CONTROLLING PHOTOLUMINESCENCE AND UNDERSTANDING CHARGE CARRIER RECOMBINATION AND TRANSFER DYNAMICS OF PEROVSKITE NANOCRYSTALS

A Thesis Submitted for the Degree of Doctor of Philosophy

by

Tasnim Ahmed



School of Chemistry
University of Hyderabad
Hyderabad – 500046
INDIA
April 2021



Dedicated to my Family



"Science cannot solve the ultimate mystery of nature. And that is because, in the last analysis, we ourselves are a part of the mystery that we are trying to solve"

-Max Planck



Contents

Declaration Certificate

4
7
9
12
14
16
20
22
24
34
34
35
35
36
37
39
42
43
46
47
49
49
50
skite ment
56
57

3.2.2 Characterization of NCs	57
3.2.3 Steady state measurements	58
3.2.4 Time resolved measurements	60
3.2.5 Mechanism of PL enhancement	61
3.3 Discussion	63
3.4 Conclusion	64
References	64 64
References	04
Chapter 4: Mechanistic Investigation of the Defect Activity Contrib	uting to the
Photoluminescence Blinking of CsPbBr ₃ Perovskite Nanocrystals	
4.1 Introduction	72
4.2 Results	
4.2.1 PL blinking study before treatment	74
4.2.2 PL blinking study after treatment	79
4.2.3 FCS study	81
4.3 Discussion	83
4.4 Conclusion	85
References	85
Chapter 5: Impact of Hole Transfer on Photoluminescence Blinkin	g of Single
FAPbBr ₃ Nanocrystals	0.4
5.1 Introduction	94
5.2 Results	0.5
5.2.1 Steady state measurements	96
5.2.2 PL blinking study	97
5.2.3 FCS study	102
5.3 Discussion	105
5.4 Conclusion	107
References	107
Chapter 6: Individual Particle Level Picture of Charge Carrier Recor	nbination in
Bi-doped CsPbBr ₃ Nanocrystals	
6.1 Introduction	116
6.2 Results	110
6.2.1 Synthesis and characterization of Bi-doped NCs	117
6.2.2 Steady state measurements	118
6.2.3 Transient absorption measurements	119
6.2.4 FCS study	121
·	121
6.2.5 Fluorescence Up-conversion measurement 6.3 Discussion	
	125
6.4 Conclusion	127
References	127
Chapter 7: Concluding Remarks	
7.1 Overview	135
7.2 Future scope and challenges	137

Declaration

I hereby declare that the matter embodied in the thesis entitled "Controlling Photoluminescence and Understanding Charge Carrier Recombination and Transfer Dynamics of Perovskite Nanocrystals" is the result of investigations carried out by me in the School of Chemistry, University of Hyderabad, India under the supervision of Professor Anunay Samanta.

In keeping with the general practice of reporting scientific investigations, the acknowledgements have been made wherever the work described is based on the findings of other investigators. Any omission or error that might have crept in is regretted.

Tasmim Ahmed

University of Hyderabad India April 2021 **Tasnim Ahmed**







Phone: (work) +91 40 2313 4813, +91 40 2301 2341

(lab): +91 40 2313 4913

Fax: +91 40 2301 1594

Email: anunay@uohyd.ac.in OR anunay.samanta@gmail.com

URL: http://chemistry.uohyd.ac.in/~as/

Certificate

This is to certify that the thesis entitled "Controlling Photoluminescence and Understanding Charge Carrier Recombination and Transfer Dynamics of Perovskite Nanocrystals" submitted by Ms. Tasnim Ahmed bearing the registration number 15CHPH31 in partial fulfilment of the requirements for the award of Doctor of Philosophy (Ph.D.) in the School of Chemistry, University of Hyderabad, India under my supervision and guidance. This thesis is free from plagiarism and has not been submitted previously in part or full to this or other University/Institution for any degree or diploma. Further, the student has following publications before submission of the thesis for adjudication and has produced evidences for the same in the form of reprints.

Parts of the thesis have been published in the following publications:

- 1. **Tasnim Ahmed**, Sudipta Seth, and Anunay Samanta, Boosting the Photoluminescence of CsPbX₃ (X= Cl, Br, I) Perovskite Nanocrystals Covering a Wide Wavelength Range by Post-Synthetic Treatment with Tetrafluoroborate Salts, *Chem. Mater.*, **2018**, 30, 3633–3637. (Chapter 3)
- Tasnim Ahmed, Sudipta Seth and Anunay Samanta, Mechanistic Investigation of the Defect Activity Contributing to the Photoluminescence Blinking of CsPbBr₃ Perovskite Nanocrystals, ACS Nano, 2019, 13, 13537–13544. (Chapter 4)

- 3. Tasnim Ahmed, Sumanta Paul and Anunay Samanta, Impact of Hole Transfer on Photoluminescence Blinking of Single FAPbBr₃ Nanocrystals (To be communicated) (Chapter 5)
- 4. **Tasnim Ahmed**, Apurba De, Sumanta Paul and Anunay Samanta, Individual Particle-Level Picture of Charge Carrier Recombination in Bidoped CsPbBr₃ Nanocrystal. *J. Phys. Chem. C* **2021**, 125, 2156–2162. (Chapter 6)

The student has made presentation in the following conferences:

- 1. "Effect of Heterovalent Metal Doping on the Optical Properties of Perovskite Nanocrystals", **International Conference on Nanoscience and Technology**, S. N. Bose National Centre for Basic Sciences, Kolkata, India, March 5-7, 2020. (*Poster presentation*)
- 2. "Mechanistic Investigation of Photoluminescence Blinking in Single CsPbBr₃ Perovskite Nanocrystals", **15**th **Trombay Symposium on Radiation and Photochemistry (TSRP-2020)**, Bhabha Atomic Research Center (BARC), Mumbai, India, January 5-9, 2020. (*Poster presentation*)
- 3. "Effect of Heterovalent Metal Doping on Optical Properties of Perovskite Nanocrystals" **17**th**Annual In-House Symposium of the School of Chemistry (Chemfest-2020),** University of Hyderabad, Hyderabad, India, February, 2018. (*Oral Presentation*)
- 4. "Dramatic Improvement of Photoluminescence of CsPbX₃ (X=Cl, Br, I) Perovskite Nanocrystals by Simple Post-Synthetic Treatment with Tetrafluoroborate Salts", **International Workshop & Conference on Perovskite & Hybrid Photovoltaics**, IIT Delhi, New Delhi, India, February 4-8, 2019. (*Poster presentation*)
- 5. "Outstanding Photoluminescence Enhancement of CsPbX₃ (X=Cl, Br, I) Perovskite Nanocrystals by Post-Synthetic Treatment with Tetrafluoroborate Salts", **15thAnnual In-House Symposium of the School of Chemistry (Chemfest-2018),** University of Hyderabad, Hyderabad, India, March 09-10, 2018. (*Poster Presentation*)

The student has passed the following courses towards the fulfilment of the coursework requirement for Ph.D. degree:

Sl. No.	Course Code	Title	Credits	Status
1	CY801	Research Proposal	3	Pass
2	CY802	Chemistry Pedagogy	3	Pass
3	CY806	Instrumental Method-B	3	Pass
4	CY453	Molecular Spectroscopy	3	Pass

Anunay Samanta

Thesis Supervisor

PROF. ANUNAY SAMANTA SCHOOL OF CHEMISTRY UNIVERSITY OF HYDERABAD HYDERABAD - 500 046 Kumare Juanum Dean 19/4/201

School of Chemistry
University of Hyderabad
Dean
SCHOOL OF CHEMISTRY
UNIVERSITY OF HYDERABAD
HYDERABAD-500 046



Acknowledgements

Last five and half years of PhD journey is the most important period of my life. During this period, I have gone through several phases which have helped me not only to improve my academic learning but also to grow me as a person.

I express my sincere gratitude to my research supervisor, Prof. Anunay Samanta for giving me the opportunity to work with him. I am thankful for his constant cooperation, guidance, and patience towards the blunders I made. I am grateful to him for giving me the freedom of work in the lab and for his enormous efforts to make our work move smoothly. My sincere gratitude to madam, Boni and Ani da. I enjoyed all the occasions associated with them, whether it was lab party or Ani da's marriage.

I would like to thank the present and former Dean(s), School of Chemistry, for providing all the facilities and their constant support. I extend my gratitude to all the faculty members of the school, especially thankful to my doctoral committee members, Prof. Samar Kumar Das and Prof. Tushar Jana for their valuable suggestions, cooperation, and encouragement.

The Centre for Nanotechnology and Central Instrumental Facility, University of Hyderabad is greatly acknowledged for providing the facilities, like TEM. I am thankful to Mr. Durga Prasad (DP anna) for not only helping me in sample measurements but also in several aspects. Sunil has also been very helpful during SEM measurements. My special thanks to Surya anna and Anil anna for their cooperation in PXRD and FT-IR measurements and also in many other occasions.

I must thank Rdhika, Shiva, Naresh and Srinivas for their efforts in smoothening official work. I am thankful to all the non-teaching staff, School of Chemistry for their cooperation in several needs. I must also mention about all the workers for their enormous effort in keeping our lab and School clean, and for the maintenance of the beautiful garden in our School.

Financial assistance from UGC and CSIR, India is greatly acknowledged. My special thanks to CSIR for providing me the fellowship during my PhD.

My sincere regards to all the teachers who have come at different stages of my life. I had great teachers during my school life like, Asokh Sir, Angshuman Sir, Bijay Sir, Jayanti Di, Namita Di, Krishna Di, and Soma Di, who had always faith in me and made me more passionate about science. Ranjit Sir (R.P Sir) and Rizabul Sir have turned my interest towards physical chemistry during my college days. I must mention Sukriti Sir, who had been an amazing teacher of organic chemistry. I am fortunate enough to have great teachers like Pranab Da, and Bidhan Da, during my M.Sc. days. Bidhan Da had been not only a good teacher to me but also a philosopher; I still remember that lecture on "there

is no existence of God". My heartfelt gratitude to Pranab Da for all his guidance and for encouraging me to opt for a doctoral degree.

I cherish those school days, which were the golden days of my life, with friends like Sabnam, Sahin, Sunny, Sudipta, Salma, Tanvi, Moumi. I shared unforgettable memories of college days with friends like Badiuzzaman. Meena, Manisha, Antara, Barsali, Anwesha, Soumi, Sumantas. I enjoyed a lot in my hostel days during B.Sc and M.Sc. time with Fancy di, Priyanka, Pratusha, Kakoli di, Menu, Madhura, Sanghita, Puja, Ritika. I value my friendship with Badiuzzaman. I have learnt many things from all the discussions we had. I am very much fortunate that I got friends like Pavel, Barun who have been always there in the difficult time, showed faith on me and taught me. I am grateful for their contribution in my life.

I feel myself lucky for being a part of this AS lab. Chandu anna had been wonderful senior whose suggestions have been always valuable to me. Thank you for cheering me up to participate in cricket and badminton tournament. I am fortunate to have a senior like Navendu da, who has always motivated me and has been always there for any kind of help. I really enjoyed any kind of discussions with you which has been always fruitful. It was an amazing experience to work with Sudipta Da. I will always be grateful to you for teaching me everything in lab, starting from synthesis of perovskite nanocrystals to handling all the instruments. I really enjoyed all the discussions with you and learnt a lot from you. Sneha di has been an excellent senior. I am thankful for your help and support in several occasions. I really admire your presentation and communication skills, which I always tried to adopt. Saddam and Apurba, both have been most supportive batch mates I can ever have. I really enjoyed all the academic and non-academic discussions with you and will cherish all the leg pulling of each other. I have always appreciated Saddam for his positive attitude and maintaining a cheerful environment in the lab. It was a nice experience to work with Apurba, I cannot mention how much I have learnt from you. I really admire you for your straightforward nature and for valuing each small details of anything in every aspect of life. I am fortunate having juniors like Sumanta, Somnath and Rajesh. I enjoyed working with Sumanta and for all the thoughtful discussions. I appreciate the efforts of Somnath for handling several things in lab. Rajesh, your optimistic attitude, and your determination is admirable. Although I had little chance to be associated with Alila, I enjoyed your company. I feel myself lucky for being able to work with such wonderful people. I thank all my lab mates for keeping a healthy atmosphere in lab.

I cherish the bonding with my batch mates like Mou, Samita, Sipra, Chandni, Ankit, Senthil, Anif, Tanmay, Manish, Venky, Sanddep. I enjoyed the time we spent together during the organization of PhD freshers' party, Chemfest, and playing cricket and badminton tournaments. I value my bonding with Divya akka.

I enjoyed several events in the campus like Saraswati puja, Diwali, Knight cup. I will cherish those days I spent with Arpita di, Debparna di, Sabari di, Sneha di, Suchana (Pramilabahini). Thank you for giving me those memories, which will last for lifetime. I

really miss those Saturday night 'adda'. Our Pune trip was really full of fun. I had great time with Sabari di and Ankit, and I really enjoyed all those campus hopping with you. Without the cheerful company of all these people the campus life would have been boring and difficult to survive. I treasure the moments shared with Sugata da, Rudra da, Kool da, Suman da, Kausikh da, Suvo da, Nitai da, Kallol da, and Olivia di. It was great to have juniors like Olivia, Somdutta, Sampita, Sarada, Daradi, Prachi, Anupam, Sautrick, Hafizur, Alim, Suman, Mujahid, Tausif, Suvam, Nilanjan. I am thankful to Maumita di for your visit to our hostel adda in several occasions. I value my close association with Debika. A big thanks to you for all those delicious foods you cooked. Although I had limited interaction with Bappa, Kuntal and Arijit, I will cherish all the moments spent with you. I had wonderful time with Taher, Ajra, Entajul, Naznin, Sohel. I have lot of memories of such a wonderful and vibrant campus.

It is very difficult to express my gratitude to my family. The blessings and sacrifices of my parents are beyond words. Thank you for being so patient and for supporting me whatever I wanted to do in my life. My sincere gratitude to my grandfathers (late) and grandmothers who always had/have encouraged me for my education. I owe a lot to my uncle 'kakamoni'; your ideology and thinking always have a great impact on me. I am grateful to 'Kesab kaku' and 'choto jamaibabu' for teaching me and guiding me. 'Di', I am blessed to have elder sister like you. I cannot thank you enough for your motivation and supports at every stages of my life. I may not have survived without you. I feel myself lucky to have brother-in-law like 'dadabhai', you have been always there to guide me. My relations with my cousins (Titly, Titas, Dola Di, Saheb) have always derive me strength, which means a lot to me. I am grateful to my 'khalamonis' for their special love and cares. I am blessed to have 'ammu' (niece) and 'ghoton' (nephew) in my life, without them my life would have been colourless. I acknowledge the love and cares of all my relatives.

I could not mention all the names but my sincere gratitude to all the people who have been associated with this journey.

7asnim



List of Publications

Thesis Chapter Publications

- Tasnim Ahmed, Sumanta Paul and Anunay Samanta, Impact of Hole Transfer on Photoluminescence Blinking of Single FAPbBr₃ Nanocrystals (To be communicated) (Chapter 6)
- Tasnim Ahmed, Apurba De, Sumanta Paul and Anunay Samanta, Individual Particle-Level Picture of Charge Carrier Recombination in Bidoped CsPbBr₃ Nanocrystal. J. Phys. Chem. C 2021, 125, 2156–2162. (Chapter 5)
- 3. <u>Tasnim Ahmed</u>, Sudipta Seth and Anunay Samanta, Mechanistic Investigation of the Defect Activity Contributing to the Photoluminescence Blinking of CsPbBr₃ Perovskite Nanocrystals, ACS Nano, 2019, 13, 13537–13544. (Chapter 4)
- 4. <u>Tasnim Ahmed</u>, Sudipta Seth, and Anunay Samanta, Boosting the Photoluminescence of CsPbX₃ (X= Cl, Br, I) Perovskite Nanocrystals Covering a Wide Wavelength Range by Post-Synthetic Treatment with Tetrafluoroborate Salts, Chem. Mater., 2018, 30, 3633–3637. (Chapter 3)

Other Publications

- 5. Navendu Mondal, Apurba De, Sudipta Seth, <u>Tasnim Ahmed</u>, Somnath Das, Sumanta Paul, Rajesh Kumar Gautam and Anunay Samanta, Dark Excitons of the Perovskites for Sensitization of Molecular Triplet. ACS Energy Lett. 2021, 6, 588–597 (Perspective)
- Manjari Chakraborty, <u>Tasnim Ahmed</u> and Moloy Sarkar, Understanding the Behavior of Monocationic and Dicationic Room Temperature Ionic Liquids through Resonance Energy Transfer (RET) Studies, Langmuir, 2019, 35, 16172–16184.
- 7. Sudipta Seth, <u>Tasnim Ahmed</u>, Apurba De and Anunay Samanta, Tackling the Defects, Stability, and Photoluminescence of CsPbX₃ Perovskite Nanocrystals, ACS Energy Letters, 2019, 4, 1610-1618. (Perspective)
- 8. Manjari Chakraborty, <u>Tasnim Ahmed</u>, Ranu Satish Dhale, Debashis Majhi, and Moloy Sarkar, Understanding the Microscopic Behavior of

- Binary Mixtures of Ionic Liquids through Various Spectroscopic Techniques, J. Phys. Chem. B, 2018, 122, 12114–12130.
- 9. Sudipta Seth, <u>Tasnim Ahmed</u>, and Anunay Samanta, Photoluminescence Flickering and Blinking of Single CsPbBr₃ Perovskite Nanocrystals: Revealing Explicit Carrier Recombination Dynamics, J. Phys. Chem. Lett., 2018, 9, 7007–7014.
- 10. Sneha Paul, <u>Tasnim Ahmed</u>, and Anunay Samanta, Influence of Divalent Counterions on the Dynamics of DNA as Probed by Using a Minor-Groove Binder, ChemPhysChem, 2017, 18, 1 8.

List of Conference Presentations

Poster Presentation

- "Effect of Heterovalent Metal Doping on the Optical Properties of Perovskite Nanocrystals", International Conference on Nanoscience and Technology, S. N. Bose National Centre for Basic Sciences, Kolkata, India, March 5-7, 2020. (Best Poster Award)
- 2. "Mechanistic Investigation of Photoluminescence Blinking in Single CsPbBr₃ Perovskite Nanocrystals", **15**th **Trombay Symposium on Radiation and Photochemistry (TSRP-2020)**, Bhabha Atomic Research Center (BARC), Mumbai, India, January 5-9, 2020.
- 3. "Dramatic Improvement of Photoluminescence of CsPbX₃ (X=Cl, Br, I) Perovskite Nanocrystals by Simple Post-Synthetic Treatment with Tetrafluoroborate Salts", **International Workshop & Conference on Perovskite & Hybrid Photovoltaics**, IIT Delhi, New Delhi, India, February 4-8, 2019.
- 4. "Outstanding Photoluminescence Enhancement of CsPbX₃ (X=Cl, Br, I) Perovskite Nanocrystals by Post-Synthetic Treatment with Tetrafluoroborate Salts", **15thAnnual In-House Symposium of the School of Chemistry (Chemfest-2018),** University of Hyderabad, Hyderabad, India, March 09-10, 2018.
- "Effect of Heterovalent Metal Doping on Optical Properties of Perovskite Nanocrystals" 17thAnnual In-House Symposium of the School of Chemistry (Chemfest-2020), University of Hyderabad, Hyderabad, India, February, 2018. (Best Poster Award)

Oral Presentation

 "Effect of Heterovalent Metal Doping on Optical Properties of Perovskite Nanocrystals" 17thAnnual In-House Symposium of the School of Chemistry (Chemfest-2020), University of Hyderabad, Hyderabad, India, February, 2018. 2. "Photoluminescence Blinking and Charge Transfer Dynamics from Single Perovskite Nanoparticles to Phenothiazine", Conference on Advances in Catalysis, Energy and Environmental Research Online Meet, TIFR Hyderabad, Dec 16 - 18, 2020

Chapter-wise organization of the thesis

This thesis is classified into seven chapters. Chapter 1 starts with a brief introduction on the semiconductor Nanocrystals (NCs) and quantum confinement. Then we have discussed about crystal structure of a newly emerging optoelectronic material, perovskites along with the characteristic properties of its NCs and surface properties of them. The importance of doping is mentioned. An overview of PL blinking of single NCs and various mechanisms responsible for PL fluctuation are discussed along with the brief idea of studying charge transfer processes from single NC. In this Chapter 2, details of preparation of different perovskite NCs, their characterization using different techniques (such as TEM, FESEM, FTIR, XPS, PXRD) are discussed. We have discussed the methods and basic principle for single molecule fluorescence spectroscopy measurements in detail. Major focus is given to the time-resolved confocal fluorescence microscope, used for the fluorescence correlation spectroscopy and photoluminescence time-traces measurements. The outline of setup used for femtosecond transient absorption and fluorescence up-conversion measurements are provided. The basic components of timecorrelated single photon counting technique, spectrofluorimeter and UV-Vis spectrophotometer are provided. The working chapter starts with Chapter 3, in which a postsynthetic treatment with tetrafluoroborate salts is performed to improve the photoluminescence (PL) of $CsPbX_3$ (X = Cl, Br, I) perovskite NCs which emits, covering a wide wavelength range. In Chapter 4, further investigation is done on the trapping mechanism of charge carriers responsible for PL blinking of single CsPbBr₃ perovskite NCs and effect of that surface treatment on the blinking of NCs. In Chapter 5, heterogeneity of hole transfer processes from single FAPbBr₃ NCs to phenothiazine and its effect on PL blinking is studied. In the Chapter 6, we investigate effects of Bi-doping on the optical properties of CsPbBr₃ NCs and charge carrier recombination processes at the individual particle level. Last Chapter 7 summarizes the findings of all those investigations and highlights the possible directions which can be investigated further based on our findings.



CHAPTER 1

Introduction

Overview

This chapter starts with a brief introduction on the bulk semiconductors and quantum confinement in nanocrystals (NCs). This is followed by an outline of the journey of lead halide based perovskites as an emerging optoelectronic material. Specific attention is given to the perovskite NCs and their surface properties. The importance of doping in these materials is highlighted. An overview of PL blinking of single NCs and various mechanisms contributing to the PL fluctuation are presented. A brief discussion on charge transfer from single NCs is also made. Finally, the motivation behind the thesis work is presented.

1.1. Semiconductors: Bulk to nanocrystals

The electrical conductivity of a semiconductor material is between a metal and an insulator. Semiconductors can be pure elements (like silicon, germanium) or compounds (like cadmium selenide, gallium arsenide) whose band gap generally lies below 4 eV. For bulk semiconductors, the band gap energy (E_p), which is the minimum energy required to excite an electron from valence band (VB) to the conduction band (CB), is composition dependent. When electron is promoted to the CB by providing energy greater than Eg in the form of heat or photon, it leaves behind a hole in the VB. The negatively charged electron and the positively charged hole can act as free carriers and may be mobilized in presence of external electric field. Their lowest energy state is electrostatically bound electron-hole pair, known as the exciton. Consequently, the exciton has slightly less energy than the unbound electron and hole. Often this bound pair moves together in the lattice and is considered as neutral quasi-particle. Relaxation of the electron back to the VB annihilates the exciton and may be accompanied by radiative recombination with emission of photon. The recombination of exciton is limited by resonance stabilization due to overlap between the wave functions of the electron and hole.

In general, exciton can be of two types, Frenkel and Wannier-Mott depending on the binding energy.² Frenkel exciton has strong binding energy (0.1-1 eV), and is observed in materials of low dielectric constant. However, the Wannier-Mott exciton possesses weak exciton binding energy (typically ~0.01 eV), and is observed in materials with high dielectric constant, where the columbic interaction between the electron and hole is reduced due to electric field screening. Wannier-Mott kind of exciton is found in most of perovskite materials³ which is the subject matter of my thesis. Energy of exciton in crystal is approximated considering Hydrogen atom model system and is expressed as 4-6

$$E_{exciton} = E_g - \frac{R_y}{n^2} + \frac{\hbar^2 \kappa^2}{2(m_e^* + m_h^*)}$$
 (1.1)

Where n is an integer, R_y is exciton Rydberg energy, \hbar is the reduced Plank's constant and m_e^* and m_h^* represent the effective mass of electron and hole respectively and κ is the exciton wave vector.

Another important parameter to consider in this context is the exciton Bohr radius, which is most probable distance between the electron and hole of exciton. Although exciton is hydrogen like system but the binding energy is smaller, because of smaller effective mass and screening of Coulomb force between the electron and the hole. Exciton Bohr radius (a₀) is expressed as⁶

$$a_0 = a_h \frac{\epsilon}{m_r} = \frac{\hbar^2 \epsilon}{e^2} \left(\frac{1}{m_e^*} + \frac{1}{m_h^*} \right)$$
 (1.2)

Where, a_h is the hydrogen Bohr radius. Exciton Bohr radius depends on the dielectric constant of the materials (ϵ) and effective mass of the electron and the hole. Depending on the nature of the material the exciton Bohr radius can vary from 0.5 nm to more than 50 nm.

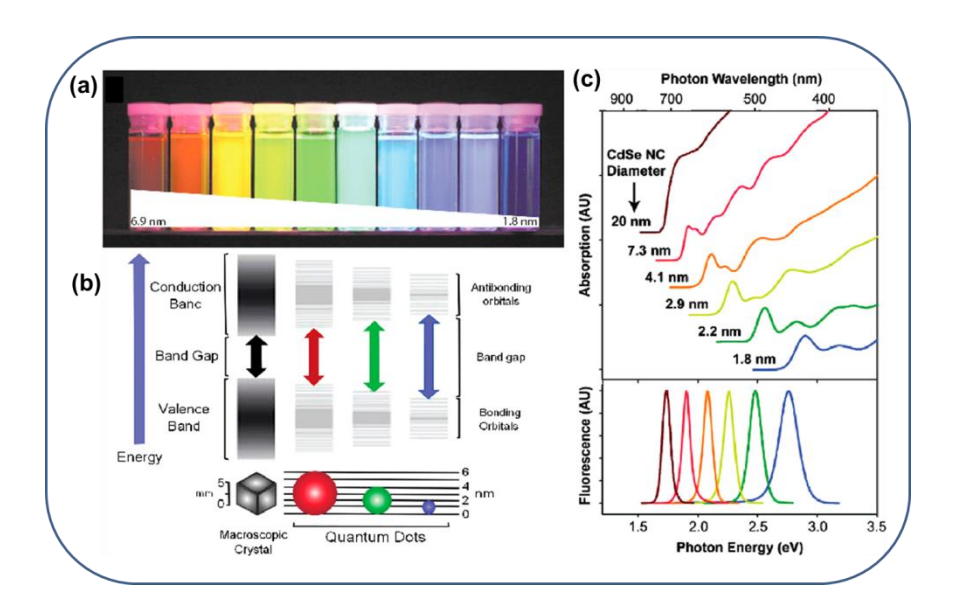


Figure 1.1: (a) Tunability of emission over the visible range with the variation of size of QDs, (b) Size dependent changes in band-gap and discrete states and (c) Absorption (top) and emission (bottom) spectra of the QDs with variation of size. Adapted from ref. 9.

The semiconductor materials in their nanocrystalline form possess some interesting properties compared to their bulk form like carrier multiplication and photoluminescence blinking.⁷⁻⁹ If the size of the NC is smaller than the size of exciton Bohr radius, the electron and the hole wave functions become spatially confined. Thus, whether a semiconductor is in the bulk or quantum confined regime depends on the exciton Bohr radius and the size of the crystal. In the quantum confined regime the nanocrystals show size dependent optical and electronic properties.^{9, 10} As the size of semiconductor crystallites becomes smaller and approaches the exciton Bohr radius, quantum confinement effect becomes effective and blue shift of exciton energy is observed. NC with dimension smaller than the exciton Bohr radius shows size dependent absorption and emission spectra with discrete electronic transition, shown in Figure 1.1. Now depending on the extent of confinement in different spatial directions, the nanocrystals can be threedimensional (3D, bulk), two-dimensional (2D, confined in one direction), onedimensional (1D, confined in two direction) and zero-dimensional (0D, confined in three direction). With increase in confinement, the band gap increases and the energy levels become more discrete in nature, which is shown in Figure 1.2.11 The band gap energy of a quantum confined system is generally expressed as^{8, 10}

$$E_Q = E_g + \frac{\hbar^2 \pi^2}{2R^2} \left(\frac{1}{m_e^*} + \frac{1}{m_h^*} \right) - \frac{1.786e^2}{\epsilon R} - 0.248E_{Ry}^*$$
 (1.3)

$$E_{Ry}^* = 13605.8 \frac{1}{\epsilon} \left(\frac{m_0}{m_e^*} + \frac{m_0}{m_h^*} \right)^{-1}$$
 (1.4)

Where E_Q and E_g represent the band gap of the quantum confined and bulk system respectively and R is the radius of the NC. The second term represents confinement energy of electron and hole. The third term arises due to Coulombic attraction between electron and hole. The last term arises due to spatial correlation between electron and hole and corresponds to the Rydberg energy. This last term is generally neglected, but

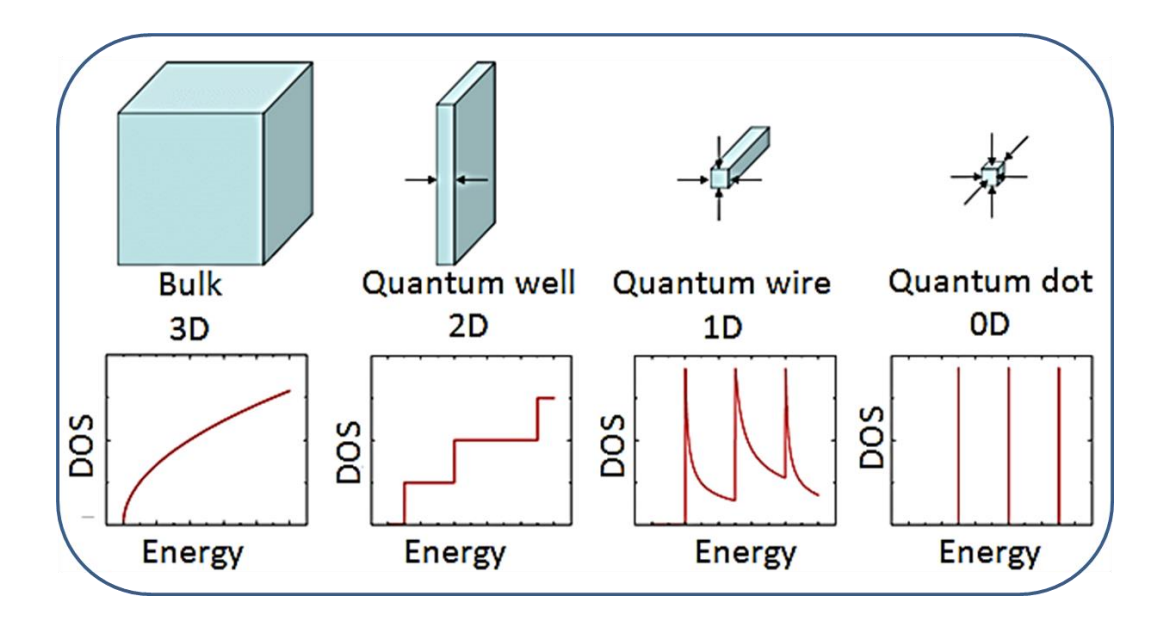


Figure 1.2: Effect of quantum confinement on the density of states of different systems (adapted from ref. 11).

becomes important for material with small dielectric constant. All these calculations have been done considering the spherical effective mass of both electron and hole and the spherically symmetric confining potentials for spherical quantum dots. Strong confinement regime is found to be valid for R=2a₀.8 In recent years, effect of quantum confinement has been studied extensively and the quantum confined materials have been applied in LEDs, lasers, biological imaging, photovoltaic devices etc. because of their tunable band gap, high PL efficiency, small size, and sharp emission properties.

1.2. Perovskites materials

 $CaTiO_3$ was named as perovskite material after mineralogist L. A. Perovski, which was discovered in 1839 in Ural mountain of Russia by Gustav Rose. Later, materials having similar crystal structure and general formula ABX_3 are termed as perovskite materials. Here, A and B are cations, where size of A is greater than B and X is an anion. In traditional ABX_3 perovskites, the B cation is octahedrally coordinated in BX_6 configuration, shown in Figure 1.3. The A cation resides at the octahedral void. The

crystal structure strongly depends on the size of those ions. The stability of crystal structure of 3D perovskite is determined by the Goldschmith tolerance factor (t), ^{12, 13}

$$t = \frac{r_A + r_X}{\sqrt{2(r_B + r_X)}}\tag{1.5}$$

Where, r_A , r_B , and r_X represent the ionic radii of A, B and X respectively. Empirically, for favorable structure the value ranges $0.81 \le t \le 1.0$. Along with the tolerance factor the second constraint is the octahedral factor (μ) which lies in the range $0.44 \le \mu \le 0.9$, ¹⁴ can be expressed as



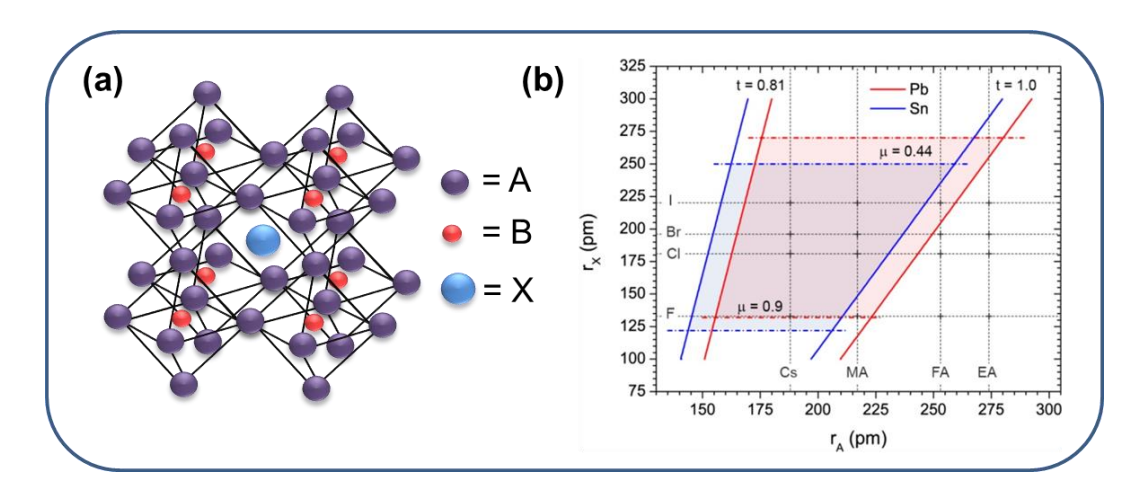


Figure 1.3: (a) Schematic representation of perovskite structure with general formula ABX_3 , (b) Formability of 3D tin (blue) and lead (red) halide perovskites as a function of halide anion and A-site cation radii. Dashed and solid lines mark the bounds of the octahedral and tolerance factors, respectively (adapted from ref. 14).

Recently synthetic metal halide based perovskites have attracted immense attention of researchers because of their intriguing optical and electronic properties which make them potential candidates for applications in optoelectronic and photovoltaic devices. Metal halide perovskites were reported first in 1893¹⁵, and main focus was on its application in

light emitting devices and transistors. However, it has come into the limelight in 2009 because of its application in solar cell as shown by Miyasaka and co-workers. 16 Since then, several developments have taken place either to improve the properties of materials or to explore its applications in different photovoltaic and optoelectronic devices. 17 In this case, in ABX₃, X is halide anion (Cl⁻, Br⁻, I⁻), B is a bivalent metal cation (Pb²⁺, Sn²⁺ etc.) and A is monovalent cation (Cs⁺, Rb⁺, CH(NH₂)₂⁺ or FA⁺, CH₃NH₃⁺ or MA⁺ etc.). The emission can be tuned by varying the halides. Depending on the A cation, it can be allinorganic (A= Cs⁺, Rb⁺) or hybrid organic-inorganic (A= FA⁺, MA⁺) halide perovskite. ¹⁸ Since the first in 2009, within very few years, the power conversion efficiency of solar cell has reached >25%. 19 High colour purity and low non-radiative rates make them potential candidates for LEDs and lasers. 20, 21 Unfortunately, bulk perovskites show low photoluminescence quantum yield (PLQY) because of (a) low exciton binding energy, and (b) low formation energy of defects arises for ionic mobility. The films prepared from those precursor solutions also show low PLQY and suffer from intrinsic defects²² and variation of PLQY is observed for different grains, which is lowest at the grain boundary.²³ Then the attention was turned towards NCs not only to improve the PLQY but also to reach the quantum confinement size regime to tune the emission by varying the size on NCs. The CsPbX₃ NCs were first reported very recently in 2015.²⁴ Overall, promising optoelectronic properties of lead halide based perovskites like large absorption coefficient, colour tunability by changing the halides and sizes of NCs, high defect tolerance and long carrier mobility make them popular as next generation semiconductor. 14, 17, 18, 20, 25

1.3. Perovskite nanocrystals

Kovalenko and co-workers first reported the synthesis of CsPbX₃ NCs following a conventional hot-injection method and reached a high PLQY (50-90%).²⁴ Since then various *in-situ* and post synthetic modification has been done to improve its optoelectronic properties and explore its potential application in different fields. The band gap of the NCs can be tuned by changing the halides, which covers emission over the visible region (Figure 1.4).²⁴ Halide exchange can be done even at room temperature.¹⁷

These perovskite materials are composed of highly ionic bonds which is one of the reasons for the easy synthesis of NCs even at room temperature. Since the first report of

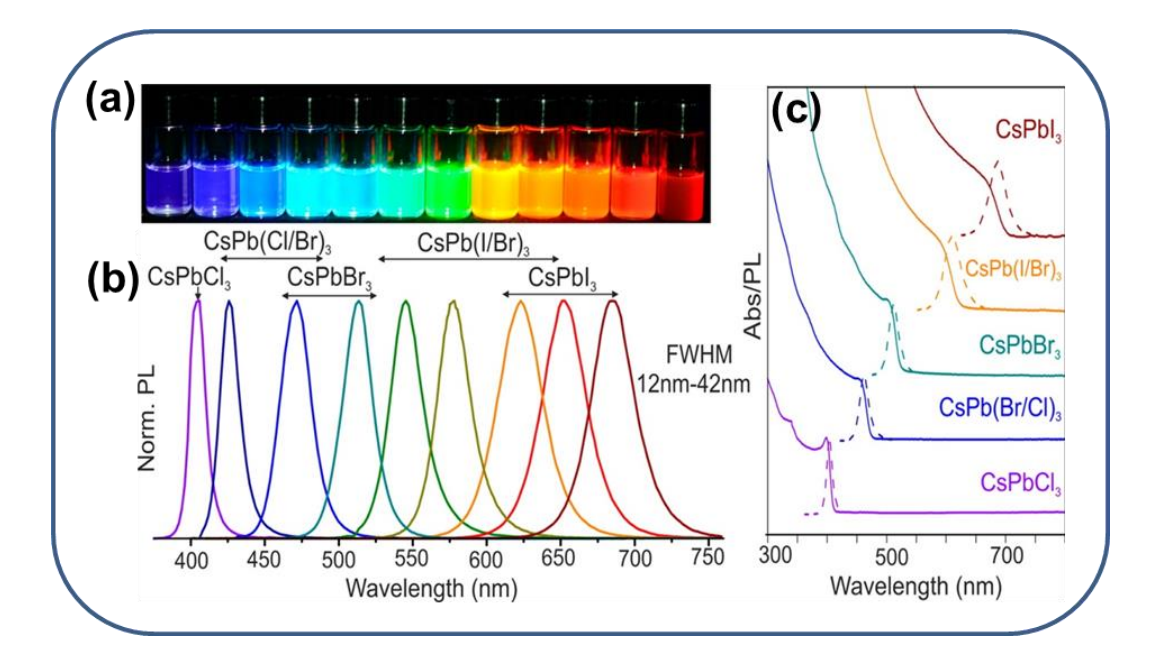


Figure 1.4: (a) Colloidal solution of perovskite NCs exhibiting composition dependent emission over the entire visible spectral region under UV lamp, (b) Tunability of emission spectra with the variation of halide and (c) Typical optical absorption and emission spectra of perovskite NCs. Adapted from ref. 24.

NCs, several processes are developed to tune the shape and size of the NCs.¹⁷ For preparation of the NCs organic ligands are used to control the growth of NCs as well as for passivation of the surface defects. In a conventional synthesis oleic acid and oleylamine are used as ligands.²⁶ However labile nature of those ligands emphasizes the need of more studies to find out alternative ligands which bind more strongly to the surface of NCs.^{26, 27}

The VB of lead halide perovskites is formed by the Pb-6s and halide-np orbitals and the CB is formed by Pb-6p orbitals. In conventional semiconductors (like GaAs, CdSe etc.),

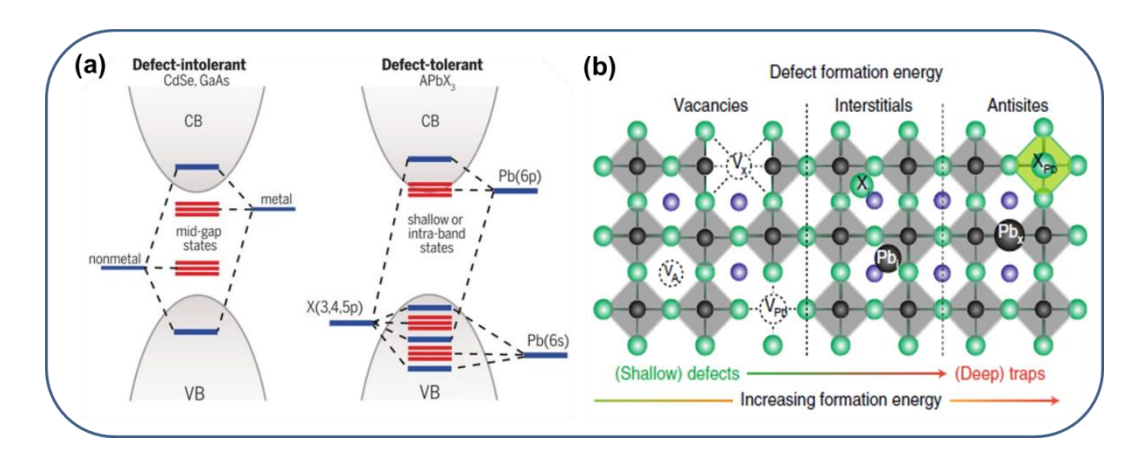


Figure 1.5: (a) Schematic representation of the electronic structure of perovskites, highlighting their defect tolerant nature compared to conventional semiconductors (adapted from ref. 30) and (b) Possible point defects and their formation energy in perovskites (adapted from ref. 28).

the band gap is formed by the gap between bonding and anti-bonding orbitals. In perovskite materials, the VB and CB contain anti-bonding and non-bonding orbitals (shown in Figure 1.5).²⁸ Thus the unpassivated surface defects or point defects form shallow trap states or are enclosed in the VB and CB. The 'A' cation has no-direct influence on band-structure. This particular nature of band structure makes these lead-halide perovskites defect-tolerant with high PL efficiency.²⁸⁻³⁰

Highly ionic nature of perovskite materials makes them soluble in polar solvent and decomposing the structure. This decomposition is accelerated in presence of moisture, light, oxygen and heat. So retention of structural and optical stability is highly challenging for this lead halide perovskites. In this regard, FA based perovskite NCs have more stability than the MA based NCs, which has low formation energy.²⁸ Hence, for its practical applications, those NCs should be protected in inert shell such as shell of silica, alumina, or BaSO₄, or polymers.²⁶ Structural instability is observed for red emitting CsPbI₃ NCs, where the structure of NCs are changed from a emitting phase to a non-emitting phase because of large size of the iodides leading to a tilting of the octahedral

unit.³¹ Although considerable work has been done to make the NCs stable, still they suffer from low stability.

Although lead halide perovskite NCs are defect tolerant, they are not completely defect free. The labile nature of ligands keeps the surface unpassivated and the uncoordinated orbitals act as traps. Formation of point defects is highly favourable due to low formation energy. Especially the halide vacancy plays a major role in the formation of traps states and lowering the PLQY of NCs.²⁶ Due to the large or small size of ions, the crystal structure of perovskite NCs can be distorted introducing defects in the NCs. For example, in case of CsPbI₃ or CsPbCl₃ NCs, large size of I or small size of Cl creates intrinsic defects in the NCs which act as trapping centres for charge carriers.^{31, 32}

Due to soft and dynamic nature of the perovskite lattice (define as crystalline liquids), the photoexcited electrons and holes can couple with the ionic displacement of lattices (phonon) and form polarons.^{33, 34} Formation of polarons can result self-trapping of charge carriers. The detrimental effect of polaron formation on the optical properties of NCs is needed to be understood properly.³³

1.4. Surface properties of perovskite nanocrystals

For semiconductor as the size of particle is approached to nanometer scale, the PL property is largely determined by the quality of the surface on the NCs. As the size of the material decreases, the ratio of surface to volume increases and the number of atoms present on the surface increases. The atoms present on the surface of a crystal facet are not completely bonded within the crystal lattice and hence, are under-coordinated. As a result, the periodicity of the crystal is disrupted with one or more dangling orbital on each atom of the surface pointed outward from the crystal. Now if the energy levels of trap states fall within the band gap of the semiconductor, they can act as carrier trapping centre and reduce the overlap of wavefunction of electron and hole promoting nonradiative recombination of exciton. Depending on the nature and position of the trap states, they can act as deep or shallow trap for electron and hole. One of the general

strategies to eliminate those trap states is passivation of those under coordinated surface atoms with suitable capping ligands.

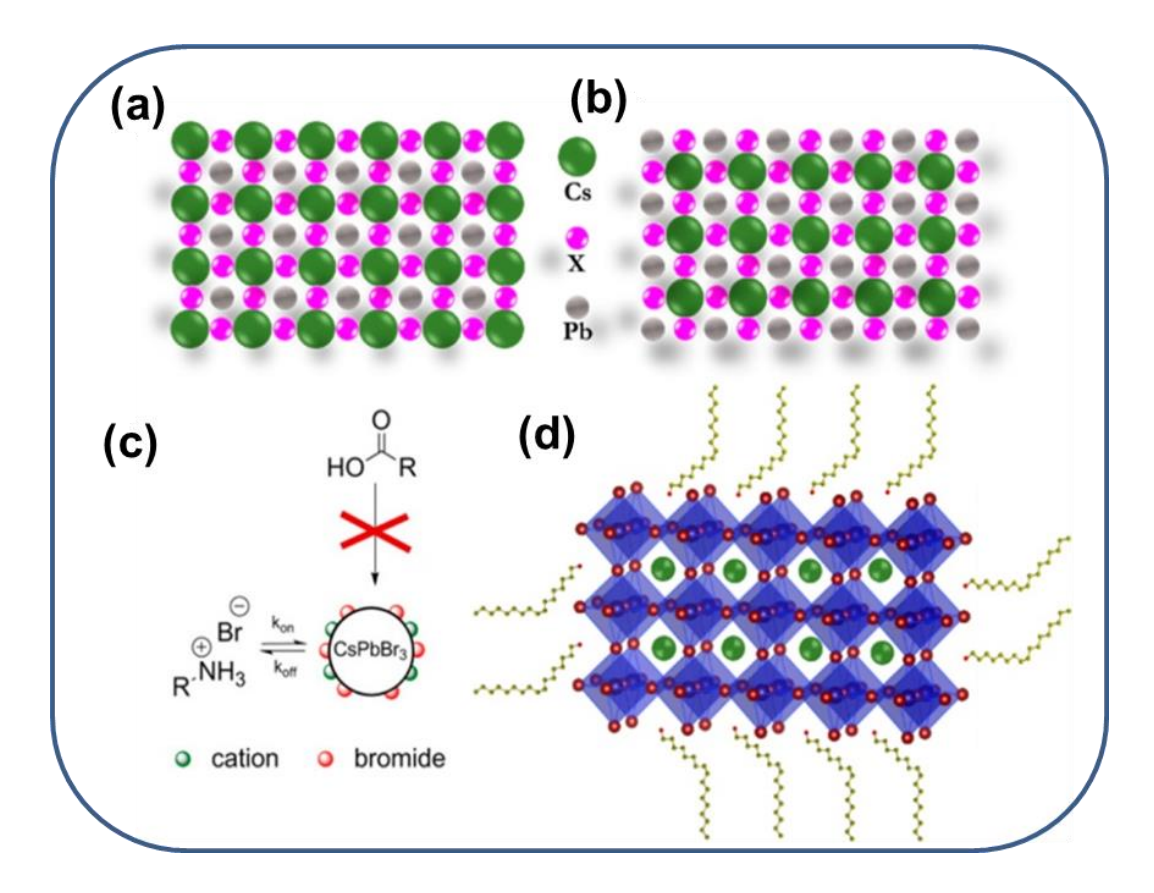


Figure 1.6: Schematic illustration of surface termination with (a) CsX or (b) PbX_2 of $CsPbX_3$, (c) Surface stabilization by dynamic oleylammonium bromide, where oleic acid is not acting as ligand, and (d) Surface passivation of perovskite NCs by oleylammonium ions, replacing surface Cs^+ ions. Adapted from ref. 17.

In case of perovskite NCs, the surfaces are passivated by ligands with long hydrocarbon chain which also inhibits the aggregation of NCs and maintains the structural integrity.^{17, 26} Conventionally oleic acid and oleylamine are used as capping ligand.²⁶ These ligands on the surface are highly dynamic in nature, which undergo rapid adsorption and desorption process on the surface.³⁵ The mode of capping depends on the surface stoichiometry and two possibilities of surface termination are [CsX] or [PbX₂] (shown in

Chapter 1 Introduction

Figure 1.6).³⁶ It is reported that oleylammonium ion binds to the Br of the surface through hydrogen bonding and it can also substitute some of Cs-ions from the surface of NCs.^{35, 37} The Br-vacancies on the surface of NCs leads naked Pb atoms, which act as one of the major surface traps and responsible for low PLQY.²⁶ Hence, modification of surface properties is an important process for modulation of the optical properties of NCs.²⁶

1.5. Doped perovskite nanocrystals

Doping is a fundamental strategy to alter the properties of any semiconducting materials. In contrast to composition engineering, doping needs incorporation of small amount of impurities in the crystal. It does not change much of the host crystal structure, but modifies the fundamental properties of the semiconductor, like stability of crystal, optoelectronic property, and magnetic property. ^{38, 39} With the aim to endow this

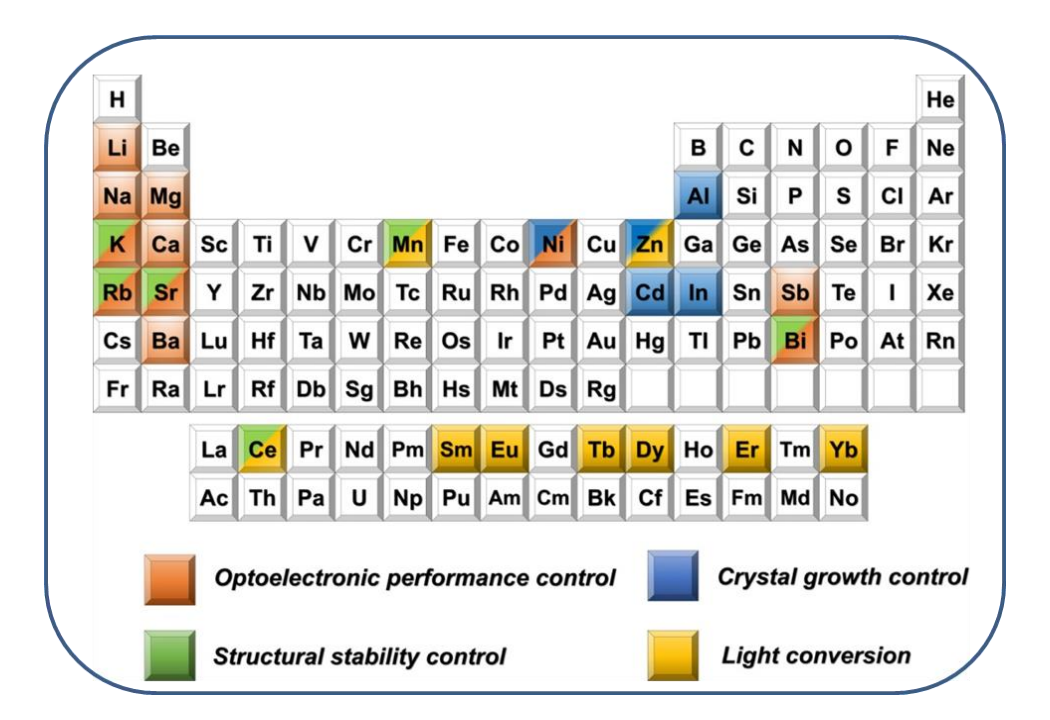


Figure 1.7: Various dopants used to alter the properties of perovskites for different purposes (adapted from ref. 42).

perovskite material with new properties several studies have been performed in the last five years. All A, B or X ions can be replaced with various dopants, but here I have discussed about B cation doping, which is the subject matter of the thesis. Several isovalent and heterovalent ions with respect to the B cation (Pb²⁺) are doped for different purposes such as structural stability, controlling the optoelectronic performance, crystal growth, light conversion and partial replacement of toxic lead (see Figure 1.7). 40-42 The dopants are chosen in such a manner that they do not disrupt the crystal structure. The soft and ionic nature of perovskite crystal makes it feasible to exchange the Pb²⁺ ion with dopants during the synthesis as well as in post synthetic manner (Figure 1.8). Interestingly, doping with ions smaller in size than Pb²⁺ (Cd²⁺, Mg²⁺, Ni²⁺ etc.), 26, 32, 43, 44 results in unprecedented enhancement of PLQY of CsPbCl₃ NCs due to correction of short-range disorder of the crystal. 44 On the other hand, doping with metal ions, like Mn²⁺,

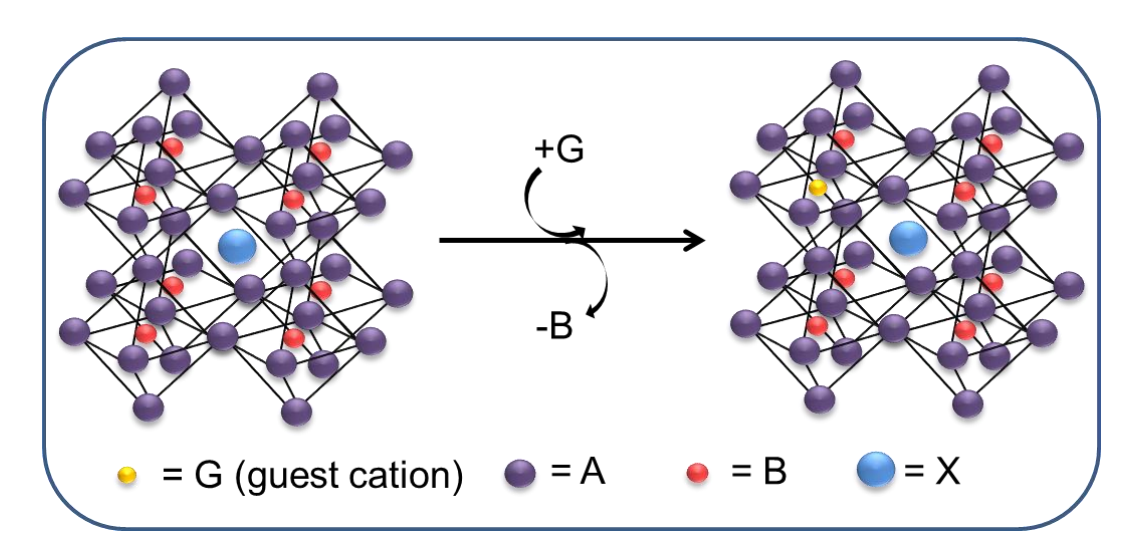


Figure 1.8: Schematic representation shows doping at B site. Replacement of B cation (Pb^{2+}) with dopant.

Sr²⁺, Bi³⁺ etc. improves the stability of the photoactive phase of CsPbI₃ NCs with the release of crystal strain.^{45, 46} Doping of Mn²⁺ and several lanthanide ions in CsPbCl₃ NCs introduces additional emission peak due to internal electronic transition of the dopants.^{47, 48} Among the several heterovalent dopants less toxic Bi³⁺ has attracted attention because

of similar electronic configuration and ionic radii of Pb²⁺.⁴⁹ It is reported that Bi³⁺ doping increases the conductivity and the concentration of free carriers as well.⁵⁰ Very recently, it is successfully doped in CsPbBr₃ NCs which show a decrease of PLQY.⁴⁹ Despite several attempts to alter the PL properties of perovskites through metal ion doping, the photoexcited carrier dynamics is not clearly understood yet and needs to be studied extensively to utilize the full potential of these substances.

1.6. Single particle photoluminescence blinking

Under constant illumination, most of the single emitters exhibit random fluctuation of PL intensity with time, which is called PL intermittency or blinking. At the ensemble level, PL blinking becomes undetectable as fluctuation is smoothed out. In case of semiconductor NCs, blinking was first observed for CdSe based NCs by Nirmal et al. in 1996.⁵¹ Blinking is attributed to the interaction of charge carriers with defect site of NCs.⁵²⁻⁵⁴

PL blinking was observed previously for fluorescent proteins and dye molecules. In case of simple emitter, blinking is attributed to the intersystem crossing to the triplet state, where a single rate is observed for blinking. However, in case of more complex NCs, the reason for blinking is the interaction of charge carriers (electron or hole) with the defect site of NCs, which can be present on the surface or internal to the NCs. 52, 53 Charge trapping hinders both radiative recombination of photo-generated excitons and their transport in the NCs, and limits the efficiency of devices. 52-54 Depending on the nature of defects charge carriers can reside on those trap states for a range of time (ns to ms) and promote non-radiative recombination of exciton causing PL blinking. PL fluctuation can happen over several intensity levels, where the high intensity states are called ON states and the low or non-emitting states are called OFF states (Figure 1.9). In most of the cases several intermediate states (or GREY) are also observed between ON and OFF states. A distribution of blinking rate is observed in case of NCs and is expressed properly with power law function. 52,53 In case of metal chalcogenide quantum dots, the blinking time is observed spanning from few microsecond to hundreds of second. 52, 53 In case of perovskite NCs, the blinking rate is observed to be faster. 52, 55, 56 This highly distributed blinking rate is attributed to the static and time dependent variation of trapping and detrapping rate of charge carriers. Thus, time resolved and statistical analyses of the blinking traces provide important information on the nature of trap states, trapping kinetics in a single NC and heterogeneity of the processes.

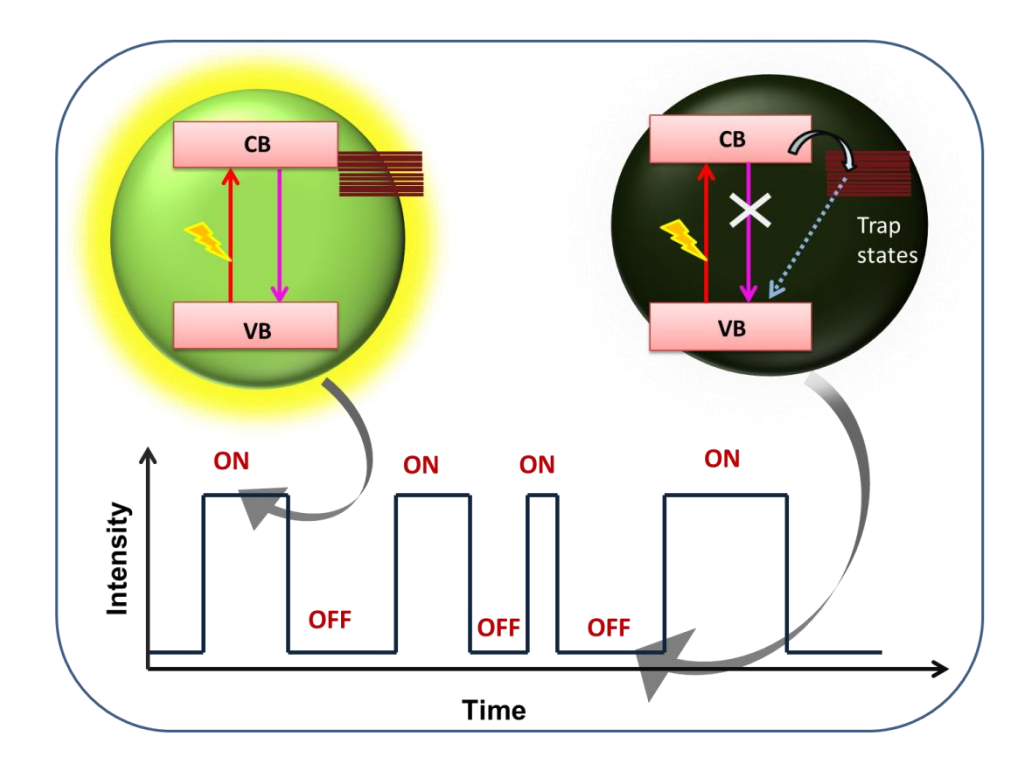


Figure 1.9: Schematic representation of blinking in semiconductor NCs due to competitive radiative and non-radiative recombination through trapping of charge carriers.

Over the past two decades of research several mechanisms have been proposed to describe the reason for blinking of single particle and development of those mechanisms are ongoing and highly debatable.⁵⁷⁻⁶⁵ Among these mechanisms charging-discharging model is very common and well accepted.⁶³⁻⁶⁵ Under continuous excitation, particles become charged due to trapping of a photoexcited carrier (electron/hole) to long-lived trap states. Generation of another exciton forms trion (positive/negative) by coupling with

the charged nanoparticle.^{57, 58, 66} The trion recombines following non-radiative Auger recombination and quenches the PL of nanoparticles via transferring the exciton

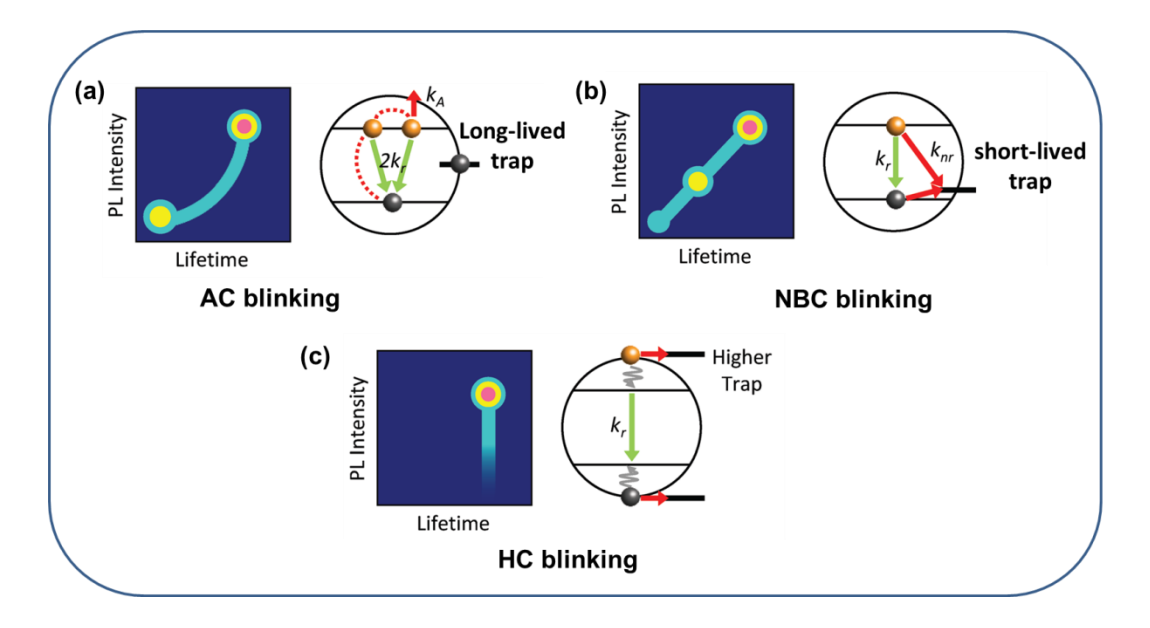


Figure 1.10: Three different types of PL blinking mechanisms are observed in semiconductor NCs. Illustration of their FLID patterns (left) which is represented by false color coding and the corresponding recombination processes of the photoexcited charge carriers (right). Green arrows indicate the radiative processes, whereas the red arrows indicate nonradiative processes (adapted from ref. 69).

recombination energy to the third carrier (either electron or hole).^{52, 53} Trion can also recombine in a radiative manner, whose rate is almost double of that neutral exciton recombination.^{56, 57} This kind of trion mediated recombination is denoted as AC blinking (Figure 1.10 a).⁵² The blinking cycle is completed once the charged nanoparticle returns back to its neutral position and restores the original high PL intensity (ON) state. However the process of neutralization is not known and remains as an active area of research. Later, this charging model is confirmed by the intensity-lifetime scaling of different intensity regions of the PL trace.⁵⁵⁻⁵⁷ Intensity-lifetime scaling represents the ratio of radiative rate of two different intensity levels (OFF to ON) and is represented as

$$\eta = k_{ON}: k_{OFF} = I_{ON}/\tau_{ON}: I_{OFF}/\tau_{OFF}$$
(1.7)

Where, I and τ are the PL intensity and lifetime of the corresponding state.

In case of trion recombination, as the extra charge exerts double Coulombic interaction, the rate for trion recombination is almost double of the neutral exciton. Hence the η value becomes 2 for trion recombination. This case correlation between intensity and lifetime is observed, but not in a linear way. A convenient way to check the correlation between intensity and lifetime is the analysis of fluorescence intensity lifetime distribution (FLID) pattern. In this representation, probability of occupying different states is shown in two dimensional lifetime-intensity space by false color coding. For AC blinking a curved trajectory is observed in FLID pattern, shown in Figure 1.10 a. Two completely discrete states are also observed for binary switching between ON and OFF states. Elementary kinetics predicted single exponential decay of distribution of ON and OFF blinking time duration. However, experimentally it is found that the decay follows power law behavior, indicating wide distribution of rates. Several modifications have been made on the charging mechanism to explain such widely distributed kinetics, such as static distribution of tarp states and later dynamically changing trapping rate is also included. The charging mechanism to explain such widely distributed kinetics, such as static distribution of tarp states and later dynamically changing trapping rate is also included.

Recently, it is observed that charging model alone cannot be enough to explain the low PLQY of the OFF state, which is observed to be lower than that, is predicted from the Auger quenching. Another blinking model is proposed, referred as NBC blinking, that does not need any charging of NCs or long-lived trap. ⁶² In this case, the trap states are short-lived ($\leq 1\mu s$) and the trapped charge recombines rapidly to its counter-charge before formation of another exciton. Several continuous emissive states are reported with fixed radiative rate with dynamic fluctuation of trapping rates. ⁵⁷ This leads to the intensity-lifetime scaling, η value 1. ⁵⁷ Intensity and lifetime are linearly correlated, and hence, a linear trajectory in the FLID pattern is observed (Figure 1.10 b). The variation of recombination rates leads to power law distribution of the ON-OFF events, which are better explained by the multiple recombination centers (MRC) model proposed by Frantsuzov et al. According to this model, there are several trap states in the NCs, which

switch between active and inactive conformation.^{52, 59} The fluctuation of trapping rate is determined by the changes in the number of available active trapping sites.

There is another mechanism, which is distinct from the NBC blinking and arises due to the interception of hot carriers. ^{58, 68, 69} This mechanism is denoted as HC blinking. Although both the NBC and HC mechanisms are related to the rapid nonradiative recombination through trap states, but the competition between the radiative and nonradiative pathway is different. Unlike NBC, in HC-blinking, some hot carriers are trapped before cooling down to the band-edge and recombines with counter charges nonradiatively. These charges do not contribute to the PL intensity and lifetime in the measurement. Therefore, in FLID pattern it shows states with abrupt change in intensity without any change in lifetime (Figure 1.10 c).

For perovskite NCs, the ON and OFF states switch rapidly and show fast blinking. In several cases, no distinct states are observed, rather a continuous distribution of emissive states are noticed, which is called as PL flickering. The blinking mechanism of perovskite NCs seems to be diverse depending on the composition and surface properties. In most of the cases, AC mechanism is reported as the reason of blinking.^{56, 70-72} Co-existence of both NBC and AC type mechanisms on the same perovskite NC is also observed.⁵⁵ Blinking limits the efficiency of devices, but elimination of the processes (discussed above) responsible for blinking is highly challenging.⁷³⁻⁷⁶ Suppression of blinking has been achieved for metal chalcogenide QDs by surface modifications or by putting shells around QDs. However, very few reports on the effect of surface treatment on the blinking mechanism of the perovskite NCs are available.^{55, 67, 75}

1.7. Interfacial charge transfer from single particle

Photoinduced charge (electron/hole) transfer processes from semiconductors are widely studied, mostly because of its applications in solar cells and photocatalysis. Especially, for application in solar cells, it has been studied more intensely because of emerging demand of renewable solar energy source. Therefore, it is essential to understand those processes at the fundamental level to utilize the full potential and optimize the

performance of the devices. For a molecular adsorbate, electron (hole) transfer from the semiconductor requires that the LUMO (HOMO) level lies below (above) the conduction band (valence band) of the harvester. Efficient quenching of PL is observed on successful charge transfer. 77

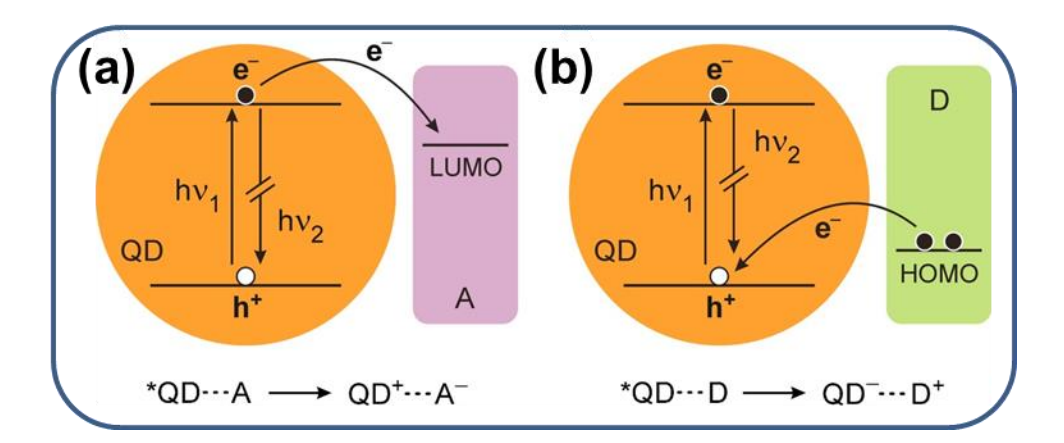


Figure 1.11. Schematic representation of electron transfer (a) from and (b) to the photoexcited QD in presence of electron or hole acceptor (adapted from ref. 77).

The electron transfer dynamics can be resolved by comparing lifetime of emitter before and after charge transfer. The lifetime of the emitter before charge transfer can be written as

$$\tau_0 = \frac{1}{k_r + k_{nr}} = \frac{1}{k_0} \tag{1.8}$$

where τ_0 is the fluorescence lifetime before charge transfer and k_r and k_{nr} are the radiative and nonradiative decay rates respectively.

The lifetime of the emitter after charge transfer can be written as

$$\tau = \frac{1}{k_0 + k_{ct}} \tag{1.9}$$

where k_{ct} is the interfacial charge transfer rate.

Chapter 1 Introduction

In case of perovskite NCs, most of the studies have been performed at the ensemble level, where all the parameters are averaged out.⁷⁸⁻⁸² Understanding the distribution of charge transfer rate is difficult from the ensemble measurements. PL spectroscopy study at the single particle level explores the hidden dynamic and static heterogeneity of processes.^{54, 83, 84} Thus, charge transfer study at the single particle level exposes how the rate of charge transfer can vary from one particle to another, how the rate can vary with time for a single particle, and how the charge transfer dynamics can affect the PL properties.

1.8. Motivation behind the thesis work

The growing demand for electricity all over the world makes it essential to find an alternative to fossil fuels, both to overcome the shortage of energy supply and to stop the detrimental effect on the environment. Renewable energies are inexhaustible natural source and have received enormous attention of researchers. Solar energy in particular is one of the most promising renewable energy sources. Until now, silicon has been the material used in commercialized solar cell, but these are still quite expensive. In this context, an emerging material is perovskite with promising optoelectronic properties, because of their low cost and high efficiency. A rapid progress has been made on the way towards the increase of conversion efficiency. Within very few years, the efficiency has reached from 3% to more than 25%. 19 Not only in solar cells but also this lead halide based perovskites have shown encouraging application in LEDs, lasers and other optoelectronic devices. In this regard, understanding the photophysical processes in these perovskites is important for utilization of full potential of these materials and development of devices. This is where the importance of spectroscopic tools comes. The major focus of the thesis is studying the photophysical processes in different photoexcited perovskite materials in their nanocrystalline form using various spectroscopic techniques, especially the single particle fluorescence techniques.

These CsPbX₃ nanocrystals possess crystal defects which have detrimental effect in the performance of the devices made of these materials. The PL properties of these substances are, however, highly sensitive to the synthetic conditions and compositions. Although the perovskite NCs are defect tolerant, they are not completely free from

Chapter 1

defects. These defects act as trapping centers for the charge carriers and lower the PL efficiency of the systems. PL properties of the NCs are largely determined by the quality of the surface because of high surface to volume ratio of them. Hence, surface treatment by appropriate reagent is key to obtaining defect-free samples with superior PL properties for light-based applications. With this motivation, we quest for a common method for improvement of the PL properties of a wide variety of CsPbX₃ NCs following a post synthetic treatment.

Efficiency of an optoelectronic device made of these materials depends on the fate of the charge carriers. Hence, understanding of the nature of trap states and dynamics of different competitive radiative and nonradiative charge carrier recombination processes is essential for proper utilization of these materials. The charge carrier recombination process can be investigated by monitoring the PL properties of individual NCs in immobilized and freely diffusing states of NCs. Single NCs show random PL fluctuations or blinking, due to involvement of trap states in carrier recombination processes. Hence, the nature and the position of trap states can be understood from the blinking mechanism it follows. This is why we have chosen CsPbBr₃ NC to study the PL blinking mechanism and effect of post synthetic surface treatment on the carrier dynamics.

The performance of photovoltaic devices depends on the charge transfer processes to and from the semiconducting materials along with the other processes. Hence, investigation of the exciton dissociation processes in presence of electron or hole acceptor, are important. Charge transfer processes introduce new nonradiative recombination channels for the photo-excited particle. The blinking dynamics of single NCs can be modulated by the charge transfer activity. More insights into the heterogeneity of charge transfer dynamics are provided from single particle level study. With this motivation, we investigate the effect of hole transfer from single FAPbBr₃ NC to PTZ on the PL blinking behavior.

Doping is a fundamental strategic route, through which semiconducting materials can be endowed with new properties. Quite naturally, the perovskite NCs also have been doped with various dopants, which include both isovalent and heterovalent ions with respect to Pb²⁺ for different purposes. Among different heterovalent dopants, less toxic Bi³⁺ has

received utmost attention as its ionic radius and electronic structure are very similar to those of Pb²⁺. Hence, we have investigated the effect of Bi doping on the PL behavior of these NCs and heterogeneity of carrier dynamics depending on the extent of doping using several spectroscopic techniques at the ensemble and single particle level.

References

- 1. YU, P.; Cardona, M., *Fundamentals of Semiconductors: Physics and Materials Properties*. Springer: 2010, ISBN 978-3-642-00710-1.
- 2. Pope, M.; Swenberg, C. E. *Electronic Processes in Organic Crystals and Polymers*, Oxford University Press: 1999.
- 3. Tilchin, J.; Dirin, D. N.; Maikov, G. I.; Sashchiuk, A.; Kovalenko, M. V.; Lifshitz, E., Hydrogen-like Wannier–Mott Excitons in Single Crystal of Methylammonium Lead Bromide Perovskite. *ACS Nano* **2016**, 10, 6363–6371.
- 4. Brus, L. E., A Simple Model for the Ionization Potential, Electron Affinity, and Aqueous Redox Potentials of Small Semiconductor Crystallites. *J. Chem. Phys.* **1983**, 79, 5566.
- 5. Henderson, B.; Imbusch, G. F., *Optical Spectroscopy of Inorganic Solids*. Clarendon Press, Oxford: 1989.
- 6. Gaponenko, S. V., *Introduction to Nanophotonics. Cambridge University Press.* 2010, ISBN-10: 0521763754.
- 7. Smith, A. M.; Nie, S., Semiconductor Nanocrystals: Structure, Properties, and Band Gap Engineering. *Acc. Chem. Res.* **2010**, 43, 190-200.
- 8. Kayanuma, Y., Quantum-Size Effects of Interacting Electrons and Holes in Semiconductor Microcrystals with Spherical Shape. *Phys. Rev. B* **1988**, 38, 9797.
- 9. Chou, K. F.; Dennis, A. M., Förster Resonance Energy Transfer between Quantum Dot Donors and Quantum Dot Acceptors. *Sensors* **2015**, 15, 13288-13325.
- 10. Einevoll, G., Confinement of Excitons in Quantum Dots. *Phys. Rev. B* **1992,** 45, 3410.
- 11. Jayawardhana, M. R. P. I.; Gamalath, K. A. I. L. W., Electronic Structures of CdSe Quantum Dots Embedded in ZnSe. *World Sci. News* **2017**, 86, 205-225.
- 12. Goldschmidt, V. M., Die Gesetze Der Krystallochemie. *Naturwissenschaften* **1926,** 14, 477-485.
- 13. Pen~a, M. A.; Fierro, J. L. G., Chemical Structures and Performance of Perovskite Oxides. *Chem. Rev.* **2001,** 101, 1981–2017.
- 14. Manser, J. S.; Christians, J. A.; Kamat, P. V., Intriguing Optoelectronic Properties of Metal Halide Perovskites. *Chem. Rev.* **2016**, 116, 12956-13008.
- 15. Wells, H. L., Über die Cäsium- und Kalium-Bleihalogenide. *Z. Anorg. Allg. Chem.* **1893,** 3, 195-210.

- Chapter 1
- 16. Kojima, A.; Teshima, K.; Shirai, Y.; Miyasaka, T., Organometal Halide Perovskites as Visible-Light Sensitizers for Photovoltaic Cells. J. Am. Chem. Soc. 2009, 131, 6050-6051.
- 17. Shamsi, J.; Urban, A. S.; Imran, M.; Trizio, L. D.; Manna, L., Metal Halide Perovskite Nanocrystals: Synthesis, Post-Synthesis Modifications, and Their Optical Properties. Chem. Rev. 2019, 119, 3296-3348.
- Jena, A. K.; Kulkarni, A.; Miyasaka, T., Halide Perovskite Photovoltaics: Background, Status, and Future Prospects. Chem. Rev. 2019, 119, 3036-3103.
- 19. NREL Best Efficiency Chart: https://www.nrel.gov/pv/assets/pdfs/best-researchcell-efficiencies.20200104.pdf.
- Le, Q. V.; Jang, H. W.; Kim, S. Y., Recent Advances toward High-Efficiency Halide 20. Perovskite Light-Emitting Diodes: Review and Perspective. Small Methods 2018, 2, 1700419.
- Stranks, S. D.; Snaith, H. J., Metal-Halide Perovskites for Photovoltaic and Light-21. Emitting Devices. Nat. Nanotechnol 2015, 10, 391–402.
- 22. Yin, W. J.; Shi, T. T.; Yan, Y. F., Unusual Defect Physics in CH₃NH₃Pbl₃ Perovskite Solar Cell Absorber. Appl. Phys. Lett. 2014, 104, 63903.
- deQuilettes, D. W.; Vorpahl, S. M.; Stranks, S. D.; Nagaoka, H.; Eperon, G. E.; Ziffer, M. E.; Snaith, H. J.; Ginger, D. S., Solar Cells. Impact of Microstructure on Local Carrier Lifetime in Perovskite Solar Cells. *Science* **2015**, 348, 683–686.
- 24. Protesescu, L.; Yakunin, S.; Bodnarchuk, M. I.; Krieg, F.; Caputo, R.; Hendon, C. H.; Yang, R. X.; Walsh, A.; Kovalenko, M. V., Nanocrystals of Cesium Lead Halide Perovskites (CsPbX₃, X = Cl, Br, and I): Novel Optoelectronic Materials Showing Bright Emission with Wide Color Gamut. Nano Lett. 2015, 15, 3692–3696.
- Swarnkar, A.; Chulliyil, R.; Ravi, V. K.; Irfanullah, M.; Chowdhury, A.; Nag, A., Colloidal CsPbBr₃ Perovskite Nanocrystals: Luminescence beyond Traditional Quantum Dots. Angew. Chem. Int. Ed. 2015, 54, 15424-15428.
- Seth, S.; Ahmed, T.; De, A.; Samanta, A., Tackling the Defects, Stability, and Photoluminescence of CsPbX₃ Perovskite Nanocrystals. ACS Energy Lett. 2019, 4, 1610-1618.
- 27. Roo, J. D.; Ibáñez, M.; Geiregat, P.; Nedelcu, G.; Walravens, W.; Maes, J.; Martins, J. C.; Driessche, I. V.; Kovalenko, M. V.; Hens, Z., Highly Dynamic Ligand Binding and Light Absorption Coefficient of Cesium Lead Bromide Perovskite Nanocrystals. ACS Nano 2016, 10, 2071-2081.
- Akkerman, Q. A.; Rainò, G.; Kovalenko, M. V.; Manna, L., Genesis, Challenges and Opportunities for Colloidal Lead Halide Perovskite Nanocrystals. Nature Mater 2018, 17, 394-405.
- 29. Huang, H.; Bodnarchuk, M. I.; Kershaw, S. V.; Kovalenko, M. V.; Rogach, A. L., Lead Halide Perovskite Nanocrystals in the Research Spotlight: Stability and Defect-Tolerance. ACS Energy Lett. 2017, 2, 2071–2083.

- Kovalenko, M. V.; Protesescu, L.; Bodnarchuk, M. I., Properties and Potential 30. Optoelectronic Applications of Lead Halide Perovskite Nanocrystals. Science 2017, (358), 745-750.
- 31. Swarnkar, A.; Marshall, A. R.; Sanehira, E. M.; Chernomordik, B. D.; Moore, D. T.; Christians, J. A.; Chakrabarti, T.; Luther, J. M., Quantum Dot-Induced Phase Stabilization of α -CsPbI₃ Perovskite for High-Efficiency Photovoltaics. *Science* **2016**, 354, 92–95.
- Mondal, N.; De, A.; Samanta, A., Achieving Near-Unity Photoluminescence Efficiency for Blue-Violet-Emitting Perovskite Nanocrystals. ACS Energy Lett. 2019, 4, 32-39.
- 33. Ghosh, D.; Welch, E.; Neukirch, A. J.; Zakhidov, A.; Tretiak, S., Polarons in Halide Perovskites: A Perspective. J. Phys. Chem. Lett. 2020, 11, 3271-3286.
- Miyata, K.; Meggiolaro, D.; Trinh, M. T.; Joshi, P. P.; Mosconi, E.; Jones, S. C.; Angelis, F. D.; Zhu, X.-Y., Large Polarons in Lead Halide Perovskites. Science 2017, 3, 1701217.
- 35. Roo, J. D.; Ibańez, M.; Geiregat, P.; Nedelcu, G.; Walravens, W.; Maes, J.; Martins, J. C.; Driessche, I. V.; Kovalenko, M. V.; Hens, Z., Highly Dynamic Ligand Binding and Light Absorption Coefficient of Cesium Lead Bromide Perovskite Nanocrystals. ACS Nano 2016, 2071-2081.
- 36. Bodnarchuk, M. I.; Boehme, S. C.; Brinck, S. t.; Bernasconi, C.; Shynkarenko, Y.; Krieg, F.; Widmer, R.; Aeschlimann, B.; Günther, D.; Kovalenko, M. V., Rationalizing and Controlling the Surface Structure and Electronic Passivation of Cesium Lead Halide Nanocrystals. ACS Energy Lett. 2019, 4, 63-74.
- Ravi, V. K.; Santra, P. K.; Joshi, N.; Chugh, J.; Singh, S. K.; Rensmo, H.; Ghosh, P.; Nag, A., Origin of the Substitution Mechanism for the Binding of Organic Ligands on the Surface of CsPbBr3 Perovskite Nanocubes. J. Phys. Chem. Lett. 2017, 8, 4988-4994.
- 38. Abram, R. A.; Rees, G. J.; Wilson, B. L. H., Heavily Doped Semiconductors and Devices. Adv. Phys. 1978, 27, 799-892.
- Khana, A.; Das, A., Diffusivity-Mobility Relationship for Heavily Doped 39. Semiconductors Exhibiting Band Tail. Phys. B 2010, 405, 817-821.
- Luo, B.; Li, F.; Xu, K.; Guo, Y.; Liu, Y.; Xia, Z.; Zhang, J. Z., B-Site Doped Lead Halide Perovskites: Synthesis, Band Engineering, Photophysics, and Light Emission Applications. J. Mater. Chem. C **2019,** 7, 2781-2808.
- Swarnkar, A.; Mir, W. J.; Nag, A., Can B-Site Doping or Alloying Improve Thermaland Phase-Stability of All-Inorganic CsPbX₃ (X = Cl, Br, I) Perovskites? ACS Energy Lett. **2018** 3, 286-289.
- Zhou, Y.; Chen, J.; Bakr, O. M.; Sun, H.-T., Metal-Doped Lead Halide Perovskites: 42. Synthesis, Properties, and Optoelectronic Applications. Chem. Mater. 2018, 30, 6589-6613.
- Das, S.; De, A.; Samanta., A., Ambient Condition Mg²⁺ Doping Producing Highly 43. Luminescent Green- and Violet-Emitting Perovskite Nanocrystals with Reduced Toxicity and Enhanced Stability. J. Phys. Chem. Lett. 2020, 11, 1178-1188.

- 44. Yong, Z.-J.; Guo, S.-Q.; Ma, J.-P.; Zhang, J.-Y.; Li, Z.-Y.; Chen, Y.-M.; Zhang, B.-B.; Zhou, Y.; Shu, J.; Gu, J.-L.; al., e., Doping-Enhanced Short-Range Order of Perovskite Nanocrystals for Near-Unity Violet Luminescence Quantum Yield. *J. Am. Chem. Soc.* **2018**, 140, 9942–9951.
- 45. Dutta, A.; Pradhan, N., Phase-Stable Red-Emitting CsPbI₃ Nanocrystals: Successes and Challenges. *ACS Energy Lett.* **2019**, 4, 709–719.
- 46. Hu, Y.; Bai, F.; Liu, X.; Ji, Q.; Miao, X.; Qiu, T.; Zhang, S., Bismuth Incorporation Stabilized α -CsPbI $_3$ for Fully Inorganic Perovskite Solar Cells. *ACS Energy Lett.* **2017**, 2, 2219–2227.
- 47. Pan, G.; Bai, X.; Yang, D.; Chen, X.; Jing, P.; Qu, S.; Zhang, L.; Zhou, D.; Zhu, J.; Xu, W.; Dong, B.; Song, H., Doping Lanthanide into Perovskite Nanocrystals: Highly Improved and Expanded Optical Properties. *Nano Lett.* **2017**, 17, 8005–8011.
- 48. De, A.; Mondal, N.; Samanta, A., Luminescence Tuning and Exciton Dynamics of Mn-doped CsPbCl₃ Nanocrystals. *Nanoscale* **2017**, 9, 16722-16727.
- 49. Begum, R.; Parida, M. R.; Abdelhady, A. L.; Murali, B.; Alyami, N. M.; Ahmed, G. H.; Hedhili, M. N.; Bakr, O. M.; Mohammed, O. F., Engineering Interfacial Charge Transfer in CsPbBr₃ Perovskite Nanocrystals by Heterovalent Doping. *J. Am. Chem. Soc.* **2017**, 139, 731-737.
- 50. Abdelhady, A. L.; Saidaminov, M. I.; Murali, B.; Adinolfi, V.; Voznyy, O.; Katsiev, K.; Alarousu, E.; Comin, R.; Dursun, I.; Sinatra, L.; Sargent, E. H.; Mohammed, O. F.; Bakr, O. M., Heterovalent Dopant Incorporation for Bandgap and Type Engineering of Perovskite Crystals. *J. Phys. Chem. Lett.* **2016**, *7*, 295-301.
- 51. Nirmal, M.; Dabbousi, B. O.; Bawendi, M. G.; Macklin, J. J.; Trautman, J. K.; Harris, T. D.; Brus, L. E., Fluorescence intermittency in single cadmium selenide nanocrystals. *Nature* **1996**, 383, 802–804.
- 52. Cordones, A. A.; Leone, S. R., Mechanisms for Charge Trapping in Single Semiconductor Nanocrystals Probed by Fluorescence Blinking. *Chem. Soc. Rev.* **2013**, 42, 3209-3221.
- 53. Efros, A. L.; Nesbitt, D. J., Origin and Control of Blinking in Quantum Dots. *Nat. Nanotechnol.* **2016**, 11, 661-671.
- 54. Jin, S.; Hsiang, J.-C.; Zhu, H.; Song, N.; Dicksonb, R. M.; Lian, T., Correlated Single Quantum Dot Blinking and Interfacial Electron Transfer Dynamics. *Chem. Sci.* **2010**, 1, 519–526.
- 55. Seth, S.; Ahmed, T.; Samanta, A., Photoluminescence Flickering and Blinking of Single CsPbBr3 Perovskite Nanocrystals: Revealing Explicit Carrier Recombination Dynamics. *J. Phys. Chem. Lett.* **2018**, 9, 7007–7014.
- 56. Park, Y. S.; Guo, S.; Makarov, N. S.; Klimov, V. I., Room Temperature Single-Photon Emission from Individual Perovskite Quantum Dots. *ACS Nano* **2015**, 9, 10386-10393.
- 57. Yuan, G.; Gómez, D. E.; Kirkwood, N.; Boldt, K.; Mulvaney, P., Two Mechanisms Determine Quantum Dot Blinking. *ACS Nano* **2018**, 12, 3397–3405.

- 58. Galland, C.; Ghosh, Y.; Steinbruck, A.; Sykora, M.; Hollingsworth, J. A.; Klimov, V. I.; Htoon, H., Two Types of Luminescence Blinking Revealed by Spectroelectrochemistry of Single Quantum Dots. *Nature* **2011**, 479, 203-207.
- 59. Frantsuzov, P. A.; Volkan-Kacso, S.; Janko, B., Model of Fluorescence Intermittency of Single Colloidal Semiconductor Quantum Dots Using Multiple Recombination Centers. *Phys. Rev. Lett.* **2009**, 103, 207402.
- 60. Busov, V. K.; Frantsuzov, P. A., Models of Semiconductor Quantum Dots Blinking based on Spectral Diffusion. *Optics and Spectroscopy* **2019**, 126, 70-82.
- 61. Frantsuzov, P.; Kuno, M.; Jánko, B.; Marcus, R. A., Universal Emission Intermittency in Quantum dots, Nanorods, and Nanowires. *Nature Physics* **2008**, 4.
- 62. Frantsuzov, P. A.; Marcus, R. A., Explanation of Quantum Dot Blinking without the Long-Lived Trap Hypothesis. *Phys. Rev. B: Condens. Matter Mater. Phys.* **2005,** 72, 155321.
- 63. Park, Y.-S.; Lim, J.; Makarov, N. S.; Klimov, V. I., Effect of Interfacial Alloying versus "Volume Scaling" on Auger Recombination in Compositionally Graded Semiconductor Quantum Dots. *Nano Lett.* **2017**, 17, 5607–5613.
- 64. Rosen, S.; Schwartz, O.; Oron, D., Transient Fluorescence of the Off State in Blinking CdSe/CdS/ZnS Semiconductor Nanocrystals Is Not Governed by Auger Recombination. *Phys Rev Lett.* **2010**, 104, 157404.
- 65. Tenne, R.; Teitelboim, A.; Rukenstein, P.; Dyshel, M.; Mokari, T.; Oron, D., Studying Quantum Dot Blinking through the Addition of an Engineered Inorganic Hole Trap. *ACS Nano* **2013**, 7, 5084–5090.
- 66. Park, Y. S.; Bae, W. K.; Pietryga, J. M.; Klimov, V. I., Auger Recombination of Biexcitons and Negative and Positive Trions in Individual Quantum Dots. *ACS Nano* **2014**, 8, 7288-7296.
- 67. Yarita, N.; Tahara, H.; Saruyama, M.; Kawawaki, T.; Sato, R.; Teranishi, T.; Kanemitsu, Y., Impact of Postsynthetic Surface Modification on Photoluminescence Intermittency in Formamidinium Lead Bromide Perovskite Nanocrystals. *J. Phys. Chem. Lett.* **2017**, 8, 6041–6047.
- 68. Trinh, C. T.; Minh, D. N.; Ahn, K. J.; Kang, Y.; Lee, K.-G., Verification of Type-A and Type-B-HC Blinking Mechanisms of Organic–Inorganic Formamidinium Lead Halide Perovskite Quantum Dots by FLID Measurements. *Sci Rep* **2020**, 10, 2172.
- 69. Kim, T.; Jung, S. I.; Ham, S.; Chung, H.; Kim, D., Elucidation of Photoluminescence Blinking Mechanism and Multiexciton Dynamics in Hybrid Organic–Inorganic Perovskite Quantum Dots. *Small* **2019**, 15, 1900355.
- 70. Yarita, N.; Tahara, H.; Ihara, T.; Kawawaki, T.; Sato, R.; Saruyama, M.; Teranishi, T.; Kanemitsu, Y., Dynamics of Charged Excitons and Biexcitons in CsPbBr₃ Perovskite Nanocrystals Revealed by Femtosecond Transient-Absorption and Single-Dot Luminescence Spectroscopy. *J. Phys. Chem. Lett.* **2017**, 8, 1413-1418.
- 71. Hu, F.; Zhang, H.; Sun, C.; Yin, C.; Lv, B.; Zhang, C.; Yu, W. W.; Wang, X.; Zhang, Y.; Xiao, M., Superior Optical Properties of Perovskite Nanocrystals as Single Photon Emitters. *ACs Nano* **2015**, 9, 12410–12416.

- 72. Yarita, N.; Aharen, T.; Tahara, H.; Saruyama, M.; Kawawaki, T.; Sato, R.; Teranishi, T.; Kanemitsu, Y., Observation of Positive and Negative Trions in Organic-Inorganic Hybrid Perovskite Nanocrystals. *Phys. Rev. Mater.* **2018**, *2*, 116003.
- 73. Zhang, A.; Bian, Y.; Wang, J.; Chen, K.; Dong, C.; Ren, J., Suppressed Blinking Behavior of CdSe/CdS QDs by Polymer Coating. *Nanoscale* **2016**, 8, 5006-5014.
- 74. Li, B.; Zhang, G.; ZaoWang; Li, Z.; RuiyunChen; ChengbingQin; YanGao; LiantuanXiao; Jia, S., Suppressing the Fluorescence Blinking of Single Quantum Dots Encased in N-type Semiconductor Nanoparticles. *Sci Rep.* **2016**, 6, 32662.
- 75. Tang, X.; Yang, J.; Li, S.; Liu, Z.; Hu, Z.; Hao, J.; Du, J.; Leng, Y.; Qin, H.; Lin, X.; Lin, Y.; Tian, Y.; Zhou, M.; Xiong, Q., Single Halide Perovskite/Semiconductor Core/Shell Quantum Dots with Ultrastability and Nonblinking Properties. *Adv. Sci.* **2019**, 6, 1900412.
- 76. Mahler, B.; Spinicelli, P.; Buil, S.; Quelin, X.; Hermier, J.-P.; Dubertret, B., Towards Non-Blinking Quantum Dots: The Effect of Thick Shell. *Proc. of SPIE* **2009**, 7189, 718903-9.
- 77. Avellini, T.; Lincheneau, C.; Vera, F.; Silvi, S.; Credi, A., Hybrids of Semiconductor Quantum Dot and Molecular Species for Photoinduced Functions. *Coord. Chem. Rev.* **2014**, 263-264, 151-160.
- 78. De, A.; Mondal, N.; Samanta, A., Hole Transfer Dynamics from Photoexcited Cesium Lead Halide Perovskite Nanocrystals: 1-Aminopyrene as Hole Acceptor. *J. Phys. Chem. C* **2018**, 122, 13617–13623.
- 79. Kobosko, S. M.; DuBose, J. T.; Kamat, P. V., Perovskite Photocatalysis. Methyl Viologen Induces Unusually Long-Lived Charge Carrier Separation in CsPbBr₃ Nanocrystals. *ACS Energy Lett.* **2020**, 5, 221–223.
- 80. DuBose, J. T.; Kamat, P. V., Surface Chemistry Matters. How Ligands Influence Excited State Interactions between CsPbBr₃ and Methyl Viologen. *J. Phys. Chem. C* **2020**, 124, 12990–12998.
- 81. Sarkar, S.; Ravi, V. K.; Banerjee, S.; Yettapu, G. R.; Ganesh B. Markad; Nag, A.; Mandal, P., Terahertz Spectroscopic Probe of Hot Electron and Hole Transfer from Colloidal CsPbBr₃ Perovskite Nanocrystals. *Nano Lett.* **2017**, 17, 5402–5407.
- 82. Wu, K.; Liang, G.; Shang, Q.; Ren, Y.; Kong, D.; Lian, T., Ultrafast Interfacial Electron and Hole Transfer from CsPbBr₃ Perovskite Quantum Dots. *J. Am. Chem. Soc.* **2015,** 137, 12792–12795.
- 83. Song, N.; Zhu, H.; Jin, S.; Lian, T., Hole Transfer from Single Quantum Dots. *ACS Nano* **2011,** 5, 8750–8759.
- 84. Issac, A.; Jin, S.; Lian, T., Intermittent Electron Transfer Activity From Single CdSe/ZnS Quantum Dots. *J. Am. Chem. Soc.* **2008**, 130, 11280–11281.

CHAPTER 2

Materials, Instrumentation and Methods

Overview

In this chapter, details of preparation of different materials, their characterization, instrumental techniques and methodologies used for the studies have been discussed. Details of the chemicals used for the work have been enlisted here. Details are on the preparation of different perovskite nanocrystals (NCs) and doped NCs are provided. Basic principles of single molecule fluorescence spectroscopy measurements and methodologies for the measurements including sample preparation have been discussed in detail. The instrumental details of time-resolved confocal fluorescence microscope have been described, especially for the fluorescence correlation spectroscopy and photoluminescence (PL) time-traces measurements. The methods used for analysis of data for single molecule spectroscopy techniques are provided. The femtosecond transient absorption and fluorescence up-conversion setups are outlined. The instrumental details time-correlated single photon counting, spectrofluorimeter and UV-Vis spectrophotometer are provided. Information on various instruments used for characterization of materials is also provided along with the details of photoluminescence quantum yield (PLQY) measurement.

2.1. Materials

Caesium carbonate (99.9%), octadecene (ODE, 90%), oleic acid (OA, 90%), oleylamine (OLA, 70%), trioctylphosphine (TOP, 97 %), lead chloride (99.999%), lead bromide (99.999%), lead iodide (PbI₂, 99%), toluene (99.8%, anhydrous), hexane (>99%, anhydrous) ammonium tetrafluoroborate (99.99%), sodium tetrafluoroborate (99.99%), bismuth bromide (98%), methyl acetate (Me-OAc, 99.5%, anhydrous), formamidinium acetate (FA-OAc, 99%), lead oxide (99%), N-bromosuccinimide (NBS, 99%) were purchased from Sigma-Aldrich. Hexane (HPLC grade) was purchased from Finar. All the chemicals were used without any purification.

2.2. Synthesis of perovskite materials

2.2.1. CsPbX₃ nanocrystals

 $CsPbX_3$ (X = Cl, Br, I) perovskite NCs were synthesized following a reported procedure, ¹ hot injection method at temperature ranges between 150 °C and 180 °C. First caesiumoleate (Cs-oleate) was prepared by mixing Cs₂CO₃ (0.10175 g) and OA (0.3125 mL) in ODE (5 mL) taken in a 50 mL double-necked round-bottom (RB) flask and kept in vacuum for 1 hr at 120 °C. Later, for complete solubilization of the solid material, the temperature was raised to 160 °C which led to the formation of a clear solution of Csoleate. This mixture was kept at 100 °C under N₂ atmosphere (as Cs-oleate precipitates out of ODE at room temperature) for its further use. ODE (5 mL), PbX₂ (0.188 mmol), OA (0.5 mL) and OLA (0.5 mL) were loaded in a 50 mL double-necked RB flask and the mixture was heated under vacuum at 120 °C for at least 1 hr. After complete solubilization of the PbX₂ salt, the mixture was transferred into N₂ atmosphere. The temperature was raised up to 170 °C and kept for 20 minutes followed by injection of preprepared Cs-oleate solution (0.4 mL). The reaction mixture was cooled in an ice-water bath after 5 sec. For chloride containing perovskite NCs, synthesis was carried out at higher temperature (180 °C) and 1 mL of TOP was used additionally for complete solubilization of PbCl₂. The obtained crude solution was centrifuged at 8000 rpm for 10

min. The precipitated NCs were dispersed in hexane, toluene or ODE (for different experimental purpose) after washing with the same solvent.

2.2.2. FAPbBr₃ nanocrystals

FAPbBr₃ NCs were synthesized following a reported procedure.² The 1st step involved preparation of FA-oleate and in the 2nd step, the NCs were prepared. For the preparation of FA-oleate, FA-acetate (2.5 mmol, 260 mg) was loaded into a two-necked 50 mL RB flask along with 10 mL oleic acid. It was then kept at 120 °C in N₂ atmosphere for 30 min to obtain a clear solution and was kept at 100 °C before its use. Next, 0.2 mmol of PbO (0.044 g) and 0.6 mmol of NBS (0.108 g) were taken into a double-necked 50 mL RB flask along with ODE (5 mL). The reaction mixture was kept under vacuum for 15 min at 120 °C and then transferred in N₂ atmosphere. OA (1 mL) and OLA (1 mL) were injected into the reaction mixture for complete solubilization of the reaction mixture. Then the temperature was increased to 200 °C and preheated FA-oleate solution (0.5 mL) was swiftly injected into the reaction mixture. The reaction mixture was cooled in an icewater bath after 15 sec. Me-OAc (8 mL) was added to the crude solution and centrifuged for 5 min at 7000 rpm. Finally, the precipitate was dispersed in hexane or ODE, which was again centrifuged at 12000 rpm for 10 min and the supernatant solution was stored for further studies.

2.2.3. Bi-doped CsPbBr₃ nanocrystals

Bi-doped CsPbBr₃ NCs were prepared following a reported procedure with few modifications.³ Cs-oleate was prepared by following a method described in section 2.2.1. Before injection, Cs-oleate was kept at 100 °C (as Cs-oleate precipitates out of ODE at room temperature) under N₂ atmosphere. In another 50 mL RB flask, PbBr₂ (0.188 mmol), BiBr₃ (2%, 5%, 10% or 20 mole % of PbBr₂), ODE (5 mL), OA (0.5 mL) and OLA (0.5 mL) were mixed and heated at 120 °C under vacuum for 1 hr. The mixture was transferred into N₂ atmosphere after complete solubilization of PbBr₂ and BiBr₃. Then the temperature was raised to 170 °C and 0.4 mL pre-prepared Cs-oleate solution was injected into it. The reaction mixture was cooled in an ice-water bath after 10 sec. Then

Me-OAc was added to the reaction mixture in 1:2 (v/v) ratio (reaction mixture: Me-OAc) and then centrifuged at 6000 rpm for 10 min. The precipitate was dispersed in ODE or hexane. These synthesized NCs were subsequently treated with a moderate mixture of OA (0.1 mL) and OLA (0.1 mL).

2.3. Methods and instrumentation

2.3.1. Single molecule fluorescence spectroscopy

Single molecule spectroscopy (SMS) is an advanced and constantly growing technique to investigate the properties of single molecule and its applications continues to span over several fields, from biology to physics to chemistry. In case of ensemble measurements, we get average value of a parameter for a large number of molecules. On the contrary, SMS completely eliminates the ensemble averaging and allows construction of the actual distribution of values for an experimental parameter. This is important for systems which are heterogeneous and reveals information about the "nanoenvironments". Along with this, for the SMS techniques, fluctuation of fluorescence intensity with time is observed for a single molecule with a constant irradiation of light due to change in its local environment or photophysical parameters. Such fluctuations of fluorescence are important to reveal unprecedented insight into behavior of molecules which is generally masked by ensemble averaging. In single molecule fluorescence spectroscopy to probe the molecule, a light beam is used for an electronic transition and the emitted photon (fluorescence) from the single molecule is detected.⁴ To probe a single molecule in mobilized or immobilized state of sample, two points are important. Firstly, assuring that single molecule is present in the probe optical volume and secondly, a good enough single to noise ratio (S/N) to detect a single molecule and to accomplish this combination of small probe volume (~fL) and ultralow concentration of interested molecules (~ nMpM) are needed. In this context, confocal fluorescence microscope (CFM) coupled with avalanche photodiode (APD) is used widely.

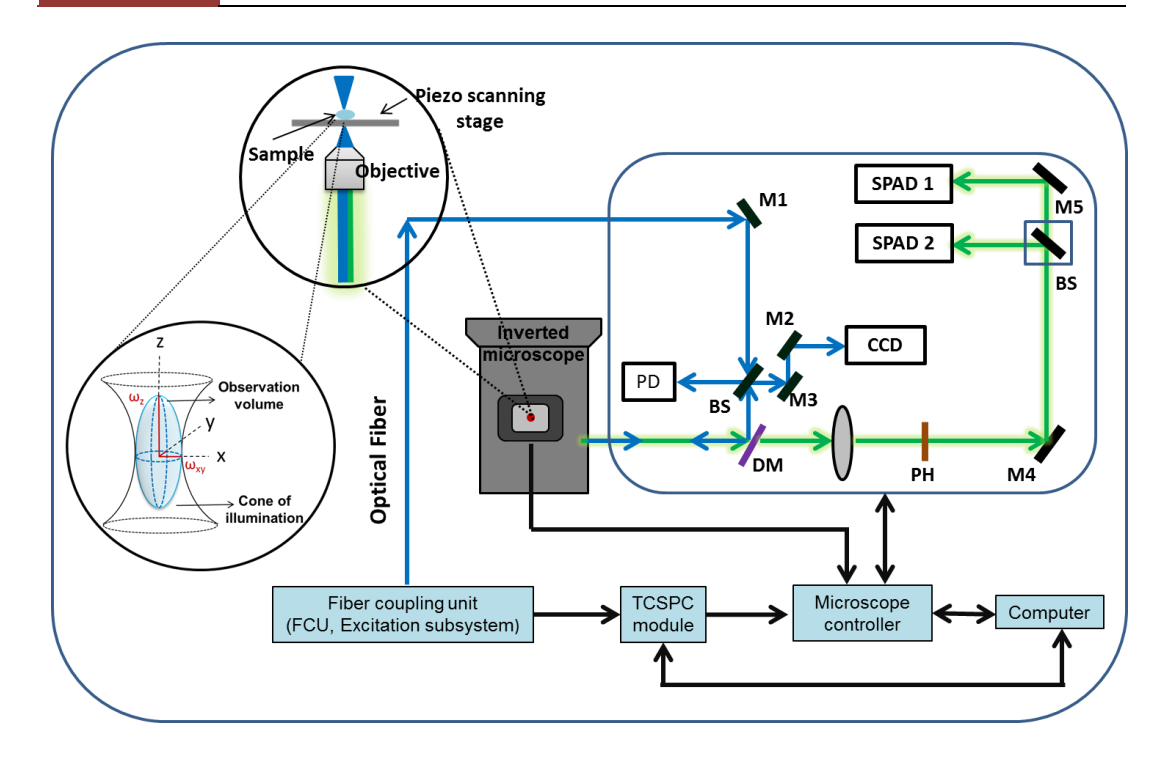
2.3.2 Time-resolved confocal fluorescence microscope

The resolution of optical microscope is given by Abbe's law

$$d = \lambda / 2NA \tag{2.1}$$

where λ is the wavelength of the light used for excitation, NA is the numerical aperture of the lens, defined as $NA = n \sin \theta$, for a medium with refractive index 'n' and ' θ ' is maximum half angle of the cone of light entering or leaving the working lens. Now in conventional wide field microscope, the whole sample is excited at a time which results into unwanted out-of-focus background signals. To avoid this limitation in CFM, point illumination is used by placing a pinhole at the conjugate focal plane of the excitation focus before the detector to eliminate the unfocused signal and improve the resolution. The observation volume defined by the combination of objective and the pinhole is ellipsoidal (shown in inset of Scheme 2.1). A schematic diagram of a CFM is shown in Scheme 2.1.

For our measurements, we have used time resolved CFM of model MicroTime 200 from PicoQuant, which consists of an inverted microscope (Olympus IX71) that forms the microscope body. For the excitation of samples, 405 nm and 485 nm pulsed diode laser (FWHM of 176 ps and 144 ps, respectively) were used. The tunability of repetition rates of the lasers was ranges between 1-80 MHz. The output of the diode laser was coupled to the main optical unit (MOU) by polarization maintained single mode optical fiber. In the MOU, the excitation light was directed to the microscope body through dichroic mirror and was focused to the sample droplet placed on the coverslip through the water immersion objective (UPlansApo NA 1.2, 60X). A photo-diode (PD) was used to record the excitation power. The back-scattered light was directed to a charged couple device (CCD) through a beam splitter to adjust the focus and light distribution. The same objective was



Scheme 2.1: Schematic diagram of time-resolved confocal fluorescence microscope setup. PD = photodiode, DM = dichroic mirror, PH = pinhole, BS = beam splitter, $M_i = mirror$ and inset shows ellipsoidal observation volume.

used to collect the emission from the sample and was passed through a dichroic mirror followed by 430 and 510 nm long-pass filter for 405 and 485 nm laser light, respectively to remove the excitation light. A 50 μ m pinhole was placed before detectors to assure the collection of tightly focused signal which was recollimated and directed to the single photon avalanche photodiode (SPAD) detector. A single or double SPAD detector was used to collect photons. A (50/50) beam splitter was used to direct the light to the two SPADs. Maximum area of 80 μ m \times 80 μ m was scanned employing raster scan. All the data acquisitions were performed using a TCSPC module (PicoHarp 300) in time-tagged time-resolved (TTTR) mode. In this TCSPC mode the time difference between the excitation to the detection of the photon from the sample is recorded using the start-stop technique, described latter. Along with this, the time-tagged mode events are also recorded in the real time, *i. e.*, arrival of each photon from the start of the experiment. We

employed this CFM with TTTR data acquisition mode to study the fluorescence properties and photo-excited carrier recombination processes of single perovskite NC. For that we have used fluorescence correlation spectroscopy (FCS) measurements of freely diffusing NCs and also studied the PL intermittency in the immobilized state of NCs using PL intensity time traces.

2.3.2.1 Fluorescence correlation spectroscopy measurement

FCS is based on fluctuation of fluorescence intensity with time of freely diffusing molecules through the observation volume. To get a sharp fluctuation there must be present single or few molecules in the tiny observation volume, where CFM is suitable for this purpose (Scheme 2.4). For nM concentration of the sample and ~ 1 fL observation volume, the average number of fluorophores present in this volume is 0.6. As fluorophores diffuses randomly in and out of the volume and the number of fluorophores in the volume is described by the Poisson distribution.

In FCS measurement, an autocorrelation function is generated from the fluctuation of fluorescence intensity of fluorophores during passing through the observation volume. It contains information related to all the dynamical processes which lead to fluorescence intensity fluctuation. The autocorrelation function is defined by the following equation^{5, 6}

$$G(\tau) = <\delta F(t)\delta F(t+\tau) > / < F(t) >^2$$
(2.2)

where $\langle F(t) \rangle$ is the average fluorescence intensity. The fluctuations of fluorescence intensity from the average fluorescence intensity at time t and $(t+\tau)$ are $\delta F(t)$ and $\delta F(t+\tau)$, respectively, and are given by

$$\delta F(t) = F(t) - \langle F(t) \rangle \text{ and } \delta F(t+\tau) = F(t+\tau) - \langle F(t) \rangle$$
 (2.3)

At different lag times (τ) , the self-similarity of fluorescence intensity time trace with itself is measured in FCS, where $G(\tau)$ gives the probability of finding photon at time $(t+\tau)$ for a fluorescence photon detection event at time t,.

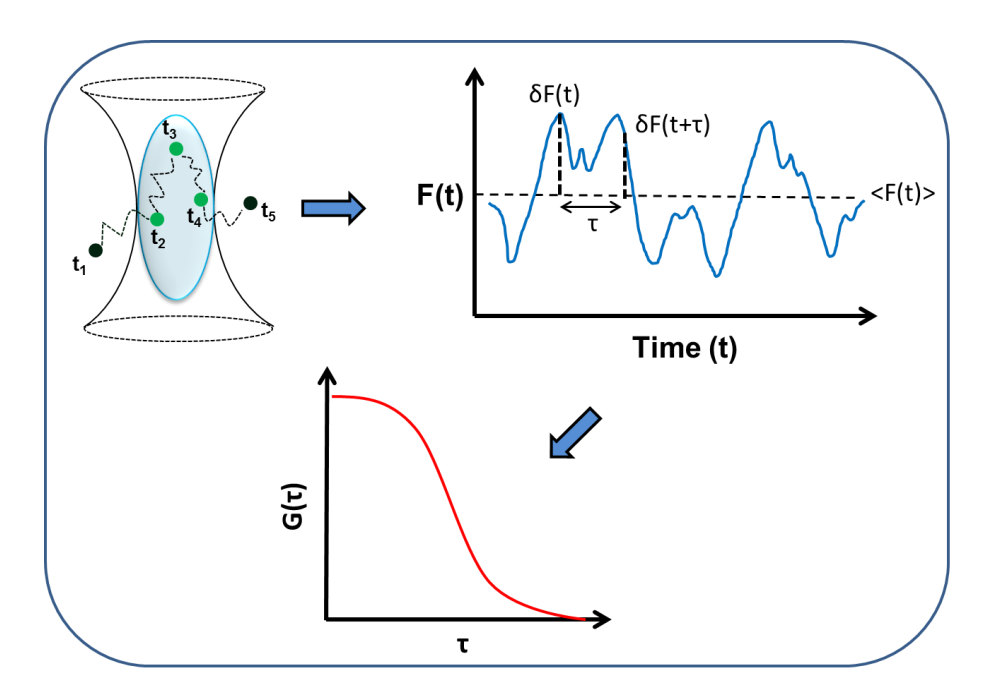
The correlation function for fluctuation of fluorescence only due to 3-dimensional diffusion of fluorophores in and out of observation volume is given by

$$G(\tau) = \frac{1}{N} \left(1 + \frac{\tau}{\tau_D} \right)^{-1} \left[1 + \frac{\tau}{\kappa^2 \tau_D} \right]^{-\frac{1}{2}}$$
(2.4)

where, τ_D is the diffusion time, N is the average number of fluorophore in the observation volume, κ (= ω_Z/ω_{xy}) is the structure parameter of the observation volume; ω_Z and ω_{xy} are axial and lateral radii, respectively. The diffusion coefficient (D) of the fluorophore can be derived as

$$D = \frac{\omega_{xy}^2}{4\tau_D} \tag{2.5}$$

The fluorophores can also undergo fast photophysical process including transitions of fluorescence between bright and dark (non-emissive) state during the passing time through the observation volume. Several factors that can cause rapid fluctuation of



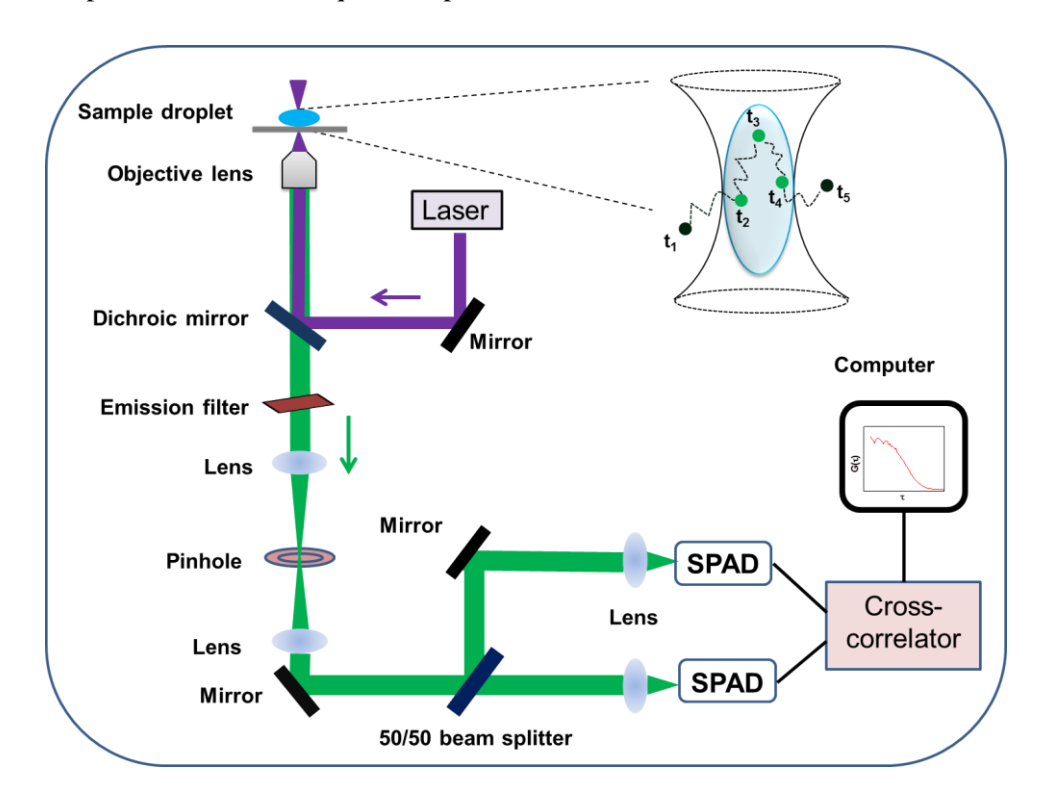
Scheme 2.2: Basic working principle of FCS measurements. Fluctuations of fluorescence intensity due to random diffusion of fluorophore in and out of the observation volume.

Chapter 2

fluorescence like intersystem crossing in the fluorophores, conformational change of molecules, trapping of charge carriers in semiconductors, etc. In these cases, the correlation function can be expressed as

$$G_{total}(\tau) = G_{diffusion}(\tau)G_{faster}(\tau) \tag{2.6}$$

The form of $G_{faster}(\tau)$ depends on the nature of the fast process. However, in case of perovskite NCs, the fast fluctuation of fluorescence can arise due to trapping of photogenerated charge carriers. The appropriate form of $G_{total}(\tau)$ will be discussed in the relevant portions of the subsequent chapters.



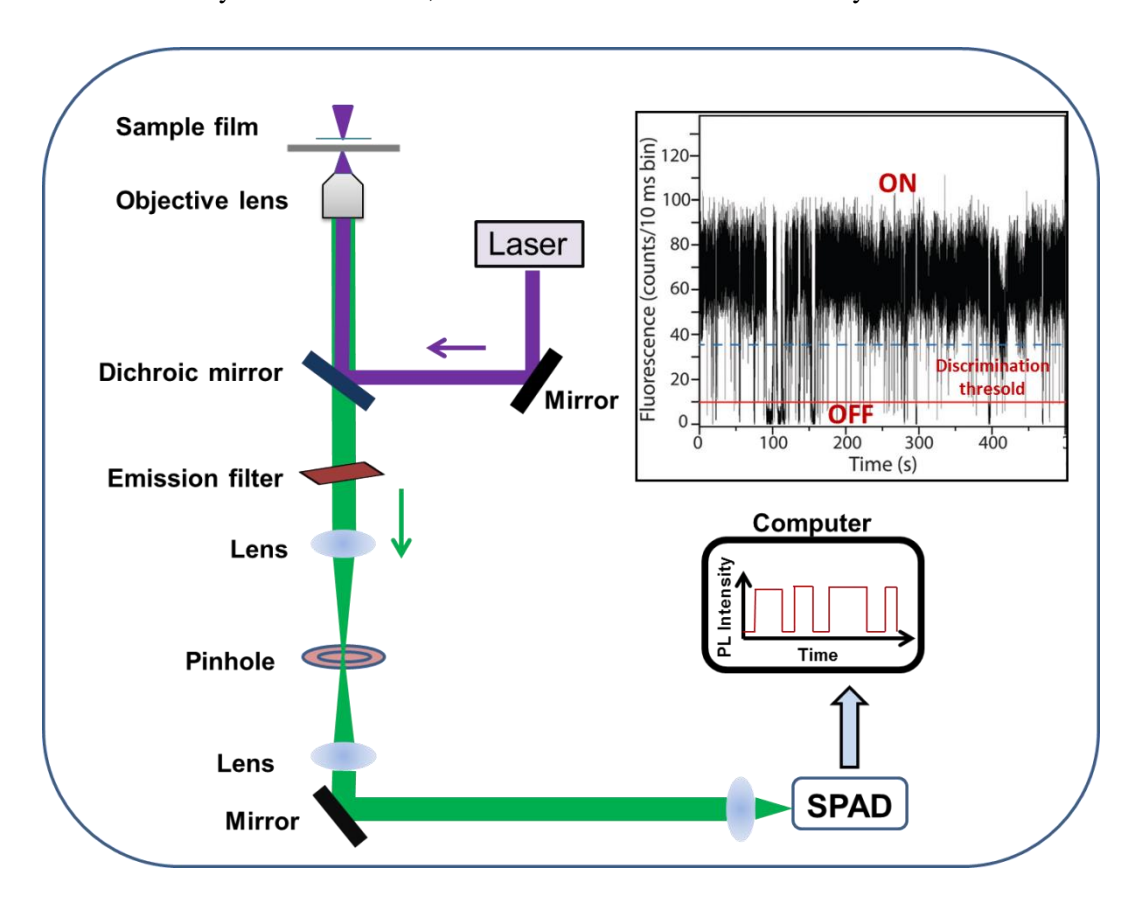
Scheme 2.3: Schematic diagram of CFM for FCS measurement, which shows crosscorrelation of signals obtained from two detectors.

All FCS measurements were performed at the room temperature using the CFM in the TTTR mode; details description of the CFM set-up is already discussed (Scheme 2.1), where a basic configuration is shown is Scheme 2.3. The measurements were performed Chapter 2

using two detectors to remove the artifacts introduced by detectors. A 50/50 beam splitter was placed before the detectors to direct the fluorescence signal to the two SPAD detectors which were then cross-correlated. All data were analyzed using the SymphoTime software.

2.3.2.2. Photoluminescence intensity time-trace

PL intensity time trace is generated in real time scale by constant excitation of an immobilized single fluorophore to study PL characteristics of that single fluorophore. In most of the single fluorophores, a random fluctuation of PL intensity is observed over several intensity levels with time, which is termed as PL intermittency or



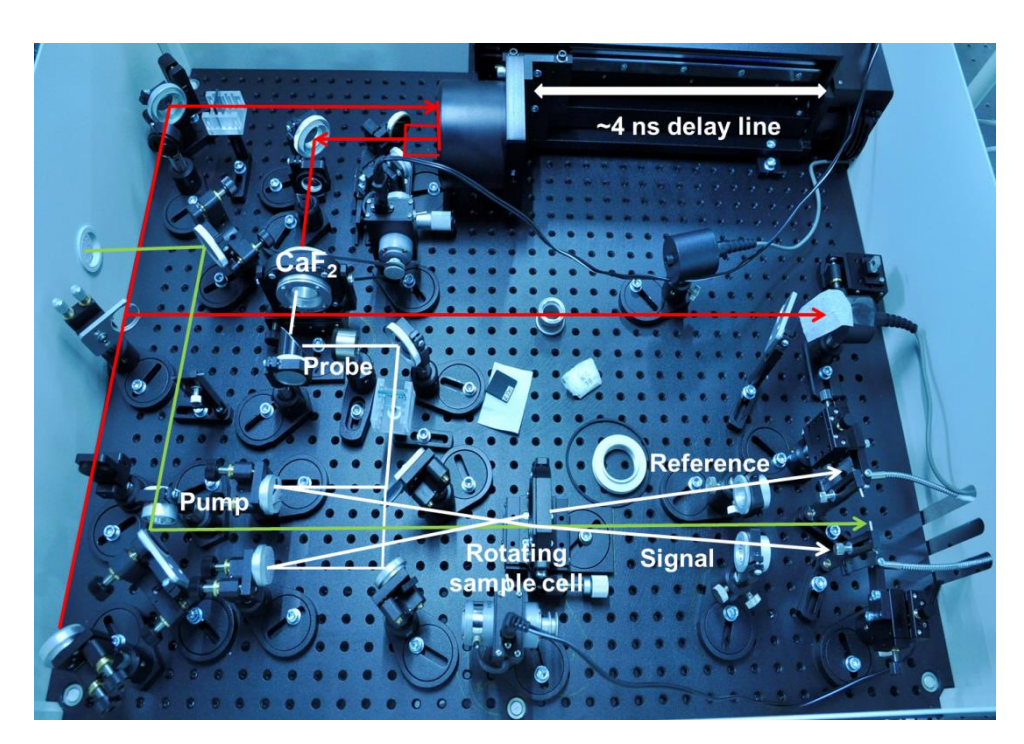
Scheme 2.4: Schematic diagram of CFM for PL blinking measurement in the immobilized states of fluorophores, shows signal is obtained from a single detector.

blinking. The high intensity levels are called as ON states and the lowest intensity levels close to the background are called as OFF states (shown in Scheme 2.4). A threshold is set to separate the ON and OFF states. To increase the signal to noise ratio and separate the ON and OFF states properly, photon arrival times are averaged over time and this bin time was used 10-20 ms for our study. To understand the mechanism of blinking, the intensity levels are separated into different regions. Analysis of lifetime of those states gives information about the possible recombination processes of the photoexcited fluorophores. When there are several intensity levels, setting a threshold becomes difficult to separate the ON and OFF states. Fluorescence lifetime intensity distribution pattern provides important information on the processes responsible for the blinking. In our study, all the measurements were performed by using CFM (Scheme 2.4) in the TTTR mode. The fluorescence signal was directed to single SPAD for detection. To get a film with well separated distribution of the fluorophores, a very dilute sample solution (pM) was drop casted on the coverslip by adding non-interacting polymers like polymethyl methacrylate (PMMA). All the measurements were performed keeping low excitation intensity of laser to avoid formation of multiexcitons. For the analysis of data SymphoTime software was used. Details of analysis will be discussed in the relevant portions of the subsequent chapters.

2.3.3. Femtosecond transient absorption (TA) measurement

TA measurement is used to measure those processes occurring in the fs-ps time region for both fluorescent and non-fluorescent sample and fs pulsed lasers are employed for the excitation of sample. In this technique, the sample is excited to higher energy states by optical pump and the fate of the excited (transient) sample is investigated by using a broad band probe at delayed time with respect to the pump. This technique is also referred as pump-probe method.^{8, 9}

The femtosecond setup we used (Shown in Scheme 2.5) consist of a mode-locked Ti:sapphire laser as oscillator (Mai-Tai, Spectra Physics) producing < 100 fs pulses centred at 800 nm (30 nJ, 80 MHz). The pulse was directed to a regenerative amplifier (Spitfire Ace, Spectra Physics), and was pumped by frequency-doubled output of Nd:YLF laser at 527 nm (Empower, Spectra Physics) to produce amplified pulse of frequency 1 KHz and pulse energy ~ 4.2 mJ (800 nm, < 100 fs). The amplified laser was divided into two parts. The intensity portion (~ 3.2 mJ) was directed to an optical parametric amplifier (TOPAS-Prime, Spectra Physics) to obtain the excitation pump beam (wavelength tenability 290-2600 nm) at 400 nm for our study. The pump beam was guided to the transient absorption spectrometer (ExciPro, CDP systems) to excite the sample and to modulate it a mechanical chopper. The remaining portion (~ 1 mJ) was passed through a step motor controlled optical delay line (~ 4 ns) and directed to CaF₂ crystal to generate white probe light (320-900 nm). The probe was divided into two beams, one used as



Scheme 2.5: Layout of optical components of the spectrometer of the pump-probe setup used for our study (adapted from ref 9).

Probing beam and another as reference beam and focused on a rotating quartz sample cell (1 mm path length). For better overlap, a collimated geometry was maintained between

pump and probe beam. The transmitted probe and reference beam were directed to a polychromator and detected by multichannel photodiode array and processed to record difference in absorbance (ΔA) in presence and absence of pump beam.⁸ To avoid any undesired non-linear processes, all our measurements were performed at low pump fluence (2 μJ cm⁻²). All data were analysed using ExciPro (CDP system) and Igor Pro software. The differential absorption is given by

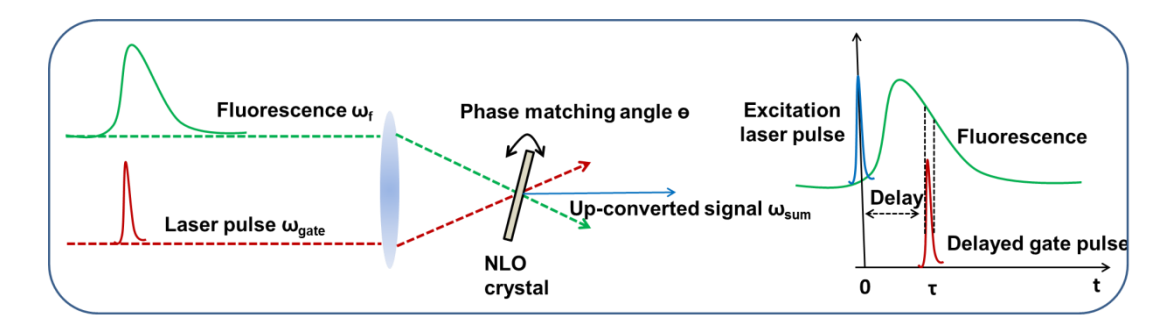
$$\Delta A(\lambda, t) = A_{pump\ on}(\lambda, t) - A_{pump\ off}(\lambda) = A_{exc}(\lambda, t) - A_{ground}(\lambda) \quad (2.7)$$

$$\Delta A(\lambda, t) = \log \left(\frac{I_{0,exct}(\lambda)}{I_{exct}(\lambda, t)} \right) - \log \left(\frac{I_{0,ground}(\lambda)}{I_{ground}(\lambda)} \right) = \log \left(\frac{I_{ground}(\lambda)}{I_{exct}(\lambda, t)} \right)$$
(2.8)

Where A_{exc} and A_{ground} are the absorbance of the excited and ground state species respectively and I_0 and I are intensities of incident and transmitted probe light. To avoid multiphoton processes, the intensity of probe light was kept low compared to the pump. The main processes which may contribute to TA spectrum for molecular systems are ground state bleach (GSB), excited state absorption (ESA) and stimulated emission (SE). The pump excites fraction of molecules to the excited states and hence when probe comes it experiences less number of molecules in the ground state than the unexcited sample for pump-off condition (more transmitted intensity). As a result ΔA appears as negative signal in the spectral region of ground state absorption. The photoexcited molecules (pump-on) can further be excited to the higher energy state or generate new transient species. In that case there is absorption of probe light at those wavelength and transmits less light, $I_{ground} > I_{exct}$. Consequently, ΔA appears as positive. Lastly, the probe pulse brings back those photo excited sample (pump on) to ground state through stimulated emission, which results additional photons and $I_{ground} < I_{exct}$, results negative ΔA signal at the spectral region corresponding to the emission.

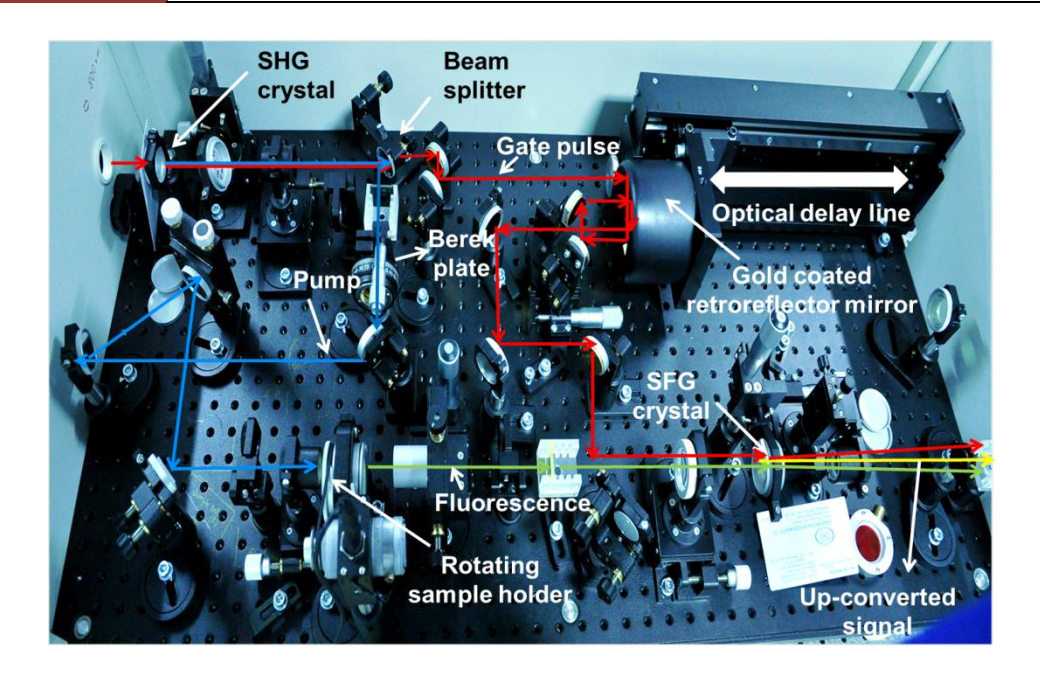
2.3.4. Femtosecond PL up-conversion setup

PL up-conversion (UC) provides high temporal resolution for PL decay of fluorescent samples. In this technique, the PL is up-converted when it is mixed with a delayed probe (or gate) beam in a sum frequency crystal (shown in Scheme 2.6). For efficient UC, phase matching of both the beam is necessary and the temporal resolution is limited by the gate pulse width. The up-converted signal is recorded with respect to the excitation pulse at different delay time of the gate pulse.



Scheme 2.6: Basic principle for the generation of up-converted signal and basic working principle of PL UC measurement.

All our measurements were made in up-conversion spectrometer (FOG 100, CDP systems, Russia) shown in Scheme 2.7, where a part of the output from Mai Tai (800 nm, 80 MHz, < 100 fs) was received. For second harmonic generation, 800 nm beam was focused onto a β -barium borate (BBO) crystal and 400 nm beam was generated and used for excitation of the sample. The 400 nm laser beam was reflected by using a dichroic mirror and the transmitted 800 nm beam (called gate bean) was passed through a mechanical



Scheme 2.7: Layout of optical components of PL UC setup used for our study (adapted from ref 9).

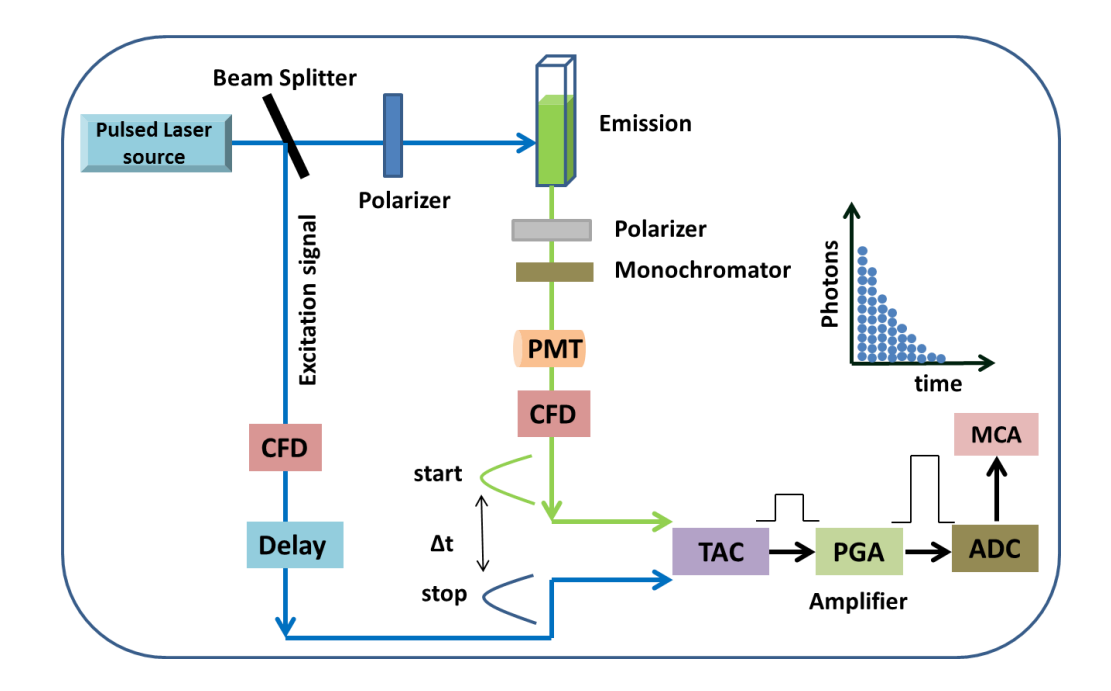
delay line ~ 4 ns. The 400 nm output was passed through a Berek plate, which was set at magic angle. A filter was placed to remove residual gate beam and was focused on the rotating sample cell. The fluorescence from the sample was focused to a second BBO crystal after passing through a collimating lens and a filter (to remove excitation beam, 400 nm). The gate beam was directed to the BBO crystal and after mixing with the fluorescence, up-converted signal was produced. The up-converted signal was passed through the monochromator (adjusted according to the up-converted signal) and was detected in a PMT.

2.3.5. Picosecond time-correlated single photon counting (TCSPC) setup

PL decays were measured using TCSPC spectrometer (Horiba Jobin Yvon IBH) in the picosecond to microsecond region. It works on the basic principle of a stop watch, where the emitted single photon events are detected and the time of detection is correlated to the

Chapter 2

arrival time of the excitation laser pulse. 10 The schematic diagram of the setup is shown in Scheme 2.8.



Scheme 2.8: The main components of the TCSPC setup and working principle.

The experiments start when a laser pulse simultaneously excites the sample and sends a signal to the constant fraction discriminator (CFD) (forward mode). CFD measures the arrival time of the laser and diverts the signal to time-to-amplitude convertor (TAC) and START the voltage ramp. The emitted photon is detected by photo multiplier tube (PMT) and directed to another CFD to measures the arrival time of the photon and makes TAC to STOP the voltage ramp. The time difference between START and STOP pulse comes as the output of TAC. The resultant voltage is amplified by programmable gain amplifier (PGA) and converted to numerical value by analog-to-digital convertor (ADC). This process is repeated several times and a histogram of PL intensity change over time is generated.

For our studies, we have used PicoBrite (405 nm, 1 MHz, 60 ps FWHM) diode laser as the excitation source and micro-channel plate (MCP) PMT (Hamamatsu R3809U-50) as

Chapter 2

the detector. A dilute solution of Ludox (as scatterer) was placed inside the sample chamber to measure the instrument response function (IRF).

Lifetimes were estimated by deconvoluting the IRF and decay profiles using nonlinear least-square iterative fitting procedure (software IBH DAS6, Version 2.2).

2.4. Photoluminescence Quantum Yield Measurement

The PLQYs of the perovskite NCs were estimated by comparing with a reference standard dye whose PLQY (QYR) is known and excitable at the same wavelength of the sample, having almost similar emission wavelength range. PLQYs were calculated by following the equation

$$QY_S = QY_R \times (I_S/I_R) \times (OD_R/OD_S) \times (n_S^2/n_R^2)$$
(2.9)

Where OD is the optical density, I represents integrated area under the PL spectra excited at the same wavelength and under similar experimental condition and n is the refractive index of the medium used. The subscript R and S refer to reference and sample respectively. 9,10-diphenylanthracene¹¹ in toluene medium (QY = 0.93), cumarine 153^{12} in ethanol (OY = 0.546) and rhodamine $6G^{13}$ in aqueous medium (OY = 0.95) were used as references.

2.5. Materials Characterization with Other Experimental Techniques

All steady state absorption and emission spectra were recorded using UV-vis spectrophotometer (Cary 100, Varian) and spectrofluorimeter (FluoroLog-3, Horiba Jobin Yvon), respectively. To measure the size and shape of NCs transmission electron microscope (TEM) were used (Tecnai G2 FE1 F12) with an accelerating voltage of 200 keV. The high resolutions TEM (HRTEM) of NCs were taken with the same instrument, which was used for estimation of the lattice spacing using the Gatan Digital Micrograph software. Powder X-ray diffraction (PXRD) patterns of the NCs were obtained using Bruker D8 advance diffractometer using Cu-K α X-radiation ($\lambda = 1.5406$ Å). Elemental composition analysis was done using energy-dispersive X-ray spectrometer (EDX)

Chapter 2

coupled with field emission-scanning electron microscope (FESEM, Ultra 55 Carl Zeiss instrument). Bruker Tensor II spectrometer was used to measure FTIR spectra. X-ray photoelectron spectroscopy (XPS) measurements were performed using Thermo Scientific K-Alpha + spectrometer using micro-focused monochromatic X-ray source, generated at 70 W with a spot size of 400 µm. The energy resolution of the spectrometer was set at 0.5 eV at pass energy of 50 eV.

References

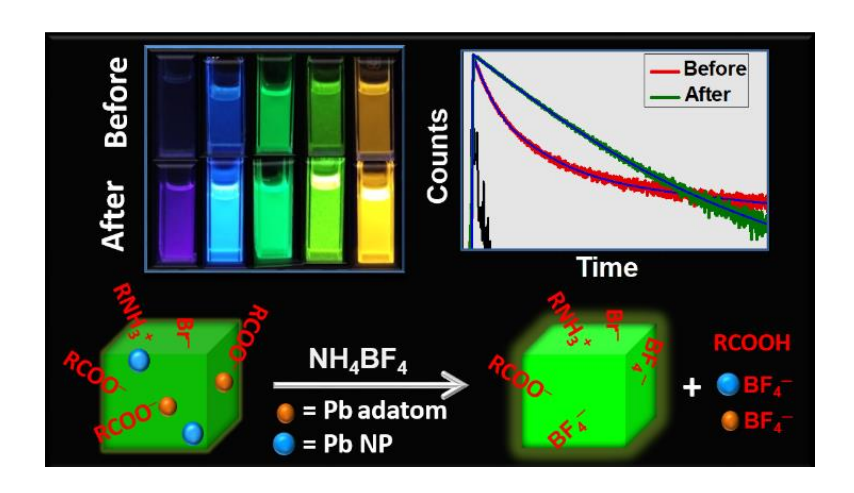
- Protesescu, L.; Yakunin, S.; Bodnarchuk, M. I.; Krieg, F.; Caputo, R.; Hendon, C. H.; Yang, R. X.; Walsh, A.; Kovalenko, M. V., Nanocrystals of Cesium Lead Halide Perovskites (CsPbX₃, X = Cl, Br, and I): Novel Optoelectronic Materials Showing Bright Emission with Wide Color Gamut. Nano Lett. 2015, 15, 3692-3696.
- Paul, S.; Samanta, A., N-Bromosuccinimide as Bromide Precursor for Direct Synthesis of Stable and Highly Luminescent Green-Emitting Perovskite Nanocrystals. ACS *Energy Lett.* **2020,** 5, 64–69.
- Begum, R.; Parida, M. R.; Abdelhady, A. L.; Murali, B.; Alyami, N. M.; Ahmed, G. H.; Hedhili, M. N.; Bakr, O. M.; Mohammed, O. F., Engineering Interfacial Charge Transfer in CsPbBr₃ Perovskite Nanocrystals by Heterovalent Doping. J. Am. Chem. Soc. **2017,** 139, 731-737.
- Moernera, W. E.; Fromm, D. P., Methods of Single-Molecule Fluorescence Spectroscopy and Microscopy. Rev. Sci. Instrum. 2003, 74, 3597-3619.
- J. R. Lakowicz, P. o. F. S., 3rd edn., Springer, New York, 2006. 5.
- Bacia, K.; Haustein, E.; Schwille, P., Fluorescence Correlation Spectroscopy: Principles and Applications. *Cold Spring Harb Protoc.* **2014,** 7, 709-725.
- Cordones, A. A.; Leone, S. R., Mechanisms for Charge Trapping in Single Semiconductor Nanocrystals Probed by Fluorescence Blinking. Chem. Soc. Rev. 2013, 42, 3209.
- Berera, R.; Grondelle, R. v.; Kennis, J. T. M., Ultrafast Transient Absorption Spectroscopy: Principles and Application to Photosynthetic Systems. Photosynth Res 2009, 101, 105-118.
- De, A 2020, Ultrafast Carrier Dynamics and Charge Transfer Processes in Photoexcited Perovskite Nanocrystals, University of Hyderabad, India.
- Valeur, B., Molecular Fluorescence: Principles and Applications. In 2nd ed.; Wiley-VCH Verlag GmbH: Weinheim, 2001.
- Maciejewski, A.; Steer, R. P., Spectral and Photophysical Properties of 9,10-Diphenylanthracene in Perfluoro-n-hexane: The Influence of Solute-Solvent Interactions 1986, (35), 59 - 69. *Journal of Photochemistry* **1986,** 35, 59-69.

Chapter 2 Materials, Instrumentation and Methods

- 12. Rurack, K.; Spieles, M., Fluorescence Quantum Yields of a Series of Red and Near-Infrared Dyes Emitting at 600-1000 nm *Anal. Chem.* **2011**, 83, 1232–1242.
- 13. Kubin, R. F.; Fletcher, A. N., Fluorescence Quantum Yields of Some Rhodamine Dyes. *J. Lumin.* **1982,** 27, 455-462.

CHAPTER 3

Boosting the Photoluminescence of CsPbX₃ (X=Cl, Br, I) Perovskite Nanocrystals Covering a Wide Wavelength Range by Post-Synthetic Treatment with Tetrafluoroborate Salts



Overview

While the caesium lead halide (CsPbX₃, X= Cl, Br, I) perovskite nanocrystals (NCs) are in limelight for their promising optical and opto-electronic properties, the trapping of charge carriers by the defect states greatly diminishes their photoluminescence quantum yield (PLQY). Herein we show how a simple treatment with sodium or ammonium tetrafluoroborate salt can dramatically improve the PL properties of a series of CsPbX₃ NCs emitting in the blue-yellow region. We have achieved near-unity PLQY for CsPbBr₃ and CsPbBr_xCl_{3-x} and substantially high PLQY for CsPbCl₃ and CsPbBr_xI_{3-x} NCs by this method. The effect of this treatment is also reflected from much-improved PL decay profiles of the NCs. The findings, which demonstrate the effectiveness of tetrafluoroborate ion in producing high quality photo-luminescent perovskite NCs by removing excess Pb from the surface, are expected to boost the utility of these materials in practical applications.

3.1. Introduction

Cesium lead halide perovskite (CsPbX₃, X=Cl, Br, I) NCs have received enormous attention in recent years as promising optoelectronic materials¹⁻⁴ due to their broad absorption, intense PL with narrow band width, high defect tolerance, and band gap tunability over the entire visible range.⁵⁻⁷

The PL properties of these substances are, however, highly sensitive to the synthetic conditions and compositions. Several reports show low PLQY of these perovskites.^{6,8-14} Even the highly luminescent perovskite NCs prepared by the hot injection method are not free from defects, which act as trapping centers for the charge carriers and lower the PL efficiency of the systems.⁶ The complex multi-exponential PL decay kinetics of these NCs is also the consequence of defects,^{10,11,13,15-19} which can arise from the surface²⁰ and/or intrinsic in nature.²¹⁻²³ Due to high surface to volume ratio of these NCs their PL properties are largely determined by the quality of the surface. Hence, surface treatment by appropriate reagent is key to obtaining defect-free samples with superior PL properties for light-based applications.

Attempts have been made previously to improve the PLQY of perovskite NCs by surface modification, during 14,17 or after the synthesis. 10,11,19,24,25 PLOY value of near unity is observed for CsPbBr₃ NCs upon treatment with Na/NH₄ thiocyanate salts²⁴ and lead bromide.¹⁹ didodecyldimethylammoniumbromide, 10 Upon treatment with didodecyldimethylammoniumsulfide¹¹ and metal bromide^{14,19} PLQY of 70-83% is achieved for these NCs. For CsPbI₃ NCs, PLQY of ~100% is achieved by treatment with trioctylphosphine-PbI₂ or 2, 2'-iminodibenzoic acid. 17,25 It is thus evident that no given method of surface treatment is effective for all or a large number of CsPbX₃ NCs. During our quest for a common method (post-synthetic treatment) for improvement of the PL properties of a wide variety of CsPbX₃ NCs, we have observed that a simple treatment with sodium/ammonium tetrafluoroborate salt is highly effective. It enhances the PLQY of several CsPbX₃ NCs emitting in the 400-600 nm region substantially. Particularly noteworthy in this context is 90-96% PLQY for CsPbBr_xCl_{3-x}, and 50-fold enhancement for CsPbCl₃.

3.2. Results

3.2.1. Post synthetic surface treatment of NCs

The colloidal CsPbX₃ NCs studied in this work were synthesized following the procedure reported by Protesescu et al.⁶ with minor modifications (see Chapter 2 for details). Then, the precipitate was finally dispersed in toluene for measurements. 2-4 mL of NC (few micro-molar) solution was stirred with solid NaBF₄ or NH₄BF₄ for 30 minutes at room temperature and open atmosphere. Majority of the changes in the NC occurs within first 10 minutes and become unaffected after 30 minutes of the treatment. Since the ionic tetrafluoroborate salts have very limited solubility in nonpolar toluene, they were separated easily from the NC solution by centrifuging for 5 minutes at 6000 rpm. Outcome of the treatment is highly reproducible. The tetrafluoroborate salts were used directly after purchase in this method. Colloidal dispersion of the NCs remained unaffected after the treatment.

3.2.2. Characterization of NCs

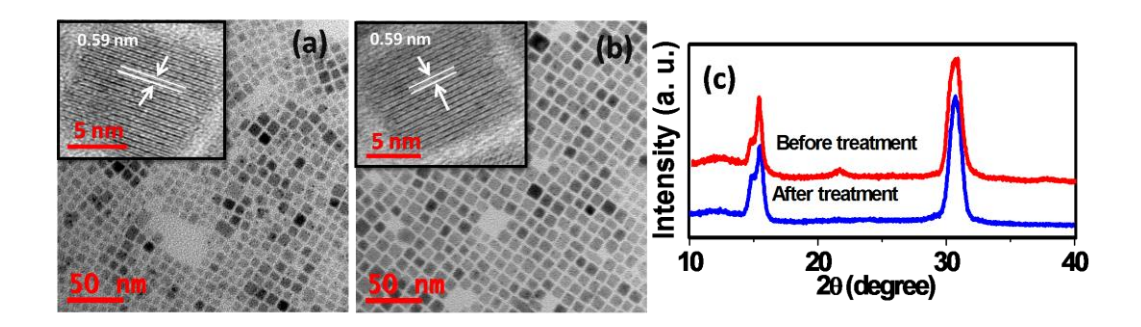


Figure 3.1: TEM images of CsPbBr₃ NCs before (a) and after (b) treatment showing an edge-length of ~9.7 nm. High resolution-TEM images in the insets show similar interplanar distance of 0.59 nm. (c) Powder X-ray diffraction patterns of CsPbBr₃NCs before and after the treatment.

Chapter 3 Boosting the photoluminescence...

To see the change in morphology and crystal structure of the NCs, before and after treatment, TEM images and powder XED patterns are used. TEM images of the assynthesized CsPbX₃ NCs show a regular cubic morphology with edge length of ~7-12 nm (depending on halide composition). No change in size of the samples after treatment is observed from TEM images (Figure 3.1, AI.1 and AI.2). The HR-TEM images (insets to Figure 3.1) show a lattice spacing of 0.59 nm for the (100) plane for CsPbBr₃ before and after the treatment.⁶ No change in crystal structure is also evident from close match of the powder XRD patterns of treated and untreated NCs.

3.2.3. Steady state measurements

The emission peak position (λ_{max}) of the samples studied here vary between ~402nm (CsPbCl₃) and ~595nm [CsPb(Br/I)₃] (Figure AI.3), thus covering a large part of the visible spectrum. Representative PL spectra (Figure 3.2) of CsPbCl₃ and CsPbBr₃ show PL peaks at 402 nm (FWHM = 14 nm) and 507 nm (FWHM = 20 nm), respectively. The PLQYs of these as-synthesized samples are measured to be ~1 % and ~30 %, respectively. Even though no noticeable change in size, shape or crystal structure of the NCs was found on treatment with the tetrafluoroborate salt, a huge improvement of the PL properties of the samples is observed. For example, the PLQY of treated CsPbBr₃ reaches a value of almost unity (\geq 95%). CsPbCl₃ shows ~50-fold enhancement of PLQY to reach a value of 50%. The other mixed halides also show excellent improvement of PLQY (Table 3.1). The PLQY values achieved for the mixed halides vary between 63-96%. We also note that no improvement of PLQY is observed only for CsPbI₃ NCs. The photographs in Figure 3.2 highlights the PL enhancement over a wide range of wavelengths is achieved in this work. The high PLQY values obtained for so many individual NCs by a single method is unprecedented. In all cases, a small but reproducible

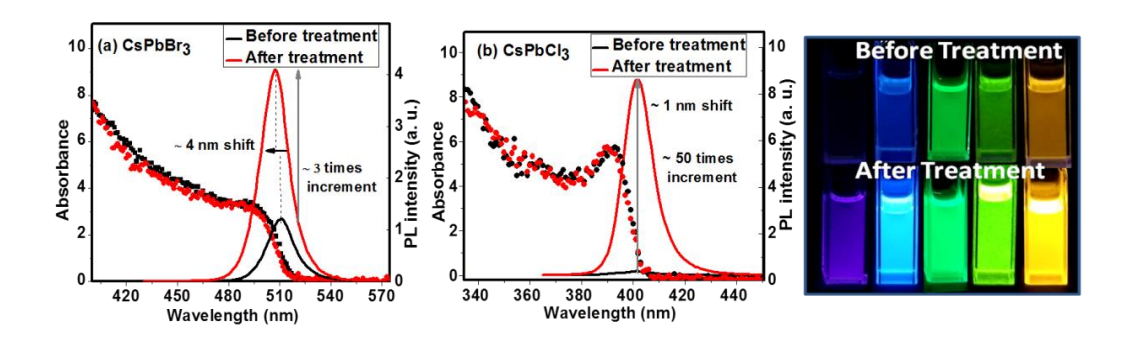


Figure 3.2: Absorption and PL spectra of (a) CsPbBr₃, (b) CsPbCl₃ and (c) Photographs of PL of colloidal solutions of CsPbX₃ NCs in toluene (under 365 nm UV lamp) before and after treatment covering the visible spectral region of 400-600 nm. Both sodium and ammonium tetrafluoroborate salts show similar effect.

Table 3.1.PL peak and QY of the NCs before and after treatment and comparison with literature values.

		PLQY (%)		
Materials	λ_{\max} $(\mathbf{nm})^*$	Before treatment	After treatment	Literature (after treatment)
CsPbCl ₃	402	1±0.4	50±5	
CsPbCl ₂ Br	427	1±0.5	90±3	
CsPbCl _{1.5} Br _{1.5}	442	2±1	95±2	
CsPbBr ₂ Cl	458	4±1	96±3	
CsPbBr ₃	507	30±8	95±2	~100 ^{19,24} ,71 ^{10,11}
CsPbBr ₂ I	540	10±5	70±5	
CsPbBr _{1.5} I _{1.5}	595	13±5	63±2	
CsPbI ₃	690	40±5	40±5	>95 ²⁵

^{*}before treatment

blue shift of the PL maximum (by 1–4 nm) is observed (Figure 3.2); though similar shift in the absorption spectra is absent. This blue shift of the PL peak for treated and more luminescent samples could be due to the removal of shallow emissive energy levels of the as-synthesized NCs. 8,9,11,12,14,24

3.2.4. Time resolved measurements

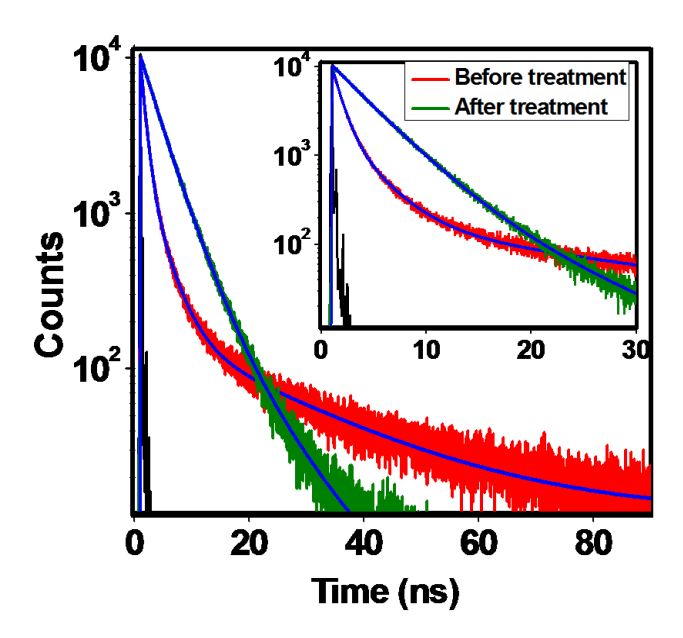


Figure 3.3: Photoluminescence decay curves of CsPbBr₃ ($\lambda_{ex} = 405$ nm). Inset shows the curves in 0-25 ns time window.

Table 3.2. Lifetime (τ/ns) components of CsPbBr₃ NCs before and after treatment.

CsPbBr ₃	$\tau_1(\alpha_1 ^*)$	$\tau_2(\alpha_2)$	$\tau_3(\alpha_3)$	${ au_{\mathrm{avg}}}^{\#}$
Before treatment	3.0(0.24)	19.8(0.02)	0.9(0.74)	1.78
After treatment	3.6(0.96)	9.3(0.04)		3.82

^{*} α_i 's are amplitudes of the lifetime components. " τ_{avg} is defined as $\sum \alpha_i \tau_{i'} \sum \alpha_i$

The PL decay profiles of the samples are also significantly improved by the treatment (Figure 3.3). The multi-exponential decay, which is characteristic of the complex/multiple radiative de-excitation pathways, 9,19,26-28 of the as-synthesized samples, is transformed to nearly single-exponential one in some cases with significant enhancement of PL lifetime. Table 3.2 shows three-component decay of CsPbBr₃ becomes nearly single exponential after the treatment. This aspect is better seen from the decay curve shown in the 0-25 ns

time window (inset of Figure 3.3). The \sim 3 ns (τ_1) component is attributed to excitonic recombination considering the literature values, 9,19,24 and enhancement of the amplitude (α_1) of this component on treatment. As the 0.9 ns component, which was the major radiative recombination process before treatment, vanishes after the treatment, it can be attributed to the trap states arising from the surface defects, which are eliminated after the treatment. The long lived component with very small (4%) contribution is presumably arising from shallow trap-mediated radiative recombination. Striking effect of the treatment is also noticed for other mixed halide NCs (Figure AI.4). The tri-exponential PL decay patterns change to bi-exponential one in almost all cases with low contribution from the long-lived component (Table AI.2).

3.2.5. Mechanism of PL enhancement

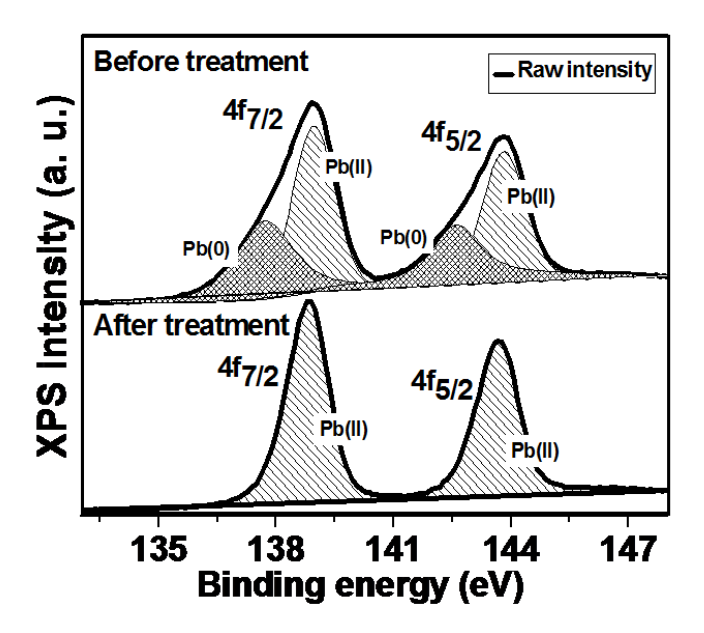


Figure 3.4: XPS spectra due to Pb 4f7/2 and 4f5/2 before and after treatment. Spectra are calibrated with respected to C 1s peak (at 285.35 eV).

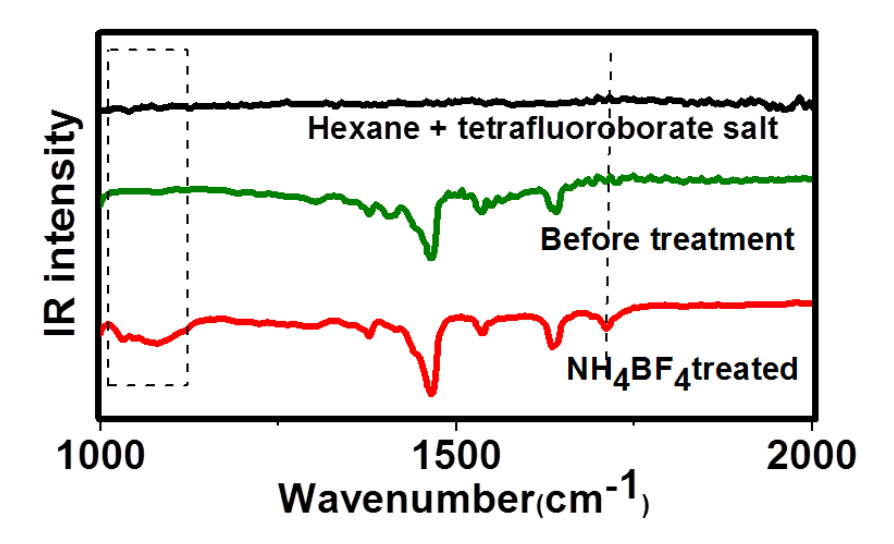


Figure 3.5: Fourior transformed infrared spectroscopy (FTIR) transmission spectra of tetrafluoroborate salt treated hexane, CsPbBr₃ NCs before treatment and after treatment with NH₄BF₄.

In order to understand the mechanism of tetrafluoroborate salt induced PL enhancement we have carefully examined the analytical data. The observation of similar PXRD pattern, lattice spacing and absorption spectrum of the samples before and after the treatment indicates that the crystal structures of the NCs are not affected by the treatment and hence, it is the surface that is modified in the process.

X-ray photoelectron spectroscopy (XPS), Infrared (IR) and energy dispersive X-ray (EDX) spectroscopy measurements have been used to assess the surface modification of the NCs and to understand the mechanism of PL enhancement. Quantitative XPS analysis for CsPbBr₃ indicates a Pb:Br ratio of 3.8 for the untreated surface, which is higher than the expected ratio of 3.0 in the bulk, but is understandable as excess Br on the NC surface arises from the capping ligands. ^{31,32}Following the salt treatment, this ratio increases to 4.0 indicating removal of some Pb from the surface. Deconvolution of the high resolution XPS spectrum of untreated NCs for Pb 4f yields 4 peaks as shown in Figure 3.4. Two intense peaks are located at 138.9 eV (4f_{7/2}) and 143.8 eV (4f_{5/2}) with a spin-orbit splitting of 4.9 eV, which corresponds to Pb in 2+ oxidation state. Additional weaker peaks at

137.6 eV and 142.6 eV, which are absent after the treatment, are attributed to Pb in its metallic state. 33,34 It is known that formation of Pb(0) nanoparticles (NPs) during the synthesis of perovskite NCs by hot injection method cannot be avoided. 32 As it is known that BF₄ can easily strip off capping ligands and labile lead atoms from lead chalcogenide NC surface, 35,36 one expects BF₄ salt treatment to remove the labile Pb adatoms and nanoparticles. This removal of lead is confirmed by the presence of excess lead (Figure AI.8) in the EDX spectrum of the salts after the treatment. Even though, no signature of fluorine (Figure AI.6) could be observed from the XPS measurements, the FTIR spectra of the NCs after the treatment (Figure 3.5) do show a broad peak around 1080 cm⁻¹ due to the B-F stretching of BF₄ bound to lead.³⁷ Another peak at 1712 cm⁻¹ corresponding to C=O stretching of oleic acid obtained from the reaction with counter ion and oleate.²⁴

3.3. Discussion

Considering IR and XPS data, long term colloidal stability and inter-particle packing of these NCs (as evident from TEM images), we conclude that BF₄ ions access only to limited places on the NC surface (sites from where stripping occurs) and do not remove all surface capping ligands as observed in earlier report.³⁸ The fact that these undercoordinated lead ions and lead NPs act as traps for charge carriers and facilitate nonradiative decay leading to low PLQY of NCs is well documented. 24,33,39 This mechanism of PL enhancement is quite similar to that observed in the case of Na/NH₄ thiocyanate-treated samples.²⁴

Having understood the mechanism of PL enhancement, it is not difficult to rationalize its observed trend as we move from CsPbCl₃ to CsPbI₃. Low PLQY of CsPbCl₃ and its 50-fold enhancement indicates the presence of both intrinsic and surface defects in the sample before treatment and effective removal of the surface defects after the treatment. This is confirmed by the presence of a large quantity of lead NPs in as-synthesized NCs and their removal after the treatment (vide TEM images, Figure AI.1 and AI.2). As we move towards CsPbBr₃ the crystals become nearly defect-free after treatment indicating that the defects in these systems arise mostly from lead-rich surface. No noticeable

enhancement for CsPbI₃ suggests that the defects in these NCs are mostly due to structural distortion arising from larger iodine (intrinsic point defects).⁴⁰

3.4. Conclusion

In short, an extraordinary improvement of the PL properties of a series of CsPbX₃ NCs covering a wide wavelength range (~200 nm) in the visible region is achieved by following a simple protocol. Unlike the previous reports, the present method enhances the PLQY of CsPbBr₃ and CsPbCl_xBr_{3-x} NCs to near unity with almost single-exponential PL decay profile in some cases. Further, even for blue-emitting CsPbCl₃ NCs, we have accomplished 50-fold enhancement, which is quite remarkable for this system. These findings, which demonstrate the effectiveness of tetrafluoroborate ion in producing high quality photo-luminescent perovskite NCs by removing excess lead atoms from the surface, are likely to boost the utility of these materials in high performance optoelectronic devices.

References

- (1) Zhang, X.; Lin, H.; Huang, H.; Reckmeier, C.; Zhang, Y.; Choy, W. C. H.; Rogach, A. L., Enhancing the Brightness of Cesium Lead Halide Perovskite Nanocrystal Based Green Light-Emitting Devices through the Interface Engineering with Perfluorinated Ionomer. Nano Lett. 2016, 16, 1415–1420.
- (2) Wang, Y.; Li, X.; Song, J.; Xiao, L.; Zeng, H.; Sun, H., All-Inorganic Colloidal Perovskite Quantum Dots: A New Class of Lasing Materials with Favorable Characteristics. Adv. Mater. 2015, 27, 7101-7108.
- (3) Swarnkar, A.; Marshall, A. R.; Sanehira, E. M.; Chernomordik, B. D.; Moore, D. T.; Christians, J. A.; Chakrabarti, T.; Luther, J. M., Quantum dot-induced phase stabilization of a-CsPbI₃ perovskite for high-efficiency photovoltaics. *Science* **2016**, 354, 92-95.
- (4) Ramasamy, P.; Lim, D.-H.; Kim, B.; Lee, S.-H.; Leeb, M.-S.; Lee, J.-S., All-inorganic cesium lead halide perovskite nanocrystals for photodetector applications. Chem. Commun. 2016, 52, 2067-2070.
- (5) Swarnkar, A.; Chulliyil, R.; Ravi, V. K.; Irfanullah, M.; Chowdhury, A.; Nag, A., Colloidal CsPbBr₃ Perovskite Nanocrystals: Luminescence beyond Traditional Quantum Dots. Angew. Chem. Int. Ed. 2015, 54, 15424 –15428.
- (6) Protesescu, L.; Yakunin, S.; Bodnarchuk, M. I.; Krieg, F.; Caputo, R.; Hendon, C. H.; Yang, R. X.; Walsh, A.; Kovalenko, M. V., Nanocrystals of Cesium Lead Halide Perovskites (CsPbX₃, X = Cl, Br, and I): Novel Optoelectronic Materials Showing Bright Emission with Wide Color Gamut. Nano Lett. 2015, 15, 3692–3696.

- (7) Akkerman, Q. A.; D'Innocenzo, V.; Accornero, S.; Scarpellini, A.; Petrozza, A.; Prato, M.; Manna, L., Tuning the Optical Properties of Cesium Lead Halide Perovskite Nanocrystals by Anion Exchange Reactions. *J. Am. Chem. Soc.* **2015**, 137, 10276–10281.
- (8) De, A.; Mondal, N.; Samanta, A., Luminescence Tuning and Exciton Dynamics of Mn-doped CsPbCl₃ Nanocrystals. *Nanoscale* **2017**, 9, 16722-16727.
- (9) Mondal, N.; Samanta, A., Complete ultrafast charge carrier dynamics in photo-excited all-inorganic perovskite nanocrystals (CsPbX₃). *Nanoscale* **2017**, 9, 1878-1885.
- (10) Pan, J.; Quan, L. N.; Zhao, Y.; Peng, W.; Murali, B.; Sarmah, S. P.; Yuan, M.; Sinatra, L.; Alyami, N. M.; Liu, J.; Yassitepe, E.; Yang, Z.; Voznyy, O.; Comin, R.; Hedhili, M. N.; Mohammed, O. F.; Lu, Z. H.; Kim, D. H.; Sargent, E. H.; Bakr, O. M., Highly Efficient Perovskite-Quantum-Dot Light-Emitting Diodes by Surface Engineering. *Adv. Mater.* **2016**, 28, (39), 8718–8725.
- (11) Pan, J.; Sarmah, S. P.; Murali, B.; Dursun, I.; Peng, W.; Parida, M. R.; Liu, J.; Sinatra, L.; Alyami, N.; Zhao, C.; Alarousu, E.; Ng, T. K.; Ooi, B. S.; Bakr, O. M.; Mohammed, O. F., Air-Stable Surface-Passivated Perovskite Quantum Dots for Ultra-Robust, Single- and Two-Photon-Induced Amplified Spontaneous Emission. *J. Phys. Chem.* **2015**, 6, 5027–5033.
- (12) Parobek, D.; Roman, B. J.; Dong, Y.; Jin, H.; Lee, E.; Sheldon, M.; Son, D. H., Exciton-to-Dopant Energy Transfer in Mn-Doped Cesium Lead Halide Perovskite Nanocrystals. *Nano Lett.* **2016**, 16, 7376–7380.
- (13) Seth, S.; Mondal, N.; Patra, S.; Samanta, A., Fluorescence Blinking and Photoactivation of All-Inorganic Perovskite Nanocrystals CsPbBr₃ and CsPbBr₂I. *J. Phys. Chem. Lett.* **2016**, 7, 266–271.
- (14) Woo, J. Y.; Kim, Y.; Bae, J.; Kim, T. G.; Kim, J. W.; Lee, D. C.; Jeong, S., Highly Stable Cesium Lead Halide Perovskite Nanocrystals through in Situ Lead Halide Inorganic Passivation. *Chem. Mater.* **2017**, 29, 7088–7092.
- (15) Quilettes, D. W. d.; Vorpahl, S. M.; Stranks, S. D.; Nagaoka, H.; Eperon, G. E.; Ziffer, M. E.; Snaith, H. J.; Ginger, D. S., Impact of microstructure on local carrier lifetime in perovskite solar cells. *Science* **2015**, 348 683-686.
- (16) Kang, J.; Wang, L.-W., High Defect Tolerance in Lead Halide Perovskite CsPbBr₃. *J. Phys. Chem. Lett.* **2017**, 8, 489–493.
- (17) Liu, F.; Zhang, Y.; Ding, C.; Kobayashi, S.; Izuishi, T.; Nakazawa, N.; Toyoda, T.; Ohta, T.; Hayase, S.; Minemoto, T.; Yoshino, K.; Dai, S.; Shen, Q., Highly Luminescent Phase-Stable CsPbI₃ Perovskite Quantum Dots Achieving Near 100% Absolute Photoluminescence Quantum Yield. *ACS Nano* **2017**, 11, 10373–10383.
- (18) Noel, N. K.; Abate, A.; Stranks, S. D.; Parrott, E. S.; Burlakov, V. M.; Goriely, A.; Snaith, H. J., Enhanced Photoluminescence and Solar Cell Performance via Lewis Base Passivation of OrganicInorganic Lead Halide Perovskites. *ACS Nano* **2014**, 8, 9815–9821.
- (19) Stasio, F. D.; Christodoulou, S.; Huo, N.; Konstantatos, G., Near-Unity Photoluminescence Quantum Yield in CsPbBr₃ Nanocrystal Solid-State Films via Postsynthesis Treatment with Lead Bromide. *Chem. Mater.* **2017**, 29, 7663–7667.
- (20) Tachikawa, T.; Karimata, I.; Kobori, Y., Surface Charge Trapping in Organolead Halide Perovskites Explored by Single-Particle Photoluminescence Imaging. *J. Phys. Chem. Lett.* **2015**, 6, 3195–3201.

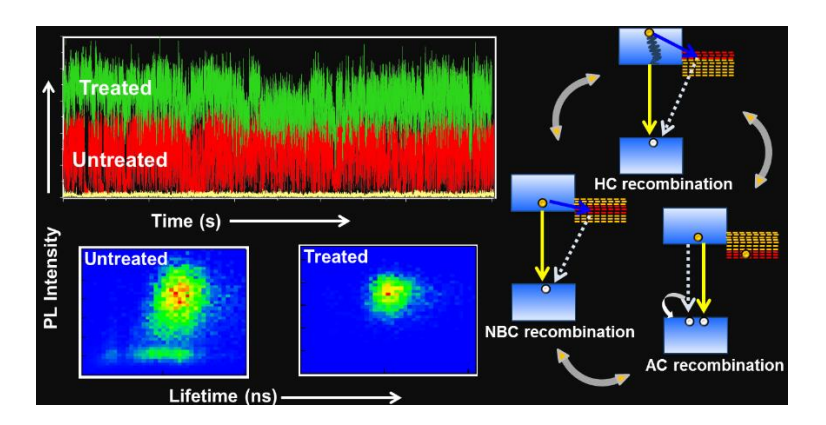
- (21) Kim, J.; Lee, S.-H.; Lee, J. H.; Hong, K.-H., The Role of Intrinsic Defects in Methylammonium Lead Iodide Perovskite. *J. Phys. Chem. Lett.* **2014**, 5, 1312–1317.
- (22) Smyth, D. M., Defects and Order in Perovskite-Related Oxides. *Annu. Rev. Mater. Sci* **1985**, 15, 329–357.
- (23) Xiao, Z.; Zhou, Y.; Hosonoab, H.; Kamiya, T., Intrinsic defects in a photovoltaic perovskite variant Cs₂SnI₆. *Phys. Chem. Chem. Phys.* **2015**, 17, 18900-18903.
- (24) Koscher, B. A.; Swabeck, J. K.; Bronstein, N. D.; Alivisatos, A. P., Essentially trapfree CsPbBr₃ colloidal nanocrystals by post-synthetic thiocyanate surface treatment. *J. Am. Chem. Soc.* **2017**, 19, (139), 6566–6569.
- (25) Pan, J.; Shang, Y.; Yin, J.; Bastiani, M. D.; Peng, W.; Dursun, I.; Sinatra, L.; El-Zohry, A. M.; Hedhili, M. N.; Emwas, A.-H.; Mohammed, O. F.; Ning, Z.; Bakr, O. M., Bidentate Ligand-Passivated CsPbI₃ Perovskite Nanocrystals for Stable Near-Unity Photoluminescence Quantum Yield and Efficient Red Light-Emitting Diodes. *J. Am. Chem. Soc.* **2018**, 140, 562–565.
- (26) Raino, G.; Nedelcu, G.; Protesescu, L.; Bodnarchuk, M. I.; Kovalenko, M. V.; Mahrt, R. F.; Stöferle, T., Single Cesium Lead Halide Perovskite Nanocrystals at Low Temperature: Fast SinglePhoton Emission, Reduced Blinking, and Exciton Fine Structure. *ACS Nano* **2016**, 10, 2485–2490.
- (27) Li, X.; Wu, Y.; Zhang, S.; Cai, B.; Gu, Y.; Song, J.; Zeng, H., CsPbX₃ Quantum Dots for Lighting and Displays: Room-Temperature Synthesis, Photoluminescence Superiorities, Underlying Origins and White Light-Emitting Diodes. *Adv. Funct. Mater.* **2016,** 26, 2435–2445.
- (28) Hu, F.; Zhang, H.; Sun, C.; Yin, C.; Lv, B.; Zhang, C.; Yu, W. W.; Wang, X.; Zhang, Y.; Xiao, M., Superior Optical Properties of Perovskite Nanocrystals as Single Photon Emitters. *ACS Nano* **2015**, 9, 12410–12416.
- (29) Roo, J. D.; Ibáñez, M.; Geiregat, P.; Nedelcu, G.; Walravens, W.; Maes, J.; Martins, J. C.; Driessche, I. V.; Kovalenko, M. V.; Hens, Z., Highly Dynamic Ligand Binding and Light Absorption Coefficient of Cesium Lead Bromide Perovskite Nanocrystals. *ACS Nano* **2016**, 10, 2071–2081.
- (30) Udayabhaskararao, T.; Kazes, M.; Houben, L.; Lin, H.; Oron, D., Nucleation, Growth, and Structural Transformations of Perovskite Nanocrystals. *Chem. Mater.* **2017**, 29, 1302–1308.
- (31) Zhang, Y.; Lv, H.; Cui, C.; Xu, L.; Wang, P.; Wang, H.; Yu, X.; Xie, J.; Huang, J.; Tang, Z.; Yang, D., Enhanced optoelectronic quality of perovskite films with excess CH₃NH₃I for high-efficiency solar cells in ambient air. *Nanotechnology* **2017**, 28, 205401-205411.
- (32) Ravi, V. K.; Santra, P. K.; Joshi, N.; Chugh, J.; Singh, S. K.; Rensmo, H.; Ghosh, P.; Nag, A., Origin of the Substitution Mechanism for the Binding of Organic Ligands on the Surface of CsPbBr₃ Perovskite Nanocubes. *J. Phys. Chem. Lett.* **2017**, 8, (20), 4988-4994.
- (33) Rosen, E. L.; Buonsanti, R.; Llordes, A.; Sawvel, A. M.; Milliron, D. J.; Helms, B. A., Exceptionally Mild Reactive Stripping of Native Ligands from Nanocrystal Surfaces by Using Meerweins Salt. *Angew. Chem. Int. Ed.* **2012**, 51, 684–689.
- (34) Dai, Q.; Zhang, Y.; Wang, Y.; Wang, Y.; Zou, B.; Yu, W. W.; Hu, M. Z., Ligand Effects on Synthesis and Post-Synthetic Stability of PbSe Nanocrystals. *J. Phys. Chem. C* 2010 **2010**, 114, 16160–16167.

Chapter 3 Boosting the photoluminescence...

- (35) Nagane, S.; Bansode, U.; Game, O.; Chhatreab, S.; Ogale, S., CH₃NH₃PbI_(3-x)(BF4)_x: molecular ion substituted hybrid perovskite. *Chem. Commun.* **2014**, 50, 9741-9744.
- (36) Doris, S. E.; Lynch, J. J.; Li, C.; Wills, A. W.; Urban, J. J.; Helms, B. A., Mechanistic Insight into the Formation of Cationic Naked Nanocrystals Generated under Equilibrium Control. *J. Am. Chem. Soc.* **2014**, 136, 15702–15710.
- (37) Zhang, W.; Pathak, S.; Sakai, N.; Stergiopoulos, T.; Nayak, P. K.; Noel, N. K.; Haghighirad, A. A.; Burlakov, V. M.; deQuilettes, D. W.; Sadhanala, A.; Li, W.; LiduoWang; Ginger, D. S.; Friend, R. H.; Snaith, H. J., Enhanced optoelectronic quality of perovskite thinfilms with hypophosphorous acid for planarheterojunction solar cells. *Nat. Commun.* **2015**, *6*, 10030.
- (38) Huang, H.; Bodnarchuk, M. I.; Kershaw, S. V.; Kovalenko, M. V.; Rogach, A. L., Lead Halide Perovskite Nanocrystals in the Research Spotlight: Stability and Defect Tolerance. *ACS Energy Lett.* **2017**, 2, 2071–2083.

CHAPTER 4

Mechanistic Investigation of the
Defect Activity Contributing to the
Photoluminescence Blinking of
CsPbBr₃ Perovskite Nanocrystals



Overview

Exploration of the full potential of the perovskite nanocrystals (NCs) for different applications requires a thorough understanding of the pathways of recombination of the photo-generated charge carriers and associated dynamics. In this work, we have tracked the recombination routes of the charge carriers by probing photoluminescence (PL) intermittency of the immobilized and freely diffusing single CsPbBr₃ NCs employing a time-tagged-time-resolved method. The immobilized single CsPbBr₃ NCs show a complex PL time-trace, a careful analysis of which reveals nonradiative band-edge recombination through trap states, trion recombination and trapping of the hot carriers contribute to the blinking behavior of any given NC. A drastically suppressed PL blinking observed for the NCs treated with a tetrafluoroborate salt indicates elimination of most of the undesired recombination processes. Fluorescence correlation spectroscopy (FCS) study on the freely diffusing single NCs shows that enhanced PL and suppressed blinking of the treated particles is the outcome of an increase in per-particle brightness, not due to any increase in the number of particles undergoing "off"-"on" transition in the observation volume. The mechanistic details obtained from this study on the origin of blinking in CsPbBr₃ NCs provide deep insight into the radiative and nonradiative charge carrier recombination pathways in these important materials and this knowledge is expected to be useful for better design and development of bright photoluminescent samples of this class for optoelectronic applications.

4.1. Introduction

Caesium lead halide CsPbX₃ (X= Cl, Br & I) perovskite NCs are in limelight as promising materials for photovoltaic and optoelectronic applications because of their excellent properties such as broad absorption with high absorption cross-section, narrow tunable emission, high PLQY, long carrier diffusion length and intrinsic defect tolerance. 1-12 These 'defect-tolerant' NCs are, however, not completely free from charge carrier trapping centres.^{3, 13-17} These are largely free from deep-trap states, but they do possess shallow trap states, which facilitate nonradiative recombination of the charge carriers and decrease PLQY of the system. 14, 18-21 As efficiency of an optoelectronic device made of these materials depends on the fate of the charge carriers, a thorough understanding of the nature of the trap states and dynamics of different competitive radiative and non-radiative charge carrier recombination processes is essential for proper utilization of these substances.

The charge carrier recombination process can be investigated by monitoring the PL properties of individual NCs. Extensive studies on (mostly CdSe based) semiconductor quantum dots have shown that these single NCs show random PL fluctuations, termed as PL intermittency or blinking, due to participation of the trap states in carrier recombination processes.²² Random fluctuation of PL between the bright (on), dim (grey) and dark (off) states arises from a number of processes depending on the size, composition and nature (density and position of the trap states) of the NCs and several models have been proposed to explain PL blinking. 23-28 These studies have revealed the contribution of the following processes on their PL blinking. 24-26, 29-34 When a charge carrier gets trapped in a short-lived shallow trap state, it relaxes rapidly through a nonradiative route before another exciton is generated. In this case, time-dependent fluctuation of the carrier trapping rate leads to PL blinking behaviour. 22, 25, 26, 30 PL fluctuation due to these shallow trap states mediated nonradiative band-edge carrier (NBC) recombination is known as NBC blinking. 22, 25, 35 When the charge carrier is trapped for a longer period, the NC becomes charged. Absorption of another photon by this charged NC, when creates an exciton, the system becomes a trion.^{25, 31, 33, 36, 37} Under

this condition, two situations can arise; (i) the exciton recombination energy can be nonradiatively transferred to a third carrier (called, Auger recombination), ^{22, 36, 38} and (ii) the exciton can recombine radiatively at a faster rate, which is almost twice that of neutral exciton recombination.^{24, 25, 38} PL blinking arising from trion mediated recombination (radiative and nonradiative) is termed as AC blinking.²⁵ Both AC and NBC recombination can cause blinking of the same NC. 25, 35 Apart from these two processes, trapping of the hot carrier prior to its relaxation to the band edge can also lead to PL blinking. When this happens, the trapped hot carrier relaxes rapidly (through a nonradiative recombination route) before generation of another exciton and one observes a large drop of PL intensity without any significant change in lifetime. This phenomenon, which is known as hot carrier (HC) blinking, is not a common process. ^{24, 39-41}

As far as the perovskite NCs are concerned, it is already known that a number of recombination processes contribute to their blinking. 10-12, 17, 25, 35, 39, 41-51 In some cases, it is claimed that PL blinking is due to the AC recombination, 10, 12, 45 whereas in some other cases, NBC recombination is found to be responsible for PL fluctuation. 43 The occurrence of both NBC and AC recombination in a single CsPbBr₃ NC is also reported.³⁵ Very recently, HC recombination, which was earlier observed in core-shell CdSe/CdS NCs, 24 has been reported for hybrid (organic-inorganic) perovskite NCs. 39, 41 Suppression of the recombination processes contributing to blinking is a challenging task, but has been achieved for metal chalcogenide quantum dots. 52-54 However, very few studies exploring the effect of surface treatment on the blinking behaviour of the perovskite NCs have been made so far. 35, 39, 55

In this work, we investigate PL blinking of both immobilized and freely diffusing CsPbBr₃ NCs and demonstrate that all three recombination processes (NBC, AC and HC) contribute to the PL blinking of each single NC. By examining the PL blinking behaviour of the tetrafluoroborate salt treated NCs, we determine which of these processes are actually suppressed by the surface treatment.

4.2. Results

4.2.1 PL blinking study before treatment of NCs

CsPbBr₃ NCs with an average edge length of 8 ± 1.5 nm and PLQY of ~(30-40)% were synthesized for this study following hot-injection method (details in 'Chapter 3.2.1'). ^{6, 14} The first absorption onset and PL peak of these NCs appear at ~495 nm and ~505 nm, respectively (Figure AII.1). For single-particle study, dilute solutions of the NCs in toluene (picomolar concentration) were drop-casted on a coverslip and dried under vacuum. Confocal PL microscopy image of a typical film of the NCs is shown in Figure 4.1a. The film was excited at 405 nm by a pulsed laser (FWHM 176 ps) with a repetition rate of 4 MHz and average power of 0.05 μ W. The low laser power was used to avoid any non-linear process. Under the experimental condition, each NC was found to absorb on average ~ 0.08 photons per pulses. ^{35, 43, 45, 56} The number of excitons generated per pulse was calculated using the formula, $\langle N \rangle = J_p \times \sigma$, where J_p is per-pulse photon fluence and the absorption cross section is, $\sigma = 1.5 \times 10^{-14}$ cm^{2, 10, 12, 42}

We examined the PL blinking of 55 single NCs among which 39 (~70%) exhibited a blinking pattern, labelled as Class-1 blinking, shown in Figure 4.1b. The occurrence of different PL intensity levels (Figure 4.1c) indicates a broad distribution of the high-intensity "on" state and a much narrower distribution of the low-intensity "grey" state; the latter is not clearly separable from the "off" states (Figure 4.1 and AII.2). To determine the origin of different intensity states we have divided the PL intensity into six levels, marked as R1 to R6, and measured the decay profiles (Figure 4.1d) for each level.

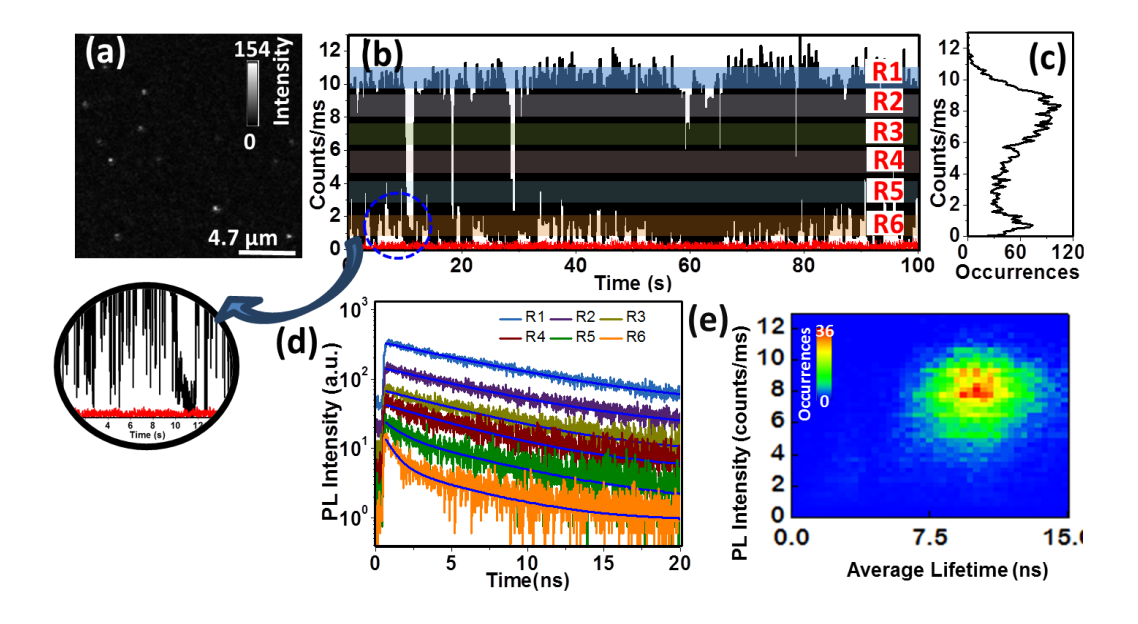


Figure 4.1: (a) PL intensity image of a film of CsPbBr₃ NCs as obtained using a confocal microscope, (b) PL intensity time-trace (binning time 10 ms) of a NC exhibiting Class-1 blinking. The zoomed portion of the circled region shows that the low intensity "grey" states are very close to the background (red line) or the "off" state. (c) Occurrences of the measured PL intensities, (d) PL decay profiles for levels, R1 to R6, and (e) FLID of a single CsPbBr₃ NC with false colour representation.

Table 4.1: Average lifetime components (τ_i) and their weightages (α_i) of different PL levels of the untreated NCs.

Region	$\tau_1(\alpha_1)$ ns	ns $ au_2(lpha_2)$ ns	
R1	8.2±0.3		
R2	7.8±0.1		
R3	7.1±0.3		
R4	6.4±0.1		
R5	6.1±0.2(0.62)	1.1±0.1(0.38)	
R6	$6.5\pm4(0.40)$	0.94±0.1(0.60)	

For the high intensity levels (R1 to R4), PL decay is found to be single-exponential, but for the lower intensity levels (R5 and R6), the decay profile is bi-exponential (Table 4.1 and AII.1).¹² The highest intensity level, which is associated with a single lifetime component of ~8.2 ns (Table 4.1), is attributed to excitonic emission.^{12, 35, 43, 45} The lifetime gradually decreases with decrease in PL intensity (Table AII.1). The computed intensity-lifetime scaling (η) of the top four different intensity regions (R1, R2, R3 and R4) is given below.

$$\eta = k_{R1} : k_{R2} : k_{R3} : k_{R4} = \frac{I_1}{\tau_1} : \frac{I_2}{\tau_2} : \frac{I_3}{\tau_3} : \frac{I_4}{\tau_4} = 1.1 : 1.0 : 0.92 : 0.75$$

A near-unity ratio of the radiative recombination rates of the three high intensity levels indicates the competition between a fixed radiative rate and variable nonradiative rates in the NC. This is typical signature of PL blinking due to NBC recombination. ^{25, 43, 44}

Even though our measurements were performed on well-separated single NCs (Figure 4.1a), one may argue that the multistate emission is not from single NC rather comes from clusters. Let us assume that each particle represents a cluster of 2 NCs. If the 2 NCs have different PL lifetime, the PL decay curve for the R1 level would have been biexponential, which is not the case. If the 2 NCs have same lifetime, the PL intensity of the particle would have been twice as large with same lifetime and hence, η would have been >1.0, which again is not the case. Hence, it is evident that each luminescent particle consists of a single NC.

A deviation of the η value (from near-unity) from level R4 onwards indicates involvement of additional process(es) competing with the NBC recombination and contributing to the lower intensity levels. For these levels, a second lifetime component (~1 ns) is observed, whose contribution increases from level R5 to R6 (Table 4.1). As multiexciton recombination processes are ruled out under our experimental condition, the short-lived component must be arising from trion recombination. The observed lifetime of this process is in agreement with literature.^{10, 35, 43} It is thus evident that AC recombination also contributes to the blinking of each NC. The involvement of two

simultaneously occurring recombination processes can be found out from the fluorescence lifetime-intensity distribution (FLID) patterns.^{25, 35, 42} However, in the present case, this is not very clear from the FLID pattern (Figure 4.1e), presumably due to low occurrence of the "grey" state population.

For further investigation of the processes contributing to PL fluctuations, we have constructed PL lifetime traces corresponding to the intensity traces and compared them together (Figure 4.2, AII.3). It is seen that the PL intensity correlates quite well with the lifetime in most of the regions, but there are some specific regions (indicated by a dashed lines, in Figure 4.2), where the lifetime is significantly high for a very low intensity state. This suggests trapping of the carriers prior to their cooling. Thus it is evident that hot-carrier trapping also contributes to PL blinking along with AC and NBC recombination processes.

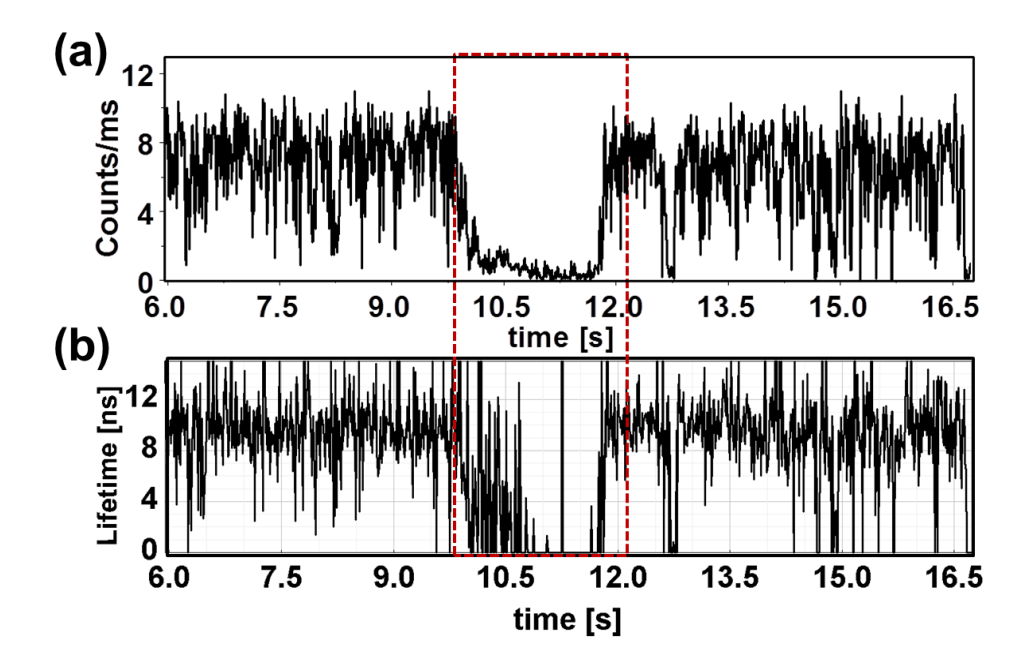


Figure 4.2: (a) PL intensity and (b) lifetime trajectories of a NC exhibiting Class-1 blinking. The region indicated by two dashed red lines shows no correlation between intensity and lifetime.

The PL time-trace and corresponding intensity histogram of the remaining 30% of the NCs, classified as Class-2 blinking, are shown in Figure 4.3. Unlike in the previous case, here the occurrence of the "grey" state is greater than that of the "on" state. Analysis of the PL decay profiles at higher intensity levels reveals contribution of the NBC recombination similar to what is observed for Class-1 NCs (Figure AII.5). As the "grey" states have greater contribution for Class-2 NCs (Figure 4.3b), the low intensity states are now more clearly visible in the FLID pattern (Figure 4.3c and AII.6). One can easily identify two distinct lifetime components for the low intensity region. The ~7.5 ns component (indicated by an arrow) is similar to the lifetime of neutral exciton. For a low intensity state, a lifetime closer to that of the neutral exciton can be explained only if the carriers are trapped before they relax to the band edge.⁵⁷ This implies that hot carrier mediated HC recombination also contributes to the blinking of CsPbBr₃ NC. Another low intensity region (circled) in Figure 4.3c, with lifetime (~1.6 ns, Table AII.2) significantly shorter than that of the neutral exciton (~8 ns), must be due to trion recombination. 10, 35, 43 Thus we find that three different channels of recombination (AC, NBC and HC) contribute to the observed blinking of these single CsPbBr₃ NCs as well. The blinking pattern of these NCs differs from that of the Class-1 blinking ones in respect of the weightages of the three recombination processes.

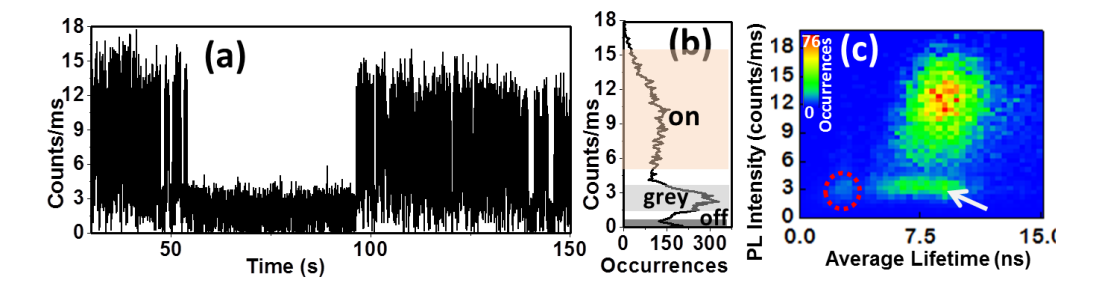


Figure 4.3: (a) PL intensity time-trace (binning time 10 ms) of a NC exhibiting Class-2 blinking. (b) Occurrences of the measured PL intensities, (c) FLID of a single NC with false colour representation.

4.2.2 PL blinking study after treatment of NCs

We have also examined the PL intensity time-trace of 51 single CsPbBr₃ NCs, which were treated with tetrafluoroborate salts to enhance the PLQY to near-unity following a recently developed method (details in 'Chapter 3'). 14 Nearly 90% of these treated NCs show significantly suppressed PL blinking displaying only one high intensity level (Figure 4.4). The disappearance of the contributions of the "grey" and "off" states, which makes the PL intensity distribution much narrower and indicates that PL blinking is effectively suppressed by the surface treatment. To investigate this aspect little deeper, we examined the PL decay profiles corresponding to three narrow intensity levels (T1, T2 and T3), as shown in Figure 4.4c. The highest intensity region (T1) exhibits singleexponential decay with a lifetime of ~ 8.8 ns (Table 4.2 and AII.3), which is not very different from that before treatment. The other two levels exhibit bi-exponential decay kinetics comprising a short component (~1.9 ns) in addition to the long one. The amplitude of this short component (~29% for T2, ~38% for T3) due to trion recombination is almost half of that before treatment (~60% for R6 in Class-2 NC). This indicates that even though trion formation is suppressed significantly due to surface treatment, it is not completely eliminated in the treated sample. A higher PLOY (evident from higher PL intensity counts), suppressed blinking and narrow distribution of the events (the "off" and "grey" states are removed) in the FLID pattern (Figure 4.4d) indicate radiative recombination as the main recombination pathway of the carriers after the treatment with highly suppressed HC and NBC processes.

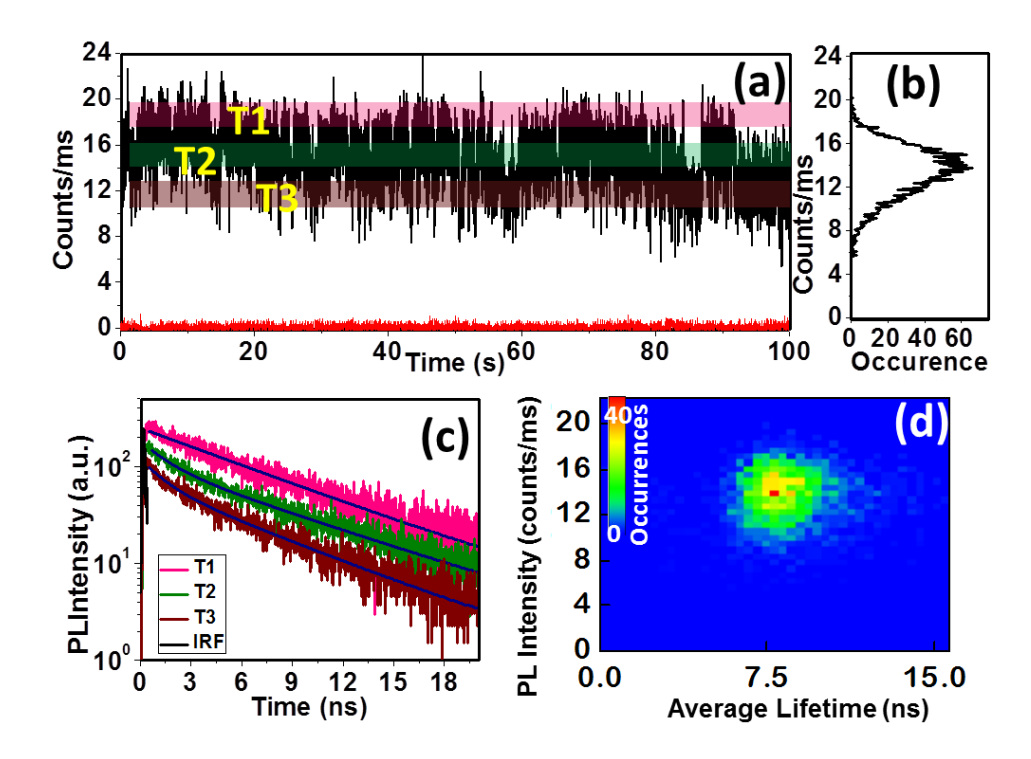


Figure 4.4: (a) PL intensity time-trace (binning time 10 ms) of a NaBF₄-treated NC. Red line indicates the background signal intensity. (b) Occurrences of the measured PL intensities, (c) PL decay profiles of the levels marked T1 to T3 and (d) FLID of single CsPbBr₃ NC after treatment with false colour representation.

Table 4.2: Average lifetime components (τ_i) and their weightages (α_i) of different PL levels of the treated NCs.

Region	$\tau_1(\alpha_1)$ ns	$\tau_2(\alpha_2)$ ns
T1	8.8±0.5	
T2	9.1±0.4(0.71)	2.1±0.2(0.29)
Т3	8.2±0.4(0.62)	1.9±0.1(0.38)

4.2.3 FCS study

As stated earlier, we have also studied the freely diffusing NCs (a colloidal solution of the NCs in octadecene) of same concentration before and after NaBF₄ treatment to understand the effect of the treatment on PL blinking dynamics. The fluorescence correlation curves are found to be best represented by equation 1 (Figure 4.5), which involves a three-dimensional diffusion along with a stretched exponential decay component due to PL blinking. The quality of the fits can be assessed from Figure AII.10 and the fitting parameters are presented in Table 4.3.

$$G(\tau) = \left[1 + \frac{\tau}{1 - T} \exp\left(-\frac{\tau}{\tau_T}\right)^{\beta}\right] \frac{1}{N} \left(1 + \frac{\tau}{\tau_D}\right)^{-1} \left(1 + \frac{\tau}{\kappa^2 \tau_D}\right)^{-\frac{1}{2}}$$
 (1)

Where τ_D is the diffusion time of the NCs, N the average number of particles undergoing reversible PL intensity fluctuation in the observation volume, T the fraction of the "off" state, and τ_T the dark-state relaxation time or blinking time. β is the stretching exponent with a value between 0 to 1 and is related to the distribution of τ_T . κ (= ω_Z/ω_{xy}) is the structure parameter of the observation volume; ω_Z and ω_{xy} are the longitudinal and transverse radii, respectively.

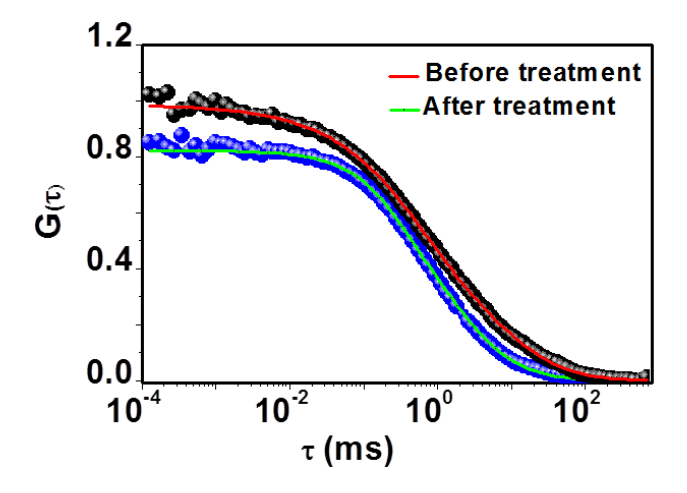


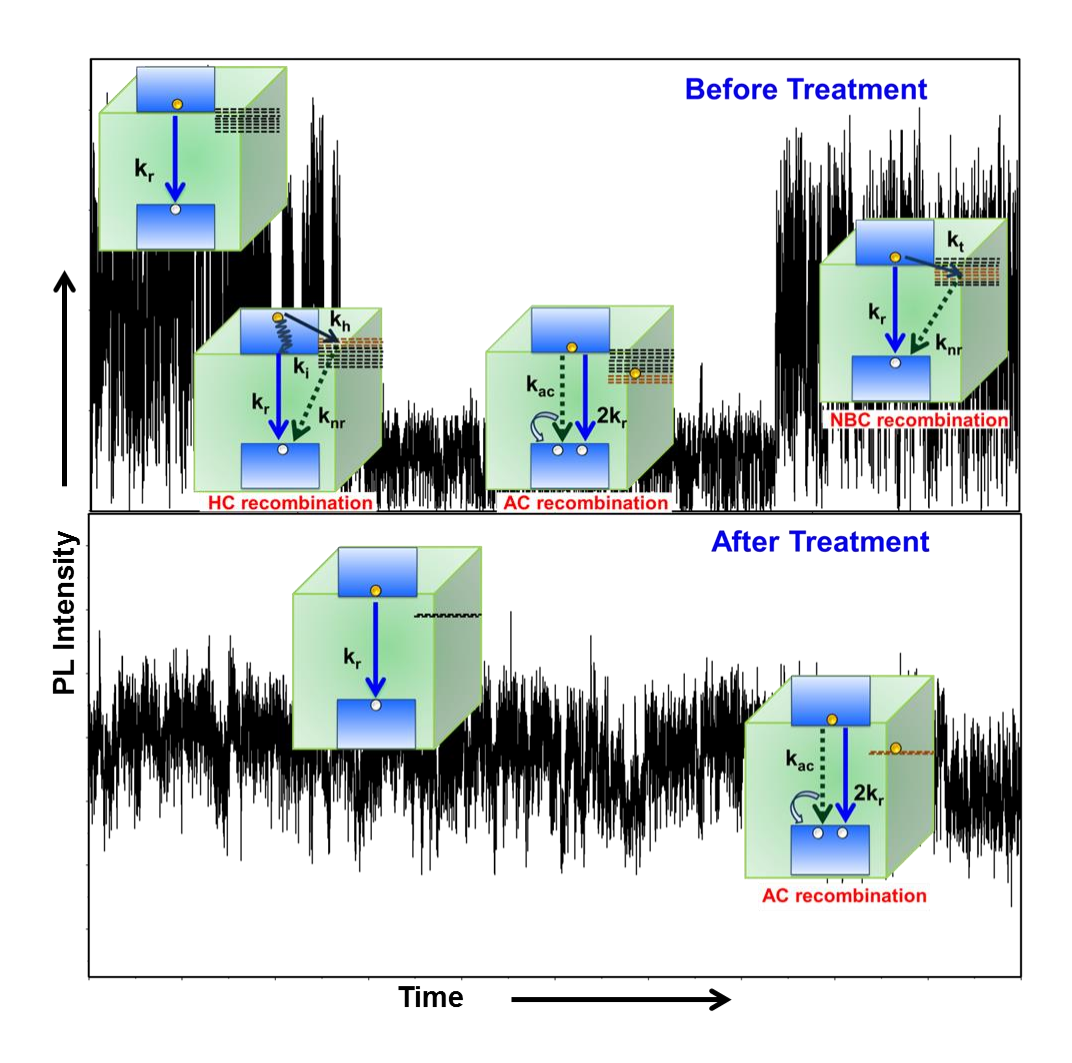
Figure 4.5: Fluorescence correlation curves of the CsPbBr₃ NCs in octadecene before and after treatment.

The β-value (0.56) obtained for the untreated NCs is substantially different from unity. This indicates a distributed kinetics of fluorescence blinking suggesting the involvement of multiple trap states. ^{10, 21, 58, 59} Interestingly, the β value of unity for the treated samples (Figure 4.5) indicates that PL fluctuation is now due to a single nonradiative recombination channel. A decrease in the T value from ~0.55 to ~0.37 upon treatment reduced off-state fraction (T) of before treatment (Table 4.3) implies that the treated particles remain mostly in the "on"-state; an observation that confirms the suppression of blinking. We note that the number of particles (N) undergoing "on"-"off" transition in the observation volume, is not altered significantly by the treatment; but, per-particle brightness (PPB) is increased (Table 4.3) by a factor of ~2.2 fold (from ~9.3K cps/particle to ~19.7K cps/particle) as a result of the treatment. This value is in agreement with ~3-fold enhancement of PLQY of the system on treatment, as we reported in an earlier work.¹⁴

Table 4.3: Estimated values of the off-state fraction (T), average number of observable particle (N) within the observable volume, stretching exponent (β) and per-particle brightness (PPB).

NCs	T	N	β	PPB(cps/particle)
Before	0.55 ± 0.03	1.89 ± 0.15	0.56 ± 0.02	9.3±0.85
treatment				
After	0.37 ± 0.02	1.84±0.16	1.0±0.01	19.7±0.91
treatment				

4.3. Discussion



Scheme 4.1: Different recombination processes in a single CsPbBr₃ NC before and after surface treatment. The black and brown dashed horizontal lines show the deactivated and activated trap states, respectively. For the sake of clarity, intra-band relaxation of the hot electrons is not shown while illustrating AC and NBC blinking. Also, hot hole cooling is not shown in all cases for the same reason.

It is generally believed that the surface defects of CsPbBr₃ NCs arise from uncoordinated lead and lead nanoparticles. ^{13, 14, 35, 39} These defects give rise to states near the conduction band that are highly effective in trapping the charge carriers. Considering these trap states

and the findings of this work, we illustrate the mechanistic details of different recombination events in single CsPbBr₃ NCs in Scheme 4.1. When the traps are in their passive state, ¹⁷ the excitons recombine radiatively with zero nonradiative rates. However, the excitons may as well recombine nonradiatively via the trap states when the latter are active.¹⁷ This study reveals that, when the exciton at the band-edge recombines through those shallow trap states before generation of another exciton (<250 ns), no charging of the NCs occurs and the blinking is due to the NBC mechanism. On the other hand, when electron is trapped for a longer duration (>250 ns) in trap states, which are relatively deeper than those involved in NBC recombination, a trion is formed on generation of another exciton. The trap states, which lie above the conduction band-edge, are involved in capturing the hot-electrons. This trapped hot electron relaxes rapidly and nonradiatively before another exciton is generated. Simultaneous occurrence of three different recombination processes in a single NC is a reflection of highly dynamic nature of the trap states due to ion migration and mobility of the charge carriers. 17, 60-62 Interestingly, though the treatment removes the "off" states, the AC recombination process is not eliminated completely after treatment, presumably because intrinsic defects and/or labile nature of the ligand on the surface. 35, 39

4.4. Conclusion

We show that three separate processes, namely NBC, HC and AC recombination, contribute to the PL blinking of each single CsPbBr₃ NC. Significant suppression of blinking, as evident from the disappearance of "off" and "grey" PL states on surface treatment of these NCs, indicates significant removal of the trap states contributing to the HC and NBC recombination processes. The AC blinking is also suppressed on treatment, but not eliminated completely. The FCS study reveals an increase in per-particle brightness of the particles on surface treatment is responsible for highly suppressed PL blinking in treated samples. The study provides new insight on the mechanism of PL blinking in CsPbBr₃ NCs, which will be useful in designing non-blinking PL materials of this class. The results also show that the treated CsPbBr₃ NCs can serve as ideal singledot light source in optoelectronic applications.

References

- 1. Gong, M.; Sakidja, R.; Goul, R.; Ewing, D.; Casper, M.; Stramel, A.; Elliot, A.; Wu, J. Z., High-Performance All-Inorganic CsPbCl₃ Perovskite Nanocrystal Photodetectors with Superior Stability. *ACS Nano* **2019**, 13, 1772-1783.
- 2. Kang, J.; Wang, L. W., High Defect Tolerance in Lead Halide Perovskite CsPbBr₃. *J. Phys. Chem. Lett.* **2017**, 8, 489-493.
- 3. Kovalenko, M. V.; Protesescu, L.; Bodnarchuk, M. I., Properties and Potential Optoelectronic Applications of Lead Halide Perovskite Nanocrystals. *Science* **2017**, 358, 745-750.
- 4. Kulbak, M.; Gupta, S.; Kedem, N.; Levine, I.; Bendikov, T.; Hodes, G.; Cahen, D., Cesium Enhances Long-Term Stability of Lead Bromide Perovskite-Based Solar Cells. *J. Phys. Chem. Lett.* **2015**, *7*, 167-172.
- 5. Nedelcu, G.; Protesescu, L.; Yakunin, S.; Bodnarchuk, M. I.; Grotevent, M. J.; Kovalenko, M. V., Fast Anion-Exchange in Highly Luminescent Nanocrystals of Cesium Lead Halide Perovskites (CsPbX₃, X = Cl, Br, I). *Nano Lett.* **2015**, 15, 5635-5640.
- 6. Protesescu, L.; Yakunin, S.; Bodnarchuk, M. I.; Krieg, F.; Caputo, R.; Hendon, C. H.; Yang, R. X.; Walsh, A.; Kovalenko, M. V., Nanocrystals of Cesium Lead Halide Perovskites (CsPb X_3 , X = Cl, Br, and I): Novel Optoelectronic Materials Showing Bright Emission with Wide Color Gamut. *Nano Lett.* **2015**, 15, 3692–3696.
- 7. Shi, Z.; Li, Y.; Zhang, Y.; Chen, Y.; Li, X.; Wu, D.; Xu, T.; Shan, C.; Du, G., High-Efficiency and Air-Stable Perovskite Quantum Dots Light-Emitting Diodes with an All-Inorganic Heterostructure. *Nano Lett.* **2016**, 17, 313-321.
- 8. Swarnkar, A.; Chulliyil, R.; Ravi, V. K.; Irfanullah, M.; Chowdhury, A.; Nag, A., Colloidal CsPbBr₃ Perovskite Nanocrystals: Luminescence beyond Traditional Quantum Dots. *Angew. Chem. Int. Ed. Engl.* **2015,** 54, 15424-15428.
- 9. Zhou, Q.; Bai, Z.; Lu, W. G.; Wang, Y.; Zou, B.; Zhong, H., *In Situ* Fabrication of Halide Perovskite Nanocrystal-Embedded Polymer Composite Films with Enhanced Photoluminescence for Display Backlights. *Adv. Mater.* **2016**, 28, 9163-9168.
- 10. Park, Y. S.; Guo, S.; Makarov, N. S.; Klimov, V. I., Room Temperature Single-Photon Emission from Individual Perovskite Quantum Dots. *ACS Nano* **2015**, 9, 10386-10393.
- 11. Hu, F.; Yin, C.; Zhang, H.; Sun, C.; Yu, W. W.; Zhang, C.; Wang, X.; Zhang, Y.; Xiao, M., Slow Auger Recombination of Charged Excitons in Nonblinking Perovskite Nanocrystals without Spectral Diffusion. *Nano Lett.* **2016**, 16, 6425-6430.
- 12. Yarita, N.; Tahara, H.; Ihara, T.; Kawawaki, T.; Sato, R.; Saruyama, M.; Teranishi, T.; Kanemitsu, Y., Dynamics of Charged Excitons and Biexcitons in CsPbBr₃ Perovskite Nanocrystals Revealed by Femtosecond Transient-Absorption and Single-Dot Luminescence Spectroscopy. *J. Phys. Chem. Lett.* **2017**, 8, 1413-1418.
- 13. Koscher, B. A.; Swabeck, J. K.; Bronstein, N. D.; Alivisatos, A. P., Essentially Trap-Free CsPbBr₃ Colloidal Nanocrystals by Postsynthetic Thiocyanate Surface Treatment. *J. Am. Chem. Soc.* **2017**, 139, 6566-6569.
- 14. Ahmed, T.; Seth, S.; Samanta, A., Boosting the Photoluminescence of CsPbX₃ (X=Cl, Br, I) Perovskite Nanocrystals Covering a Wide Wavelength Range by Post-Synthetic Treatment with Tetrafluoroborate Salts. *Chem. Mater.* **2018**, 30, 3633–3637.

- 15. Mondal, N.; De, A.; Samanta, A., Achieving Near-Unity Photoluminescence Efficiency for Blue-Violet-Emitting Perovskite Nanocrystals. *ACS Energy Lett.* **2019**, 4, 32-39.
- 16. Li, F.; Liu, Y.; Wang, H.; Zhan, Q.; Liu, Q.; Xia, Z., Postsynthetic Surface Trap Removal of CsPbX₃ (X = Cl, Br, or I) Quantum Dots *via* a ZnX₂/Hexane Solution toward an Enhanced Luminescence Quantum Yield. *Chem. Mater.* **2018**, 30, 8546–8554.
- 17. Gerhard, M.; Louis, B.; Camacho, R.; Merdasa, A.; Li, J.; Kiligaridis, A.; Dobrovolsky, A.; Hofkens, J.; Scheblykin, I. G., Microscopic Insight into Non-Radiative Decay in Perovskite Semiconductors from Temperature-Dependent Luminescence Blinking. *Nature Communications* **2019**, 10, 1698.
- 18. Huang, H.; Bodnarchuk, M. I.; Kershaw, S. V.; Kovalenko, M. V.; Rogach, A. L., Lead Halide Perovskite Nanocrystals in the Research Spotlight: Stability and Defect Tolerance. *ACS Energy Lett.* **2017**, 2, 2071-2083.
- 19. Mondal, N.; Samanta, A., Complete Ultrafast Charge Carrier Dynamics in Photo-Excited All-Inorganic Perovskite Nanocrystals (CsPbX₃). *Nanoscale* **2017**, 9, 1878-1885.
- 20. Pan, J.; Quan, L. N.; Zhao, Y.; Peng, W.; Murali, B.; Sarmah, S. P.; Yuan, M.; Sinatra, L.; Alyami, N. M.; Liu, J.; Yassitepe, E.; Yang, Z.; Voznyy, O.; Comin, R.; Hedhili, M. N.; Mohammed, O. F.; Lu, Z. H.; Kim, D. H.; Sargent, E. H.; Bakr, O. M., Highly Efficient Perovskite-Quantum-Dot Light-Emitting Diodes by Surface Engineering. *Adv. Mater.* **2016**, 28, 8718-8725.
- 21. Seth, S.; Mondal, N.; Patra, S.; Samanta, A., Fluorescence Blinking and Photoactivation of All-Inorganic Perovskite Nanocrystals CsPbBr₃ and CsPbBr₂I. *J. Phys. Chem. Lett.* **2016**, 7, 266-271.
- 22. Cordones, A. A.; Leone, S. R., Mechanisms for Charge Trapping in Single Semiconductor Nanocrystals Probed by Fluorescence Blinking. *Chem. Soc. Rev.* **2013**, 42, 3209-3221.
- 23. Efros, A. L.; Nesbitt, D. J., Origin and Control of Blinking in Quantum Dots. *Nat. Nanotechnol.* **2016,** 11, 661-671.
- 24. Galland, C.; Ghosh, Y.; Steinbruck, A.; Sykora, M.; Hollingsworth, J. A.; Klimov, V. I.; Htoon, H., Two Types of Luminescence Blinking Revealed by Spectroelectrochemistry of Single Quantum Dots. *Nature* **2011**, 479, 203-207.
- 25. Yuan, G.; Gomez, D. E.; Kirkwood, N.; Boldt, K.; Mulvaney, P., Two Mechanisms Determine Quantum Dot Blinking. *ACS Nano* **2018**, 12, 3397-3405.
- 26. Frantsuzov, P. A.; Volkan-Kacso, S.; Janko, B., Model of Fluorescence Intermittency of Single Colloidal Semiconductor Quantum Dots Using Multiple Recombination Centers. *Phys. Rev. Lett.* **2009**, 103, 207402.
- 27. Kuno, M.; Fromm, D. P.; Hamann, H. F.; Gallagher, A.; Nesbitt, D. J., "On"/"Off" Fluorescence Intermittency of Single Semiconductor Quantum Dots. *J. Chem. Phys.* **2001**, 115, 1028-1040.
- 28. Busov, V. K.; Frantsuzov, P. A., Models of Semiconductor Quantum Dots Blinking based on Spectral Diffusion. *Optics and Spectroscopy* **2019**, 126, 70-82.
- 29. Frantsuzov, P.; Kuno, M.; Jánko, B.; Marcus, R. A., Universal Emission Intermittency in Quantum Dots, Nanorods and Nanowires. *Nature Physics* **2008**, 4.

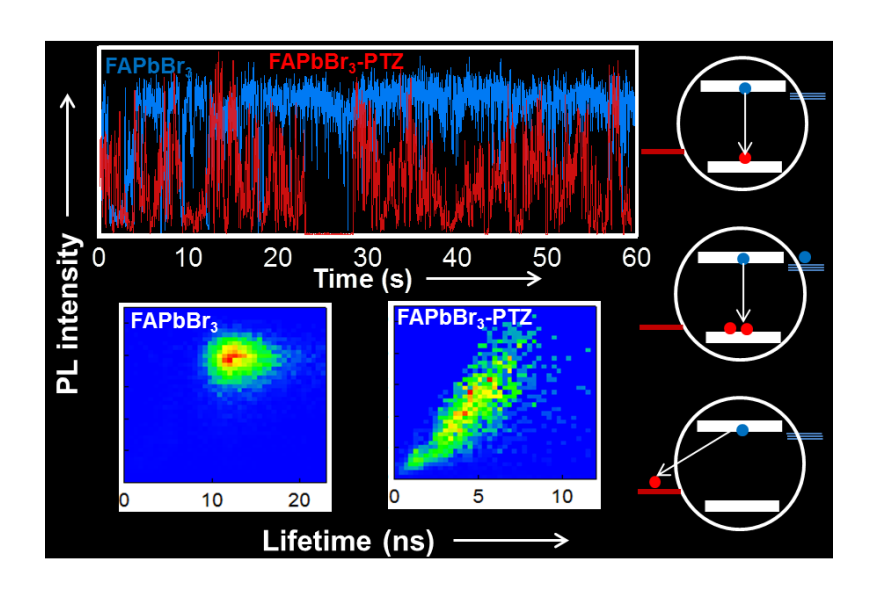
- 30. Frantsuzov, P. A.; Marcus, R. A., Explanation of Quantum Dot Blinking without the Long-Lived Trap Hypothesis. *Phys. Rev. B: Condens. Matter Mater. Phys.* **2005**, 72, 155321.
- 31. Park, Y.-S.; Lim, J.; Makarov, N. S.; Klimov, V. I., Effect of Interfacial Alloying *versus* "Volume Scaling" on Auger Recombination in Compositionally Graded Semiconductor Quantum Dots. *Nano Lett.* **2017**, 17, 5607–5613.
- 32. Rosen, S.; Schwartz, O.; Oron, D., Transient Fluorescence of the Off State in Blinking CdSe/CdS/ZnS Semiconductor Nanocrystals Is Not Governed by Auger Recombination. *Phys Rev Lett.* **2010**, 104, 157404.
- 33. Tenne, R.; Teitelboim, A.; Rukenstein, P.; Dyshel, M.; Mokari, T.; Oron, D., Studying Quantum Dot Blinking through the Addition of an Engineered Inorganic Hole Trap. *ACS Nano* **2013**, 7, 5084–5090.
- 34. Zhao, J.; Nair, G.; Fisher, B. R.; Bawendi, M. G., Challenge to the Charging Model of Semiconductor-Nanocrystal Fluorescence Intermittency from Off-State Quantum Yields and Multiexciton Blinking. *Phys Rev Lett.* **2010**, 104, 157403.
- 35. Seth, S.; Ahmed, T.; Samanta, A., Photoluminescence Flickering and Blinking of Single CsPbBr₃ Perovskite Nanocrystals: Revealing Explicit Carrier Recombination Dynamics. *J. Phys. Chem. Lett.* **2018**, 9, 7007–7014.
- 36. Nirmal, M.; Dabbousi, B.; Bawendi, M. G.; Macklint, J. J.; Trautmant, J. K.; Harrist, T. D.; Brus, L. E., Fluorescence Intermittency in Single Cadmium Selenide Nanocrystals. *Nature* **1996**, 383, 802–804.
- 37. Park, Y. S.; Bae, W. K.; Pietryga, J. M.; Klimov, V. I., Auger Recombination of Biexcitons and Negative and Positive Trions in Individual Quantum Dots. *ACS Nano* **2014**, 8, 7288-7296.
- 38. Spinicelli, P.; Buil, S.; X, X. Q.; Mahler, B.; Dubertret, B.; Hermier, J. P., Bright and Grey States in CdSe-CdS Nanocrystals Exhibiting Strongly Reduced Blinking. *Phys Rev Lett.* **2009**, 102, 136801.
- 39. Yarita, N.; Tahara, H.; Saruyama, M.; Kawawaki, T.; Sato, R.; Teranishi, T.; Kanemitsu, Y., Impact of Postsynthetic Surface Modification on Photoluminescence Intermittency in Formamidinium Lead Bromide Perovskite Nanocrystals. *J. Phys. Chem. Lett.* **2017**, 8, 6041–6047.
- 40. Reid, K. R.; McBride, J. R.; Croix, A. D. L.; Freymeyer, N. J.; Click, S. M.; Macdonald, J. E.; Rosenthal, S. J., Role of Surface Morphology on Exciton Recombination in Single Quantum Dot-in- Rods Revealed by Optical and Atomic Structure Correlation. *ACS Nano* **2018**, 12, 11434–11445.
- 41. Kim, T.; Jung, S. I.; Ham, S.; Chung, H.; Kim, D., Elucidation of Photoluminescence Blinking Mechanism and Multiexciton Dynamics in Hybrid Organic–Inorganic Perovskite Quantum Dots. *Small* **2019**, 15, 1900355.
- 42. Gibson, N. A.; Koscher, B. A.; Alivisatos, A. P.; Leone, S. R., Excitation Intensity Dependence of Photoluminescence Blinking in CsPbBr₃ Perovskite Nanocrystals. *J. Phys. Chem. C* **2018**, 122, 12106–12113.
- 43. Li, B.; Huang, H.; Zhang, G.; Yang, C.; Guo, W.; Chen, R.; Qin, C.; Gao, Y.; Biju, V.; Rogach, A. L.; Xiao, L.; Jia, S., Excitons and Biexciton Dynamics in Single CsPbBr₃ Perovskite Quantum Dots. *J. Phys. Chem. Lett.* **2018**, 9, 6934–6940.

- 44. Yuan, G.; Ritchie, C.; Ritter, M.; Murphy, S.; Gómez, D. E.; Mulvaney, P., The Degradation and Blinking of Single CsPbI₃ Perovskite Quantum Dots. *J. Phys. Chem. C* **2018.** 122, 13407–13415.
- 45. Hu, F.; Zhang, H.; Sun, C.; Yin, C.; Lv, B.; Zhang, C.; Yu, W. W.; Wang, X.; Zhang, Y.; Xiao, M., Superior Optical Properties of Perovskite Nanocrystals as Single Photon Emitters. *ACs Nano* **2015**, *9*, 12410–12416.
- 46. Tachikawa, T.; Karimata, I.; Kobori, Y., Surface Charge Trapping in Organolead Halide Perovskites Explored by Single-Particle Photoluminescence Imaging. *J. Phys. Chem. Lett.* **2015**, 6, 3195–3201.
- 47. Halder, A.; Pathoor, N.; Chowdhury, A.; Sarkar, S. K., Photoluminescence Flickering of Micron-Sized Crystals of Methylammonium Lead Bromide: Effect of Ambience and Light Exposure. *J. Phys. Chem. C* **2018**, 122, 15133–15139.
- 48. Merdasa, A.; Tian, Y.; Camacho, R.; Dobrovolsky, A.; Debroye, E.; Unger, E. L.; Hofkens, J.; Sundstrom, V.; Scheblykin, I. G., "Supertrap" at Work: Extremely Efficient Nonradiative Recombination Channels in MAPbI₃ Perovskites Revealed by Luminescence Super-Resolution Imaging and Spectroscopy. *ACS Nano* **2017**, 11, 5391-5404.
- 49. Pathoor, N.; Halder, A.; Mukherjee, A.; Mahato, J.; Sarkar, S. K.; Chowdhury, A., Fluorescence Blinking Beyond Nanoconfinement: Spatially Synchronous Intermittency of Entire Perovskite Microcrystals. *Angew. Chem.* **2018**, 130, 11777–11781.
- 50. Zhang, A.; Dong, C.; Ren, J., Tuning Blinking Behavior of Highly Luminescent Cesium Lead Halide Nanocrystals through Varying Halide Composition. *J. Phys. Chem. C* **2017**, 121, 13314–13323.
- 51. Raino, G.; Nedelcu, G.; Protesescu, L.; Bodnarchuk, M. I.; Kovalenko, M. V.; Mahrt, R. F.; Stöferle, T., Single Cesium Lead Halide Perovskite Nanocrystals at Low Temperature: Fast SinglePhoton Emission, Reduced Blinking, and Exciton Fine Structure. *ACS Nano* **2016**, 10, 2485–2490.
- 52. Zhang, A.; Bian, Y.; Wang, J.; Chen, K.; Dong, C.; Ren, J., Suppressed Blinking Behavior of CdSe/CdS QDs by Polymer Coating. *Nanoscale* **2016**, 8, 5006-5014.
- 53. Li, B.; Zhang, G.; ZaoWang; Li, Z.; RuiyunChen; ChengbingQin; YanGao; LiantuanXiao; Jia, S., Suppressing the Fluorescence Blinking of Single Quantum Dots Encased in *N*-type Semiconductor Nanoparticles. *Sci Rep.* **2016**, 6, 32662.
- 54. Mahler, B.; Spinicelli, P.; Buil, S.; Quelin, X.; Hermier, J.-P.; Dubertret, B., Towards Non-Blinking Quantum Dots: The Effect of Thick Shell. *Proc. SPIE* **2009**, 7189, 718903.
- 55. Tang, X.; Yang, J.; Li, S.; Liu, Z.; Hu, Z.; Hao, J.; Du, J.; Leng, Y.; Qin, H.; Lin, X.; Lin, Y.; Tian, Y.; Zhou, M.; Xiong, Q., Single Halide Perovskite/Semiconductor Core/Shell Quantum Dots with Ultrastability and Nonblinking Properties. *Adv. Sci.* **2019**, 6, 1900412.
- 56. Mondal, N.; De, A.; Samanta, A., Biexciton Generation and Dissociation Dynamics in Formamidinium- and Chloride-Doped Cesium Lead Iodide Perovskite Nanocrystals. *J. Phys. Chem. Lett.* **2018**, 9, 3673–3679.
- 57. Chen, J.; Messing, M. E.; Zheng, K.; Pullerits, T., Cation-Dependent Hot Carrier Cooling in Halide Perovskite Nanocrystals. *J. Am. Chem. Soc.* **2019**, 141, 3532–3540.

- Dong, C.; Qian, H.; Fang, N.; Ren, J., Study of Fluorescence Quenching and 58. Dialysis Process of CdTe Quantum Dots, Using Ensemble Techniques and Fluorescence Correlation Spectroscopy. J. Phys. Chem. B 2006, 110, 11069-11075.
- Patra, S.; Samanta, A., A Fluorescence Correlation Spectroscopy, Steady-State, and Time-Resolved Fluorescence Study of the Modulation of Photophysical Properties of Mercaptopropionic Acid Capped CdTe Quantum Dots upon Exposure to Light. J. Phys. Chem. C 2013, 117, 23313-23321.
- Yettapu, G. R.; Talukdar, D.; Sarkar, S.; Swarnkar, A.; Nag, A.; Ghosh, P.; 60. Mandal, P., Terahertz Conductivity within Colloidal CsPbBr₃ Perovskite Nanocrystals: Remarkably High Carrier Mobilities and Large Diffusion Lengths. Nano Lett. 2016, 16, 4838-4848.
- 61. Mosconi, E.; Angelis, F. D., Mobile Ions in Organohalide Perovskites: Interplay of Electronic Structure and Dynamics. ACS Energy Lett. 2016, 1, 182–188.
- Chen, S.; Wen, X.; Sheng, R.; Huang, S.; Deng, X.; Green, M. A.; Ho-Baillie, A., Mobile Ion Induced Slow Carrier Dynamics in Organic-Inorganic Perovskite CH₃NH₃PbBr₃. ACS Appl. Mater. Interfaces **2016**, 8, 5351-5357.

CHAPTER 5

Impact of Hole Transfer on Photoluminescence Blinking of Single FAPbBr₃ Nanocrystals



Overview

Transfer or extraction of charge carriers from photoexcited perovskite nanocrystals (NCs) is a process of great interest in photovoltaic applications. In this work, we report our findings interfacial hole transfer dynamics from immobilized and freely diffusing single NCs of FAPbBr₃ to surface adsorbed phenothiazine (PTZ) by using single particle fluorescence spectroscopy employing time-tagged-time-resolved method. While FAPbBr₃ NCs show two-state (ON-OFF) blinking, FAPbBr₃-PTZ NCs exhibit a complex blinking pattern comprising several levels of photoluminescence (PL) intensity due to the hole transfer process. A careful analysis of the PL decay behavior of different intensity levels and fluorescence lifetime intensity distribution (FLID) pattern reveals a heterogeneous nature of the hole transfer dynamics. Both particle to particle and time-dependent variation of hole transfer rate of a given particle are identified. Direct observation of short-lived (<100 ns) charge separated state, FAPbBr₃-PTZ⁺, in immobilized state of NCs, is again supported by the FCS measurement. Increase of dispersive nature of blinking dynamics due to heterogeneity in hole transfer rate is further revealed by FCS measurements.

5.1. Introduction

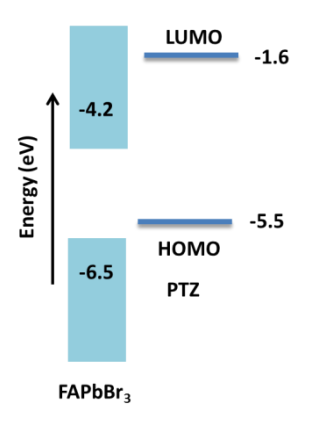
Lead halide based perovskites NCs continue to receive enormous attention as a promising semiconducting material for photovoltaic and optoelectronic applications because of their excellent properties such as broad absorption with high absorption crosssection, tunable emission with narrow band width, high photoluminescence quantum vield (PLOY), long carrier diffusion length, and intrinsic defect tolerance. 1-7 Since the first report in 2009,8 the power conversion efficiency of solar cells based on these materials has improved rapidly and reached to 25% till now. As the performance of these devices depends on the efficiency of the extraction/transfer of the charge carriers from these semiconducting materials along with the other processes. 10 investigation of the exciton dissociation processes in presence of electron or hole acceptor is important. In this regard most of our current understanding of charge carrier dynamics from perovskite is derived by using ultrafast transient spectroscopy and ensemble-averaged measurements, 11-17 where most of the time, we get an average of charge transfer dynamics.

However there is possibility that these processes can generate heterogeneity of charge transfer rates, which is difficult to estimate in ensemble-averaged measurement. The heterogeneity can be static (varies among different single NCs) and dynamic (varies with time for a single NC) depending on the number of adsorbed charge acceptors on the surface of NCs as well as fluctuating electronic coupling strength among them. 18-24 In this context single particle fluorescence spectroscopy is a powerful tool to probe those distributions ^{18, 20, 25, 26} and can provide further insights into the heterogeneity of charge transfer dynamics. Hence it is important to study the charge transfer processes at the single particle level to understand the distribution of processes and the nature of those NCs.

Distribution of charge transfer processes has been studied most extensively for single metal chalcogenide based quantum dots (QDs) by studying the PL intermittency or blinking. 18-24 PL blinking arises due to participation of trap states in the charge carrier recombination processes. 27-34 Several mechanisms have been proposed to understand the blinking behavior and, radiative and nonradiative recombination paths. Among them trion-mediated recombination (AC blinking) through long-lived trap states and,³⁵ nonradiative band-edge carrier recombination (NBC blinking)³⁵ and hot-carrier trapping mediated recombination (HC blinking)³⁶ through short-lived trap states, are widely accepted mechanisms for blinking of semiconductors. Now in presence of charge acceptor there is introduction of another nonradiative recombination channels (along with the trap mediated recombination) in the photo-excited QDs and the blinking dynamics of those QDs is modulated by the charge transfer process. More insights into the heterogeneity of charge transfer dynamics have been obtained through studies of charge transfer in single metal chalcogenide based QD-charge acceptor complexs.¹⁸⁻²⁴

Single perovskite nanocrystals (NCs) exhibit PL blinking due to the involvement of trap states in recombination of the photo-generated charge carriers. Although the blinking mechanism can be quite diverse for the perovskite NCs depending on the composition and surface properties, they show many similarities with PL blinking in conventional metal chalcogenide QDs. 27, 29, 34, 37-45 Introduction of additional pathways for charge recombination/transfer leads to a change in PL blinking pattern of the NCs. There is modulation of blinking dynamics of the single FAPbBr₃ perovskite NCs for electron transfer to ITO and n-type TiO₂. 31, 46 and hole to CuSCN³⁰. There are very few reports

Scheme 5.1: Alignment of the energy levels of FAPbBr₃ NCs and PTZ. 20, 47



Chapter 5 Impact of hole transfer...

available till now which probe the interfacial charge transfer from single NCs. Hence further extensive studies are needed at the single particle level for different charge acceptors to understand charge transfer process and its distribution in details and have an efficient charge acceptor to build novel devices.

In this work, we investigate hole transfer from single FAPbBr₃ NCs to phenothiazine (PTZ) whose HOMO and LUMO levels and the valence and conduction bands of the FAPbBr₃ NCs (Scheme 5.1) permit hole transfer from photoexcited NCs to PTZ. Ensemble averaged measurements, ultrafast transient and time resolved terahertz spectroscopy,^{15, 16} has been used previously for studying hole transfer dynamics from CsPbBr₃ perovskite NCs to PTZ. For the former study half-life of hole transfer and subsequent charge recombination are reported as 49 ps and 1 ns respectively¹⁶ and for the later hot-hole transfer is observed with time scale of sub-300 fs.¹⁵ However, understanding those processes at the single particle level and studying the distribution of hole transfer rate is still lacking. This study of PL blinking in the mobilized and freely diffusing state of FAPbBr₃ NCs with and without PTZ provides further details of hole transfer dynamics and heterogeneity of hole transfer rate. We observed not only static but also dynamic heterogeneity of hole transfer rate. Finally we proposed a model to account for the observed effects of hole transfer on single NC blinking dynamics.

5.2. Results

5.2.1. Steady-state measurements

The FAPbBr₃ NCs (average edge length ~12 nm, Figure AIII.1), prepared following a reported procedure, ⁴⁸ details of which are provided in the 'Chapter 2', were centrifuged and dispersed in hexane or ODE for studies. Absorption and emission spectra of the NCs are presented in Figure 5.1a. These NCs are highly fluorescent (PLQY >90%) and the emission peak is observed at 527 nm. PTZ adsorbed NCs (indicated hereafter as FAPbBr₃-PTZ NCs) were obtained by sonication of a mixture of a colloidal dispersion of the NCs and PTZ. While the absorption spectra of FAPbBr₃ and FAPbBr₃-PTZ NCs are

almost identical, the PL of FAPbBr $_3$ -PTZ NCs much lower (Figure 5.1a) due to hole transfer from photoexcited FAPbBr $_3$ NCs to the adsorbed PTZ moiety. $^{15,\,16}$

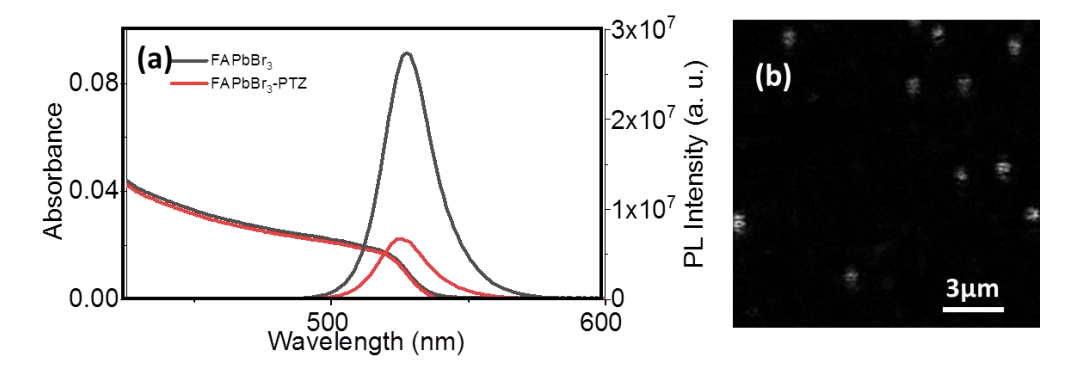


Figure 5.1: (a) Absorption and emission spectra (λ_{ex} = 405 nm) of FAPbBr₃ and FAPbBr₃-PTZ NCs. (b) PL intensity image of a film of a very dilute solution of the sample with well separated NCs obtained using confocal microscope.

5.2.2. PL blinking study

To examine the effect of hole transfer on the blinking dynamics of single NCs, by confocal fluorescence microscopy technique employing a time-tagged time-resolved PL (TTTR-PL) method. For this study, a diluted dispersion (\sim pM) of the NCs was mixed with polystyrene (PS) in toluene and drop-casted on a cover glass and dried under vacuum. This film was excited by a 485 nm pulsed laser (fwhm 176 ps) with a repetition rate of 10 MHz and average power of 0.05 μ W. Under this experimental condition, each NC was found to absorb on an average \sim 0.08 photon per pulse. A confocal PL microscopy image of a typical film of well separated NCs is shown in Figure 5.1b.

Among the ~50 single FAPbBr₃ NCs examined, a large majority of these particles (44 NCs) show low fluctuations of PL intensity and remains mostly in the high intensity (ON) state. A representative PL trace of this class of single FAPbBr₃ NCs is shown in Figure 5.2a. The corresponding histograms of fluorescence intensity indicates very low occurrence of low intensity states compared to the ON states. The binary switching

between ON and OFF states (states near to background) are prominent in rest of the NCs, which is discussed in Figure AIII.3.

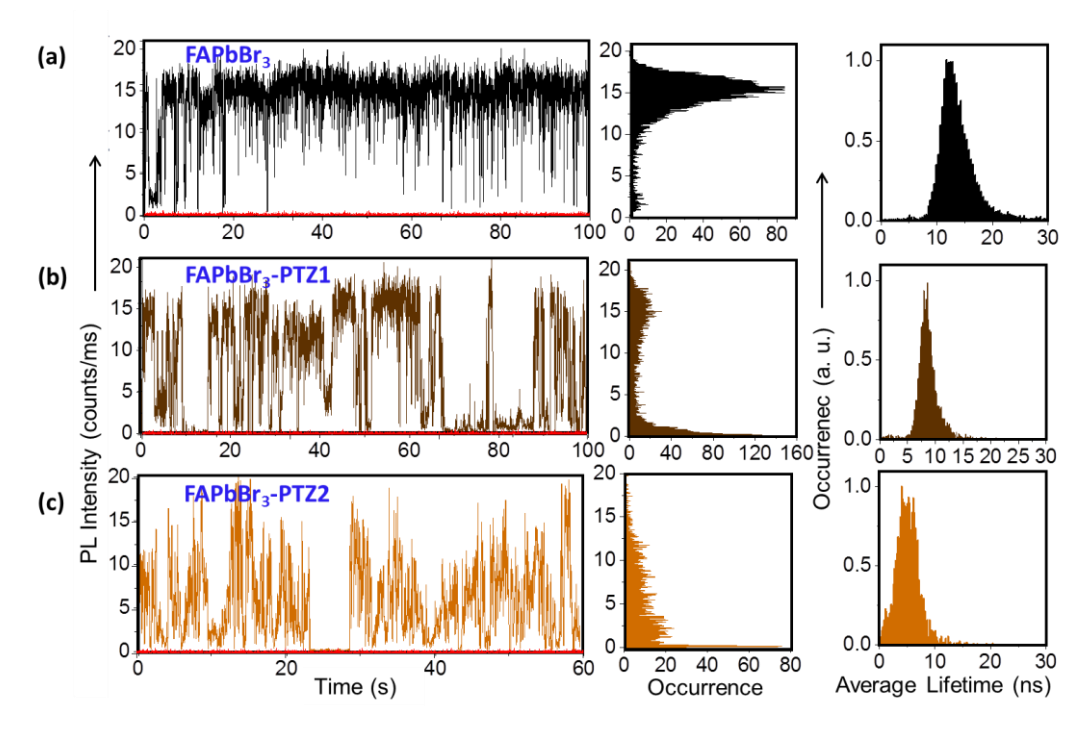


Figure 5.2: PL intensity trajectories with bin time of 20 ms (where the background is shown by red line) and their corresponding PL intensity and lifetime distributions of FAPbBr₃ (a), FAPbBr₃-PTZ1 (b) and FAPbBr₃-PTZ2 (c) NCs.

Interestingly FAPbBr₃-PTZ NCs exhibit strikingly different blinking behavior. These NCs exhibit several intermediate states between the ON and OFF states. Moreover, the blinking pattern is found to vary from particle to particle. Among the 50 NCs examined, PL intensity traces of two such representative NCs (labelled as FAPbBr₃-PTZ1 and FAPbBr₃-PTZ2) are shown here in Figure 5.2b and 5.2c. A wide distribution of the PL intensity states with low occurance for the high intensity states is clearly evident. This blinking pattern is quite different from the observation of a single intermediate state in case of CuSCN as hole acceptoer.³⁰ It is also evident from those occurrence histograms (Figure 5.2a, 5.2b and 5.2c) that after hole transfer the fraction of ON states has decreased along with the increase of OFF state fraction. A decrease of average lifetime in FAPbBr₃-

PTZ NCs (Figure 5.2b and 5.2c) compared to FAPbBr₃ NCs (Figure 5.2a) alone is due to the hole transfer process. The decrease in lifetime is more in case of FAPbBr₃-PTZ2 NC compared to FAPbBr₃-PTZ1 presumably because of a large number of adsorbed PTZ on the surface of NCs in the case of former.²⁰

To understand the origin of different intensity states we have analyzed the PL decay dynamics of different PL intensity levels. For FAPbBr₃, we have analyzed two different levels, denoted as R1 and R2 (Figure 5.3a), whereas for FAPbBr₃-PTZ NCs, as there are several intermediate states, we have examined four different levels (T1, T2, T3 and T4 for FAPbBr₃-PTZ1 and P1, P2, P3 and P4 for FAPbBr₃-PTZ2), displayed in Figure 5.3b and 5.3c. The PL decay curve corresponding to the highest intensity level of all the NCs is single exponential. For FAPbBr₃ NCs, the highest intensity level (R1) is associated with a lifetime component of 12 ns (τ_1) , and is attributed to the neutral exciton emission. ^{29, 31} For the lowest intensity level (R2) of FAPbBr₃ NCs, the PL decay profile is biexponential with lifetime components of 3.5 ns (τ_1) and 0.45 ns (τ_2) . This short component (τ_2) can be attributed to trion recombination, based on literature.³⁰ This suggests trion mediated recombination; referred to earlier as AC mechanism is responsible for blinking of FAPbBr₃ NCs. Due to low occurrence compared to exciton recombination, the trion recombination is not visible from the fluorescence lifetime intensity distribution (FLID) pattern (Figure 5.3b). For the rest of the NCs (5 NCs out of 49) along with the AC, hot carrier trapping mediated HC kind of blinking is also observed (Figure AIII.3), but that kind of NCs are less in number.

For FAPbBr₃-PTZ1 and FAPbBr₃-PTZ2 NCs, the lifetime component of the highest intensity level is 8 ns (for T1 region) and 6 ns (for P1 region), respectively. Average exciton lifetimes for the highest intensity ON state calculated for all the ~50 studied NCs are ~12 ns and ~6.5 ns for the FAPbBr₃ and FAPbBr₃-PTZ NCs respectively (Figure AIII.2). A lower lifetime of the highest intensity state is attributed to the hole transfer process, which introduces a new non-radiative recombination channel that increases the exciton decay rate. A distribution of lifetime of the highest intensity state (Figure AIII.2) indicates a heterogeneity of the hole transfer rates. This heterogeneity is much greater in

FAPbBr₃-PTZ NCs compared to FAPbBr₃ due to the different number of PTZ molecules adsorbed on the NCs surface in addition to different surface environment.¹⁸

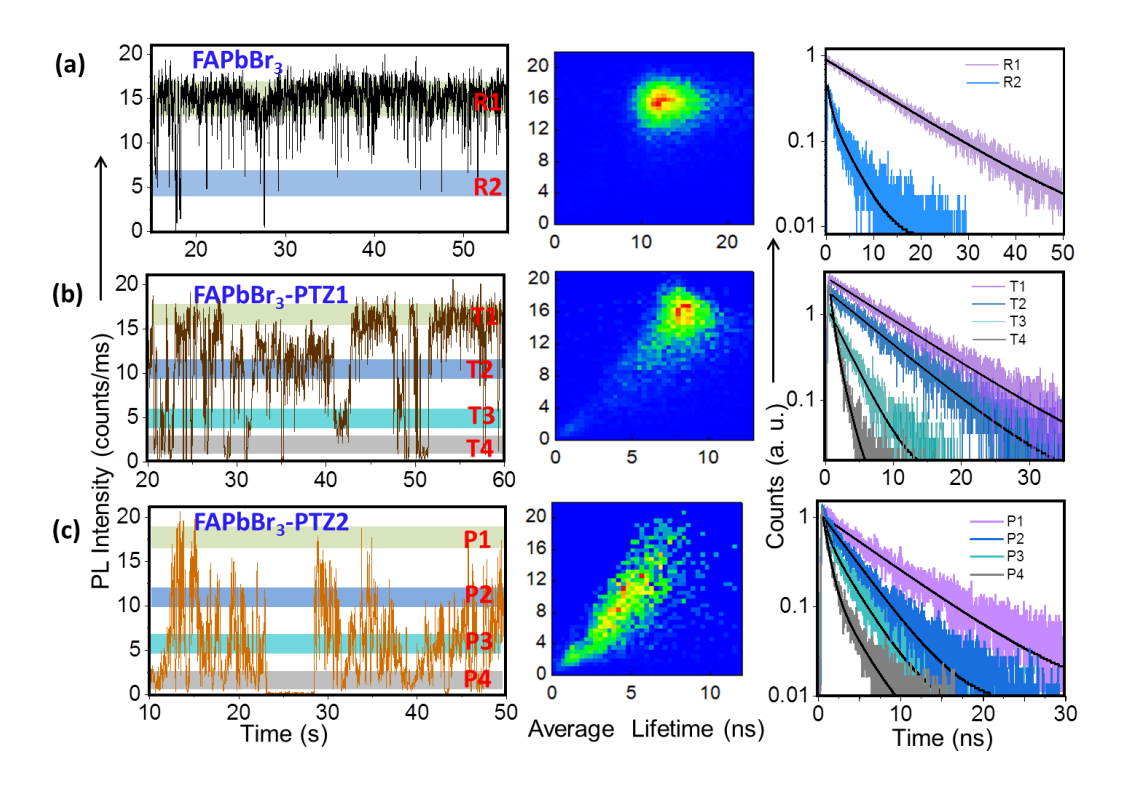


Figure 5.3: PL intensity trajectories (in short time region) for (a) FAPbBr₃, (d) FAPbBr₃-PTZ1 and (g) FAPbBr₃-PTZ2 NCs. Different intensity levels of which PL decay profiles were measured are indicated by color bars, FLID patterns and PL intensity decay of corresponding intensity regions.

We have analyzed the PL decay profiles for the lower intensity levels for FAPbBr₃-PTZ NCs to understand the reason for appearance of several PL intensity levels due to hole transfer. The lifetime decreases as we move from the highest intensity levels (T1 or P1) to the lower intensity levels of FAPbBr₃-PTZ1 and FAPbBr₃-PTZ2 NCs. For the FAPbBr₃-PTZ1 NCs PL decay is single exponential up to T3 level and lifetime (τ_1) gradually decreases from 8.6 ns to 2.2 ns (Table AIII.2). Intensity–lifetime scaling of the three different intensity regions (T1, T2 and T3) is as follows

$$\eta = k_{T1}: k_{T2}: k_{T3} = \frac{I_{T1}}{\tau_{T1}}: \frac{I_{T2}}{\tau_{T2}}: \frac{I_{T3}}{\tau_{T3}} = 1.1: 1.0: 0.92$$

A near-unity ratio of the radiative recombination rates of these intensity regions suggests the competition between a fixed radiative rate and variable nonradiative rates, which is typical signature of PL blinking following non-radiative band-edge carrier (NBC) recombination.³⁵ This kind of near-unity ratio is also observed for FAPbBr₃-PTZ2 for P1 and P2 regions. From this analysis, we obtain two important informations. The observation of varying nonradiative rate in PTZ adsorbed systems, which in the present case is due to hole transfer, is dynamic in nature. This consequently results continuous emissive states of different levels.⁴⁹ Secondly, in our case, η being far from 2, indicates that hole transfer to PTZ does not lead to formation of trion (as the rate for trion mediated recombination is almost double of the neutral exciton recombination). Trion (negative) formation was observed previously for hole transfer from FAPbBr₃ NC to CuSCN and also for core-shell CdSe QD to PTZ due to formation of long-lived charge separated state. 20, 35 However, in our case the hole in PTZ and electron in the NC recombines at a faster rate before generation of another exciton and consequently no negative trion is formed, which indicates the formation of short-lived (<100 ns, as repetition rate of excitation pulse 10 MHz) charge separated states (FAPbBr₃-PTZ⁺). Moreover at the lower intensity levels (T4 for FAPbBr₃-PTZ1 and P3 and P4 for FAPbBr₃-PTZ2) a very short component of ~0.45 ns arises, which well matches with the value of trion recombination due to presence of long-lived traps in the NCs which is observed in the FAPbBr₃ NC before hole transfer and yet present in FAPbBr₃-PTZ NCs also. Unlike to FAPbBr₃, several states are clearly visible in the FLID patterns of FAPbBr₃-PTZ NCs (Figure 5.3b and 5.3c) and presence of those intermediate states is more prominent in FAPbBr₃-PTZ2 NC than FAPbBr₃-PTZ1. The FLID patterns (for 50 FAPbBr₃-PTZ NCs are shown in Figure AIII.5) look like a mixture of linear and curvature nature as along with trion mediated recombination process (AC, due to presence of electron trap in the NC) nonradiative band edge carrier recombination through short-lived charge separated state, FAPbBr₃-PTZ⁺ is also responsible for the blinking of PL of FAPbBr₃-PTZ NCs.

Although all the measurements were carried out on well separated single NCs (Figure 5.1b), considering the several intermediate intensity states one can think that the emission is not from single NC but rather from clusters. This possibility can be nullified considering the following argument: Let us assume that cluster consist of two NCs. (i) If the two NCs have different PL lifetime then the decay curve for the P1 and T1 would have been bi-exponential which is not the case. (ii) If they have same lifetime then η would have been >1.0, because then intensity would have been twice with same lifetime, which is again not the case. Hence it is evident that the emission is from single FAPbBr₃-PTZ NC.

Further we provide an estimate range of hole transfer rate distribution. For that we consider 12 ns as the intrinsic lifetime ($1/k_0$) of FAPbBr₃ NC, which is the average lifetime of ON states of ~50 NCs. There is a distribution of hole transfer rates ($k = k_0 + k_{HT}$), considering static and dynamic heterogeneity. The latter can be estimated from a single NC PL trajectory. For FAPbBr₃-PTZ1 and FAPbBr₃-PTZ2 NCs, the estimated hole transfer rate (k_{HT}) fluctuates from ~0.5X10⁸ to >0.5X10⁹ s⁻¹ and ~1X10⁸ to >0.5X10⁹ s⁻¹ respectively. The distribution of lifetime shown in Figure AIII.2 corresponds to a static variation of k_{HT} from 0 to >0.4X10⁹ s⁻¹. Such heterogeneity of charge transfer rate is reported previously by Lian group for electron transfer from single CdSe/ZnS QDs.²²

5.2.1. FCS study

Additional insight on blinking dynamics due to hole transfer process is obtained from FCS studies on the freely diffusing NCs with and without PTZ in the μ s-ms time domain. In this technique, fluctuation of PL intensity of a highly dilute solution (nM) of the NCs in a small volume of the sample (typically ~ 1 fL) is measured using a confocal fluorescence microscope. Correlation curves generated from the fluctuation of PL intensity (which can be due to diffusion, physical or chemical reactions, aggregation, etc) are analyzed using equations corresponding to different models. In our case, the fluorescence correlation curves are found to be best represented by equation 5.1 (Figure 5.4), according to which two processes contribute to the PL fluctuation; a three-

dimensional diffusion process along with a stretched exponential decay component representing hole transfer process.^{27, 50} This model has been used previously for metal-chalcogenide quantum dots as well as perovskite NCs also.⁵¹⁻⁵³ The amplitude of correlation at time τ , $G(\tau)$, is expressed as

$$G(\tau) = \left[1 + \frac{\tau}{1 - T} exp\left(-\frac{\tau}{\tau_T}\right)^{\beta}\right] 1 / < N > (1 + \tau/\tau_D)^{-1} (1 + \tau/\kappa^2 \tau_D)^{-1/2}$$
(5.1)

Where, $\langle N \rangle$ is the average number of particles undergoing reversible PL intensity fluctuation in the observation volume, τ_D is the diffusion time of the NCs, T is the fraction of particles in their "off" state, and τ_T is the dark-state relaxation time or blinking time. β is a stretching exponent having a value between 0 to 1 indicating the distribution of τ_T . κ (= ω_Z/ω_{xy}) is the structure parameter of the observation volume; ω_z and ω_{xy} are the longitudinal and transverse radii, respectively.

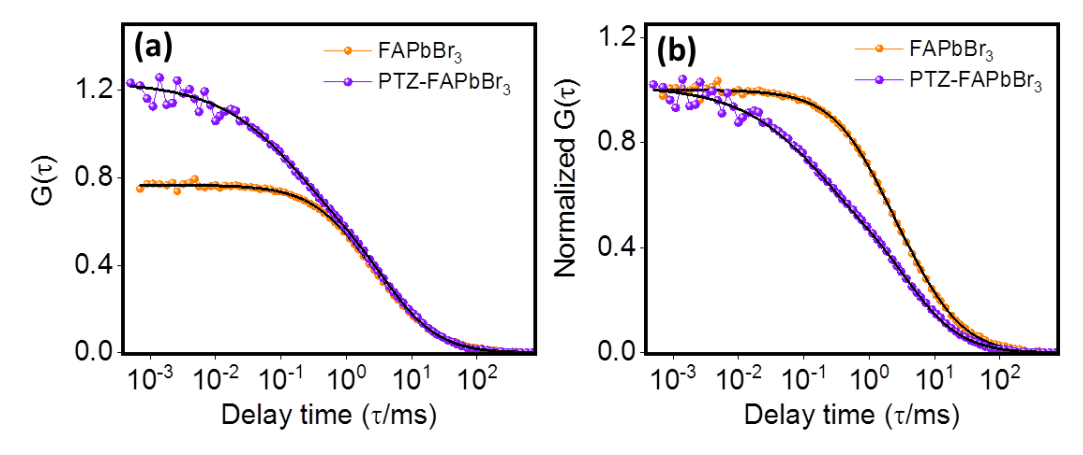


Figure 5.4: Fluorescence correlation curves of FAPbBr₃ and FAPbBr₃-PTZ NC solutions in ODE in (a) absolute and (b) normalized scale.

Table 5.1: Estimated blinking parameters, G(0), τ_D , <N>, β , τ_T and T values of the FAPbBr₃ and FAPbBr₃-PTZ NCs, as obtained from FCS measurements

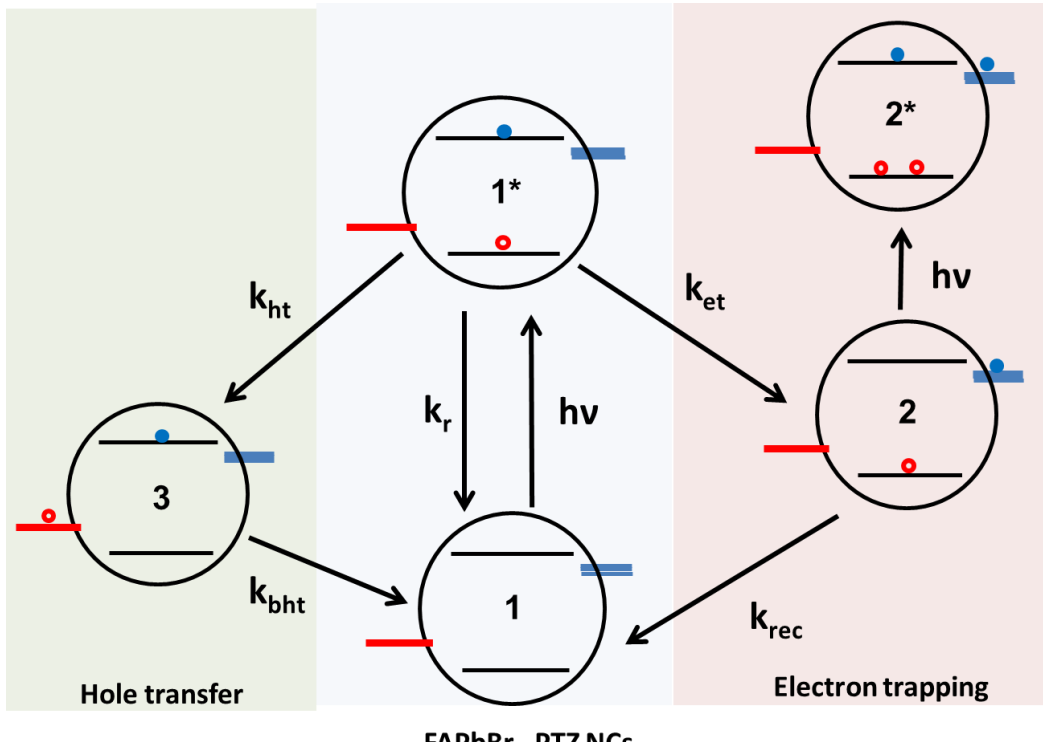
NCs	$\tau_{\mathrm{D}}\left(\mathrm{ms}\right)$	G(0)	<n></n>	β	$\tau_{\rm T}({\rm ms})$	T
FAPbBr	4.2±0.22	0.75±0.02	1.6±0.10	1	0.96±0.04	0.18±0.02
FAPbBr	4.1±0.36	1.2±0.11	1.6±0.31	0.52±0.06	0.15±0.04	0.47±0.03
₃ -PTZ						

Figure 5.4 indicates an increase in amplitude of the correlation at zero time delay, G(0), on addition of PTZ along with a change in shape of the correlation curve. A close examination of the various parameters associated with blinking (Table 5.1), as obtained from analysis of the data, shows that for FAPbBr₃ NCs the correlation data is represented by simple exponential (β =1), whereas for FAPbBr₃-PTZ NCs it fits with stretched exponential $(0 \le \beta \le 1)$ with β value 0.52±0.02. This indicates that charge carrier trapping process occurs nearly with a single rate in FAPbBr₃ NCs (consistent with the high PLQY of NCs), whereas in FAPbBr₃-PTZ NCs β <1 indicates that hole transfer opens up additional non-radiative recombination channels, causing heterogeneous hole transfer process with distribution of rate constants. It leads to increase of T value from 0.18 to 0.47 and further justifies the increase of G(0) value (from 0.75 to 1.2), as G(0) is defined as 1/[<N>(1-T)], and <N> remains fixed. Interestingly we observed decrease of dark state relaxation time (τ_T) from 0.96 ms to 0.15 ms upon hole transfer. Now in case of only FAPbBr₃ NCs dark states arises due to non-radiative recombination through trap states whereas in FAPbBr₃-PTZ NCs in addition to trap states hole transfer is also responsible. This decrease of τ_T consequently suggests that hole transfer induces short-lived chargeseparated state in FAPbBr₃-PTZ NCs. 21, 51 These observations are in agreement with the blinking kinetics in the immobilized state.

5.3. Discussion

To account for the effect of the hole acceptor on the blinking of single NC, we propose a model considering various states and their interconversion in FAPbBr₃-PTZ system. As shown in Scheme 2, a neutral NC is excited from the ground state (1) to excited state (1*), which can relax to ground state (1) by intrinsic relaxation process. This overall generates ON state with decay rate of $\sim 10^8 \, \text{s}^{-1}$. The electron can be trapped (intrinsic trap state) with rate constant, k_{et} . When the electron stays there in this state (at state 2 in Scheme 2) for a long duration (>100 ns, in our case excitation repetition pulse rate 10 MHz), the excitation of the NC generates a positive trion (2*) which can relax radiatively or via a rapid nonradiative Auger recombination process (not shown in Scheme 2). This leads to AC mechanism as the reason for blinking in both the FAPbBr₃ and FAPbBr₃-PTZ NCs. Those rate constants and states are assumed to be same in free FAPbBr₃ and FAPbBr₃-PTZ NCs.

Scheme 5.2: Possible charge separation and recombination processes in FAPbBr₃-PTZ NCs. 1 and 1* are the ground and excited states of neutral FAPbBr₃-PTZ NC in ON state; k_r is the intrinsic decay rate of NCs. Electron trapping (with rate constant k_{et}) to long-lived traps converts 1* to state 2; again excited and converts to 2*, which is low emissive (grey) or OFF state. In presence of hole acceptor additional pathway is created. 1* can be quenched due to hole transfer (with rate constant k_{ht}) to PTZ forming state 3. State 3 is short-lived and converts back to state 1 (with rate constant k_{bht}). Time dependent fluctuation of hole transfer rate creates several emissive states [$k_{ht}(t)$].



FAPbBr₃-PTZ NCs

On the other hand, the presence of hole acceptor introduces additional pathways for relaxation of the carriers in FAPbBr₃-PTZ NCs. Hole transfer from excited FAPbBr₃ NC to PTZ (with rate k_{ht}) generates a charge separated state (3). Now as the charge separated state has short lifetime (<100 ns), hence before generation of another exciton (consequently negative trion), the electron in NCs and hole in the PTZ recombines to neutral state (1). A large dynamic fluctuation of hole transfer rate [kht(t)] is observed in a single FAPbBr₃-PTZ NC which leads to fluctuation of PL intensity over different intensity regions. Hence hole transfer induces another mechanism of blinking in single FAPbBr₃-PTZ NC.³⁵ This fluctuation of hole transfer rate in a single FAPbBr₃-PTZ NC can be due to change of strength of electronic coupling and driving force with time between the NC and the adsorbate. Such change is also observed for electron transfer from CdSe/ZnS QDs and is attributed to fluctuation of conformation of adsorbate or charge present in the QD.²²

5.4. Conclusion

In summary, photoinduced hole transfer from single FAPbBr₃ NC to the surface adsorbed PTZ molecules has been studied in immobilized and freely diffusing state of single NCs by monitoring the PL blinking. The hole transfer process enhances the fluctuation of the PL intensity and introduces several intermediate intensity and low intensity states. The hole transfer process shortens the lifetimes of ON-states in the FAPbBr₃-PTZ NCs. A distribution of hole transfer rate among the particles, likely reflecting the distribution of PTZ-NC ratio in the sample. Fluctuation of hole transfer rate is observed with fixed radiative rate for a single FAPbBr₃-PTZ NC. Thus dynamic heterogeneity increases the possibility of more intermediate emissive states. Short lived charge separated state is evident from no formation of negative trions. This is further supported by the FCS study, showed shortening of dark state relaxation time. Hence due to presence of long lived trap states, only FAPbBr₃ NC shows AC blinking mechanism, whereas in FAPbBr₃-PTZ NC in addition to AC mechanism non-radiative band edge recombination through hole acceptor is also responsible for blinking. We believe that the fundamental insight obtained from our study will be helpful in better utilization of these materials in devices.

References

- Chen, Q.; Wu, J.; Ou, X.; Huang, B.; Almutlaq, J.; Zhumekenov, A. A.; Guan, X.; 1. Han, S.; Liang, L.; Yi, Z.; Li, J.; Xie, X.; Wang, Y.; Li, Y.; Fan, D.; Teh, D. B. L.; All, A. H.; Mohammed, O. F.; Bakr, O. M.; Wu, T.; Bettinelli, M.; Yang, H.; Huang, W.; Liu, X., Allinorganic Perovskite Nanocrystal Scintillators. Nature 2018, 561, 88-93.
- Gong, M.; Sakidja, R.; Goul, R.; Ewing, D.; Casper, M.; Stramel, A.; Elliot, A.; Wu, J. Z., High-Performance All-Inorganic CsPbCl₃ Perovskite Nanocrystal Photodetectors with Superior Stability. ACS Nano 2019, 13, 1772-1783.
- Kang, J.; Wang, L. W., High Defect Tolerance in Lead Halide Perovskite CsPbBr₃. J. Phys. Chem. Lett. **2017**, 8, 489-493.
- Kovalenko, M. V.; Protesescu, L.; Bodnarchuk, M. I., Properties and Potential Optoelectronic Applications of Lead Halide Perovskite Nanocrystals. Science 2017, 358, 745-750.
- 5. Protesescu, L.; Yakunin, S.; Bodnarchuk, M. I.; Krieg, F.; Caputo, R.; Hendon, C. H.; Yang, R. X.; Walsh, A.; Kovalenko, M. V., Nanocrystals of Cesium Lead Halide Perovskites (CsPbX₃, X = Cl, Br, and I): Novel Optoelectronic Materials Showing Bright Emission with Wide Color Gamut. Nano Lett. 2015, 15, 3692-3696.

- 6. Shi, Z.; Li, Y.; Zhang, Y.; Chen, Y.; Li, X.; Wu, D.; Xu, T.; Shan, C.; Du, G., High-Efficiency and Air-Stable Perovskite Quantum Dots Light-Emitting Diodes with an All-Inorganic Heterostructure. *Nano Lett.* **2016**, 17, 313-321.
- 7. Swarnkar, A.; Chulliyil, R.; Ravi, V. K.; Irfanullah, M.; Chowdhury, A.; Nag, A., Colloidal CsPbBr₃ Perovskite Nanocrystals: Luminescence beyond Traditional Quantum Dots. *Angew. Chem. Int. Ed.* **2015**, 54, 15424-15428.
- 8. Kojima, A.; Teshima, K.; Shirai, Y.; Miyasaka, T., Organometal Halide Perovskites as Visible-Light Sensitizers for Photovoltaic Cells. *J. Am. Chem. Soc.* **2009**, 131, 6050–6051.
- 9. National Renewable Energy Laboratory NREL. https://www.nrel.gov/pv/assets/pdfs/best-research-cell-efficiencies.20200925.pdf.
- 10. Kamat, P. V., Quantum Dot Solar Cells. Semiconductor Nanocrystals as Light Harvesters. *J. Phys. Chem. C* **2008**, 112, 18737–18753.
- 11. De, A.; Mondal, N.; Samanta, A., Hole Transfer Dynamics from Photoexcited Cesium Lead Halide Perovskite Nanocrystals: 1-Aminopyrene as Hole Acceptor. *J. Phys. Chem. C* **2018**, 122, 13617–13623.
- 12. De, A.; das, S.; Samanta, A., Hot Hole Transfer Dynamics from CsPbBr₃ Perovskite Nanocrystals. *ACS Energy Lett.* **2020**, 5, 2246–2252.
- 13. Kobosko, S. M.; DuBose, J. T.; Kamat, P. V., Perovskite Photocatalysis. Methyl Viologen Induces Unusually Long-Lived Charge Carrier Separation in CsPbBr₃ Nanocrystals. *ACS Energy Lett.* **2020**, 5, 221–223.
- 14. DuBose, J. T.; Kamat, P. V., Surface Chemistry Matters. How Ligands Influence Excited State Interactions between CsPbBr₃ and Methyl Viologen. *J. Phys. Chem. C* **2020**, 124, 12990–12998.
- 15. Sarkar, S.; Ravi, V. K.; Banerjee, S.; Yettapu, G. R.; Ganesh B. Markad; Nag, A.; Mandal, P., Terahertz Spectroscopic Probe of Hot Electron and Hole Transfer from Colloidal CsPbBr₃ Perovskite Nanocrystals. *Nano Lett.* **2017**, 17, 5402–5407.
- 16. Wu, K.; Liang, G.; Shang, Q.; Ren, Y.; Kong, D.; Lian, T., Ultrafast Interfacial Electron and Hole Transfer from CsPbBr₃ Perovskite Quantum Dots. *J. Am. Chem. Soc.* **2015,** 137, 12792–12795.
- Thang, Y.-X.; Wang, H.-Y.; Zhang, Z.-Y.; Zhang, Y.; Sun, C.; Yue, Y.-Y.; Wang, L.; Chen, Q.-D.; Sun, H.-B., Photoluminescence Quenching of Inorganic Cesium Lead Halides Perovskite Quantum Dots (CsPbX₃) by Electron/Hole Acceptor. *Phys.Chem.Chem.Phys.* **2017,** 19, 1920--1926.
- 18. Jin, S.; Hsiang, J.-C.; Zhu, H.; Song, N.; Dicksonb, R. M.; Lian, T., Correlated Single Quantum Dot Blinking and Interfacial Electron Transfer Dynamics. *Chem. Sci.* **2010**, 1, 519–526.
- 19. Jin, S.; Lian, T., Electron Transfer Dynamics from Single CdSe/ZnS Quantum Dots to TiO₂ Nanoparticles. *Nano Lett.* **2009**, 9, 2448-2454.
- 20. Song, N.; Zhu, H.; Jin, S.; Lian, T., Hole Transfer from Single Quantum Dots. *ACS Nano* **2011**, 5, 8750–8759.

- 21. Cui, S.-C.; Tachikawa, T.; Fujitsuka, M.; Majima, T., Interfacial Electron Transfer Dynamics in a Single CdTe Quantum Dot-Pyromellitimide Conjugate. *J. Phys. Chem. C* **2008**, 112, 19625–19634.
- 22. Issac, A.; Jin, S.; Lian, T., Intermittent Electron Transfer Activity From Single CdSe/ZnS Quantum Dots. *J. Am. Chem. Soc.* **2008**, 130, 11280–11281.
- 23. Song, N.; Zhu, H.; Jin, S.; Zhan, W.; Lian, T., Poisson-Distributed Electron-Transfer Dynamics from Single Quantum Dots to C60 Molecules. *ACS Nano* **2011**, *5*, 613-621.
- 24. Jin, S.; Song, N.; Lian, T., Suppressed Blinking Dynamics of Single QDs on ITO. *ACS Nano* **2010**, 4, 1545–1552.
- 25. Biju, V.; Micic, M.; Hu, D.; Lu, H. P., Intermittent Single-Molecule Interfacial Electron Transfer Dynamics. *J. Am. Chem. Soc.* **2004**, 126, 9374-9381.
- 26. Lu, H. P.; Xie, X. S., Single-Molecule Kinetics of Interfacial Electron Transfer. *J. Phys. Chem. B* **1997**, 101, 2753-2757.
- 27. Ahmed, T.; Seth, S.; Samanta, A., Mechanistic Investigation of the Defect Activity Contributing to the Photoluminescence Blinking of CsPbBr₃ Perovskite Nanocrystals. *ACS Nano* **2019**, 13, 13537–13544.
- 28. Yuan, G.; Ritchie, C.; Ritter, M.; Murphy, S.; Gómez, D. E.; Mulvaney, P., The Degradation and Blinking of Single CsPbl₃ Perovskite Quantum Dots. *J. Phys. Chem. C* **2018**, 122, 13407–13415.
- 29. Yarita, N.; Tahara, H.; Saruyama, M.; Kawawaki, T.; Sato, R.; Teranishi, T.; Kanemitsu, Y., Impact of Postsynthetic Surface Modification on Photoluminescence Intermittency in Formamidinium Lead Bromide Perovskite Nanocrystals. *J. Phys. Chem. Lett.* **2017**, 8, 6041–6047.
- 30. Yarita, N.; Aharen, T.; Tahara, H.; Saruyama, M.; Kawawaki, T.; Sato, R.; Teranishi, T.; Kanemitsu, Y., Observation of Positive and Negative Trions in Organic-Inorganic Hybrid Perovskite Nanocrystals. *Phys. Rev. Mater.* **2018**, 2, 116003.
- 31. Trinh, C. T.; Minh, D. N.; Nguyen, V. L.; Ahn, K. J.; Kang, Y.; Lee, K.-G., An experimental study on the blinking suppression mechanism of organicinorganic formamidinium lead halide perovskite quantum dots on N-Type semiconductors. *APL Mater.* **2020**, 8, 031102.
- 32. Trinh, C. T.; Minh, D. N.; Ahn, K. J.; Kang, Y.; Lee, K.-G., Verification of Type-A and Type-B-HC Blinking Mechanisms of Organic–Inorganic Formamidinium Lead Halide Perovskite Quantum Dots by FLID Measurements. *Sci Rep* **2020**, 10, 2172.
- 33. Park, Y. S.; Bae, W. K.; Pietryga, J. M.; Klimov, V. I., Auger Recombination of Biexcitons and Negative and Positive Trions in Individual Quantum Dots. *ACS Nano* **2014**, 8, 7288-7296.
- 34. Seth, S.; Ahmed, T.; Samanta, A., Photoluminescence Flickering and Blinking of Single CsPbBr₃ Perovskite Nanocrystals: Revealing Explicit Carrier Recombination Dynamics. *J. Phys. Chem. Lett.* **2018**, 9, 7007–7014.
- 35. Yuan, G.; Gómez, D. E.; Kirkwood, N.; Boldt, K.; Mulvaney, P., Two Mechanisms Determine Quantum Dot Blinking. *ACS Nano* **2018**, 12, 3397–3405.

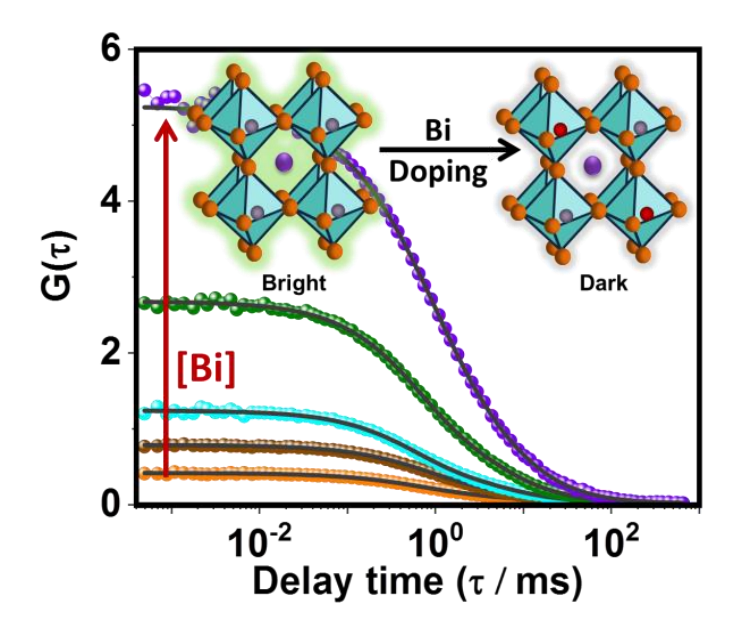
- 36. Galland, C.; Ghosh, Y.; Steinbruck, A.; Sykora, M.; Hollingsworth, J. A.; Klimov, V. I.; Htoon, H., Two Types of Luminescence Blinking Revealed by Spectroelectrochemistry of Single Quantum Dots. *Nature* **2011**, 479, 203-207.
- 37. Kim, T.; Jung, S. I.; Ham, S.; Chung, H.; Kim, D., Elucidation of Photoluminescence Blinking Mechanism and Multiexciton Dynamics in Hybrid Organic–Inorganic Perovskite Quantum Dots. *Small* **2019**, 15, 1900355.
- 38. Li, B.; Huang, H.; Zhang, G.; Yang, C.; Guo, W.; Chen, R.; Qin, C.; Gao, Y.; Biju, V.; Rogach, A. L.; Xiao, L.; Jia, S., Excitons and Biexciton Dynamics in Single CsPbBr₃ Perovskite Quantum Dots. *J. Phys. Chem. Lett.* **2018**, *9*, 6934–6940.
- 39. Zhang, A.; Dong, C.; Ren, J., Tuning Blinking Behavior of Highly Luminescent Cesium Lead Halide Nanocrystals through Varying Halide Composition. *J. Phys. Chem. C* **2017**, 121, 13314–13323.
- 40. Gerhard, M.; Louis, B.; Camacho, R.; Merdasa, A.; Li, J.; Kiligaridis, A.; Dobrovolsky, A.; Hofkens, J.; Scheblykin, I. G., Microscopic Insight into Non-Radiative Decay in Perovskite Semiconductors from Temperature-Dependent Luminescence Blinking. *Nature Communications* **2019**, 10, 1698.
- 41. Hu, F.; Yin, C.; Zhang, H.; Sun, C.; Yu, W. W.; Zhang, C.; Wang, X.; Zhang, Y.; Xiao, M., Slow Auger Recombination of Charged Excitons in Nonblinking Perovskite Nanocrystals without Spectral Diffusion. *Nano Lett.* **2016**, 16, 6425-6430.
- 42. Park, Y. S.; Guo, S.; Makarov, N. S.; Klimov, V. I., Room Temperature Single-Photon Emission from Individual Perovskite Quantum Dots. *ACS Nano* **2015**, 9, 10386-10393.
- 43. Hu, F.; Zhang, H.; Sun, C.; Yin, C.; Lv, B.; Zhang, C.; Yu, W. W.; Wang, X.; Zhang, Y.; Xiao, M., Superior Optical Properties of Perovskite Nanocrystals as Single Photon Emitters. *ACs Nano* **2015**, *9*, 12410–12416.
- 44. Gibson, N. A.; Koscher, B. A.; Alivisatos, A. P.; Leone, S. R., Excitation Intensity Dependence of Photoluminescence Blinking in CsPbBr₃ Perovskite Nanocrystals. *J. Phys. Chem. C* **2018**, 122, 12106–12113.
- 45. Park, J.; Kim, Y.; Ham, S.; Woo, J. Y.; Kim, T.; Jeong, S.; Kim, D., A relationship between the surface composition and spectroscopic properties of cesium lead bromide (CsPbBr₃) perovskite nanocrystals: focusing on photoluminescence efficiency. *Nanoscale* **2020**, 12, 1563–1570.
- 46. Li, B.; Chen, R.; Qin, C.; Yang, C.; Guo, W.; Han, X.; Gao, Y.; Zhang, G.; Xiao, L.; Jia, S., Interfacial charge transfer between CsPbBr₃ quantum dots and ITO nanoparticles revealed by single-dot photoluminescence spectroscopy. *Appl. Phys. Express* **2019**, 12, 112003.
- 47. Perumal, A.; Shendre, S.; Li, M.; Tay, Y. K. E.; Sharma, V. K.; Chen, S.; Wei, Z.; Liu, Q.; Gao, Y.; Buenconsejo, P. J. S.; Tan, S. T.; Gan, C. L.; Xiong, Q.; Sum, T. C.; Demir, H. V., High Brightness Formamidinium Lead Bromide Perovskite Nanocrystal Light EmittingDevices. *Sci. Rep.* **2016**, 6, 36733.

Chapter 5 Impact of hole transfer...

- 48. Paul, S.; Samanta, A., N-Bromosuccinimide as Bromide Precursor for Direct Synthesis of Stable and Highly Luminescent Green-Emitting Perovskite Nanocrystals. *ACS Energy Lett.* **2020**, 5, 64–69.
- 49. Chen, S.; Wen, X.; Sheng, R.; Huang, S.; Deng, X.; Green, M. A.; Ho-Baillie, A., Mobile Ion Induced Slow Carrier Dynamics in Organic–Inorganic Perovskite CH₃NH₃PbBr₃. *ACS Appl. Mater. Interfaces* **2016**, 8, 5351-5357.
- 50. Seth, S.; Mondal, N.; Patra, S.; Samanta, A., Fluorescence Blinking and Photoactivation of All-Inorganic Perovskite Nanocrystals CsPbBr₃ and CsPbBr₂I. *J. Phys. Chem. Lett.* **2016**, 7, 266-271.
- 51. Ito, S.; Toitani, N.; Pan, L.; Tamai, N.; Miyasaka, H., Fluorescence Correlation Spectroscopic Study on Water-Soluble Cadmium Telluride Nanocrystals: Fast Blinking Dynamics in the μs–ms Region. *J. Phys.: Condens. Matter* **2007**, 19, 486208.
- 52. Patra, S.; Samanta, A., A Fluorescence Correlation Spectroscopy, Steady-State, and Time- Resolved Fluorescence Study of the Modulation of Photophysical Properties of Mercaptopropionic Acid Capped CdTe Quantum Dots upon Exposure to Light. *J. Phys. Chem. C* **2013**, 117, 23313–23321.
- 53. Cui, S.-C.; Tachikawa, T.; Fujitsuka, M.; Majima, T., Photoinduced Electron Transfer in a Quantum Dot-Cucurbituril Supramolecular Complex. *J. Phys. Chem. C* **2011**, 115, 1824–1830.

CHAPTER 6

Individual Particle Level Picture of Charge Carrier Recombination in Bi-doped CsPbBr₃ Nanocrystals



Overview

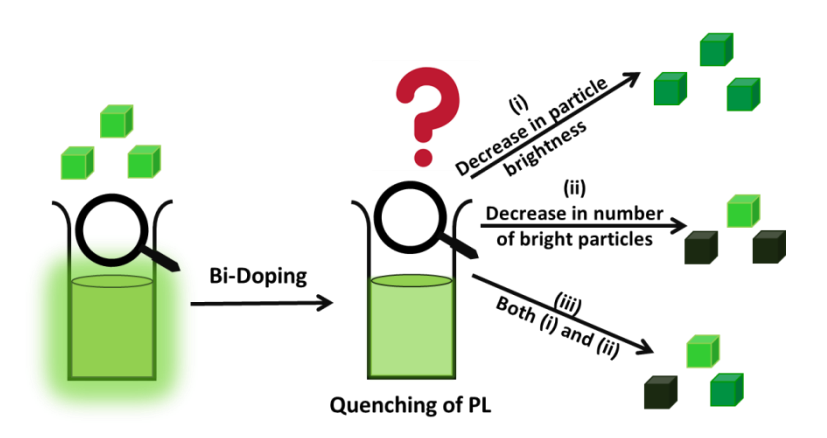
Doping is an important strategy both for introducing new properties and modifying the intrinsic properties of a semiconductor. In this work, we investigate the Bi-doped CsPbBr₃ nanocrystals (NCs), which are less toxic and weakly luminescent compared to the parent system, employing ultrafast pump-probe and fluorescence upconversion techniques and single-particle based fluorescence correlation spectroscopy technique to obtain individual particle-level understanding of the charge carrier recombination pathways and dynamics in these systems. The results reveal heterogeneity of the system in terms of photoluminescence (PL) brightness/efficiency of the individual NCs. Three different types of NCs (bright, dim and dark) have been identified in doped samples that arise from the difference in extent of doping and consequent variation in the density of Bi-induced states; the latter act as traps for the electrons and assist in nonradiative recombination of the charge carriers. An ultrafast trapping process (~2-6 ps), which renders a majority of the Bi-doped NCs into dark ones, is found to be the primary cause of weak PL of the doped systems. The individual particle-level information obtained in this work using a combination of techniques provides new insight on low PL of the Bidoped CsPbBr₃ perovskite NCs.

6.1. Introduction

The lead halide based perovskites have attracted great attention as next generation semiconducting materials for photovoltaic and optoelectronic applications because of their broad absorption with high cross-section, long carrier diffusion length, intrinsic defect-tolerance and high photoluminescence quantum yield (PLQY). 1-9 Moreover, the properties of these materials can be tuned by adjusting the composition, size and dimensionality of the systems.^{6, 10} As doping is another strategic route through which these materials can be endowed with new properties, 11-13 a large number of studies have also been performed on perovskites doped with various dopants, which include both isovalent14-21 and hetero-valent ions21, 22 with respect to Pb2+ for different purposes, like controlling the optoelectronic performance, structural stability, crystal growth, light conversion and partial replacement of toxic lead. 10, 21, 23

While the effect of doping iso-valent metal ion on the optical properties of the perovskites has been studied quite extensively 14-19, 21 not so much has been done with the hetero-valent metal ion dopants. 21, 22, 24 Among different hetero-valent dopants, less toxic Bi³⁺ has received the most attention as its ionic radius and electronic structure are very similar to those of Pb²⁺. ²⁵ Bi³⁺ doped perovskite films, nanocrystals (NCs) and large single crystals (SCs) have been studied. 24-33 As far as the optical properties are concerned, Bi-doping results in a significant drop of PLQY of the perovskites. 24, 25, 28, 30, 32 For example, Bi-doping (5%) of the MAPbBr₃ SCs leads to ~99% reduction in PL intensity and carrier lifetime. 28, 30 Very recent ultrafast time-resolved THz spectroscopy study shows a notable decrease in charge carrier mobility in MAPbBr₃ film on Bi-doping, attributed to enhanced electron-trapping defects, leading to a decrease in PL efficiency and carrier lifetime.³² A decrease of PLQY from 78% to 8% (for 2.1% doping) and substantial decrease of carrier lifetime is also reported for the CsPbBr₃ NCs by Mohammed and co- workers.^{24, 25} All these measurements provide an average PL behavior of the NCs, without revealing any information on the PL characteristics of the individual NCs. For example, an overall decrease in PLQY of the system on Bi-doping can result from (shown in Scheme 6.1) (i) a decrease in the PL brightness (photon counts per unit time) of each particle, (ii) a decrease in the number of bright particles due to

conversion of some of these particles to dark ones and (iii) both due to (i) and (ii). We attempt to obtain individual particle-level information of these doped NCs employing a fluorescence correlation spectroscopy (FCS), ultrafast transient absorption (TA) and PL upconversion (UC) techniques, which were not used previously for the study of these systems.



Scheme 6.1: Possible reasons for PL quenching on Bi-doping

6.2. Results

6.2.1 Synthesis and characterization of Bi-doped CsPbBr₃ NCS

The undoped and Bi-doped CsPbBr₃ NCs with different Bi-content were prepared following reported procedures, ^{6, 24} the details of which are provided in the 'Experimental Section'. To eliminate any possible contribution of surface-adsorbed Bi on the optical properties of the NCs, the doped samples were thoroughly washed with methyl acetate and dispersed in hexane/ODE were treated using optimum amount of OA and OAm and used for studies (details in 'Chapter 3.2'). The last treatment, which was not recommended in the reported procedure, ²⁴ was to make up for possible removal of some of protective ligands from the surface during washing.

The Bi-content in doped NCs, estimated by the inductively coupled plasma optical emission spectrometry (ICP-OES) measurements, was found to be 0.3%, 0.5%, 2.7% and

8.2%, respectively for the 2%, 5%, 10% and 20% of Bi-feed solutions. The TEM images (Figure AIV.1) of the undoped and doped (8.2% Bi) CsPbBr₃ NCs show no noticeable change in morphology (a cubic shape with an average edge length of ~9 nm). The HR-TEM images indicate (Figure AIV.1) a lattice spacing of ~0.59 nm for the (100) planes both for doped and undoped systems and confirm negligible influence of doping on the crystal structure of the NCs. Similar PXRD peak positions (Figure AIV.2) for the undoped and doped NCs further supports this statement. No change in crystal structure of the NCs upon doping is understandable as both Pb²⁺ and Bi³⁺ have an identical ionic radii $(\sim 119 \text{ pm})^{25}$

6.2.2 Steady state measurements

Doping, however, leads to a change in color of the colloidal dispersion, as observed by naked eyes, from green (0% Bi) to brown (8.2% Bi) (Figure 6.1).²⁴ The electronic absorption spectra of the NCs show (Figure 6.1a and AIV.3) a reduction of the excitonic peak intensity and slight blue-shift of the peak position with increase in Bi-content. The PL spectra (Figure 6.1b and AIV.4) of the samples also show a progressive blue shift with increasing Bi-content in the NCs. A shift in PL peak position from 513 nm to 506 nm is observed between undoped and 8.2% doped NCs. A similar shift, observed earlier for Bidoped CsPbBr₃ NCs and PbS quantum dots, was attributed to Burstein-Moss effect.^{24, 34, 35} Increase in Bi-content also leads to progressive quenching of PL. The PLQY drops from ~93% (undoped) to ~8% (8.2% Bi-doped) with no significant change in width of the PL spectra (FWHM 17-20 nm). Although this drastic decrease of PLOY is consistent with literature, 24, 25 the PL quenching can be due to surface defects arising from surfaceadsorbed Bi or/and detachment of the surface ligands. These possibilities are however ruled out by washing the doped NCs with methyl acetate and treating them with the ligands, OA and OAm. Additional control experiments (vide Appendix IV) were performed to establish that the PL quenching of CsPbBr₃ NCs in our study was solely due to Bi-doping.

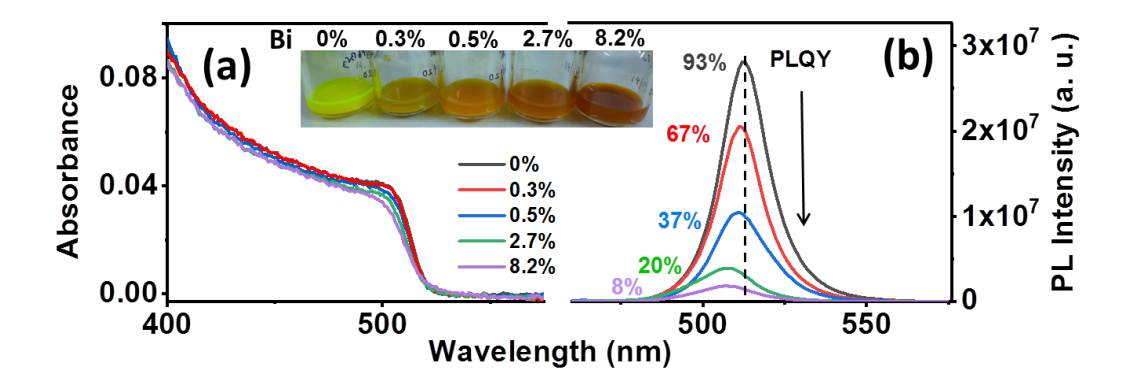


Figure 6.1: (a) Absorption and (b) emission spectra ($\lambda_{ex} = 400$ nm) of Bi-doped (0%, 0.3%, 0.5%, 2.7% and 8.2%) CsPbBr₃ NCs dispersed in hexane.

6.2.3 Transient absorption measurement

We have studied the spectral and temporal characteristics of the transients produced on photoexcitation of the undoped and doped NCs using femtosecond pulses under similar experimental conditions to understand the influence of doping on the charge carrier dynamics. The TA spectra (Figure 6.2a) are found to be characterized by a sharp bleach signal at ~509 nm, which arises due to filling of the band edge states by the charge carriers. ^{36, 37} Even though the spectral features are quite similar for the undoped and doped NCs, with increase in Bi-content in the samples, a blue shift (509 nm to 505 nm) of the bleach peak is observed (Figure 6.2), which is consistent with the shift of the excitonic peak in the steady state absorption spectra.

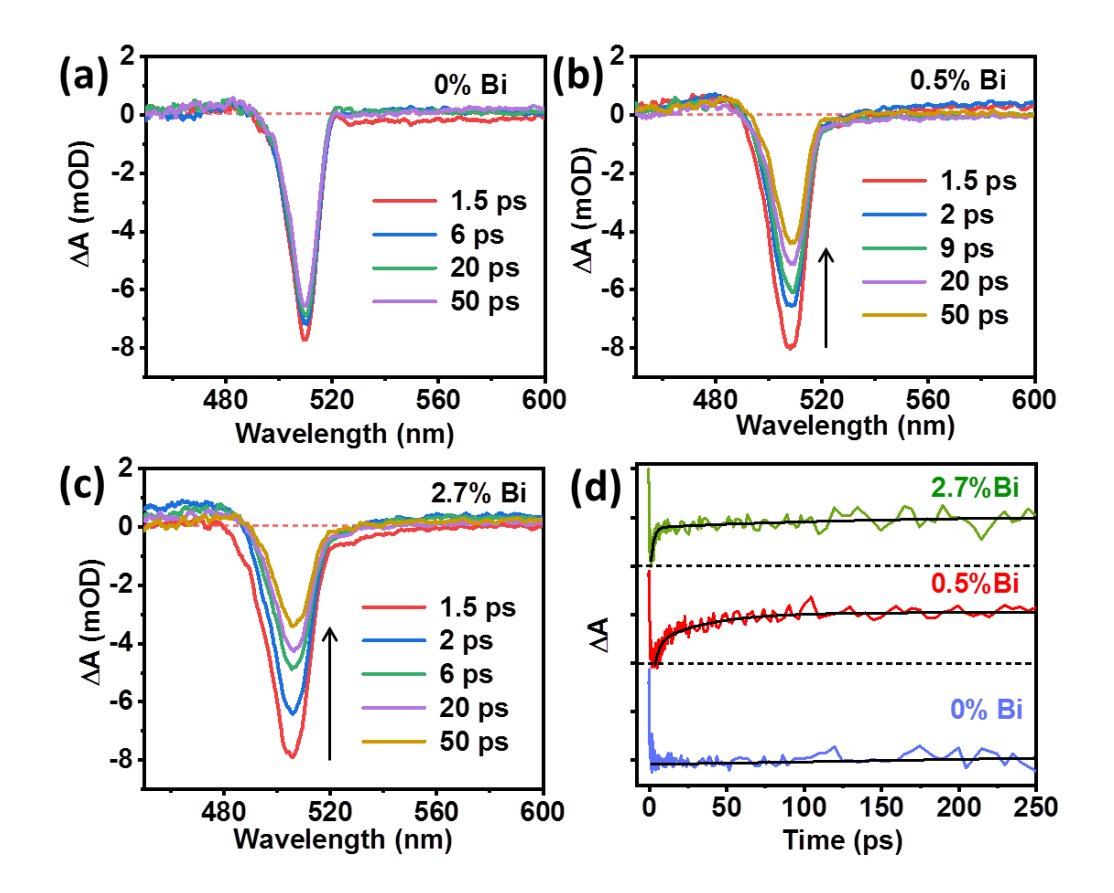


Figure 6.2: TA spectra of (a) 0% (b) 0.5% and (c) 2.7% Bi-doped CsPbBr₃ NCs dispersed in hexane ($\lambda_{ex} = 400$ nm). (d) Comparison of the bleach recovery kinetics monitored at their respective bleach maximum (505-509 nm) of the samples with different Bi-content.

The bleach recovery kinetics of the undoped CsPbBr₃ NCs is found to be single exponential (Figure 6.2d) with a time constant of >500 ps³⁸ (Table AIV.2), which represents the excitonic recombination of the charge carriers.^{17, 37} For the doped samples, the bleach recovery is, however, biexponential. In addition to the slow component (>500 ps), another ultrafast component, whose value decreases with increase in Bi-content, is observed. For example, the lifetime decreases from 3.2 to 1.9 ps on increase in dopant content in the NCs from 0.5% to 2.7% (Table AIV.2). This time constant corresponds to the trapping process. It is thus evident that Bi-doping promotes rapid nonradiative

recombination of the charge carriers through the dopant-introduced trap states and quenches the PL of the NCs. Careful inspection of the data reveals that even though the maximum bleach amplitude (measured under identical conditions) is similar for undoped, 0.5% and 2.7% doped NCs, it is substantially (75%) lower for 8.2% Bi doped sample (Figure AIV.5) indicating that for this sample, all photo-generated charge carriers do not return to the band edge states; some are leaked through another channel in competition with the hot carrier cooling process. ^{39, 40} Hence, it is evident that while carrier trapping becomes faster with increase in Bi-content, for sample with higher Bi-content, trapping of the hot carriers is also an important process. ^{17, 40} The hot carrier trapping process is further confirmed by acceleration of the *formation* of the bleach kinetics for 8.2% Bi-doped NCs as compared to the other samples (Figure AIV.5). ⁴⁰

6.2.4 FCS study

Additional insight on low PLQY of the Bi-doped CsPbBr₃ NCs is obtained from the FCS measurements. In this technique, we measure the fluctuations of PL of a highly dilute solution (nM) of the NCs in a small volume of the sample (typically \sim 1 fL) using a confocal fluorescence microscope. For this purpose, we have studied solutions of the NCs (in ODE) with identical absorbance at the excitation wavelength, 405 nm. The measured time-dependence of the fluorescence correlation data of the undoped and doped NCs is shown in Figure 6.3. The data is found to be best represented by a model (equation 6.1) according to which the PL fluctuations arise from (i) diffusion of the NCs in and out of the observation volume and (ii) involvement of the trap states, the latter are represented by a stretched exponential decay component. This model has been used previously for metal-chalcogenide quantum dots as well as for perovskite NCs. 41-44 The amplitude of correlation at time τ , $G(\tau)$, is expressed as

$$G(\tau) = \left[1 + \frac{T}{1 - T} exp \left(-\frac{\tau}{\tau_T} \right)^{\beta} \right] 1 / \langle N \rangle (1 + \tau/\tau_D)^{-1} (1 + \tau/\kappa^2 \tau_D)^{-1/2}$$
 (6.1)

Where, τ_D is the diffusion time of the NCs, $\langle N \rangle$ is the average number of particles undergoing reversible PL intensity fluctuation in the observation volume, T is the fraction

of particles in their "off" state, and τ_T is the dark-state relaxation time or blinking time. β is a stretching exponent having a value between 0 to 1 indicating the distribution of τ_T . κ (= ω_Z/ω_{xy}) is the structure parameter of the observation volume; ω_Z and ω_{xy} are the longitudinal and transverse radii, respectively. The per-particle brightness (PPB) of the NCs is given by I/<N>, where, I is the average count rate of the PL intensity trace. ⁴⁵

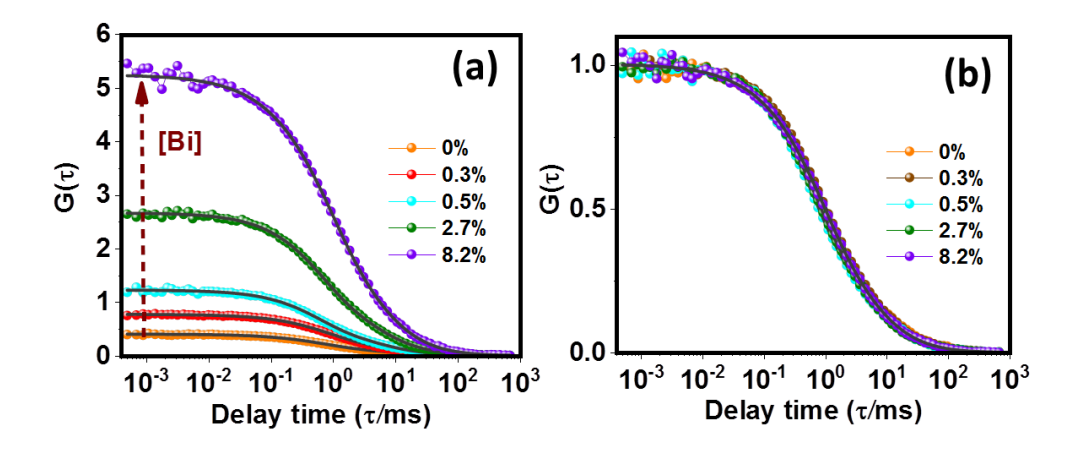


Figure 6.3: Fluorescence correlation curves of the Bi-doped (0%, 0.3%, 0.5%, 2.7% and 8.2%) CsPbBr₃ NC solutions in ODE in (a) absolute and (b) normalized scale.

Table 6.1: Estimated blinking parameters, G(0), τ_D , <N>, β , τ_T , T and PPB values of the Bi-doped (0%, 0.3%, 0.5%, 2.7% & 8.2%) CsPbBr₃ NCs, as obtained from FCS measurements.

Bi- %	G(0)	$\tau_{_{D}}$ (ms)	<n></n>	β	τ _T (ms)	Т	PPB (K cps)
0	0.44±0.02	4.1±0.27	5.6±0.41	0.78±0.01	0.63±0.03	0.52±0.05	3.27±0.21
0.3	0.71±0.03	4.2±0.25	3.01±0.37	0.79 ± 0.02	0.77 ± 0.05	0.49 ± 0.02	3.72±0.28
0.5	1.2±0.15	3.8±0.28	1.73±0.20	0.83 ± 0.06	0.60 ± 0.06	0.47±0.03	3.93±0.20
2.7	2.7±0.21	3.9±0.27	0.91±0.15	0.80 ± 0.03	0.65 ± 0.03	0.46 ± 0.04	3.59±0.25
8.2	5.3±0.25	4.1±0.26	0.43±0.02	0.75±0.05	0.75±0.05	0.48±0.02	3.27±0.28

The time-dependence of the fluorescence correlation data of the samples and the fits to equation 6.1, are shown in Figure 6. 3 With increase in Bi-content, the G(0) value, which is the amplitude of correlation at time zero, increases (Table 6.1), but the shape of the correlation curves remains the same despite significant difference in PL efficiency of different samples. A close look at different parameters associated with blinking (Table 6.1), as obtained from analysis of the data, shows that the β value is not very far from unity (~0.8) for undoped NCs, indicating that only a few trap states contribute to PL blinking of these systems. This is in agreement with high PLQY (~93%) of the undoped NCs.41 Interestingly, even though the doped systems exhibit much lower PLQY, the blinking parameters such as T, τ_T and PPB values including the β -values are very similar for doped and undoped samples. No noticeable effect of doping on the blinking dynamics (in the us-ms time scale) of the NCs, as observed here, is possible only when undoped NCs are present in an ensemble of doped NCs. Considering that G(0) is defined as 1/[<N>(1-T)], its value can increase (Figure 6.3a) due to a decrease of <N> or/and increase in T. However, as the T value remains unchanged on doping (Table 6.1), it is thus evident that the increase in the G(0) value for higher dopant content is due to a

decrease in <N> (Table 6.1). This decrease in the <N> value for higher dopant content could be due to conversion of bright NCs to permanently dark ones or/and due to slowing down of blinking dynamics ($\tau_T > \tau_D$). The number of these particles increases with increase in Bi-content in the sample, which are not observable in these measurements and causes lowering of PL efficiency. ⁴⁵⁻⁴⁷

6.2.5 Fluorescence up-conversion measurement

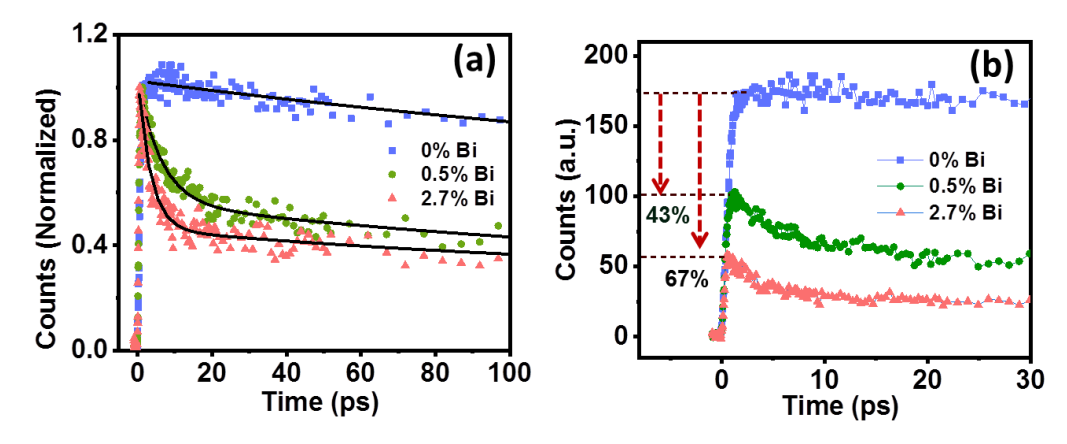


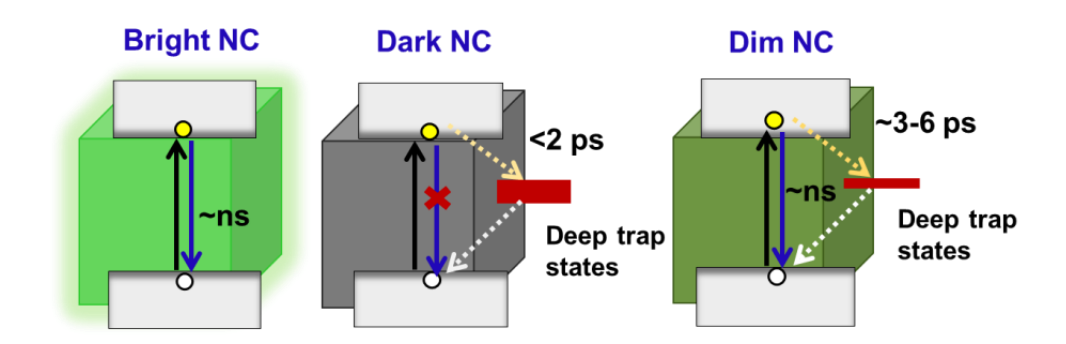
Figure 6.4: PL decays of different Bi-doped (0%, 0.5%, and 2.7%) CsPbBr₃ NCs (dispersed in hexane) obtained in PL UC measurement ($\lambda_{ex} = 400 \text{ nm}$) in (a) normalized and (b) absolute scale.

The excited state dynamics of the systems were further studied by monitoring the PL decay profiles with a time-resolution of ~200 fs using PL UC technique. Figure 6.4a depicts the normalized PL decay profiles of undoped and 0.5% and 2.7% Bi-doped NCs. While the undoped NCs exhibit a single exponential PL decay with a time constant >500 ps, the doped NCs show a biexponential decay behavior with an additional fast component due to carrier trapping process. On increase in doping content from 0.5% to 2.7%, this decay component becomes faster (from 6.2 to 3.4 ps) and the PL intensity at time zero decreases progressively (Figure 6.4b). For the 8.2% Bi-doped NCs, the initial PL counts drops to such a low level that the PL decay dynamics cannot be measured under similar experimental conditions. This decrease in time-zero PL intensity can be due

to (i) hot carrier trapping or/and (ii) increase in the number of dark particles. ⁴⁹ However, as the TA data, indicated same bleach amplitude for 0.5% and 2.7% doped NCs, it is evident that with increase in Bi-content from 0.5% and 2.7%, the number of photoluminescent NCs decreases. This finding is consistent with that obtained from the FCS study confirms the conversion of fraction of bright NCs to permanently dark ones. A quantitative analysis of the time-zero PL intensity reveals ~43% and ~67% conversion of the NCs into the dark ones for 0.5% and 2.7% Bi-doped NCs, respectively.

6.3. Discussion

Replacement of Pb²⁺ by Bi³⁺ in CsPbBr₃ NCs creates deep electron trap states, which serve as nonradiative recombination channels for the carriers and quenches the PL.^{24, 25, 28, 50} Our measurements (TA and PL UC) not only confirms that an efficient nonradiative ultrafast carrier recombination pathway introduced by the dopant is responsible for low PL efficiency of the system, but they provide the first particle-level insight on the lower PL efficiency of the Bi-doped CsPbBr₃ NCs. Let us combine the findings of three different measurements and attempt to construct the picture that we obtain from this study (Scheme 6.2).



Scheme 6.2: Recombination processes in Bi-doped CsPbBr₃ NCs, which comprise a mixture of three different kinds of NCs.

The FCS study reveals two important pieces of information. First, there remain some NCs, which exhibit blinking characteristics remarkably similar to those of the undoped

NCs that remain undoped in the doped samples. Second, the decrease of number of observable photoluminescent particles upon doping *i.e.*, conversion of the photoluminescent particles into dark ones could be the one of the possible reasons for lowering the PL efficiency upon Bi-doping.

The decrease of PL intensity at t=0 in PL UC study further confirms conversion of some bright NCs into permanently dark ones. However, had there been only the bright and dark NCs, the PL decay kinetics would not have been affected. The short lifetime component arises from the NCs with intermediate brightness, is termed as dim NCs. These are the particles, which are characterized by short PL lifetime, in which nonradiative recombination of the carriers competes with the radiative recombination processes, but does not prevent it completely (like in dark NCs). The fraction of bright NCs converting into dark ones upon doping is estimated to be ~69% (0.5% Bi) and ~84% (2.7% Bi) in FCS measurements (from the drop in the value of <N>) and ~43% and ~67% for the respective samples in PL UC measurements (from the decrease in PL intensity at t=0). This difference arises because the dim particles appeared wrongly as dark NCs in the FCS measurements. That could be due to weak PL intensities of these particles, too low to be detected under identical experimental conditions and/or slow blinking dynamics. 46, 51

A close look at the estimated time constants of the carrier trapping process (Table AIV.2) shows that the process appears faster in TA measurement than that obtained by PL UC technique. This is because PL UC measurement probes the dynamics of only the fluorescent particles (bright and dim NCs), whereas the TA studies captures the data for all particles (bright, dim and dark). With increase in Bi-content as the density of Bi-associated trap states increases, the carrier recombination process becomes faster. The dark and dim NCs differ in terms of the density of the trap states depending on the Bi-content in the individual particles.⁵¹

6.4. Conclusion

In short, investigation of the Bi-doped CsPbBr₃ NCs using a combination of techniques reveals three types of NCs differing in PL brightness and charge carrier recombination dynamics. Nonuniform doping of the NCs is found to be responsible for the heterogeneous nature of the sample. A difference in dopant content leads to a change in the density of the dopant-introduced states and consequent difference in the rate of trapping of the carriers and PL brightness of the NCs. This study provides first insight into the individual particle-level information on the carrier dynamics and PL efficiency of the Bi-doped CsPbBr₃ NCs.

References

- 1. National Renewable Energy Laboratory NREL. https://www.nrel.gov/pv/assets/pdfs/best-research-cell-efficiencies.20200803.pdf.
- 2. Chen, Q.; Wu, J.; Ou, X.; Huang, B.; Almutlaq, J.; Zhumekenov, A. A.; Guan, X.; Han, S.; Liang, L.; Yi, Z.; Li, J.; Xie, X.; Wang, Y.; Li, Y.; Fan, D.; Teh, D. B. L.; All, A. H.; Mohammed, O. F.; Bakr, O. M.; Wu, T.; Bettinelli, M.; Yang, H.; Huang, W.; Liu, X., All-inorganic Perovskite Nanocrystal Scintillators. *Nature* **2018**, 561, 88-93.
- 3. Gong, M.; Sakidja, R.; Goul, R.; Ewing, D.; Casper, M.; Stramel, A.; Elliot, A.; Wu, J. Z., High-Performance All-Inorganic CsPbCl₃ Perovskite Nanocrystal Photodetectors with Superior Stability. *ACS Nano* **2019**, 13, 1772–1783.
- 4. Kang, J.; Wang, L. W., High Defect Tolerance in Lead Halide Perovskite CsPbBr₃. *J. Phys. Chem. Lett.* **2017**, 8, 489-493.
- 5. Kovalenko, M. V.; Protesescu, L.; Bodnarchuk, M. I., Properties and Potential Optoelectronic Applications of Lead Halide Perovskite Nanocrystals. *Science* **2017**, 358, 745-750.
- 6. Protesescu, L.; Yakunin, S.; Bodnarchuk, M. I.; Krieg, F.; Caputo, R.; Hendon, C. H.; Yang, R. X.; Walsh, A.; Kovalenko, M. V., Nanocrystals of Cesium Lead Halide Perovskites (CsPbX₃, X = Cl, Br, and I): Novel Optoelectronic Materials Showing Bright Emission with Wide Color Gamut. *Nano Lett.* **2015**, 15, 3692–3696.
- 7. Shi, Z.; Li, Y.; Zhang, Y.; Chen, Y.; Li, X.; Wu, D.; Xu, T.; Shan, C.; Du, G., High-Efficiency and Air-Stable Perovskite Quantum Dots Light-Emitting Diodes with an All-Inorganic Heterostructure. *Nano Lett.* **2016**, 17, 313-321.
- 8. Swarnkar, A.; Chulliyil, R.; Ravi, V. K.; Irfanullah, M.; Chowdhury, A.; Nag, A., Colloidal CsPbBr₃ Perovskite Nanocrystals: Luminescence beyond Traditional Quantum Dots. *Angew. Chem. Int. Ed.* **2015**, 54, 15424-15428.

- 9. Zhou, Q.; Bai, Z.; Lu, W.-g.; Wang, Y.; Zou, B.; Zhong, H., In Situ Fabrication of Halide Perovskite Nanocrystal-Embedded Polymer Composite Films with Enhanced Photoluminescence for Display Backlights. *Adv. Mater.* **2016**, 28, 9163–9168.
- 10. Zhou, Y.; Chen, J.; Bakr, O. M.; Sun, H.-T., Metal-Doped Lead Halide Perovskites: Synthesis, Properties, and Optoelectronic Applications. *Chem. Mater.* **2018**, 30, 6589–6613.
- 11. Abram, R. A.; Rees, G. J.; Wilson, B. L. H., Heavily Doped Semiconductors and Devices. *Adv. Phys.* **1978**, 27, 799–892.
- 12. Khana, A.; Das, A., Diffusivity–Mobility Relationship for Heavily Doped Semiconductors Exhibiting Band Tail. *Phys. B* **2010**, 405, 817-821.
- 13. Palankovski, V.; Kaiblinger-Grujin, G.; Selberherr, S., Dopant-Dependent Band Gap Narrowing in Compound Semiconductor Devices. *Mater. Sci. Eng. B* **1999**, 66, 46-49.
- 14. De, A.; Das, S.; Mondal, N.; Samanta, A., Highly Luminescent Violet- and Blue-Emitting Stable Perovskite Nanocrystals. *ACS Mater. Lett.* **2019**, 1, 116-122.
- 15. Chen, J.-K.; Ma, J.-P.; Guo, S.-Q.; Chen, Y.-M.; Zhao, Q.; Zhang, B.-B.; Li, Z.-Y.; Zhou, Y.; Hou, J.; Kuroiwa, Y.; Moriyoshi, C.; Bakr, O. M.; Zhang, J.; Sun, H.-T., High-Efficiency Violet-Emitting All-Inorganic Perovskite Nanocrystals Enabled by Alkaline-Earth Metal Passivation. *Chem. Mater.* **2019**, 31, 3974-3983.
- 16. Yong, Z.-J.; Guo, S.-Q.; Ma, J.-P.; Zhang, J.-Y.; Li, Z.-Y.; Chen, Y.-M.; Zhang, B.-B.; Zhou, Y.; Shu, J.; Gu, J.-L.; Zheng, L.-R.; Bakr, O. M.; Sun, H.-T., Doping-Enhanced Short-Range Order of Perovskite Nanocrystals for Near-Unity Violet Luminescence Quantum Yield. *J. Am. Chem. Soc.* **2018**, 140, 9942–9951.
- 17. Das, S.; De, A.; Samanta., A., Ambient Condition Mg²⁺ Doping Producing Highly Luminescent Green- and Violet-Emitting Perovskite Nanocrystals with Reduced Toxicity and Enhanced Stability. *J. Phys. Chem. Lett.* **2020**, 11, 1178-1188.
- 18. De, A.; Mondal, N.; Samanta, A., Luminescence Tuning and Exciton Dynamics of Mn-doped CsPbCl₃ Nanocrystals. *Nanoscale* **2017**, 9, 16722-16727.
- 19. Mondal, N.; De, A.; Samanta, A., Achieving Near-Unity Photoluminescence Efficiency for Blue-Violet-Emitting Perovskite Nanocrystals. *ACS Energy Lett.* **2019**, 4, 32-39.
- 20. Wang, H.-C.; Wang, W.; Tang, A.-C.; Tsai, H.-Y.; Bao, Z.; Ihara, T.; Yarita, N.; Tahara, H.; Kanemitsu, Y.; Chen, S.; Liu, R.-S., High-Performance $CsPb_{1-x}Sn_xBr_3$ Perovskite Quantum Dots for Light-Emitting Diodes. *Angew. Chem. Int. Ed.* **2017**, 56, 13650 –13654.
- 21. Luo, B.; Li, F.; Xu, K.; Guo, Y.; Liu, Y.; Xia, Z.; Zhang, J. Z., B-Site Doped Lead Halide Perovskites: Synthesis, Band Engineering, Photophysics, and Light Emission Applications. *J. Mater. Chem. C* **2019**, 7, 2781-2808.
- 22. Swarnkar, A.; Mir, W. J.; Nag, A., Can B-Site Doping or Alloying Improve Thermaland Phase-Stability of All-Inorganic CsPbX₃ (X = Cl, Br, I) Perovskites? *ACS Energy Lett.* **2018** 3, 286–289.
- 23. Seth, S.; Ahmed, T.; De, A.; Samanta, A., Tackling the Defects, Stability, and Photoluminescence of CsPbX₃ Perovskite Nanocrystals. *ACS Energy Lett.* **2019**, 4, 1610–1618.

- 24. Begum, R.; Parida, M. R.; Abdelhady, A. L.; Murali, B.; Alyami, N. M.; Ahmed, G. H.; Hedhili, M. N.; Bakr, O. M.; Mohammed, O. F., Engineering Interfacial Charge Transfer in CsPbBr₃ Perovskite Nanocrystals by Heterovalent Doping. *J. Am. Chem. Soc.* **2017**, 139, 731-737.
- 25. Yin, J.; Ahmed, G. H.; Bakr, O. M.; Brédas, J.-L.; Mohammed, O. F., Unlocking the Effect of Trivalent Metal Doping in All-Inorganic CsPbBr₃ Perovskite. *ACS Energy Lett.* **2019**, 4, 789–795.
- 26. Abdelhady, A. L.; Saidaminov, M. I.; Murali, B.; Adinolfi, V.; Voznyy, O.; Katsiev, K.; Alarousu, E.; Comin, R.; Dursun, I.; Sinatra, L.; Sargent, E. H.; Mohammed, O. F.; Bakr, O. M., Heterovalent Dopant Incorporation for Bandgap and Type Engineering of Perovskite Crystals. *J. Phys. Chem. Lett.* **2016**, *7*, 295-301.
- 27. Hu, Y.; Bai, F.; Liu, X.; Ji, Q.; Miao, X.; Qiu, T.; Zhang, S., Bismuth Incorporation Stabilized α -CsPbl₃ for Fully Inorganic Perovskite Solar Cells. *ACS Energy Lett.* **2017**, 2, 2219–2227.
- 28. Nayak, P. K.; Sendner, M.; Wenger, B.; Wang, Z.; Sharma, K.; Ramadan, A. J.; Lovrincic, R.; Pucci, A.; Madhu, P. K.; Snaith, H. J., Impact of Bi³⁺ Heterovalent Doping in Organic–Inorganic Metal Halide Perovskite Crystals. *J. Am. Chem. Soc.* **2018**, 140, 574–577.
- 29. Lozhkina, O. A.; Murashkina, A. A.; Shilovskikh, V. V.; Kapitonov, Y. V.; Ryabchuk, V. K.; Emeline, A. V.; Miyasaka, T., Invalidity of Band-Gap Engineering Concept for Bi³⁺ Heterovalent Doping in CsPbBr₃ Halide Perovskite. *J. Phys. Chem. Lett.* **2018**, 9, 5408–5411.
- 30. Yamada, Y.; Hoyano, M.; Akashi, R.; Oto, K.; Kanemitsu, Y., Impact of Chemical Doping on Optical Responses in Bismuth-Doped CH₃NH₃PbBr₃ Single Crystals: Carrier Lifetime and Photon Recycling. *J. Phys. Chem. Lett.* **2017**, 8, 5798-5803.
- 31. Zhou, Y.; Yong, Z. J.; Zhang, K. C.; Liu, B. M.; Wang, Z. W.; Hou, J. S.; Fang, Y. Z.; Sun, H. T.; Song, B., Ultrabroad Photoluminescence and Electroluminescence at New Wavelengths from Doped Organometal Halide Perovskites. *J. Phys. Chem. Lett.* **2016,** 7, 2735-41.
- 32. Ulatowski, A. M.; Wright, A. D.; Wenger, B.; Buizza, L. R. V.; Motti, S. G.; Eggimann, H. J.; Savill, K. J.; Borchert, J.; Snaith, H. J.; Johnston, M. B.; Herz, L. M., Charge-Carrier Trapping Dynamics in Bismuth-Doped Thin Films of MAPbBr₃ Perovskite. *J. Phys. Chem. Lett.* **2020**, 11, 3681–3688.
- 33. Meng, R.; GuangbaoWu; Zhou, J.; Zhou, H.; HonghuaFang; Loi, M. A.; Zhang, Y., Understanding the Impact of Bismuth Heterovalent Doping on the Structural and Photophysical Properties of CH₃NH₃PbBr₃ Halide Perovskite Crystals with Near-IR Photoluminescence. *Chem. Eur. J.* **2019**, 25, 5480–5488.
- 34. Stavrinadis, A.; Rath, A. K.; Arquer, F. P. G. a. d.; Diedenhofen, S. L.; Mage'n, C. s.; Martinez, L.; So, D.; Konstantatos, G., Heterovalent Cation Substitutional Doping for Quantum Dot Homojunction Solar Cells. *Nat. Commun.* **2013**, 4, 2981-2987.
- 35. Kamat, P. V.; Dimitrijevic, N. M.; Nozik, A. J., Dynamic Burstein-Moss Shift in Semiconductor Colloids. *J. Phys. Chem. Lett.* **1989**, 93, 2873-2875.

- 36. Mondal, N.; De, A.; Das, S.; Paul, S.; Samanta, A., Ultrafast Carrier Dynamics of Metal Halide Perovskite Nanocrystals and Perovskite Composites. *Nanoscale* **2019**, 11, 9796–9818.
- 37. Wu, K.; Liang, G.; Shang, Q.; Ren, Y.; Kong, D.; Lian, T., Ultrafast Interfacial Electron and Hole Transfer from CsPbBr₃ Perovskite Quantum Dots. *J. Am. Chem. Soc.* **2015**, 137, 12792–12795.
- 38. Exact estimation of this long time-constant is not possible in this setup, which is suited for measurements in the fs-ps time window.
- 39. Mondal, N.; Paul, S.; Samanta, A., Photoinduced 2-way Electron Transfer in composites of Metal Nanoclusters and Semiconductor Quantum Dots. *Nanoscale* **2016**, 8, 14250-14256.
- 40. Yu, P.; Wen, X.; Lee, Y.-C.; Lee, W.-C.; Kang, C.-C.; Tang, J., Photoinduced Ultrafast Charge Separation in Plexcitonic CdSe/Au and CdSe/Pt Nanorods. *J. Phys. Chem. Lett.* **2013**, 4, 3596–3601.
- 41. Ahmed, T.; Seth, S.; Samanta, A., Mechanistic Investigation of the Defect Activity Contributing to the Photoluminescence Blinking of CsPbBr₃ Perovskite Nanocrystals. *ACS Nano* **2019**, 13, 13537-13544.
- 42. Seth, S.; Mondal, N.; Patra, S.; Samanta, A., Fluorescence Blinking and Photoactivation of All-Inorganic Perovskite Nanocrystals CsPbBr₃ and CsPbBr₂l. *J. Phys. Chem. Lett.* **2016**, 7, 266-271.
- 43. Ito, S.; Toitani, N.; Pan, L.; Tamai, N.; Miyasaka, H., Fluorescence Correlation Spectroscopic Study on Water-Soluble Cadmium Telluride Nanocrystals: Fast Blinking Dynamics in the μs–ms Region. *J. Phys.: Condens. Matter* **2007**, 19, 486208.
- 44. Patra, S.; Samanta, A., A Fluorescence Correlation Spectroscopy, Steady-State, and Time- Resolved Fluorescence Study of the Modulation of Photophysical Properties of Mercaptopropionic Acid Capped CdTe Quantum Dots upon Exposure to Light. *J. Phys. Chem. C* **2013**, 117, 23313–23321.
- 45. Dong, C.; Qian, H.; Fang, N.; Ren, J., Study of Fluorescence Quenching and Dialysis Process of CdTe Quantum Dots, Using Ensemble Techniques and Fluorescence Correlation Spectroscopy. *J. Phys. Chem. B* **2006**, 110, 11069-11075.
- 46. Dong, C.; Liu, H.; Ren, J., Assessing the Blinking State of Fluorescent Quantum Dots in Free Solution by Combining Fluorescence Correlation Spectroscopy with Ensemble Spectroscopic Methods. *Langmuir* **2014**, 30, 12969–12976.
- 47. Yao, J.; Larson, D. R.; Vishwasrao, H. D.; Zipfel, W. R.; Webb, W. W., Blinking and Nonradiant Dark Fraction of Water-Soluble Quantum Dots in Aqueous Solution. *PNAS* **2005**, 102, 14284–14289.
- 48. Mondal, N.; Samanta, A., Complete Ultrafast Charge Carrier Dynamics in Photo-Excited All-Inorganic Perovskite Nanocrystals (CsPbX₃). *Nanoscale* **2017**, *9*, 1878-1885.
- 49. Lai, R.; Wu, K., Picosecond electron trapping limits the emissivity of CsPbCl₃ perovskite nanocrystals. *J. Chem. Phys.* **2019**, 151, 194701-194706.

Chapter 6 Individual Particle Level....

- 50. Mosconi, E.; Merabet, B.; Meggiolaro, D.; Zaoui, A.; Angelis, F. D., First-Principles Modeling of Bismuth Doping in the MAPbI₃ Perovskite. *J. Phys. Chem. C* **2018**, 122, 14107–14112.
- 51. Durisic, N.; Godin, A. G.; Walters, D.; tter, P. G.; Wiseman, P. W.; Heyes, C. D., Probing the "Dark" Fraction of Core Shell Quantum Dots by Ensemble and Single Particle pH-Dependent Spectroscopy. *ACS Nano* **2011**, 5, 9062–9073.

CHAPTER 7

Concluding Remarks

7.1 Overview

The thesis deals with photophysical properties of an emerging class of semiconductor materials, lead halide perovskites, which are the focus of great attention in recent times due to their potential applications in photovoltaics and light-emitting devices. The objective of this study is to control photoluminescence (PL) efficiency of perovskite nanocrystals (NCs) and investigate charge carrier recombination and interfacial charge transfer processes in those photoexcited NCs. As the efficiency of devices made of these materials depends on the fate of the charge carriers, a thorough understanding of the dynamics of different competing radiative and nonradiative charge carrier recombination processes is essential for proper utilization of these substances. We have studied carrier relaxation processes in photoexcited perovskite nanocrystals of various compositions and interfacial hole transfer employing single particle fluorescence spectroscopy techniques by studying the PL blinking in the immobilized or freely diffusing [fluorescence correlation spectroscopy (FCS) measurements] states of NCs using a time-tagged timeresolved confocal fluorescence microcopy setup. Femtosecond transient absorption, PL upconversion and time correlated single photon counting (TCSPC) technique have also been employed along with other steady state techniques for various optical measurements for the works described in the thesis. We have synthesized the perovskite NCs in the colloidal medium following the hot injection method and characterized those NCs following techniques such as TEM, FESEM, FTIR, XPS, ICP and PXRD. A summary of the overall findings of this work is given below.

Even though the perovskite NCs are highly defect tolerant, they are not completely defect free. The defects mostly arise from the surface and/or intrinsic in nature. The optical properties of the NCs are highly dependent on the surface quality of them due to high surface to volume ratio. Hence surface treatment with proper reagent is one of the key methods to obtain defect-free NCs with superior PL properties for light-based applications. Here we explore a post-synthetic surface treatment with sodium/ammonium tetrafluoroborate salts for a large number of CsPbX₃ NCs. We observed that this simple

treatment improves substantially the PL properties of several CsPbX₃ NCs emitting in the 400-600 nm region substantially. It is noteworthy that unlike previous reports, this method enhances the PLQY to near-unity, not only for CsPbBr₃ but also for CsPbBr_xCl_{3-x} NCs. Complex multi-exponential PL decay converts to single-exponential decay in some cases after treatment. Further, even for blue-emitting CsPbCl₃ NCs, a remarkable PL enhancement of 50-fold is achieved. Apart from this we also found that tetrafluoroborate ion is effective in removing excess lead (lead nanoparticles or under coordinated lead) from the surface, which acts as non-radiative carrier trapping centers.

Understanding the carrier trapping mechanisms and effect of surface treatment is important for exploration of the full potential of the perovskite NCs for different applications. We have tracked recombination routes of the photoexcited charge carriers by probing the PL blinking of the immobilized and freely diffusing single CsPbBr₃ NC. We found that nonradiative band-edge recombination through trap states, trion recombination, and trapping of the hot carriers are responsible for the blinking of any given NC. Significant suppression of blinking is observed upon surface treatment with tetrafluoborate salt, as evident from the disappearance of "off" and "gray" PL states.

Doping is an important strategy to introduce new properties or to modify the intrinsic properties of a semiconductor. We investigated Bi-doped (less-toxic) CsPbBr₃ NCs, which are weakly luminescent compared to the parent system. Using a combination of ensemble and single particle techniques and varying the Bi-dopant in the NCs, we found three types of NCs differing in PL brightness in Bi-doped CsPbBr₃ NCs. We also studied the change in charge carrier recombination dynamics upon doping. Nonuniform doping is tracked to be responsible for the heterogeneous nature of the sample. The difference in the rate of trapping of the carriers and PL brightness of the NCs arises due to difference in dopant content in the NCs which consequently leads to a change in the density of the dopant introduced trap states.

7.2 Future scope and challenges

In first two working chapter (chapter 3), we have shown enhancement of PLQY by post synthetic surface modifications. However we could not achieve PLQY of near-unity for CsPbCl₃ and CsPbI₃ NCs. Our treatment removes the defects due to excess lead on the surface. In case of CsPbCl₃ NCs we could improve the PLQY only upto 50%, which indicates that along with the surface defects, intrinsic defects are also present in those NCs. Literature shows that doping is an important strategy to remove such intrinsic defects. It is reported that dopants like Cd, Ni etc. can improve the PLQY to near-unity for CsPbCl₃ NCs. Hence one needs to look for appropriate dopants and protocol to achieve trap-free violet emitting CsPbCl₃ NCs. No change in PL efficiency for CsPbI₃ NCs with our tetrafluoroborate salts indicates that defects in these NCs arise mostly because of structural distortion. In this regard more studies are needed to obtain defect free red emitting CsPbI₃ NCs.

In chapter 4, our study is focused only to blinking and its suppression in CsPbBr₃ NCs with the aforementioned surface treatment. It will be interesting to examine the blinking in other halide NCs, especially in those NCs which emit in the blue region. Understanding the mechanism of blinking in this region is still lacking. Again, non-blinking semiconductor NCs is always desirable in high efficiency photovoltaic and optoelectronic devices. With our surface treatment we have shown suppression of blinking of CsPbBr₃ NCs, however for other NCs it is still unexplored. Again several methods have been developed to prepare near-unity CsPbX₃ NCs. Investigation of blinking nature at the single particle level is needed to prepare non-blinking NCs.

Understanding the dynamics of charge transfer to and from the NCs is important for application in photovoltaic devices. In case of perovskite NCs most of our understanding of those processes is from ensemble average study. Single particle level study provides more understanding on the static and dynamic heterogeneity of those processes. There lies a huge opportunity to explore the charge transfer processes from perovskite NCs to various suitable charge acceptors at the single particle level.

Several reports are available on the preparation of different fluorescent lead free perovskite or perovskite related materials, like Cs₄PbBr₆ semiconductors. In this regard understanding the nature of trapping and investigation of radiative and nonradiative recombination in these systems by probing their blinking nature is an interesting and under-explored area of research.

Appendix

Appendix I

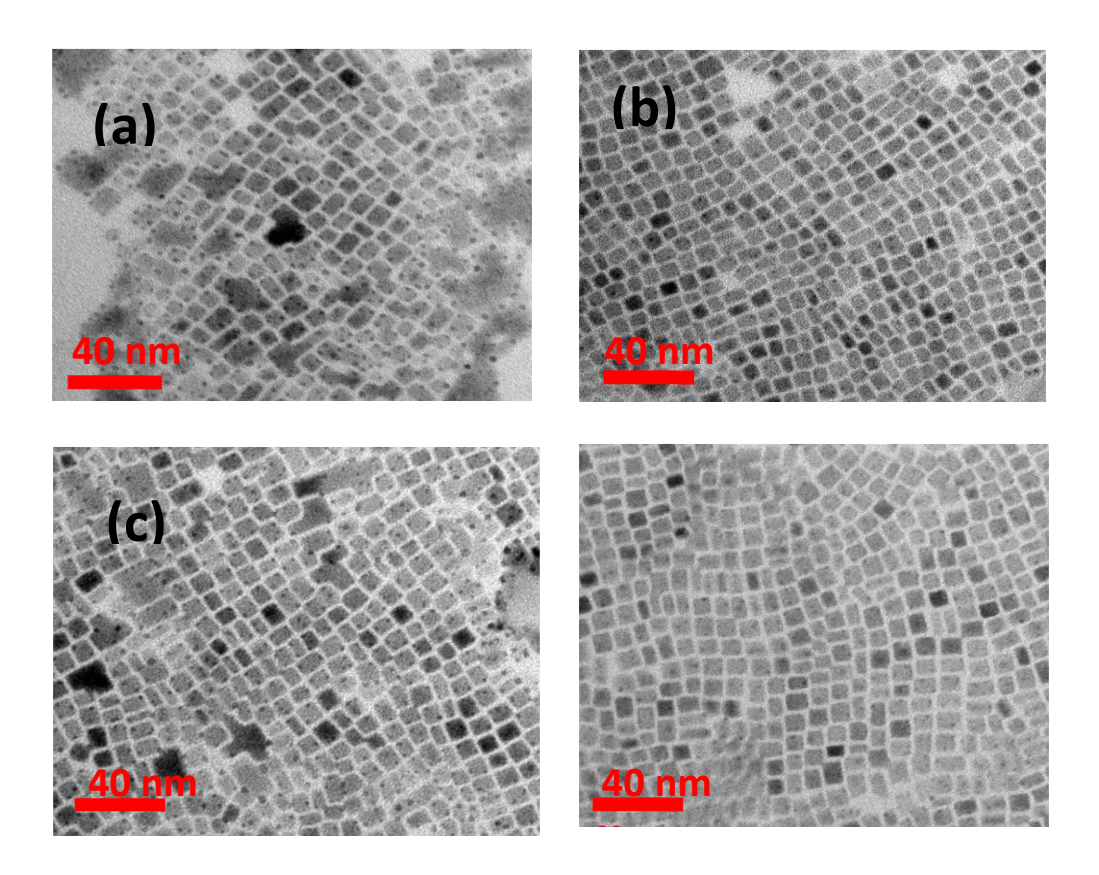
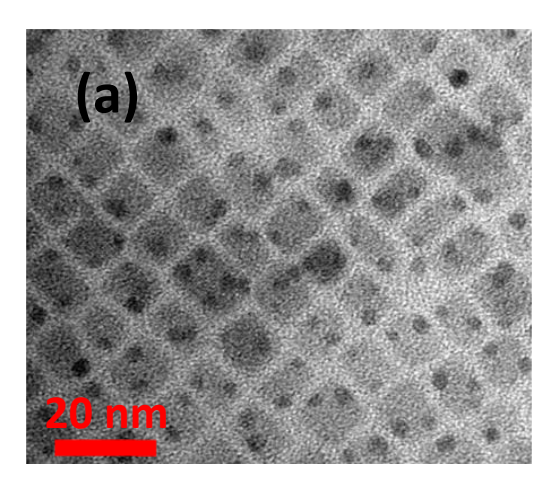


Figure AI.1: TEM images of $CsPbBr_{1.5}Cl_{1.5}$ and $CsPbBr_{1.5}I_{1.5}$ before (a & c) and after (b & d) treatment with tetrafluoroborate salts. Removal of lead NPs on treatment is evident from the TEM images.



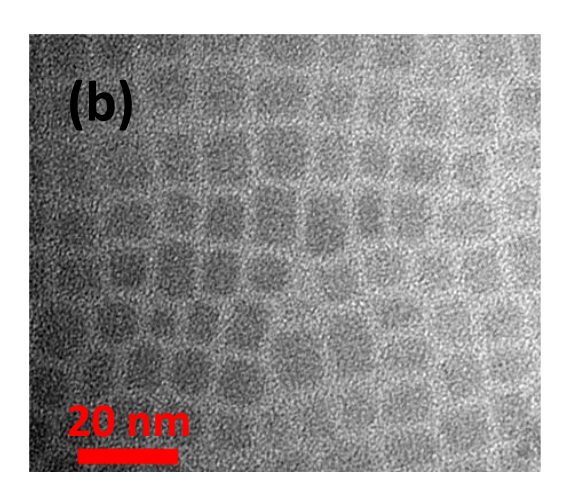


Figure AI.2: TEM images of CsPbCl₃ before (a) and after (b) treatment with tetrafluoroborate salts. Removal of black spots corresponding to Pb(0) nanoparticles on the NCs on treatment is clearly observable.

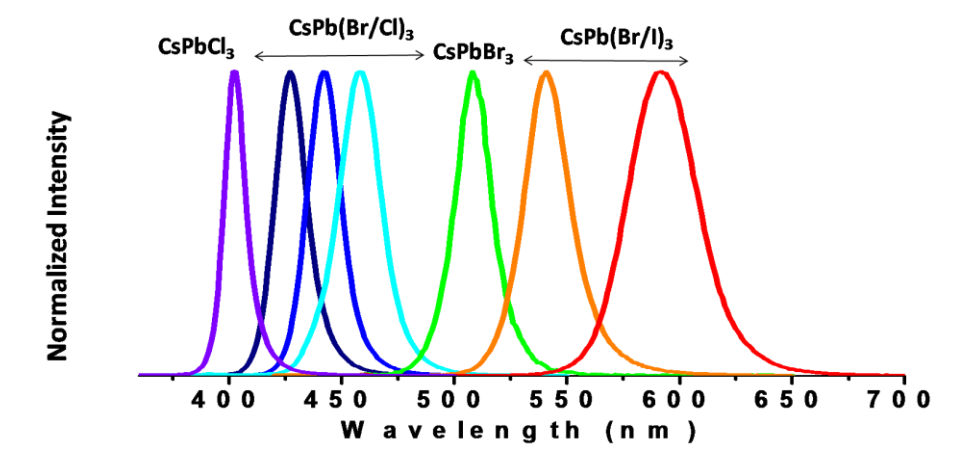


Figure AI.3: PL spectra of the NCs with different halide composition covering almost the entire visible range.

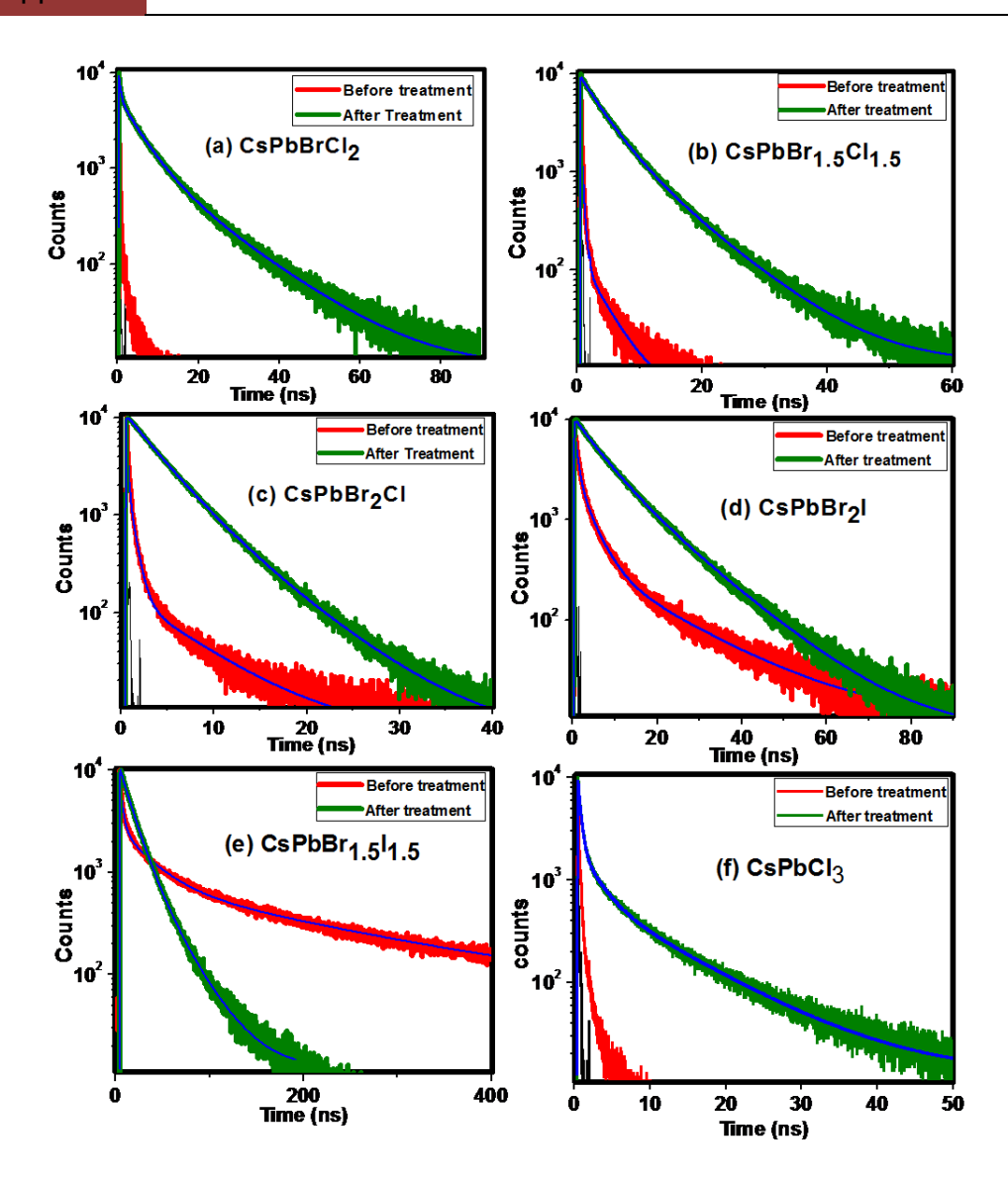


Figure AI.4: Comparison of the photoluminescence decay curves of different mixed halide NCs before and after treatment. The decay profile for CsPbCl₃, CsPbBrCl₂ and CsPbBr_{1.5}Cl_{1.5} before treatment could not be fitted properly as the PL lifetime is shorter than the instrument resolution (65 ps).

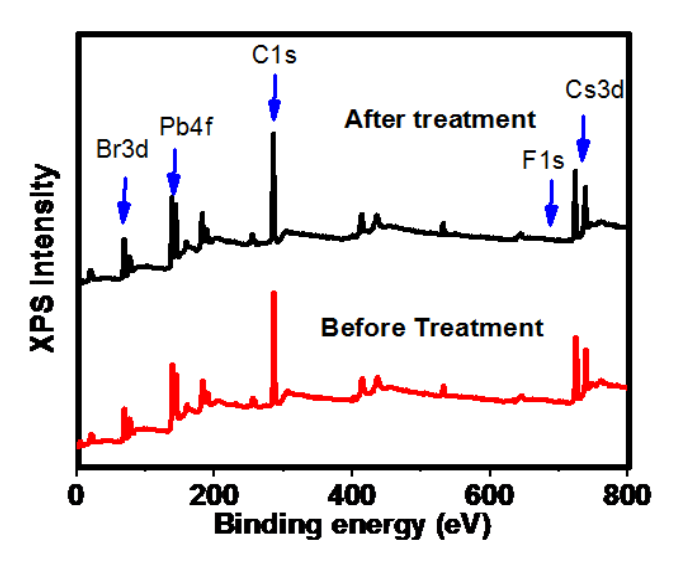


Figure AI.5: XPS survey spectra of CsPbBr₃ NCs before and after treatment. No peak for F could be seen at around 685 eV after treatment.

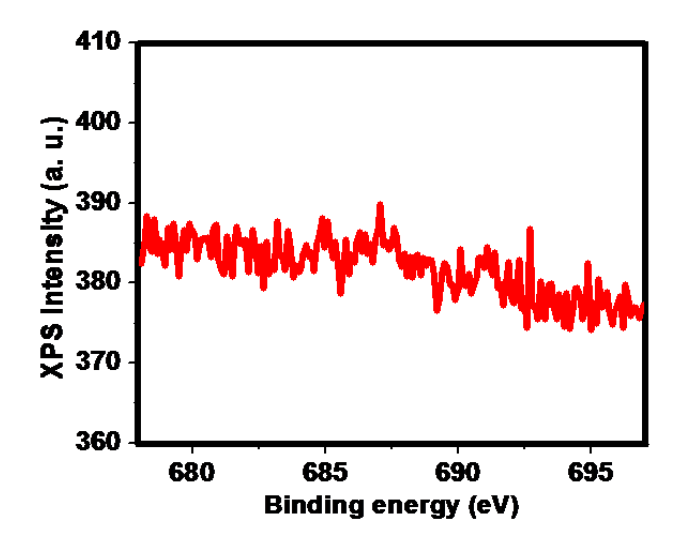


Figure AI.6: XPS spectra shows no peak for F 1s after treatment.

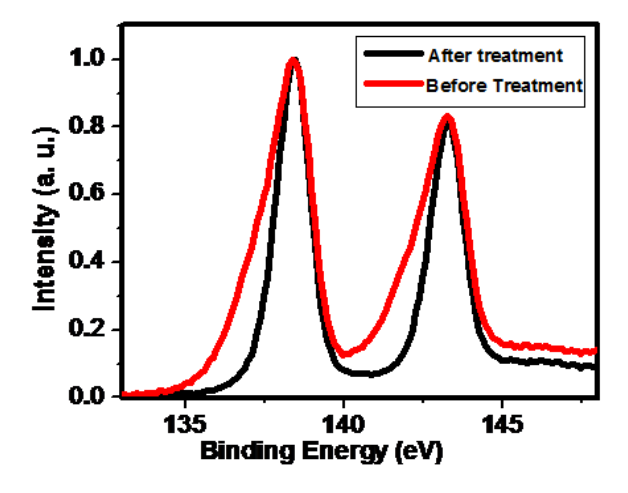


Figure AI.7: Overlap of the XPS spectra of Pb 4f7/2 and 4f5/2 before and after treatment from surface level.

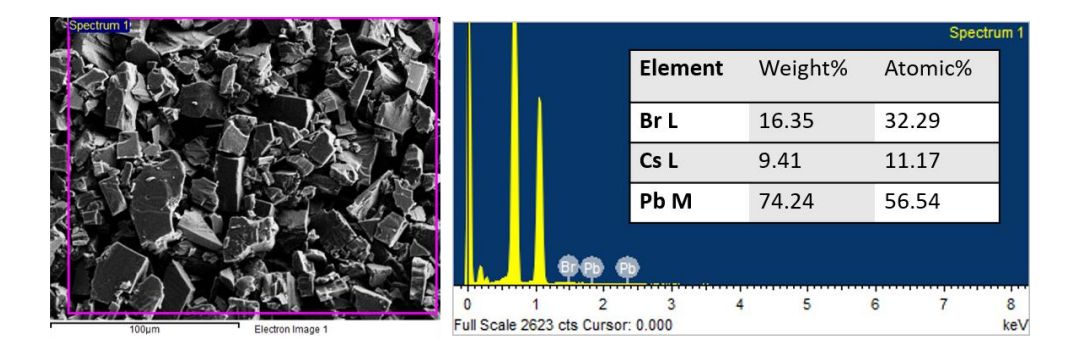


Figure AI.8: SEM image, EDX spectrum and atomic composition of constituent elements of excess unreacted solid tetrafluoroborate salt after treatment upon removal of NCs from the solid salt by several washing with toluene and centrifugation for five times. Presence of excess lead is observed (Br:Pb = 0.57:10) which is higher than that of the lead present in the NCs.

Appendix

Table AI.1: Ratio of halides taken during the synthesis and in the NCs (estimated using Energy dispersive X-ray analysis).

Notation of mixed	Precursor ratio of	The Br:Cl/I ratio in	
halide NCs Studied	PbBr ₂ :PbCl ₂ /PbI ₂	the NCs	
CsPbBrCl ₂	1:2	1:2	
CsPbBr _{1.5} Cl _{1.5}	1:1	1.1 : 1	
CsPbBr ₂ Cl	2:1	2.2:1	
CsPbBr _{1.5} I _{1.5}	1:1	1.2:1	
CsPbBr ₂ I	2:1	2.3:1	

Table AI.2: PL decay parameters of the NCs (*PL decay is found to be too fast to be measured accurately in our setup having a time resolution of ~ 65 ps).

Materials	$\tau_1(a_1)$ ns	$\tau_2(a_2)$ ns	$\tau_3(a_3)$ ns	τ_{avr} ns
CsPbCl ₃ *				
T-CsPbCl ₃	0.37(0.80)	2.25(0.14)	9.94(0.06)	1.3
CsPbBrCl ₂ *				
T-CsPbBrCl ₂	0.39(0.49)	5.23(0.36)	15(0.15)	4.3
CsPbBr _{1.5} Cl _{1.5} *				
T-CsPbBr _{1.5} Cl _{1.5}	3.51(0.70)	8.38(.30)		4.9
CsPbBr ₂ Cl	0.10(0.85)	5.09(.01)	0.51(0.14)	0.2
T-CsPbBr ₂ Cl	2.41(0.63)	6.1(0.37)		3.8
CsPbBr ₃	2.99(0.24)	19.8(0.02)	0.86(0.74)	1.8
T-CsPbBr ₃	3.55(0.96)	9.26(0.04)		3.8
CsPbBr ₂ I	3.80(0.26)	46(0.04)	1.2(0.70)	3.7
T-CsPbBr ₂ I	10.00(0.72)	22.4(0.28)		13.4
CsPbBr _{1.5} I _{1.5}	16.70(0.29)	90.3(0.10)	2.22(0.61)	15.2
T-CsPbBr _{1.5} I _{1.5}	17.60(.82)	47.0(0.18)		22.9

Appendix II

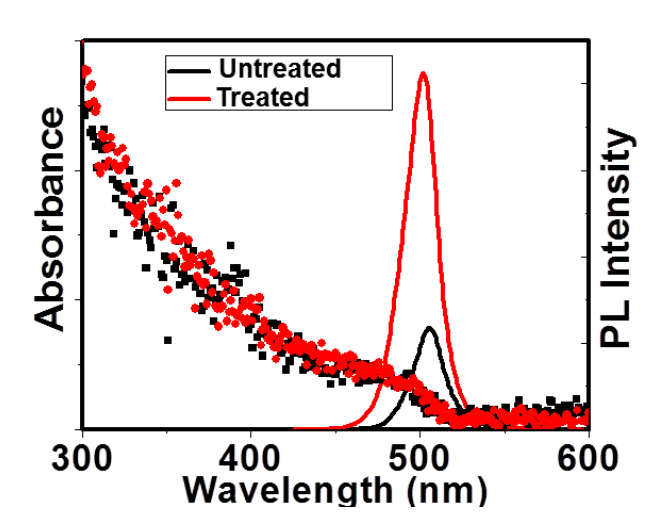


Figure AII.1: Absorption and PL spectra of untreated and treated NCs in ODE.

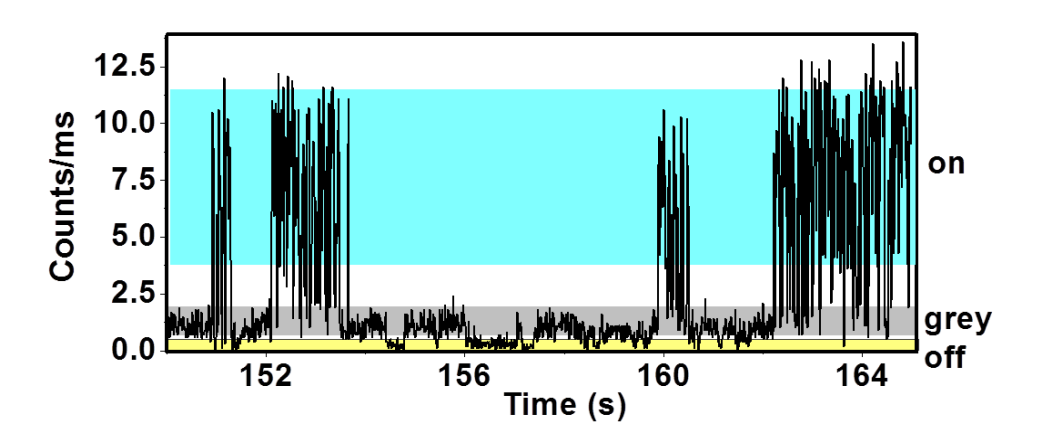


Figure AII.2: PL intensity time-trace shows the "grey" states very close to the "off" states.

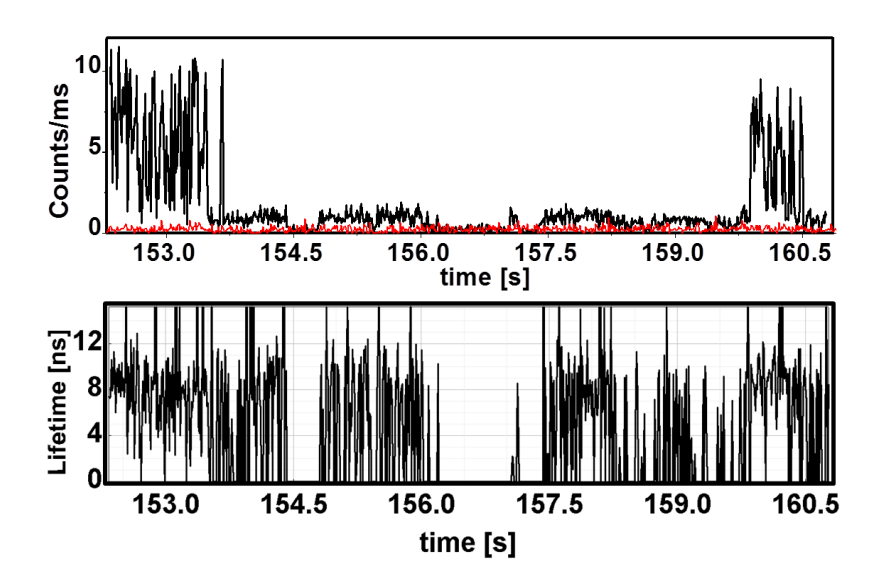


Figure AII.3: PL intensity (upper panel) and lifetime trajectories (lower panel) of another single NC, which shows Class-1 blinking.

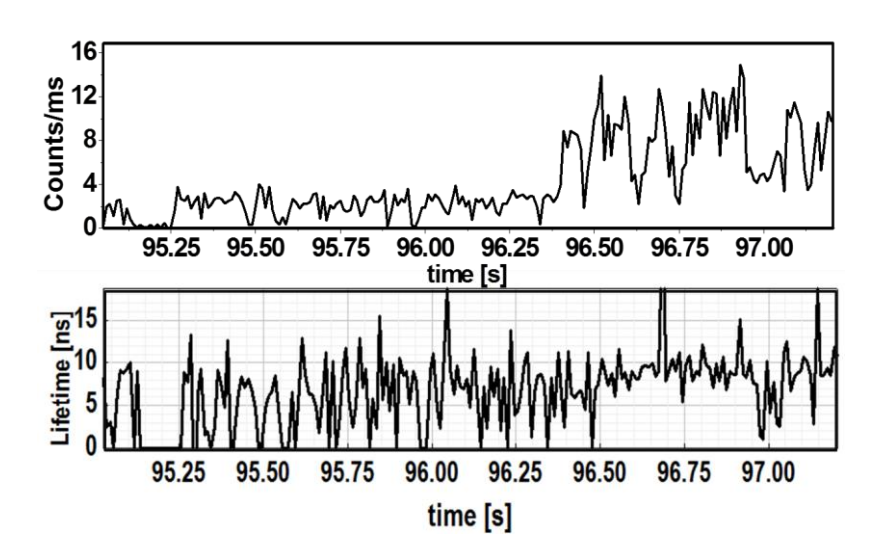


Figure AII.4: PL intensity (upper panel) and lifetime trajectories (lower panel) of single NC, which shows Class-2 blinking.

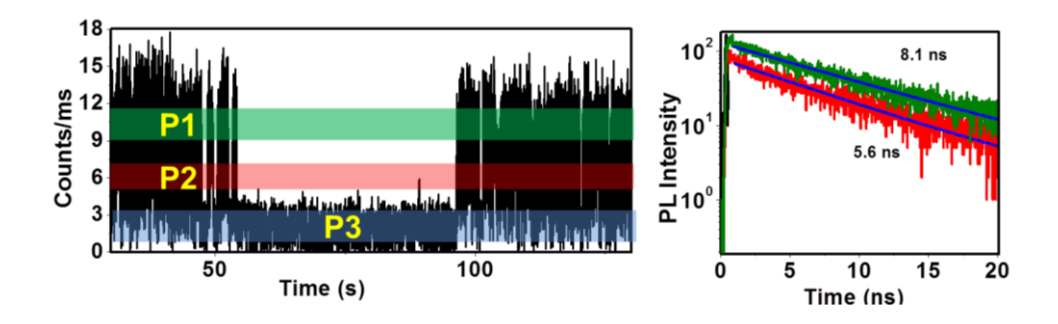


Figure AII.5: PL lifetime decay profiles of two high intensity levels (P1 and P2) of NCs showing Class-2 blinking. $\eta = k_r(P1):k_r(P2) = 1.1$.

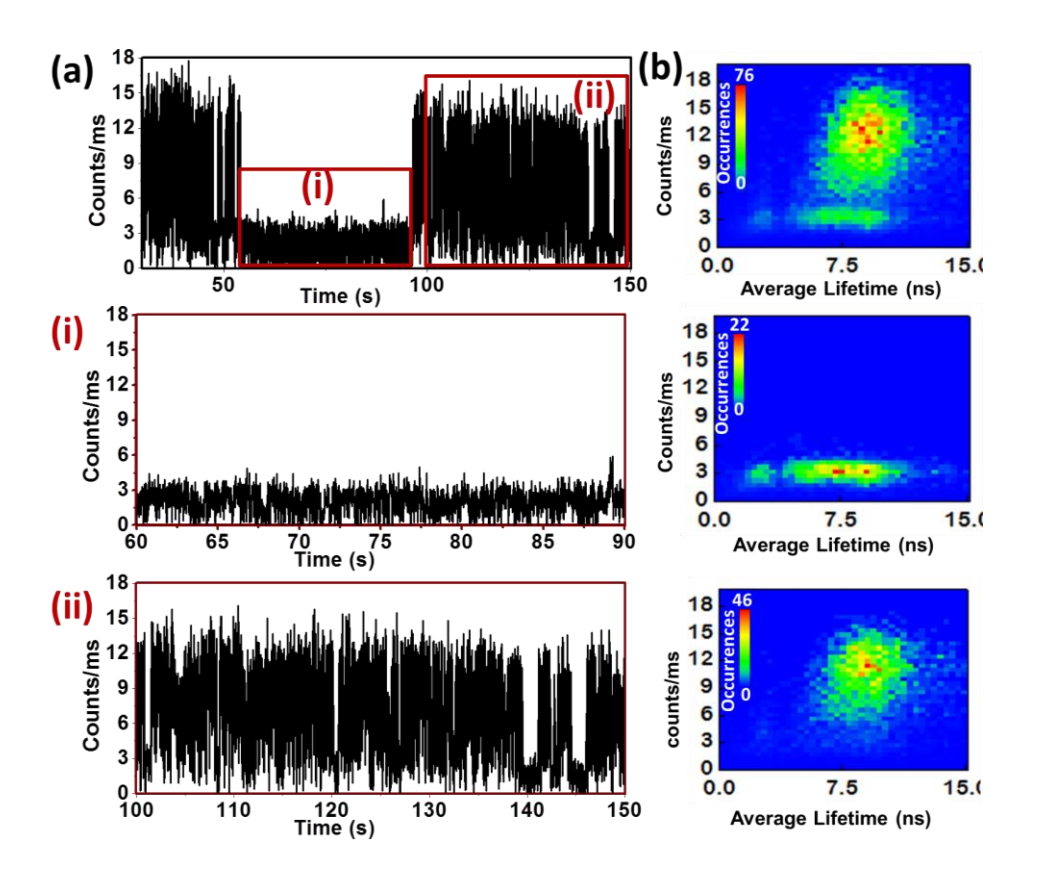


Figure AII.6: PL intensity trajectory (complete range) of the untreated NCs exhibiting Class-2 blinking (a) and the FLID pattern (b). The FLID pattern for region (i) ("grey"

states) shows two states for trion and hot carrier recombination and that for region (ii) is similier to Class-1 blinking which has less grey states.

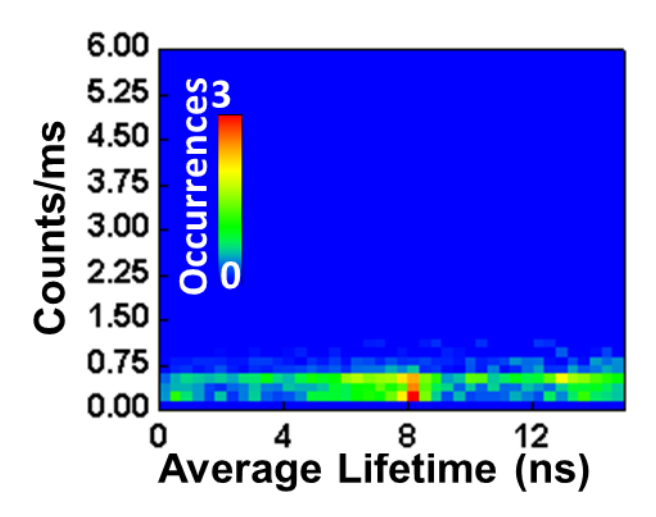


Figure AII.7: The FLID pattern of the background with very low occurrences.

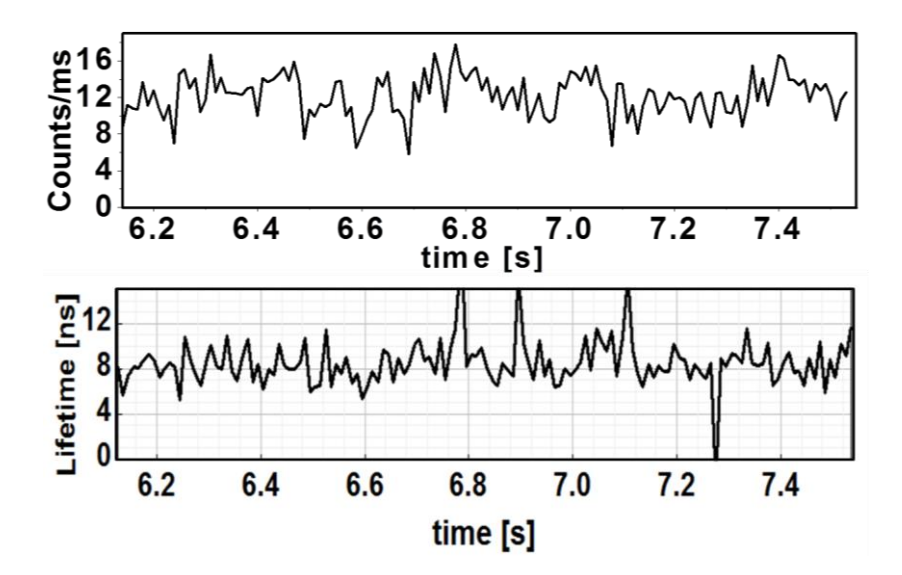


Figure AII.8: PL intensity (upper panel) and lifetime trajectories (lower panel) of the treated NCs.

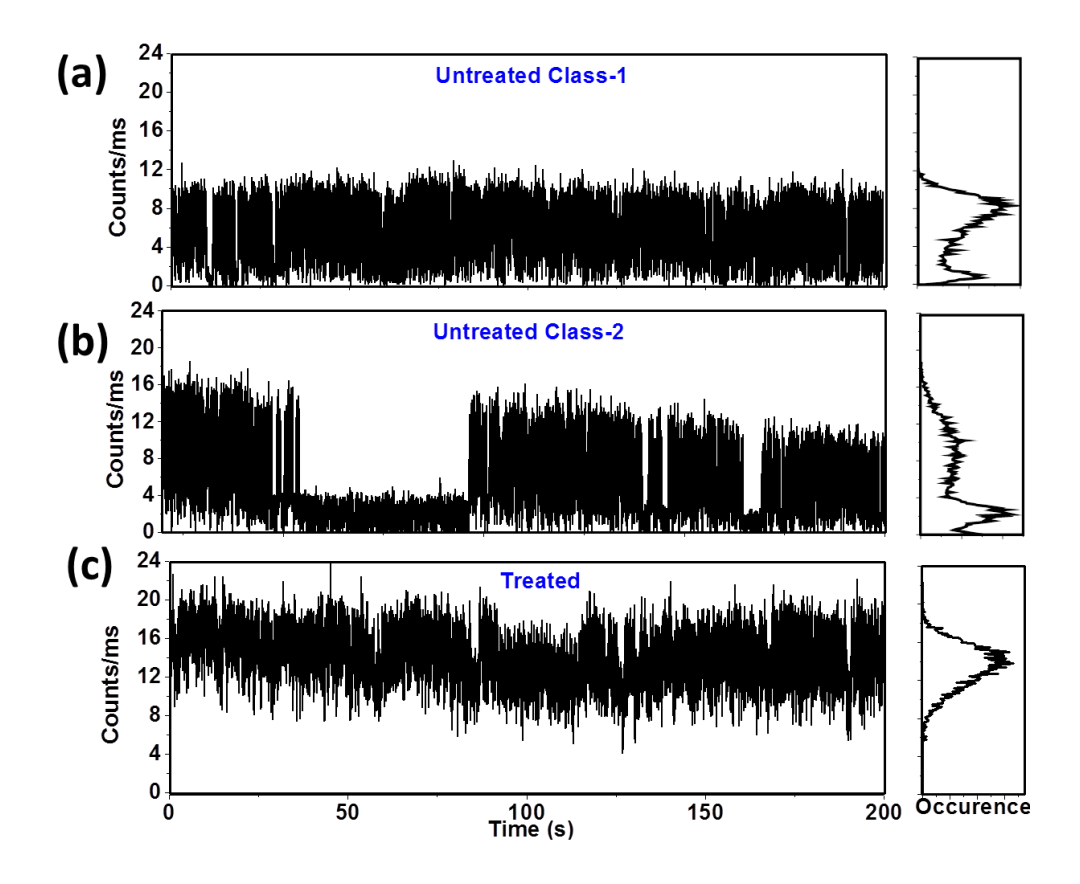


Figure AII.9: PL intensity time traces and occurrences of the measured PL intensities of untreated (a and b) and treated (c) NCs.

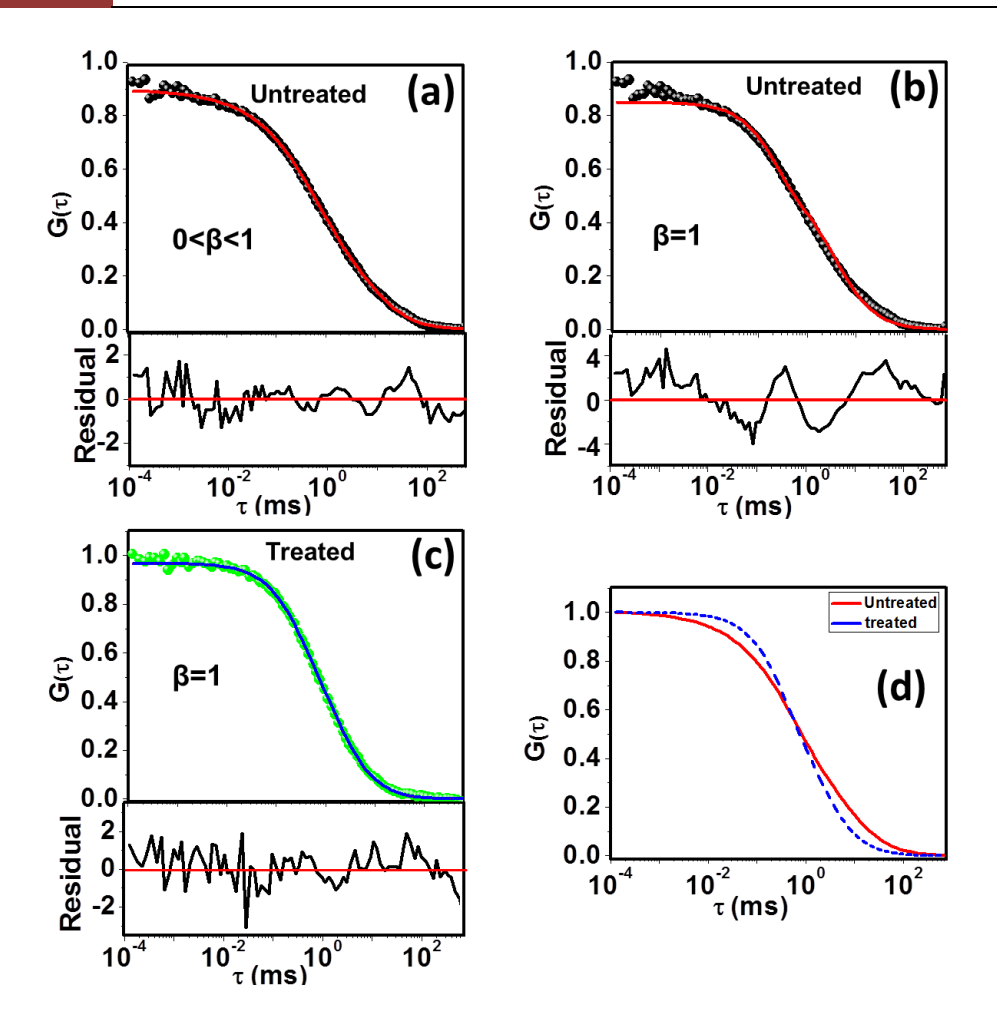


Figure AII.10: The fitted correlation curves with corresponding residuals (shown below) for untreated (a and b) and treated (c) NCs. For the untreated NCs, it is evident from the fits and residuals shown in panels (a and b), 3D diffusion model with stretched exponential $(0 < \beta < 1)$ fits the data much better compared to an exponential $(\beta = 1)$ fit. Whereas, for the treated sample, the data fits quite with exponential function $(\beta = 1)$. (d) Fitted correlation curves (normalized) for treated and untreated samples highlighting the difference.

Appendix

Table AII.1: Lifetime components (τ_i) and their weightages (α_i) of the different PL levels shown in Figure 4.1.

Region	$\tau_1(\alpha_1)$ ns	$\tau_2(\alpha_2)$ ns
R1	8.1	
R2	7.4	
R3	6.5	
R4	6.0	
R5	6.9(0.62)	1.1(0.38)
R6	5.6(.40)	0.75(0.60)

Table AII.2: Lifetime components and associated amplitudes of different intensity levels for the untreated NC showing Class-2 blinking, whose PL intensity trace is shown in Figure 4.3.

Level	$\tau_1(\alpha_1)$ ns	$\tau_2(\alpha_2)$ ns
P1	8.8	
P2	6.1	
P4	6.9(0.60)	1.6(0.40)

Table AII.3: After-treatment lifetime components (τ_i) and their weightages (α_i) of the different PL levels shown in Figure 4.4.

Region	$\tau_1(\alpha_1)$ ns	$\tau_2(\alpha_2)$ ns
T1	7.6	
T2	8.1(0.71)	1.9(0.29)
Т3	6.6(0.62)	1.7(0.38)

Appendix

Table AII.4: Estimated values of amplitude of correlation at zero time-delay [G(0)] and diffusion time (τ_D) .

NCs	G(0)	$\tau_{\mathrm{D}}\left(\mathrm{ms}\right)$
Untreated	1.19±0.04	4.39±0.47
treated	0.86 ± 0.03	2.28±0.50

Appendix III

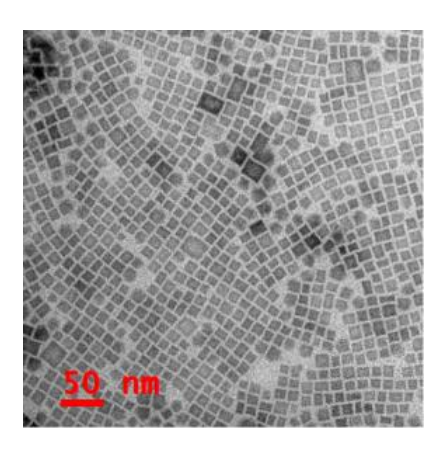


Figure AIII.1: TEM images of FAPbBr₃ NCs.

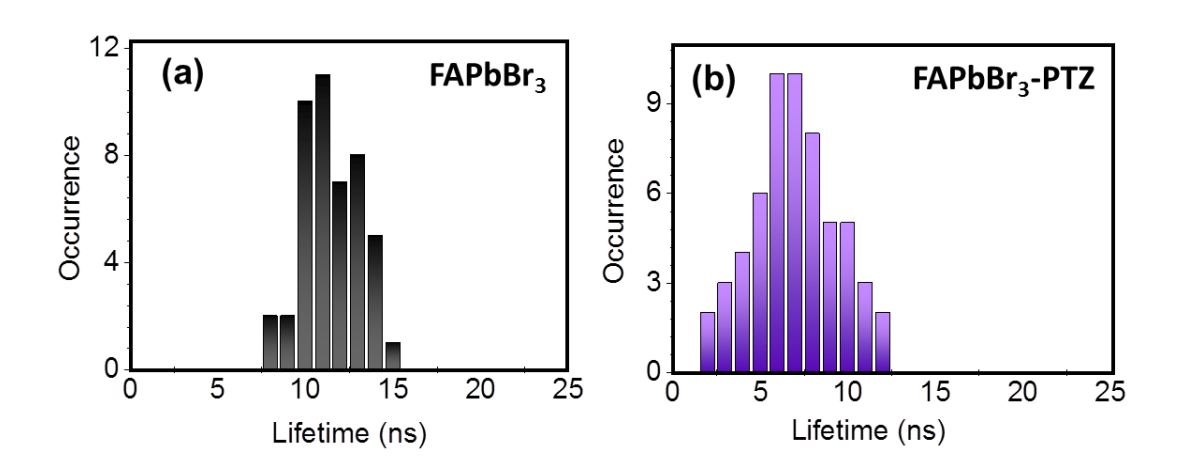


Figure AIII.2: Lifetime histogram of highest intensity state (ON state) of all the studied (a) FAPbBr₃ and (b) FAPbBr₃-PTZ NCs.

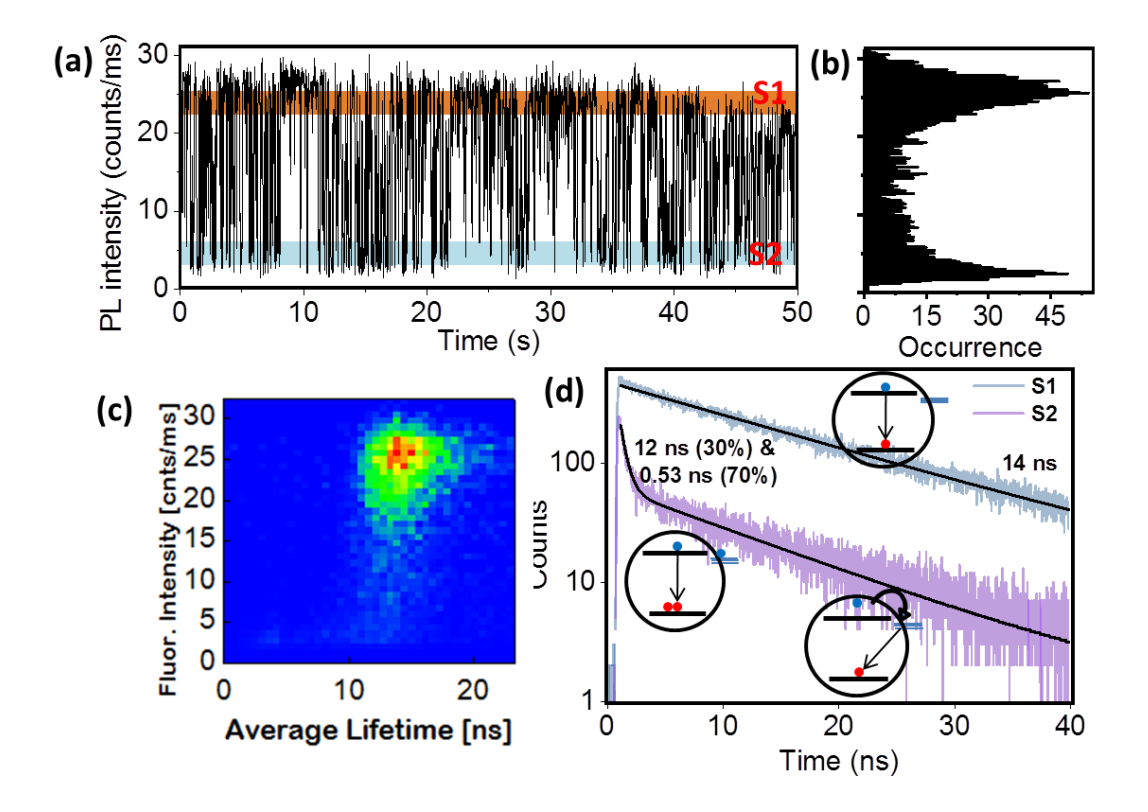
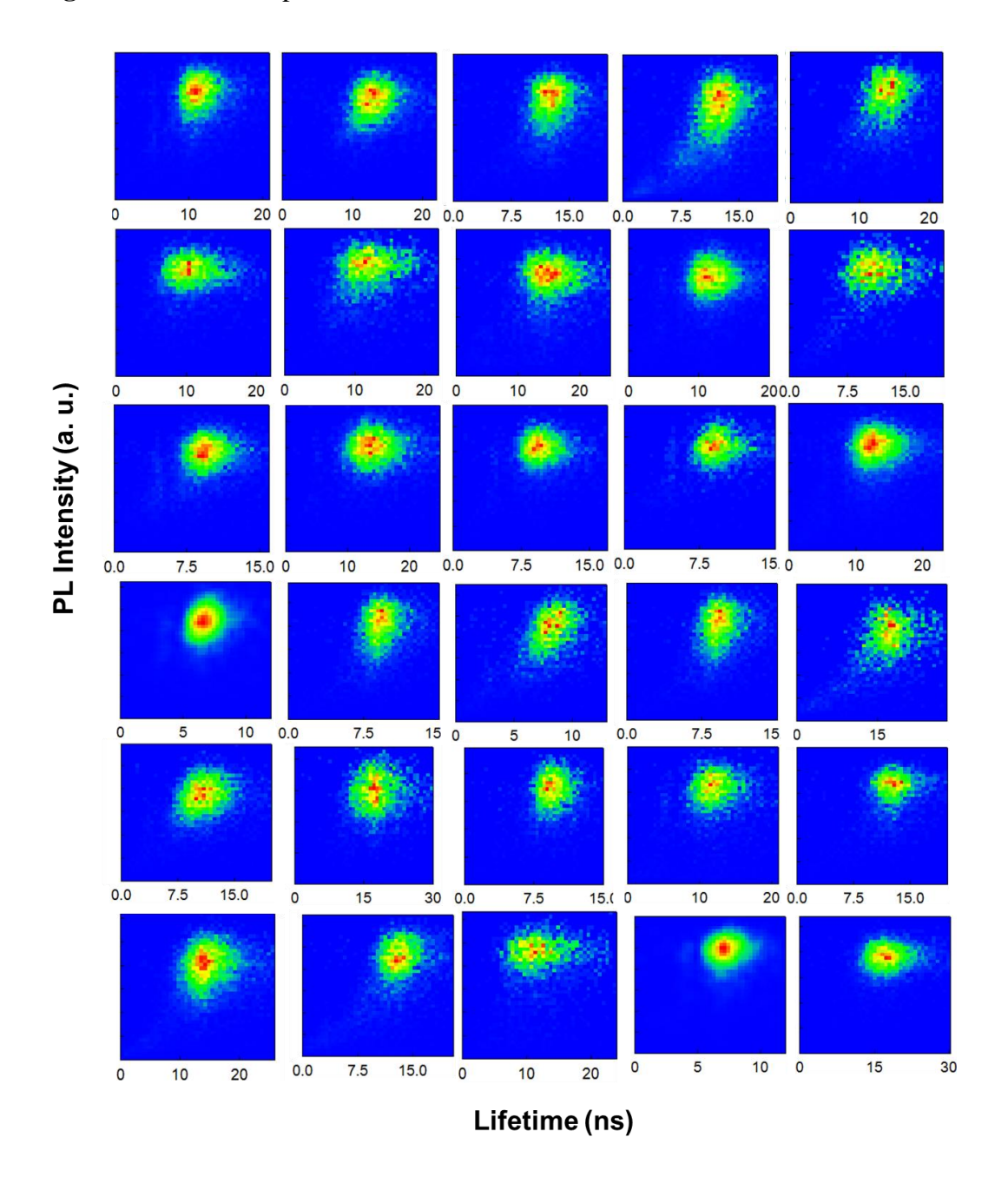


Figure AIII.3: (a) PL intensity trajectory, its corresponding (b) intensity distribution, (c) FLID pattern and (d) PL intensity decay of FAPbBr₃ NCs, where along with AC mechanism, HC is also responsible for PL blinking. Out of 49 studied NCs 5 showed this kind of blinking mechanism.

Figure AIII.4: FLID patterns of all studied FAPbBr₃ NCs



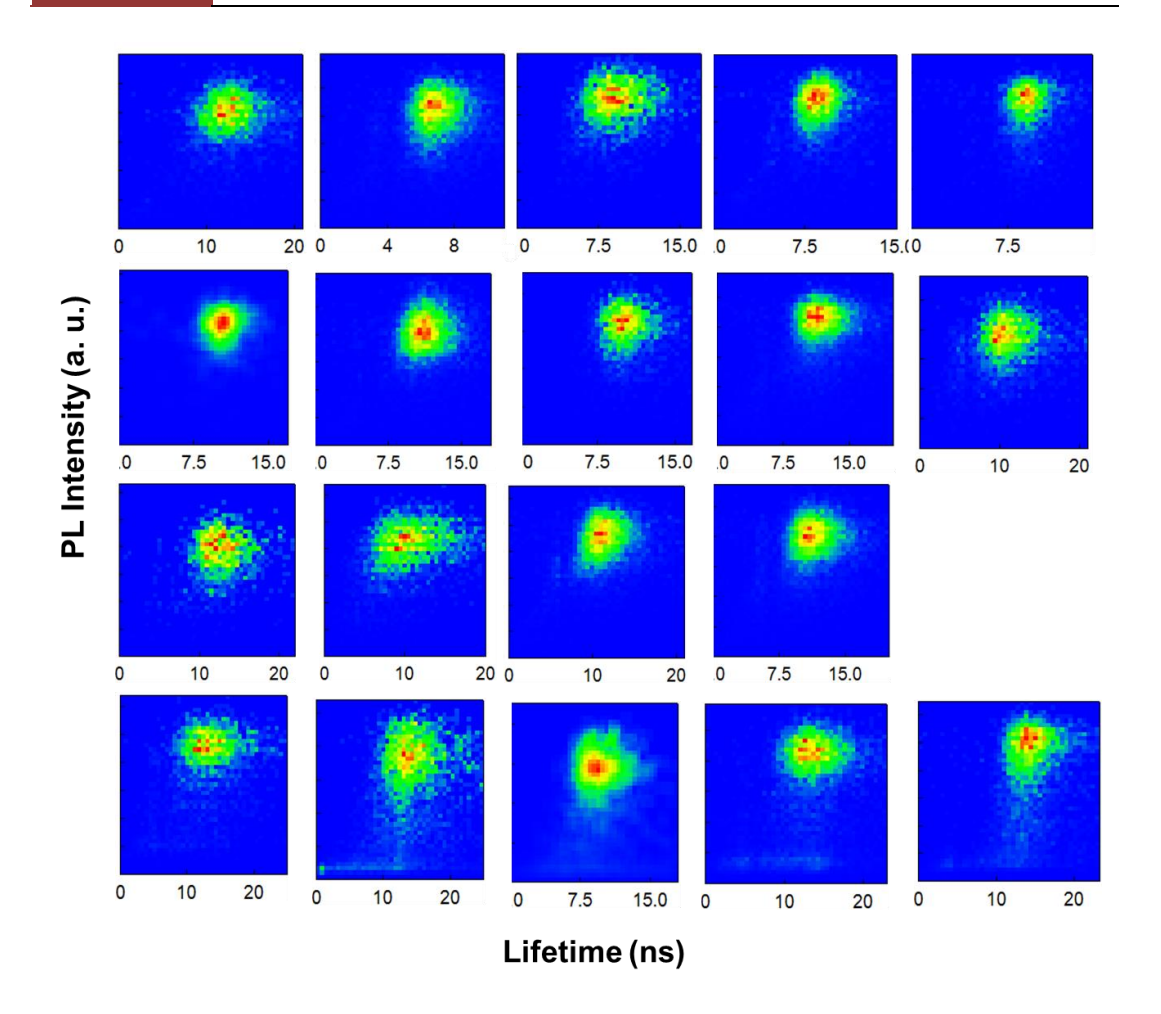
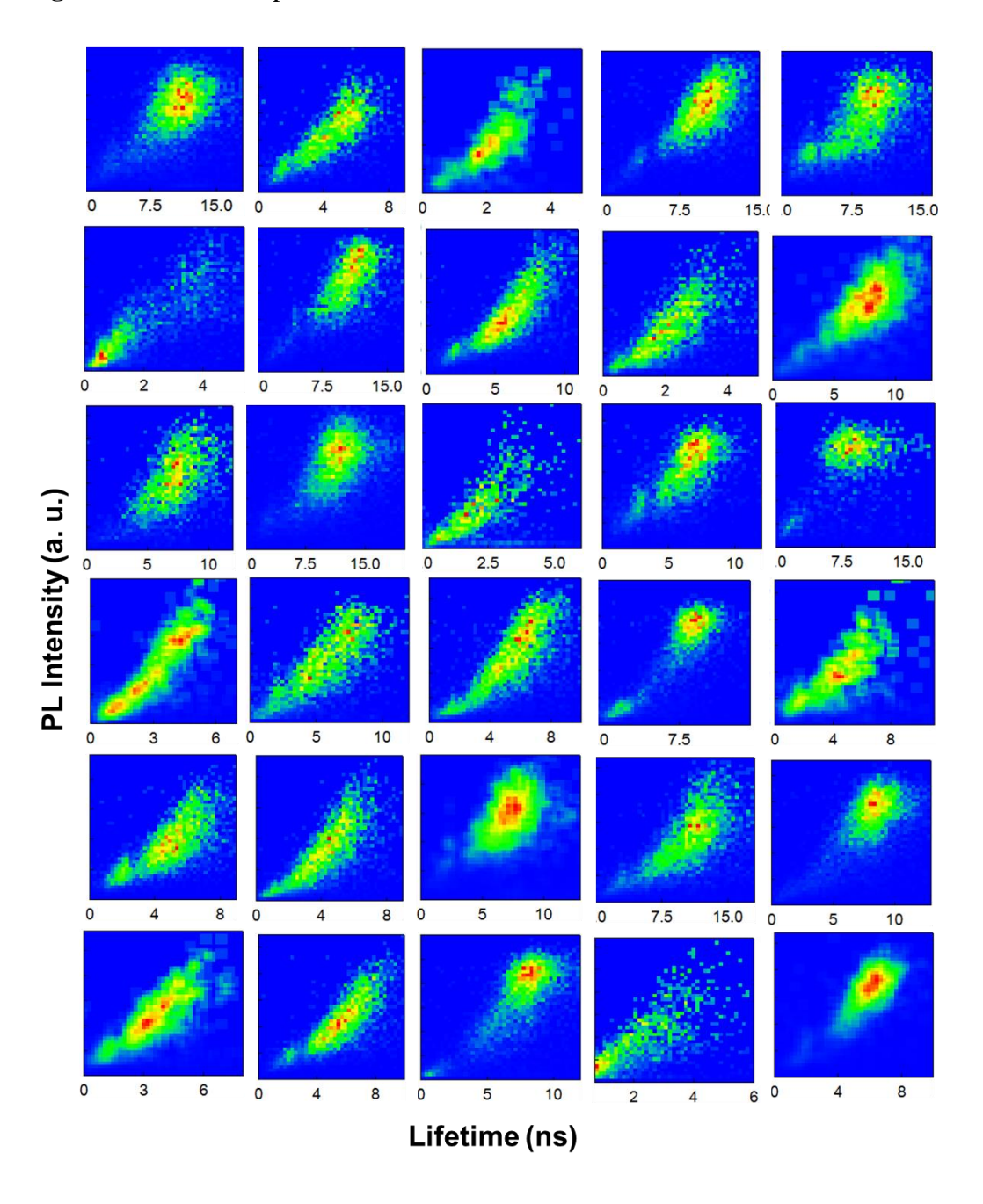
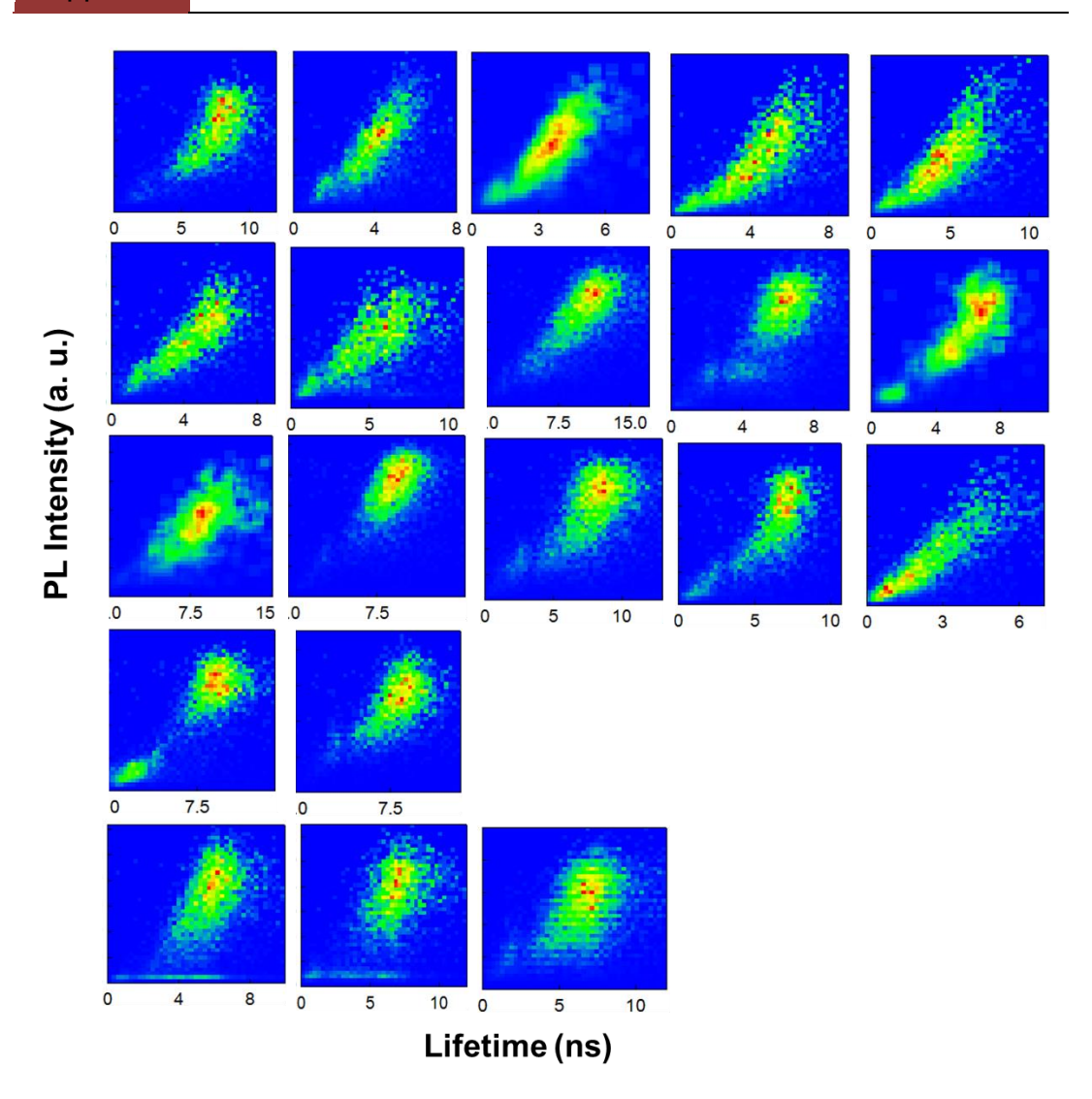


Figure AIII.5: FLID patterns of all studied FAPbBr₃-PTZNCs.





Appendix

Table AIII.1: Lifetime components (τ_i) and their weightages (α_i) of the different PL levels of FAPbBr₃ NC shown in Figure 3.

Region	$\tau_1(\alpha_1)$ ns	$\tau_2(\alpha_2)$ ns
R1	12.7	
R2	3.7 (0.5)	0.45(0.5)

Table AIII.2: Lifetime components (τ_i) and their weightages (α_i) of the different PL levels of FAPbBr₃-PTZ1 NC shown in Figure 3.

Region	$\tau_1(\alpha_1)$ ns	$\tau_2(\alpha_2)$ ns
T1	8.6	
T2	6.7	
Т3	2.2	
T4	1.2(0.6)	0.47(0.4)

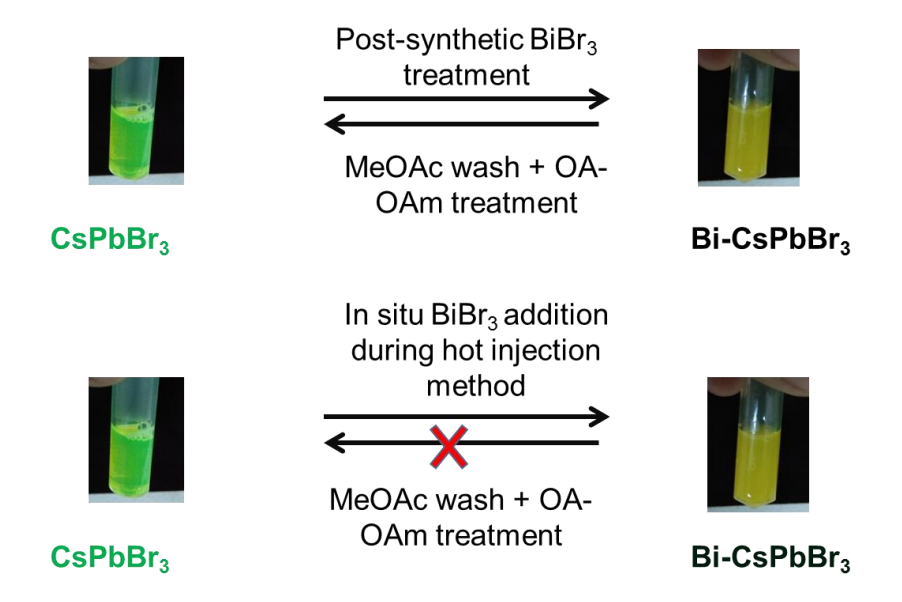
Table AIII.3: Lifetime components (τ_i) and their weightages (α_i) of the different PL levels of FAPbBr₃-PTZ2 NC shown in Figure 3.

Region	$\tau_1(\alpha_1)$ ns	$\tau_2(\alpha_2)$ ns
P1	6	
P2	4.5	
P3	2.8(0.6)	0.67(0.4)
P4	1.5(0.8)	0.45(0.2)

Appendix IV

Control Experiment: In a post synthetic treatment, 1 μ L of a saturated solution of BiBr₃ was added to 2 mL of hexane solution (nM) of CsPbBr₃ NCs and sonicated for 2 mins. A change in colour of the solution with a decrease in PL intensity is observed almost immediately. To remove the excess/surface adsorbed Bi, the sample solution was mixed with methyl acetate in 1: 2 (v/v) sample solutions: methyl acetate ratio and centrifuged at 7000 rpm. The precipitate when dispersed in hexane and then treated with OA and OAm mixture, the initial green colour of the solution returned and PLQY enhanced to ~90% like the undoped system.

On the other hand, for the *in situ* prepared Bi-doped sample using the hot injection method, the PL did not come back to a state like that of the undoped sample (shown in Scheme S1). This indicates that decrease in PLQY of the CsPbBr₃ NCs on post-synthetic treatment with BiBr₃ is due to surface-adsorbed Bi. Washing with methyl acetate followed by the ligand treatment removes them from the surface. This also establishes that decrease in PLQY of the system prepared by the hot-injection method is due to incorporation of Bi into the NCs.



Scheme AIV.1: A pictorial representation of sequential treatment of the Bi-treated CsPbBr₃ NCs (post synthetic or *in situ*) with methyl acetate (MeOAc) and a mixture of OA-OAm.

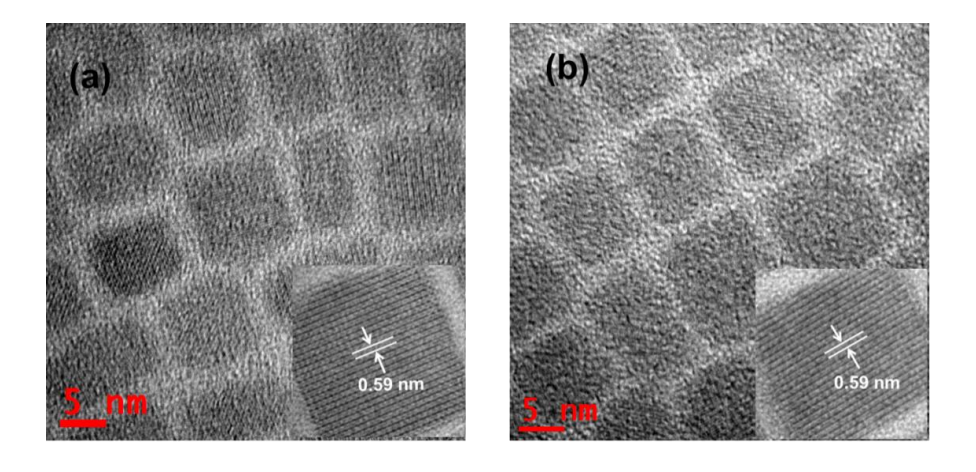


Figure AIV.1: TEM images of the (a) undoped and (b) 8.2% Bi-doped CsPbBr₃ NCs.

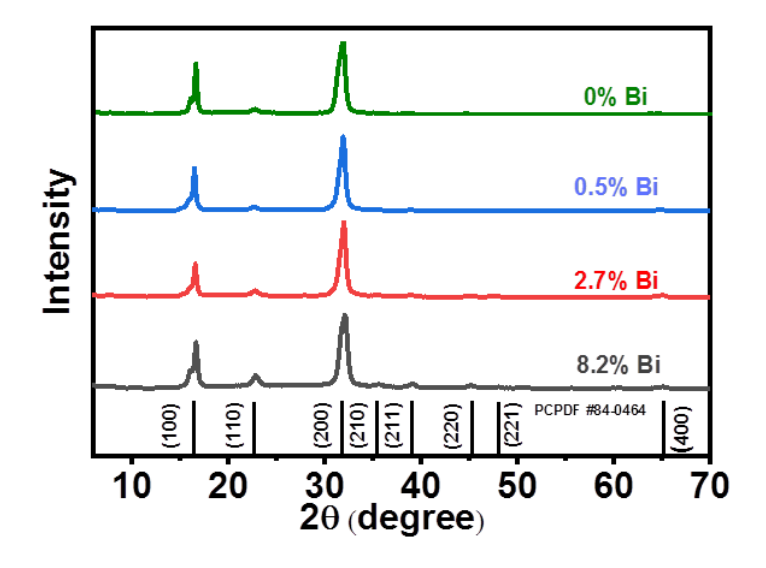


Figure AIV.2: PXRD patterns of the Bi-doped (0%, 0.5%, 2.7% and 8.2%) CsPbBr₃ NCs.

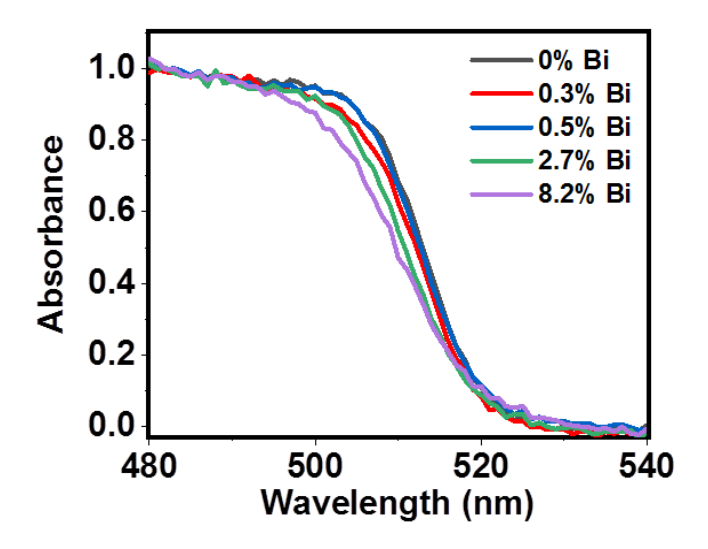


Figure AIV.3: Normalized absorption spectra of Bi-doped (0%, 0.3%, 0.5%, 2.7% and 8.2%) CsPbBr₃ NCs dispersed in hexane.

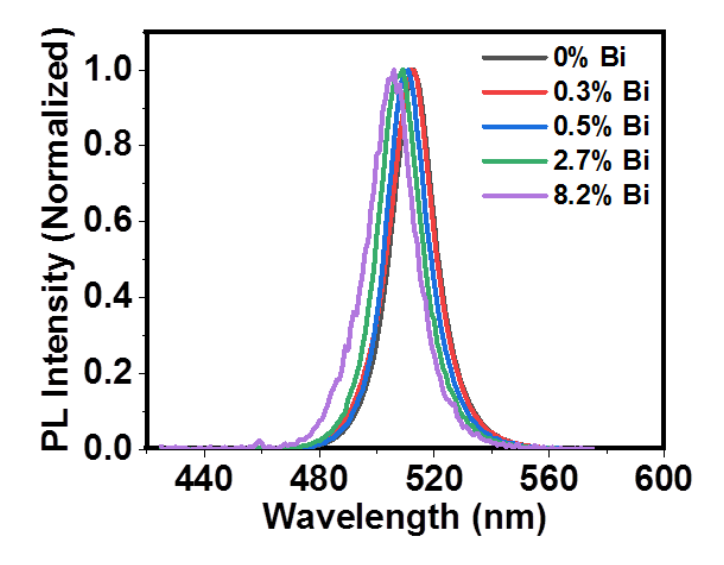


Figure AIV.4: Normalized emission spectra ($\lambda_{ex} = 400$ nm) of Bi-doped (0%, 0.3%, 0.5%, 2.7% and 8.2%) CsPbBr₃ NCs dispersed in hexane.

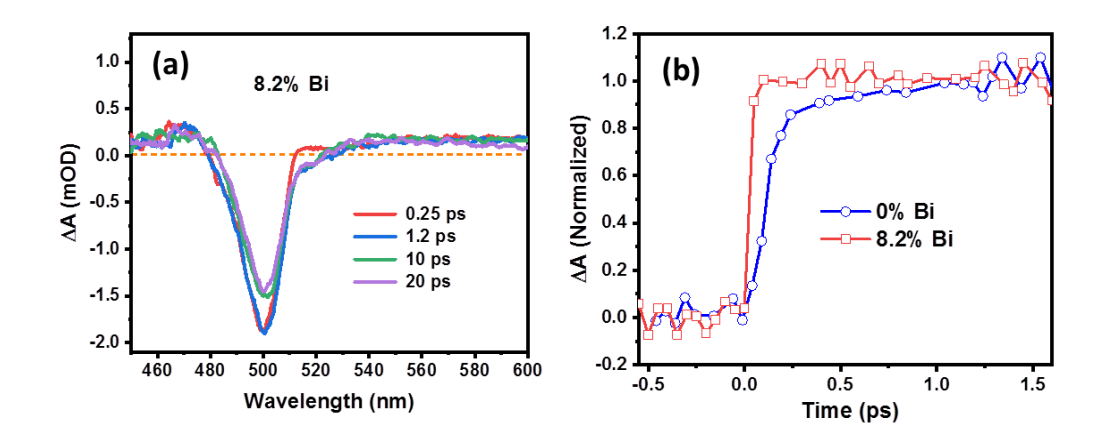


Figure AIV.5: (a) TA spectra ($\lambda_{ex} = 400$ nm) of 8.2% Bi-doped CsPbBr₃ NCs in hexane, (b) bleach formation kinetics of 0% and 8.2% Bi-doped NCs.

Table AIV.1: ICP-OES estimated Bi content in the precursor solutions

Bi/Pb (%) in feed solutions	Bi/Pb (%) ICP data
2	0.3
5	0.5
10	2.7
20	8.2

Table AIV.2: Estimated time constants[#] from TA and PL UC measurements for different samples.

Di content in	τ ₁ [ps]	τ ₂ [ps]	
Bi-content in CsPbBr ₃ NCs	TA	UC	TA	UC
0%			> 500 (1.0)	> 500 (1.0)
0.5%	3.2±0.5 (0.43)	6.2±0.2 (0.59)	> 500 (0.57)	> 500 (0.41)
2.7%	1.9±0.3 (0.73)	3.4±0.4 (0.72)	> 500 (0.27)	> 500 (0.28)

*For samples with 8.2% Bi-content, the time constants could not be estimated using TA measurements as due to the dominance of hot carrier trapping process, the bleach recovery signal does not represent the actual carrier trapping time scale and in PL UC measurements, the PL intensity (at zero time) of the system is so low that no reliable decay kinetics could be recorded.



Boosting the Photoluminescence of $CsPbX_3$ (X = Cl, Br, I) Perovskite Nanocrystals Covering a Wide Wavelength Range by Postsynthetic Treatment with Tetrafluoroborate Salts

Tasnim Ahmed, Sudipta Seth, and Anunay Samanta*®

School of Chemistry, University of Hyderabad, Hyderabad 500046, India

Supporting Information

esium lead halide perovskite (CsPb X_{3} , X = Cl, Br, I) NCs have received enormous attention in recent years as promising optoelectronic materials¹⁻⁴ due to their broad absorption, intense photoluminescence (PL) with narrow bandwidth, high defect tolerance, and band gap tunability over the entire visible range. 5-7

The PL properties of these substances are, however, highly sensitive to the synthetic conditions and compositions. Several reports show low photoluminescence quantum yield (PLQY) of these perovskites.^{6,8–14} Even the highly luminescent perovskite NCs prepared by the hot injection method are not free from defects, which act as trapping centers for the charge carriers and lower the PL efficiency of the systems.⁶ The complex multiexponential PL decay kinetics of these NCs is also the consequence of defects, ^{[10,1],1,3,15–19} which can be due to the surface.²⁰ or intrinsic in nature.^{21–23} Because of high surface to volume ratio of these NCs, their PL properties are largely determined by the quality of the surface. Hence, surface treatment by appropriate reagent is key to obtaining defect-free samples with superior PL properties for light-based applications.

Attempts have been made previously to improve the PLQY of perovskite NCs by surface modification, during ^{14,17} or after the synthesis. ^{10,11,19},24,25 A PLQY value of near unity is observed for CsPbBr3 NCs upon treatment with Na/NH4 thiocyanate salts²⁴ and lead bromide.¹⁹ Upon treatment with didodecyldimethylammonium bromide,¹⁰ didodecyldimethylammonium sulfide¹¹ and metal bromides, ^{14,19} PLQY values of 70-83% are achieved for these NCs. For CsPbI3 NCs, a PLQY of $\sim 100\%$ is achieved by treatment with trioctylphosphine-PbI $_2$ or 2,2'-iminodibenzoic acid. 17,25 It is thus evident that no given method of surface treatment is effective for all or a large number of CsPbX3 NCs. During our quest for a common method (postsynthetic treatment) for improvement of the PL properties of a wide variety of CsPbX3 NCs, we observed that a simple treatment with sodium/ammonium tetrafluoroborate salt is highly effective. It enhances the PLQY of several CsPbX₃ NCs emitting in the 400-600 nm region substantially. Particularly noteworthy in this context is 90-96% PLQY for CsPbBrxCl3-x, and 50-fold enhancement for

The colloidal CsPbX₃ NCs studied in this work were synthesized following the procedure reported by Protesescu et al.⁶ with minor modifications (see Supporting Information for details). Purified NCs were dispersed in distilled, anhydrous toluene for further measurements. 2–4 mL of NC (few micromolar) solution was stirred with solid NaBF₄ or NH₄BF₄

for 30 min at room temperature and open atmosphere. The majority of the changes in the NC occur within the first 10 min and become unaffected after 30 min of the treatment. Because the ionic tetrafluoroborate salts have very limited solubility in nonpolar toluene, they were separated easily from the NC solution by centrifuging for 5 min at 6000 rpm. The outcome of the treatment is highly reproducible. The tetrafluoroborate salts were used directly after purchase in this method. Colloidal dispersion of the NCs remained unaffected after the treatment.

TEM images of the as-synthesized CsPbX3 NCs show a regular cubic morphology with edge length of ~7-12 nm (depending on halide composition). No change in size of the samples after treatment is observed from TEM images (Figures 1, S1 and S2). The HR-TEM images (insets to Figure 1) show a lattice spacing of 0.59 nm for the (100) plane for CsPbBr₃ before and after the treatment.⁶ No change in crystal structure is also evident from close match of the powder XRD patterns of treated and untreated NCs. The emission peak position (λ_{max}) of the samples studied here vary between ~402 (CsPbCl₃) and ~595 nm [CsPb(Br/I)₃](Figure S3), thus covering a large part of the visible spectrum. Representative PL spectra (Figure 2) of CsPbCl₃ and CsPbBr₃ show PL peaks at 402 nm (fwhm = 14 nm) and 507 nm (fwhm = 20 nm), respectively. The PLQYs of these as-synthesized samples are measured to be ~1% and ~30%, respectively. Even though no noticeable change in size. shape or crystal structure of the NCs was found on treatment with the tetrafluoroborate salt, a huge improvement of the PL properties of the samples is observed. For example, the PLQY of treated CsPbBr₃ reaches a value of almost unity (≥95%). CsPbCl₃ shows ~50-fold enhancement of PLQY to reach a value of 50%. The other mixed halides also show excellent improvement of PLQY (Table 1). The PLQY values achieved for the mixed halides vary between 63% and 96%. We also note that no improvement of PLQY is observed only for CsPbI3 NCs. The photographs in Figure 2 highlight the PL enhancement over a wide range of wavelengths achieved in this work. The high PLQY values obtained for so many individual NCs by a single method is unprecedented. In all cases, a small but reproducible blue shift of the PL maximum (by 1-4 nm) is observed (Figure 2), though similar shift in the absorption spectra is absent. This blue shift of the PL peak for treated and more luminescent samples could be due to the

Received: March 24, 2018 Revised: May 22, 2018 Published: May 22, 2018

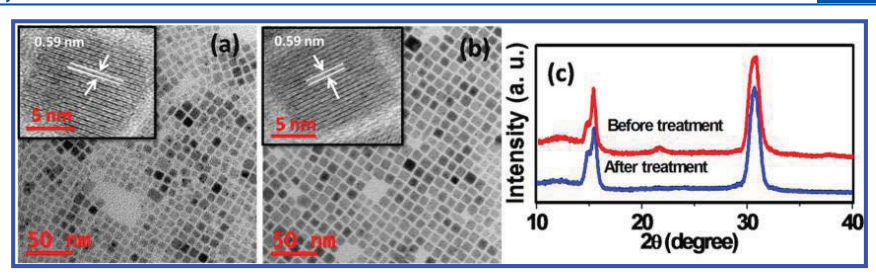


Figure 1. TEM images of $CsPbBr_3$ NCs before (a) and after (b) treatment showing an edge-length of \sim 9.7 nm. High resolution-TEM images in the insets show similar interplanar distance of 0.59 nm. (c) Powder X-ray diffraction patterns of $CsPbBr_3$ NCs before and after the treatment.

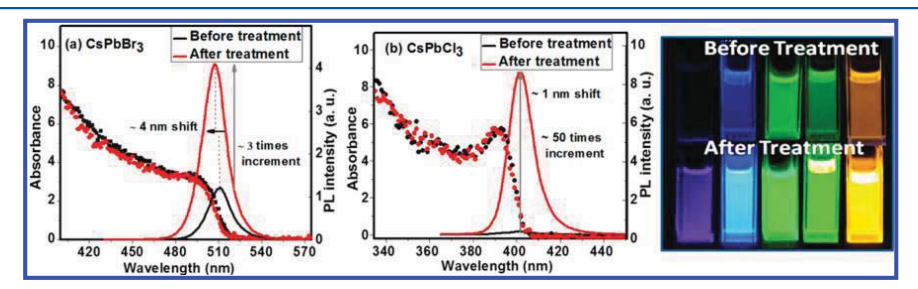


Figure 2. Absorption and PL spectra of (a) CsPbBr₃, (b) CsPbCl₃ and (c) photographs of PL of colloidal solutions of CsPbX₃ NCs in toluene (under 365 nm UV lamp) before and after treatment covering the visible spectral region of 400–600 nm. Both sodium and ammonium tetrafluoroborate salts show similar effect.

Table 1. PL Peak and QY of the NCs before and after Treatment and Comparison with Literature Values

		PLQY (%)			
Materials	$\begin{pmatrix} \lambda_{\max} \\ (nm)^a \end{pmatrix}$	Before treatment	After treatment	Literature (after treatment)	
CsPbCl ₃	402	1 ± 0.4	50 ± 5		
CsPbCl ₂ Br	427	1 ± 0.5	90 ± 3		
$CsPbCl_{1.5}Br_{1.5}$	442	2 ± 1	95 ± 2		
CsPbBr ₂ Cl	458	4 ± 1	96 ± 3		
CsPbBr ₃	507	30 ± 8	95 ± 2	~100, 19,24 71 10,11	
CsPbBr ₂ I	540	10 ± 5	70 ± 5		
$CsPbBr_{1.5}I_{1.5}$	595	13 ± 5	63 ± 2		
$CsPbI_3$	690	40 ± 5	40 ± 5	>95 ²⁵	
^a Before treatme	ent.				

removal of shallow emissive energy levels of the as-synthesized NCs. 8,9,11,12,14,24

The PL decay profiles of the samples are also significantly improved by the treatment (Figure 3). The multiexponential decay, which is characteristic of the complex/multiple radiative de-excitation pathways, $^{9,19,26-28}$ of the as-synthesized samples, is transformed to a nearly single-exponential one in some cases with significant enhancement of PL lifetime. Table 2 shows three-component decay of CsPbBr3 becomes nearly single exponential after treatment. This aspect is better seen from the decay curve shown in the 0–25 ns time window (inset of Figure 3). The $\sim\!3$ ns (τ_1) component is attributed to excitonic recombination considering the literature values, 9,19,24 and enhancement of the amplitude (α_1) of this component on treatment. As the 0.9 ns component, which was the major radiative recombination process before treatment, vanishes after the treatment, it can be attributed to the trap states arising from

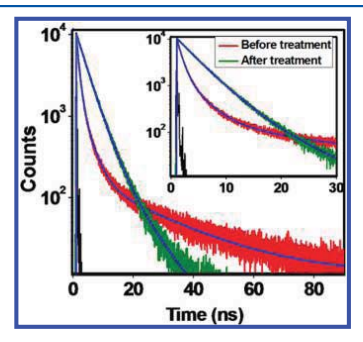


Figure 3. Photoluminescence decay curves of CsPbBr₃ (λ_{ex} = 405 nm). Inset shows the curves in 0–25 ns time window.

Table 2. Lifetime (τ/ns) Components of CsPbBr₃ NCs before and after Treatment

CsPbBr ₃	$\tau_1(\alpha_1^a)$	$ au_2(lpha_2)$	$\tau_3(\alpha_3)$	$\tau_{\rm avg}^{b}$
Before treatment	3.0(0.24)	19.8(0.02)	0.9(0.74)	1.78
After treatment	3.6(0.96)	9.3(0.04)		3.82
α_{i} 's are amplitudes $\sum \alpha_{i} \tau_{i} / \sum \alpha_{i}$	of the lifeti	me componen	ts. ${}^b au_{ m avg}$ is de	fined as

the surface defects, which are eliminated after the treatment. The long-lived component with very small (4%) contribution is presumably arising from shallow trap-mediated radiative recombination. A striking effect of the treatment is also noticed for other mixed halide NCs (Figure S4). The triexponential PL decay patterns change to a biexponential one in almost all cases

with low contribution from the long-lived component (Table S2).

In order to understand the mechanism of tetrafluoroborate salt induced PL enhancement, we carefully examined the analytical data. The observation of similar PXRD pattern, lattice spacing, and absorption spectrum of the samples before and after the treatment indicates that the crystal structures of the NCs are not affected by the treatment and, hence, it is the surface that is modified in the process.

X-ray photoelectron spectroscopy (XPS), infrared (IR) and energy dispersive X-ray (EDX) spectroscopy measurements have been used to assess the surface modification of the NCs and to understand the mechanism of PL enhancement. Quantitative XPS analysis for CsPbBr₃ indicates a Br:Pb ratio of 3.8 for the untreated surface, which is higher than the expected ratio of 3.0 in the bulk, but is understandable as excess Br on the NC surface arises from the capping ligands. ^{29,30} Following the salt treatment, this ratio increases to 4.0 indicating removal of some Pb from the surface. Deconvolution of the high resolution XPS spectrum of untreated NCs for Pb 4f yields 4 peaks as shown in Figure 4. Two intense peaks are

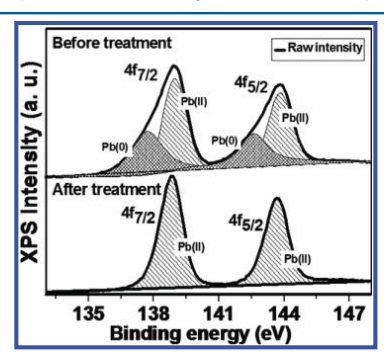


Figure 4. XPS spectra due to Pb $4f_{7/2}$ and $4f_{5/2}$ before and after treatment. Spectra are calibrated with respect to C 1s peak (at 285.35 eV).

located at 138.9 eV $(4f_{7/2})$ and 143.8 eV $(4f_{5/2})$ with a spinorbit splitting of 4.9 eV, which corresponds to Pb in 2+ oxidation state. Additional weaker peaks at 137.6 and 142.6 eV, which are absent after the treatment, are attributed to Pb in its metallic state. ^{31,32} It is known that formation of Pb(0) nanoparticles (NPs) during the synthesis of perovskite NCs by hot injection method cannot be avoided.³⁰ As it is known that $\mathrm{BF_4}^-$ can easily strip off capping ligands and labile lead atoms from lead chalcogenide NC surface, 33,34 one expects BF₄ salt treatment to remove the labile Pb adatoms and nanoparticles. This removal of lead is confirmed by the presence of excess lead (Figure S8) in the EDX spectrum of the salts after the treatment. Even though no signature of fluorine (Figure S6) could be observed from the XPS measurements. the FTIR spectra of the NCs after the treatment (Figure S9) do show a broad peak around 1080 cm⁻¹ due to the B-F stretching of BF₄⁻ bound to lead.³⁵ Another peak at 1712 cm⁻¹ corresponding to C=O stretching of oleic acid obtained from the reaction with counterion and oleate.²⁴ Considering this, long-term colloidal stability and interparticle packing of these NCs (as evident from TEM images), we conclude that BF₄ ions access only to limited places on the NC surface (sites from where stripping occurs) and do not remove all surface capping ligands as observed in earlier report. Removal of these lead adatoms and lead NPs, which act as traps for charge carriers and responsible for low PLQY of these NCs, results in improvement of PL of the system. Remains of PL enhancement is quite similar to that observed in the case of Na/NH₄ thiocyanate-treated samples.

Having understood the mechanism of PL enhancement, it is not difficult to rationalize its observed trend as we move from CsPbCl₃ to CsPbI₃. Low PLQY of CsPbCl₃ and its 50-fold enhancement indicates the presence of both intrinsic and surface defects in the sample before treatment and effective removal of the surface defects after the treatment. This is confirmed by the presence of a large quantity of lead NPs in assynthesized NCs and their removal after the treatment (vide TEM images, Figure S1). As we move toward CsPbBr₃, the crystals become nearly defect-free after treatment indicating that the defects in these systems arise mostly from lead-rich surface. No noticeable enhancement for CsPbI₃ suggests that the defects in these NCs are mostly due to structural distortion arising from larger iodine (intrinsic point defects). 38

In short, an extraordinary improvement of the PL properties of a series of CsPbX₃ NCs covering a wide wavelength range (~200 nm) in the visible region is achieved by following a simple protocol. Unlike the previous reports, the present method enhances the PLQY of CsPbBr₃ and CsPbCl₃Br_{3-x} NCs to near unity with an almost single-exponential PL decay profile in some cases. Further, even for blue-emitting CsPbCl₃ NCs, we have accomplished 50-fold enhancement, which is quite remarkable for this system. These findings, which demonstrate the effectiveness of tetrafluoroborate ion in producing high quality photoluminescent perovskite NCs by removing excess lead atoms from the surface, are likely to boost the utility of these materials in high performance optoelectronic devices.

■ ASSOCIATED CONTENT

Supporting Information

The Supporting Information is available free of charge on the ACS Publications website at DOI: 10.1021/acs.chemmater.8b01235.

Detailed information on synthesis, characterizations (XPS, TEM, PL, FTIR and time-resolved photoluminescence decay) (PDF)

AUTHOR INFORMATION

Corresponding Author

*A.S. E-mail: anunay@uohyd.ac.in.

ORCID ®

Tasnim Ahmed: 0000-0002-5990-3891 Anunay Samanta: 0000-0003-1551-0209

Notes

The authors declare no competing financial interest.

ACKNOWLEDGMENTS

This work is supported by J.C. Bose Fellowship and Research Grant No EMR/2015/000582(to AS) from SERB, and PURSE Grant (to UOH) of DST. We thank Centre for Nanotechnology and M. Durga Prasad for the TEM measurements and ACRHEM for IR. The XPS measurements have been made

using the National Chemical Laboratory (Pune) facility. T.A. and S.S. thank CSIR for Fellowships.

REFERENCES

- (1) Zhang, X.; Lin, H.; Huang, H.; Reckmeier, C.; Zhang, Y.; Choy, W. C. H.; Rogach, A. L. Enhancing the Brightness of Cesium Lead Halide Perovskite Nanocrystal Based Green Light-Emitting Devices through the Interface Engineering with Perfluorinated Ionomer. Nano Lett. 2016, 16, 1415–1420.
- (2) Wang, Y.; Li, X.; Song, J.; Xiao, L.; Zeng, H.; Sun, H. All-Inorganic Colloidal Perovskite Quantum Dots: A New Class of Lasing Materials with Favorable Characteristics. Adv. Mater. 2015, 27, 7101–7108.
- (3) Swarnkar, A.; Marshall, A. R.; Sanehira, E. M.; Chernomordik, B. D.; Moore, D. T.; Christians, J. A.; Chakrabarti, T.; Luther, J. M. Quantum dot–induced phase stabilization of α -CsPbI₃ perovskite for high-efficiency photovoltaics. *Science* **2016**, 354, 92–95.
- (4) Ramasamy, P.; Lim, D.-H.; Kim, B.; Lee, S.-H.; Lee, M.-S.; Lee, J.-S. All-inorganic cesium lead halide perovskite nanocrystals for photodetector applications. *Chem. Commun.* **2016**, *52*, 2067–2070.
- (5) Swarnkar, A.; Chulliyil, R.; Ravi, V. K.; Irfanullah, M.; Chowdhury, A.; Nag, A. Colloidal CsPbBr₃ Perovskite Nanocrystals: Luminescence beyond Traditional Quantum Dots. *Angew. Chem., Int. Ed.* 2015, 54, 15424–15428.
- (6) Protesescu, L.; Yakunin, S.; Bodnarchuk, M. I.; Krieg, F.; Caputo, R.; Hendon, C. H.; Yang, R. X.; Walsh, A.; Kovalenko, M. V. Nanocrystals of Cesium Lead Halide Perovskites (CsPbX₃, X = Cl, Br,and 1): Novel Optoelectronic Materials Showing Bright Emission with Wide Color Gamut. Nano Lett. 2015, 15, 3692–3696.
- (7) Akkerman, Q. A.; D'Innocenzo, V.; Accornero, S.; Scarpellini, A.; Petrozza, A.; Prato, M.; Manna, L. Tuning the Optical Properties of Cesium Lead Halide Perovskite Nanocrystals by Anion Exchange Reactions. J. Am. Chem. Soc. 2015, 137, 10276—10281.
- (8) De, A.; Mondal, N.; Samanta, A. Luminescence Tuning and Exciton Dynamics of Mn-doped CsPbCl₃ Nanocrystals. *Nanoscale* 2017. 9, 16722–16727.
- (9) Mondal, N.; Samanta, A. Complete ultrafast charge carrier dynamics in photo-excited all-inorganic perovskite nanocrystals (CsPbX₃). Nanoscale **2017**, *9*, 1878–1885.
- (10) Pan, J.; Quan, L. N.; Zhao, Y.; Peng, W.; Murali, B.; Sarmah, S. P.; Yuan, M.; Sinatra, L.; Alyami, N. M.; Liu, J.; Yassitepe, E.; Yang, Z.; Voznyy, O.; Comin, R.; Hedhili, M. N.; Mohammed, O. F.; Lu, Z. H.; Kim, D. H.; Sargent, E. H.; Bakr, O. M. Highly Efficient Perovskite-Quantum-Dot Light-Emitting Diodes by Surface Engineering. Adv. Mater. 2016, 28, 8718–8725.
- (11) Pan, J.; Sarmah, S. P.; Murali, B.; Dursun, I.; Peng, W.; Parida, M. R.; Liu, J.; Sinatra, L.; Alyami, N.; Zhao, C.; Alarousu, E.; Ng, T. K.; Ooi, B. S.; Bakr, O. M.; Mohammed, O. F. Air-Stable Surface-Passivated Perovskite Quantum Dots for Ultra-Robust, Single- and Two-Photon-Induced Amplified Spontaneous Emission. J. Phys. Chem. Lett. 2015, 6, 5027–5033.
- (12) Parobek, D.; Roman, B. J.; Dong, Y.; Jin, H.; Lee, E.; Sheldon, M.; Son, D. H. Exciton-to-Dopant Energy Transfer in Mn-Doped Cesium Lead Halide Perovskite Nanocrystals. *Nano Lett.* **2016**, *16*, 7376–7380.
- (13) Seth, S.; Mondal, N.; Patra, S.; Samanta, A. Fluorescence Blinking and Photoactivation of All-Inorganic Perovskite Nanocrystals $CsPbBr_3$ and $CsPbBr_2$ l. J. Phys. Chem. Lett. **2016**, 7, 266–271.
- (14) Woo, J. Y.; Kim, Y.; Bae, J.; Kim, T. G.; Kim, J. W.; Lee, D. C.; Jeong, S. Highly Stable Cesium Lead Halide Perovskite Nanocrystals through in Situ Lead Halide Inorganic Passivation. Chem. Mater. 2017, 29, 7088–7092.
- (15) de Quilettes, D. W.; Vorpahl, S. M.; Stranks, S. D.; Nagaoka, H.; Eperon, G. E.; Ziffer, M. E.; Snaith, H. J.; Ginger, D. S. Impact of microstructure on local carrier lifetime in perovskite solar cells. *Science* 2015, 348, 683–686.
- (16) Kang, J.; Wang, L.-W. High Defect Tolerance in Lead Halide Perovskite CsPbBr₃. J. Phys. Chem. Lett. **2017**, 8, 489–493.

- (17) Liu, F.; Zhang, Y.; Ding, C.; Kobayashi, S.; Izuishi, T.; Nakazawa, N.; Toyoda, T.; Ohta, T.; Hayase, S.; Minemoto, T.; Yoshino, K.; Dai, S.; Shen, Q. Highly Luminescent Phase-Stable CsPbI₃ Perovskite Quantum Dots Achieving Near 100% Absolute Photoluminescence Quantum Yield. ACS Nano 2017, 11, 10373—10383.
- (18) Noel, N. K.; Abate, A.; Stranks, S. D.; Parrott, E. S.; Burlakov, V. M.; Goriely, A.; Snaith, H. J. Enhanced Photoluminescence and Solar Cell Performance via Lewis Base Passivation of OrganicInorganic Lead Halide Perovskites. ACS Nano 2014, 8, 9815–9821.
- (19) Di Stasio, F. D.; Christodoulou, S.; Huo, N.; Konstantatos, G. Near-Unity Photoluminescence Quantum Yield in CsPbB₁₃, Nanocrystal Solid-State Films via Postsynthesis Treatment with Lead Bromide. *Chem. Mater.* **2017**, *29*, 7663–7667.
- (20) Tachikawa, T.; Karimata, I.; Kobori, Y. Surface Charge Trapping in Organolead Halide Perovskites Explored by Single-Particle Photoluminescence Imaging. J. Phys. Chem. Lett. 2015, 6, 3195–3201.
- (21) Kim, J.; Lee, S.-H.; Lee, J. H.; Hong, K.-H. The Role of Intrinsic Defects in Methylammonium Lead Iodide Perovskite. *J. Phys. Chem. Lett.* **2014**, *5*, 1312–1317.
- (22) Smyth, D. M. Defects and Order in Perovskite-Related Oxides. Annu. Rev. Mater. Sci. 1985, 15, 329–357.
- (23) Xiao, Z.; Zhou, Y.; Hosono, H.; Kamiya, T. Intrinsic defects in a photovoltaic perovskite variant Cs₂SnI₆. *Phys. Chem. Chem. Phys.* **2015**, 17, 18900–18903.
- (24) Koscher, B. A.; Swabeck, J. K.; Bronstein, N. D.; Alivisatos, A. P. Essentially trap-free CsPbBr₃ colloidal nanocrystals by post-synthetic thiocyanate surface treatment. *J. Am. Chem. Soc.* **2017**, *139*, 6566–6569
- (25) Pan, J.; Shang, Y.; Yin, J.; De Bastiani, M.; Peng, W.; Dursun, I.; Sinatra, L.; El-Zohry, A. M.; Hedhili, M. N.; Emwas, A.-H.; Mohammed, O. F.; Ning, Z.; Bakr, O. M. Bidentate Ligand-Passivated CsPbI₃ Perovskite Nanocrystals for Stable Near-Unity Photoluminescence Quantum Yield and Efficient Red Light-Emitting Diodes. J. Am. Chem. Soc. 2018, 140, 562–565.
- (26) Raino, G.; Nedelcu, G.; Protesescu, L.; Bodnarchuk, M. I.; Kovalenko, M. V.; Mahrt, R. F.; Stöferle, T. Single Cesium Lead Halide Perovskite Nanocrystals at Low Temperature: Fast Single-Photon Emission, Reduced Blinking, and Exciton Fine Structure. ACS Nano 2016, 10, 2485—2490.
- (27) Li, X.; Wu, Y.; Zhang, S.; Cai, B.; Gu, Y.; Song, J.; Zeng, H. CsPbX₃ Quantum Dots for Lighting and Displays: Room-Temperature Synthesis, Photoluminescence Superiorities, Underlying Origins and White Light-Emitting Diodes. *Adv. Funct. Mater.* **2016**, 26, 2435–2445
- (28) Hu, F.; Zhang, H.; Sun, C.; Yin, C.; Lv, B.; Zhang, C.; Yu, W. W.; Wang, X.; Zhang, Y.; Xiao, M. Superior Optical Properties of Perovskite Nanocrystals as Single Photon Emitters. ACS Nano 2015, 9, 12410–12416.
- (29) De Roo, J.; Ibáñez, M.; Geiregat, P.; Nedelcu, G.; Walravens, W.; Maes, J.; Martins, J. C.; Van Driessche, I.; Kovalenko, M. V.; Hens, Z. Highly Dynamic Ligand Binding and Light Absorption Coefficient of Cesium Lead Bromide Perovskite Nanocrystals. ACS Nano 2016, 10, 2071–2081.
- (30) Udayabhaskararao, T.; Kazes, M.; Houben, L.; Lin, H.; Oron, D. Nucleation, Growth, and Structural Transformations of Perovskite Nanocrystals. *Chem. Mater.* **2017**, *29*, 1302–1308.
- (31) Zhang, Y.; Lv, H.; Cui, C.; Xu, L.; Wang, P.; Wang, H.; Yu, X.; Xie, J.; Huang, J.; Tang, Z.; Yang, D. Enhanced optoelectronic quality of perovskite films with excess CH₃NH₃I for high-efficiency solar cells in ambient air. *Nanotechnology* **2017**, *28*, 205401–205411.
- (32) Ravi, V. K.; Santra, P. K.; Joshi, N.; Chugh, J.; Singh, S. K.; Rensmo, H.; Ghosh, P.; Nag, A. Origin of the Substitution Mechanism for the Binding of Organic Ligands on the Surface of CsPbBr₃ Perovskite Nanocubes. J. Phys. Chem. Lett. 2017, 8, 4988–4994.
- (33) Rosen, E. L.; Buonsanti, R.; Llordes, A.; Sawvel, A. M.; Milliron, D. J.; Helms, B. A. Exceptionally Mild Reactive Stripping of Native Ligands from Nanocrystal Surfaces by Using Meerweins Salt. Angew. Chem., Int. Ed. 2012, 51, 684–689.

(34) Dai, Q.; Zhang, Y.; Wang, Y.; Wang, Y.; Zou, B.; Yu, W. W.; Hu, M. Z. Ligand Effects on Synthesis and Post-Synthetic Stability of PbSe Nanocrystals. *J. Phys. Chem. C* **2010**, *114*, 16160–16167.

- (35) Nagane, S.; Bansode, U.; Game, O.; Chhatre, S.; Ogale, S. CH₃NH₃PbI_(3.x)(BF4)_x: molecular ion substituted hybrid perovskite. *Chem. Commun.* **2014**. *50*. 9741–9744.
- CH₃/NT₃POI_(3×)(DF4)₂: molecular ion substituted nyorid perovskite. Chem. Commun. **2014**, 50, 9741–9744.

 (36) Doris, S. E.; Lynch, J. J.; Li, C.; Wills, A. W.; Urban, J. J.; Helms, B. A. Mechanistic Insight into the Formation of Cationic Naked Nanocrystals Generated under Equilibrium Control. *J. Am. Chem. Soc.* **2014**, 136, 15702–15710.
- (37) Zhang, W.; Pathak, S.; Sakai, N.; Stergiopoulos, T.; Nayak, P. K.; Noel, N. K.; Haghighirad, A. A.; Burlakov, V. M.; deQuilettes, D. W.; Sadhanala, A.; Li, W.; Wang, L.; Ginger, D. S.; Friend, R. H.; Snaith, H. J. Enhanced optoelectronic quality of perovskite thinfilms with hypophosphorous acid for planarheterojunction solar cells. *Nat. Commun.* 2015, 6, 10030.
- (38) Huang, H.; Bodnarchuk, M. I.; Kershaw, S. V.; Kovalenko, M. V.; Rogach, A. L. Lead Halide Perovskite Nanocrystals in the Research Spotlight: Stability and Defect Tolerance. *ACS Energy Lett.* **2017**, *2*, 2071–2083.



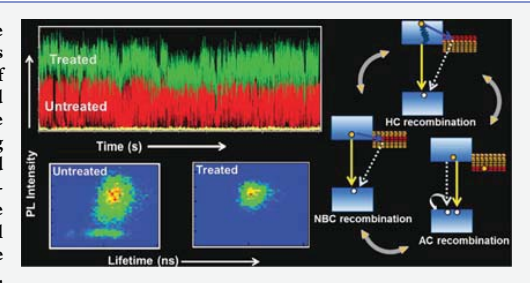
Mechanistic Investigation of the Defect Activity Contributing to the Photoluminescence Blinking of CsPbBr₃ **Perovskite Nanocrystals**

Tasnim Ahmed, Sudipta Seth, and Anunay Samanta*

School of Chemistry, University of Hyderabad, Hyderabad 500046, India

Supporting Information

ABSTRACT: Exploration of the full potential of the perovskite nanocrystals (NCs) for different applications requires a thorough understanding of the pathways of recombination of the photogenerated charge carriers and associated dynamics. In this work, we have tracked the recombination routes of the charge carriers by probing photoluminescence (PL) intermittency of the immobilized and freely diffusing single CsPbBr3 NCs employing a timetagged-time-resolved method. The immobilized single CsPbBr3 NCs show a complex PL time-trace, a careful analysis of which reveals that nonradiative band-edge recombination through trap states, trion recombination,



and trapping of the hot carriers contribute to the blinking behavior of any given NC. A drastically suppressed PL blinking observed for the NCs treated with a tetrafluoroborate salt indicates elimination of most of the undesired recombination processes. A fluorescence correlation spectroscopy (FCS) study on the freely diffusing single NCs shows that enhanced PL and suppressed blinking of the treated particles are the outcome of an increase in per-particle brightness, not due to any increase in the number of particles undergoing "off"-"on" transition in the observation volume. The mechanistic details obtained from this study on the origin of blinking in CsPbBr3 NCs provide deep insight into the radiative and nonradiative charge carrier recombination pathways in these important materials, and this knowledge is expected to be useful for better design and development of bright photoluminescent samples of this class for optoelectronic applications.

KEYWORDS: perovskite nanocrystals, photoluminescence blinking, trion recombination, Auger recombination, hot carriers, band-edge carriers

esium lead halide CsPbX3 (X = Cl, Br, and I) perovskite nanocrystals (NCs) are in the limelight as promising materials for photovoltaic and optoelectronic applications because of their excellent properties such as broad absorption with high absorption cross-section, narrow tunable emission, high photoluminescence quantum yield (PLQY), long carrier diffusion length, and intrinsic defect tolerance. 1-12 These "defect-tolerant" NCs are, however, not completely free from charge carrier trapping centers. 3,13-17 These are largely free from deep trap states, but they do possess shallow trap states, which facilitate nonradiative recombination of the charge carriers and decreased PLQY of the system. 14,18-21 As efficiency of an optoelectronic device made of these materials depends on the fate of the charge carriers, a thorough understanding of the nature of the trap states and dynamics of different competitive radiative and

nonradiative charge carrier recombination processes is essential for proper utilization of these substances.

The charge carrier recombination process can be investigated by monitoring the PL properties of individual NCs. Extensive studies on (mostly CdSe-based) semiconductor quantum dots have shown that these single NCs show random PL fluctuations, termed PL intermittency or blinking, due to participation of the trap states in carrier recombination processes.²² Random fluctuation of PL between the bright (on), dim (gray), and dark (off) states arises from a number of processes depending on the size, composition, and nature (density and position of the trap states) of the NCs, and several models have been proposed to explain PL blink-

Received: September 21, 2019 Accepted: November 12, 2019 Published: November 12, 2019

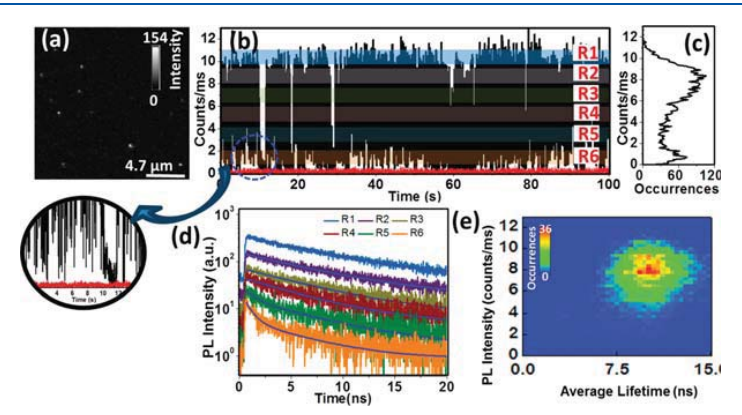


Figure 1. (a) PL intensity image of a film of CsPbBr₃ NCs as obtained using a confocal microscope. (b) PL intensity time-trace (binning time 10 ms) of an NC exhibiting class-1 blinking. The zoomed-in portion of the circled region shows that the low-intensity "gray" states are very close to the background (red line) or the "off" state. (c) Occurrences of the measured PL intensities, (d) PL decay profiles for levels R1 to R6, and (e) FLID of a single CsPbBr₃ NC with false color representation.

ing. $^{23-28}$ These studies have revealed the contribution of the following processes on their PL blinking.^{24-26,29-34} When a charge carrier gets trapped in a short-lived shallow trap state, it relaxes rapidly through a nonradiative route before another exciton is generated. In this case, time-dependent fluctuation of the carrier trapping rate leads to PL blinking behavior.²² PL fluctuation due to these shallow trap states mediated nonradiative band-edge carrier (NBC) recombination is known as NBC blinking.^{22,25,35} When the charge carrier is trapped for a longer period, the NC becomes charged. On absorption of another photon by this charged NC, which creates an exciton, the system becomes a trion.2 Under this condition, two situations can arise: (i) the exciton recombination energy can be nonradiatively transferred to a third carrier (called Auger recombination)^{2,3,6,38} and (ii) the exciton can recombine radiatively at a faster rate, which is almost twice that of neutral exciton recombination. blinking arising from trion-mediated recombination (radiative and nonradiative) is termed AC blinking.²⁵ Both AC and NBC recombination can cause blinking of the same NC. 25,35 Apart from these two processes, trapping of the hot carrier prior to its relaxation to the band edge can also lead to PL blinking. When this happens, the trapped hot carrier relaxes rapidly (through a nonradiative recombination route) before generation of another exciton, and one observes a large drop of PL intensity without any significant change in lifetime. This phenomenon, which is known as hot carrier (HC) blinking, is not a common

As far as the perovskite NCs are concerned, it is already known that a number of recombination processes contribute to their blinking. 10-12,17,25,35,39,41-51 In some cases, it is claimed that PL blinking is due to the AC recombination, 10,12,45 whereas in some other cases, NBC recombination is found to be responsible for PL fluctuation. The occurrence of both NBC and AC recombination in a single CsPbBr₃ NC is also reported. Very recently, HC recombination, which was earlier observed in core—shell CdSe/CdS NCs, 24 has been reported for hybrid (organic—inorganic) perovskite NCs. 39,41 Suppression of the recombination processes contributing to blinking is a challenging task, but has been achieved for metal

chalcogenide quantum dots.^{52–54} However, very few studies exploring the effect of surface treatment on the blinking behavior of the perovskite NCs have been made so far.^{35,39,58}

In this work, we investigate PL blinking of both immobilized and freely diffusing CsPbBr₃ NCs and demonstrate that all three recombination processes (NBC, AC, and HC) contribute to the PL blinking of each single NC. By examining the PL blinking behavior of the tetrafluoroborate salt-treated NCs, we determine which of these processes are actually suppressed by the surface treatment.

RESULTS AND DISCUSSION

CsPbBr₃ NCs with an average edge length of 8 \pm 1.5 nm (Figure S1) and PLQY of $\sim\!30-40\%$ were synthesized for this study following a hot-injection method (details in the Methods section). 6,14 The first absorption onset and PL peak of these NCs appear at $\sim\!495$ and $\sim\!505$ nm, respectively (Figure S2). For single-particle study, dilute solutions of the NCs in toluene (picomolar concentration) were drop-casted on a coverslip and dried under vacuum. A confocal PL microscopy image of a typical film of the NCs is shown in Figure 1a. The film was excited at 405 nm by a pulsed laser (fwhm 176 ps) with a repetition rate of 4 MHz and average power of 0.05 μ W. The low laser power was used to avoid any nonlinear process. Under the experimental condition, each NC was found to absorb on average $\sim\!0.08$ photon per pulse (see Methods section for details). 35,43,45,566

We examined the PL blinking of 55 single NCs, among which 39 (~70%) exhibited a blinking pattern, labeled as class-1 blinking, shown in Figure 1b. The occurrence of different PL intensity levels (Figure 1c) indicates a broad distribution of the high-intensity "on" state and a much narrower distribution of the low-intensity "gray" state; the latter is not clearly separable from the "off" state (Figures 1 and S3). To determine the origin of different intensity states, we have divided the PL intensity into six levels, marked R1 to R6, and measured the decay profiles (Figure 1d) for each level.

For the high-intensity levels (R1 to R4), PL decay is found to be single-exponential, but for the lower intensity levels (R5 and R6), the decay profile is biexponential (Tables 1 and

Table 1. Average Lifetime Components (τ_i) and Their Weightages (α_i) of Different PL Levels of the Untreated NCs

region	$\tau_1(\alpha_1)$, ns	$\tau_2(\alpha_2)$, ns
R1	8.2 ± 0.3	
R2	7.8 ± 0.1	
R3	7.1 ± 0.3	
R4	6.4 ± 0.1	
R5	$6.1 \pm 0.2(0.62)$	$1.1 \pm 0.1(0.38)$
R6	$6.5 \pm 4(0.40)$	$0.94 \pm 0.1(0.60)$

S1). The highest intensity level, which is associated with a single lifetime component of \sim 8.2 ns (Table 1), is attributed to excitonic emission. 12,35,43,45 The lifetime gradually decreases with a decrease in PL intensity (Table S1). The computed intensity—lifetime scaling (η , for details, see the SI) of the top four different intensity regions (R1, R2, R3, and R4) is given below

$$\eta = k_{\rm R1} : k_{\rm R2} : k_{\rm R3} : k_{\rm R4} = \frac{I_1}{\tau_1} : \frac{I_2}{\tau_2} : \frac{I_3}{\tau_3} : \frac{I_4}{\tau_4} = 1.1 : 1.0 : 0.92 : 0.75$$

A near-unity ratio of the radiative recombination rates of the three high-intensity levels indicates the competition between a fixed radiative rate and variable nonradiative rates in the NC. This is a typical signature of PL blinking due to NBC recombination. 25,43,44

Even though our measurements were performed on well-separated single NCs (Figure 1a), one may argue that the multistate emission is not from a single NC but rather comes from clusters. Let us assume that each particle represents a cluster of 2 NCs. If the 2 NCs have different PL lifetimes, the PL decay curve for the R1 level would have been biexponential, which is not the case. If the 2 NCs have same lifetime, the PL intensity of the particle would have been twice as large with the same lifetime, and hence, η would have been >1.0, which again is not the case. Hence, it is evident that each luminescent particle consists of a single NC.

A deviation of the η value (from near-unity) from level R4 onward indicates involvement of additional process(es) competing with the NBC recombination and contributing to the lower intensity levels. For these levels, a second lifetime component (~1 ns) is observed, whose contribution increases from level R5 to R6 (Table 1). As multiexciton recombination processes are ruled out under our experimental condition, the short-lived component must be arising from trion recombination. The observed lifetime of this process is in agreement with literature. 10,35,43 It is thus evident that AC recombination also contributes to the blinking of each NC. The involvement of two simultaneously occurring recombination processes can be found out from the fluorescence lifetime-intensity distribution (FLID) patterns.^{25,35,42} However, in the present case, this is not very clear from the FLID pattern (Figure 1e), presumably due to low occurrence of the "gray" state population.

For further investigation of the processes contributing to PL fluctuations, we have constructed PL lifetime traces corresponding to the intensity traces and compared them (Figures 2, S4). It is seen that the PL intensity correlates quite well with the lifetime in most of the regions, but there are some specific regions (indicated by dashed lines, in Figure 2), where the lifetime is significantly high for a very low intensity state. This suggests trapping of the carriers prior to their cooling. Thus, it

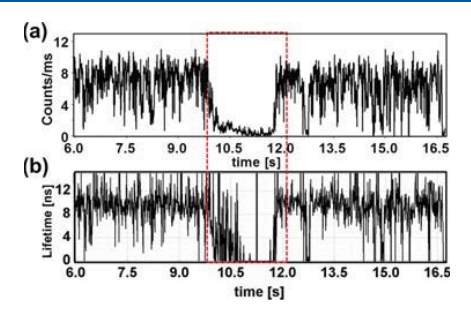


Figure 2. (a) PL intensity and (b) lifetime trajectories of an NC exhibiting class-1 blinking. The region indicated by two dashed red lines shows no correlation between intensity and lifetime.

is evident that hot carrier trapping also contributes to PL blinking along with AC and NBC recombination processes.

The PL time-trace and corresponding intensity histogram of the remaining 30% of the NCs, classified as class-2 blinking, are shown in Figure 3. Unlike in the previous case, here the occurrence of the "gray" state is greater than that of the "on" state. Analysis of the PL decay profiles at higher intensity levels reveals contribution of the NBC recombination similar to what is observed for class-1 NCs (Figure S6). As the "gray" states have greater contribution for class-2 NCs (Figure 3b), the lowintensity states are now more clearly visible in the FLID pattern (Figures 3c and S7). One can easily identify two distinct lifetime components for the low-intensity region. The ~7.5 ns component (indicated by an arrow) is similar to the lifetime of a neutral exciton. For a low-intensity state, a lifetime closer to that of the neutral exciton can be explained only if the carriers are trapped before they relax to the band edge. 57 implies that hot carrier mediated HC recombination also contributes to the blinking of a CsPbBr3 NC. Another lowintensity region (circled) in Figure 3c, with a lifetime (~1.6 ns, Table S2) significantly shorter than that of the neutral exciton (~8 ns), must be due to trion recombination. 10,35,43 Thus, we find that three different channels of recombination (AC, NBC, and HC) contribute to the observed blinking of these single CsPbBr3 NCs as well. The blinking pattern of these NCs differs from that of the class-1 blinking ones with respect to the weightages of the three recombination processes.

We have also examined the PL intensity time-trace of 51 single CsPbBr3 NCs, which were treated with tetrafluoroborate salts to enhance the PLQY to near-unity following a recently developed method (details in Methods). ¹⁴ Nearly 90% of these treated NCs show significantly suppressed PL blinking, displaying only one high-intensity level (Figure 4). The disappearance of the contributions of the "gray" and "off" states makes the PL intensity distribution much narrower and indicates that PL blinking is effectively suppressed by the surface treatment. To investigate this aspect a little deeper, we examined the PL decay profiles corresponding to three narrow intensity levels (T1, T2, and T3), as shown in Figure 4c. The highest intensity region (T1) exhibits single-exponential decay with a lifetime of ~8.8 ns (Tables 2 and S3), which is not very different from that before treatment. The other two levels exhibit biexponential decay kinetics comprising a short component (~1.9 ns) in addition to the long one. The amplitude of this short component (~29% for T2, ~38% for T3) due to trion recombination is almost half of that before

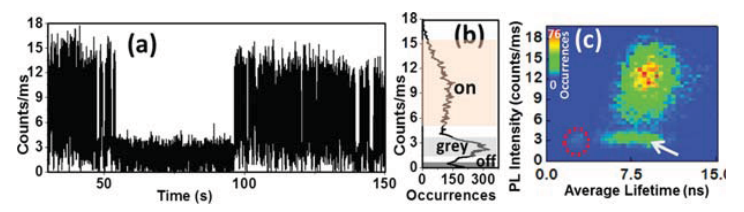


Figure 3. (a) PL intensity time-trace (binning time 10 ms) of an NC exhibiting class-2 blinking. (b) Occurrences of the measured PL intensities. (c) FLID of a single NC with false color representation.

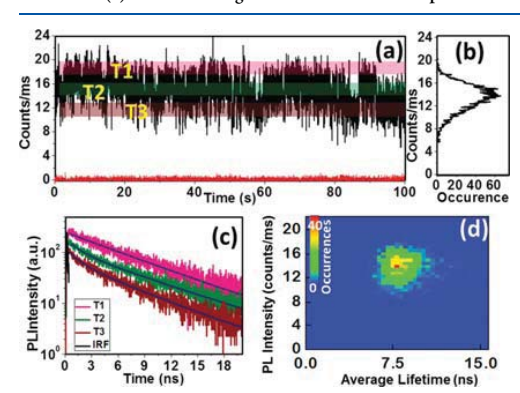


Figure 4. (a) PL intensity time-trace (binning time 10 ms) of a NaBF₄-treated NC. Red line indicates the background signal intensity. (b) Occurrences of the measured PL intensities. (c) PL decay profiles of the levels marked T1 to T3. (d) FLID of single CsPbBr₃ NC after treatment with false-color representation.

Table 2. Average Lifetime Components (τ_i) and Their Weightages (α_i) of Different PL Levels of the Treated NCs

region	$\tau_1(\alpha_1)$, ns	$\tau_2(\alpha_2)$, ns
T1	8.8 ± 0.5	
T2	$9.1 \pm 0.4(0.71)$	$2.1 \pm 0.2(0.29)$
T3	$8.2 \pm 0.4(0.62)$	$1.9 \pm 0.1(0.38)$

treatment (~60% for R6 in class-1 NC). This indicates that even though trion formation is suppressed significantly due to surface treatment, it is not completely eliminated in the treated sample. A higher PLQY (evident from higher PL intensity counts) suppressed blinking and a narrow distribution of the events (the "off" and "gray" states are removed) in the FLID pattern (Figure 4d) indicate radiative recombination as the main recombination pathway of the carriers after the treatment with highly suppressed HC and NBC processes.

As stated earlier, we have also studied the freely diffusing NCs (a colloidal solution of the NCs in octadecene) of the same concentration before and after NaBF₄ treatment to understand the effect of the treatment on PL blinking dynamics. The fluorescence correlation curves are found to be best represented by eq 1 (Figure 5), which involves a three-dimensional diffusion along with a stretched exponential decay component due to PL blinking. The quality of the fits can be assessed from Figure S11, and the fitting parameters are presented in Table 3.

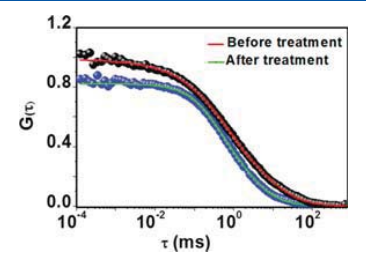


Figure 5. Fluorescence correlation curves of the $CsPbBr_3$ NCs in octadecene before and after treatment.

$$G(\tau) = \left[1 + \frac{T}{1 - T} \exp\left(-\frac{\tau}{\tau_{\rm T}}\right)^{\beta} \frac{1}{N} \left(1 + \frac{\tau}{\tau_{\rm D}}\right)^{-1} - \left(1 + \frac{\tau}{\kappa^2 \tau_{\rm D}}\right)^{-1/2} \right]$$

$$(1)$$

Table 3. Estimated Values of the Off-State Fraction (T), Average Number of Observable Particles (N) within the Observable Volume, Stretching Exponent (β) , and per-Particle Brightness (PPB)

NCs	T	N	β	PPB (K cps/ particle)
before treatment	0.55 ± 0.03	1.89 ± 0.15	0.56 ± 0.02	9.3 ± 0.85
after treatment	0.37 ± 0.02	1.84 ± 0.16	1.0 ± 0.01	19.7 ± 0.91

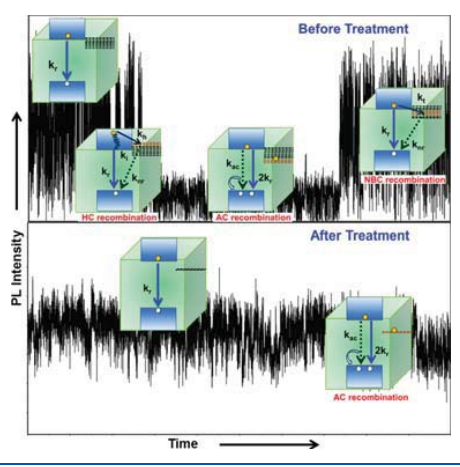
where $\tau_{\rm D}$ is the diffusion time of the NCs, N the average number of particles undergoing reversible PL intensity fluctuation in the observation volume, T the fraction of the "off" state, and $\tau_{\rm T}$ the dark-state relaxation time or blinking time. β is the stretching exponent with a value between 0 and 1 and is related to the distribution of $\tau_{\rm T}$. κ (= ω_z/ω_{xy}) is the structure parameter of the observation volume; ω_z and ω_{xy} are the longitudinal and transverse radii, respectively.

The β -value (0.56) obtained for the untreated NCs is substantially different from unity. This indicates a distributed kinetics of fluorescence blinking suggesting the involvement of multiple trap states. 10,21,58,59 Interestingly, the β -value of unity for the treated samples (Figures 5 and S11) indicates that PL fluctuation is now due to a single nonradiative recombination channel. A decrease in the off-state fraction (T) value from \sim 0.55 to \sim 0.37 upon treatment (Table 3) implies that the treated particles remain mostly in the "on" state, an

observation that confirms the suppression of blinking. We note that the number of particles (N) undergoing "on"—"off" transition in the observation volume is not altered significantly by the treatment, but per-particle brightness (PPB) is increased (Table 3) by a factor of ~2.2-fold (from ~9.3K cps/particle to ~19.7K cps/particle) as a result of the treatment. This value is in agreement with ~3-fold enhancement of the PLQY of the system on treatment, as we reported in an earlier work.

It is generally believed that the surface defects of $CsPbBr_3$ NCs arise from uncoordinated lead and lead nanoparticles. 13,14,35,39 These defects give rise to states near the conduction band that are highly effective in trapping the charge carriers. Considering these trap states and the findings of this work, we illustrate the mechanistic details of different recombination events in single $CsPbBr_3$ NCs in Scheme 1.

Scheme 1. Different recombination processes in a single CsPbBr₃ NC before and after surface treatment. The black and brown dashed horizontal lines show the deactivated and activated trap states, respectively. For the sake of clarity, intraband relaxation of the hot electrons is not shown while illustrating AC and NBC blinking. Also, hot hole cooling is not shown in all cases for the same reason.



When the traps are in their passive state, 17 the excitons recombine radiatively with zero nonradiative rates. However, the excitons may as well recombine nonradiatively via the trap states when the latter are active. 17 This study reveals that, when the exciton at the band-edge recombines through those shallow trap states before generation of another exciton (<250 ns), no charging of the NCs occurs and the blinking is due to the NBC mechanism. On the other hand, when an electron is trapped for a longer duration (>250 ns) in trap states, which are relatively deeper than those involved in NBC recombination, a trion is formed on generation of another exciton. The trap states, which lie above the conduction band-edge, are involved in capturing the hot electrons. This trapped hot electron relaxes rapidly and nonradiatively before another exciton is generated. The simultaneous occurrence of three different recombination processes in a single NC is a reflection of the highly dynamic nature of the trap states due to ion migration and mobility of the charge carriers.

Interestingly, though the treatment removes the "off" states, the AC recombination process is not eliminated completely after treatment, presumably because of intrinsic defects and/or the labile nature of the ligand on the surface. 35,39

CONCLUSION

We show that three separate processes, namely, NBC, HC, and AC recombination, contribute to the PL blinking of each single CsPbBr₃ NC. Significant suppression of blinking, as evident from the disappearance of "off" and "gray" PL states on surface treatment of these NCs, indicates significant removal of the trap states contributing to the HC and NBC recombination processes. The AC blinking is also suppressed on treatment, but not eliminated completely. The FCS study reveals that an increase in per-particle brightness of the particles on surface treatment is responsible for highly suppressed PL blinking in treated samples. The study provides insight into the mechanism of PL blinking in CsPbBr₃ NCs, which will be useful in designing nonblinking PL materials of this class. The results also show that the treated CsPbBr₃ NCs can serve as ideal single-dot light sources in optoelectronic applications.

METHODS

Synthesis of CsPbBr₃ NCs. Cs₂CO₃ (0.10175 g), oleic acid (OA) (0.3125 mL), and octadecene (ODE) (5 mL) were mixed in a 50 mL double-necked round-bottom (RB) flask and kept under vacuum for 1 h at 120 °C. Subsequently the temperature was raised to 170 °C for complete solubilization of the solid material and formation of a clear solution of cesium oleate (Cs-oleate). As Cs-oleate precipitates out of ODE at room temperature, and it was kept at 100 °C under a N2 atmosphere. ODE (5 mL), PbBr₂ (0.188 mmol), OA (0.5 mL), and oleylamine (OLA) (0.5 mL) were loaded in a 50 mL double-necked RB flask, and the mixture was heated under vacuum at 120 °C for at least 1 h. After complete solubilization of the PbBr2 salt, the mixture was transferred into a N2 atmosphere. The temperature was raised to 170 °C and kept for 20 min followed by injection of a Cs-oleate solution (0.4 mL). The reaction mixture was cooled in an ice-water bath after 5 s. The crude solution was centrifuged at 8000 rpm for 10 min. The supernatant containing unreacted precursors was discarded, and the precipitate was washed with toluene and centrifuged at 3000 rpm for 5 min to remove trace amounts of unreacted species. Then, the precipitate was finally dispersed in toluene or ODE for measurements.

Postsynthetic Surface Treatment. Purified NCs were dispersed in toluene or ODE for further measurements. A 2–4 mL amount of a few micromolar solution of NC was stirred with solid NaBF $_4$ for 30 min at room temperature and in an open atmosphere. 14 Ionic tetrafluoroborate salts were separated from the NC solution in nonpolar toluene or ODE by centrifuging for 5 min at 6000 rpm.

Single-Particle Measurement. A confocal fluorescence microscope (MicroTime 200, PicoQuant) was used for single-molecule PL and for the FCS study. The microscope body was attached to an inverted microscope (Olympus IX71) equipped with a water immersion objective (UPlansApo NA 1.2, 60×). NCs were excited at 405 nm from a pulsed diode laser (PDL 828 S Sepia II, PicoQuant) with a full width at half-maximum of 176 ps. For the single-molecule PL study, a diluted NC solution in toluene (around picomolar) was passed through the coverslip and dried under vacuum. We performed time-tagged-time-resolved photoluminescence measurements at room temperature. For FCS measurement the sample was prepared in ODE medium and placed on a coverslip. Fluorescence from the samples was collected by the same objective and passed through the dichroic mirror, filtered by using a 430 nm long-pass filter to cut off the exciting light. A 50 μ m diameter pinhole was used to remove the outof-focus signal. The signal was directed to a single-photon avalanche photodiode (SPADs). The fluorescence correlation traces were generated by cross-correlating signals from the two SPAD detectors

by using a 50/50 beam splitter. The data acquisition was performed with a SymPhoTime software controlled PicoHarp 300 time-correlated single-photon counting module in a time-tagged time-resolved method. The number of excitons generated per pulse was calculated using the formula $\langle N \rangle = J_{\rm p} \times \sigma$, where $J_{\rm p}$ is the per-pulse photon fluence and the absorption cross-section is $\sigma = 1.5 \times 10^{-14}$ cm $^{2.10,12,42}$

ASSOCIATED CONTENT

Supporting Information

The Supporting Information is available free of charge on the ACS Publications website at DOI: 10.1021/acsnano.9b07471.

Intensity—lifetime scaling, FCS study, absorption, emission spectra, and TEM images before and after treatment, additional blinking time-traces, FLID patterns, fitting of FCS data, and tables containing fitting parameters (PDF)

AUTHOR INFORMATION

Corresponding Author

*E-mail: anunay@uohyd.ac.in.

ORCID

Tasnim Ahmed: 0000-0002-5990-3891 Sudipta Seth: 0000-0002-8666-4080 Anunay Samanta: 0000-0003-1551-0209

Present Address

[†]Department of Chemical Physics and NanoLund, Chemical Centre, Lund University, P.O. Box 124, SE-22100, Lund, Sweden.

Notes

The authors declare no competing financial interest.

ACKNOWLEDGMENTS

This work is supported by the J.C. Bose Fellowship (to A.S.) from SERB and the PURSE Grant (to U.O.H.) of DST. We thank M. Durga Prasad for the TEM measurements at the Centre for Nanotechnology, University of Hyderabad. T.A. and S.S. thank CSIR for Fellowships.

REFERENCES

- (1) Gong, M.; Sakidja, R.; Goul, R.; Ewing, D.; Casper, M.; Stramel, A.; Elliot, A.; Wu, J. Z. High-Performance All-Inorganic $CsPbCl_3$ Perovskite Nanocrystal Photodetectors with Superior Stability. *ACS Nano* **2019**, *13*, 1772–1783.
- (2) Kang, J.; Wang, L. W. High Defect Tolerance in Lead Halide Perovskite CsPbBr₃. J. Phys. Chem. Lett. **2017**, 8, 489–493.
- (3) Kovalenko, M. V.; Protesescu, L.; Bodnarchuk, M. I. Properties and Potential Optoelectronic Applications of Lead Halide Perovskite Nanocrystals. Science 2017, 358, 745–750.
- (4) Kulbak, M.; Gupta, S.; Kedem, N.; Levine, I.; Bendikov, T.; Hodes, G.; Cahen, D. Cesium Enhances Long-Term Stability of Lead Bromide Perovskite-Based Solar Cells. *J. Phys. Chem. Lett.* **2016**, *7*, 167–172.
- (5) Nedelcu, G.; Protesescu, L.; Yakunin, S.; Bodnarchuk, M. I.; Grotevent, M. J.; Kovalenko, M. V. Fast Anion-Exchange in Highly Luminescent Nanocrystals of Cesium Lead Halide Perovskites (CsPbX₃, X = Cl, Br, 1). Nano Lett. 2015, 15, 5635–5640.
- (6) Protesescu, L.; Yakunin, S.; Bodnarchuk, M. I.; Krieg, F.; Caputo, R.; Hendon, C. H.; Yang, R. X.; Walsh, A.; Kovalenko, M. V. Nanocrystals of Cesium Lead Halide Perovskites (CsPbX₃, X = Cl, Br, and I): Novel Optoelectronic Materials Showing Bright Emission with Wide Color Gamut. *Nano Lett.* **2015**, *15*, 3692–3696.
- (7) Shi, Z.; Li, Y.; Zhang, Y.; Chen, Y.; Li, X.; Wu, D.; Xu, T.; Shan, C.; Du, G. High-Efficiency and Air-Stable Perovskite Quantum Dots

Light-Emitting Diodes with an All-Inorganic Heterostructure. *Nano Lett.* **2017**, *17*, 313–321.

- (8) Swarnkar, A.; Chulliyil, R.; Ravi, V. K.; Irfanullah, M.; Chowdhury, A.; Nag, A. Colloidal CsPbBr₃ Perovskite Nanocrystals: Luminescence beyond Traditional Quantum Dots. Angew. Chem, Int. Ed. 2015, 54, 15424–15428.
- (9) Zhou, Q.; Bai, Z.; Lu, W. G.; Wang, Y.; Zou, B.; Zhong, H. In Situ Fabrication of Halide Perovskite Nanocrystal-Embedded Polymer Composite Films with Enhanced Photoluminescence for Display Backlights. Adv. Mater. 2016, 28, 9163–9168.
- (10) Park, Y. S.; Guo, S.; Makarov, N. S.; Klimov, V. I. Room Temperature Single-Photon Emission from Individual Perovskite Quantum Dots. ACS Nano 2015, 9, 10386–10393.
- (11) Hu, F.; Yin, C.; Zhang, H.; Sun, C.; Yu, W. W.; Zhang, C.; Wang, X.; Zhang, Y.; Xiao, M. Slow Auger Recombination of Charged Excitons in Nonblinking Perovskite Nanocrystals without Spectral Diffusion. *Nano Lett.* **2016**, *16*, 6425–6430.
- (12) Yarita, N.; Tahara, H.; Ihara, T.; Kawawaki, T.; Sato, R.; Saruyama, M.; Teranishi, T.; Kanemitsu, Y. Dynamics of Charged Excitons and Biexcitons in CsPbBr₃ Perovskite Nanocrystals Revealed by Femtosecond Transient-Absorption and Single-Dot Luminescence Spectroscopy. *J. Phys. Chem. Lett.* **2017**, *8*, 1413–1418.
- (13) Koscher, B. A.; Swabeck, J. K.; Bronstein, N. D.; Alivisatos, A. P. Essentially Trap-Free CsPbB₁₃ Colloidal Nanocrystals by Postsynthetic Thiocyanate Surface Treatment. J. Am. Chem. Soc. 2017, 139, 6566–6569.
- (14) Ahmed, T.; Seth, S.; Samanta, A. Boosting the Photoluminescence of $CsPbX_3$ (X = Cl, Br, I) Perovskite Nanocrystals Covering a Wide Wavelength Range by Post-Synthetic Treatment with Tetrafluoroborate Salts. *Chem. Mater.* **2018**, *30*, 3633–3637.
- (15) Mondal, N.; De, A.; Samanta, A. Achieving Near-Unity Photoluminescence Efficiency for Blue-Violet-Emitting Perovskite Nanocrystals. ACS Energy Lett. 2019, 4, 32–39.
- (16) Li, F.; Liu, Y.; Wang, H.; Zhan, Q.; Liu, Q.; Xia, Z. Postsynthetic Surface Trap Removal of CsPbX₃ (X = Cl, Br, or I) Quantum Dots *via* a ZnX₂/Hexane Solution toward an Enhanced Luminescence Quantum Yield. *Chem. Mater.* **2018**, *30*, 8546–8554.
- (17) Gerhard, M.; Louis, B.; Camacho, R.; Merdasa, A.; Li, J.; Kiligaridis, A.; Dobrovolsky, A.; Hofkens, J.; Scheblykin, I. G. Microscopic Insight into Non-Radiative Decay in Perovskite Semiconductors from Temperature-Dependent Luminescence Blinking. Nat. Commun. 2019, 10, 1698.
- (18) Huang, H.; Bodnarchuk, M. I.; Kershaw, S. V.; Kovalenko, M. V.; Rogach, A. L. Lead Halide Perovskite Nanocrystals in the Research Spotlight: Stability and Defect Tolerance. *ACS Energy Lett.* **2017**, *2*, 2071–2083.
- (19) Mondal, N.; Samanta, A. Complete Ultrafast Charge Carrier Dynamics in Photo-Excited All-Inorganic Perovskite Nanocrystals (CsPbX₃). Nanoscale **2017**, *9*, 1878–1885.
- (20) Pan, J.; Quan, L. N.; Zhao, Y.; Peng, W.; Murali, B.; Sarmah, S. P.; Yuan, M.; Sinatra, L.; Alyami, N. M.; Liu, J.; Yassitepe, E.; Yang, Z.; Voznyy, O.; Comin, R.; Hedhili, M. N.; Mohammed, O. F.; Lu, Z. H.; Kim, D. H.; Sargent, E. H.; Bakr, O. M. Highly Efficient Perrovskite-Quantum-Dot Light-Emitting Diodes by Surface Engineering, Adv. Mater. 2016, 28, 8718–8725.
- (21) Seth, S.; Mondal, N.; Patra, S.; Samanta, A. Fluorescence Blinking and Photoactivation of All-Inorganic Perovskite Nanocrystals CsPbBr₃ and CsPbBr₂I. J. Phys. Chem. Lett. **2016**, 7, 266–271.
- (22) Cordones, A. A.; Leone, S. R. Mechanisms for Charge Trapping in Single Semiconductor Nanocrystals Probed by Fluorescence Blinking. *Chem. Soc. Rev.* **2013**, *42*, 3209–3221.
- (23) Efros, A. L.; Nesbitt, D. J. Origin and Control of Blinking in Quantum Dots. *Nat. Nanotechnol.* **2016**, *11*, 661–671.
- (24) Galland, C.; Ghosh, Y.; Steinbruck, A.; Sykora, M.; Hollingsworth, J. A.; Klimov, V. I.; Htoon, H. Two Types of Luminescence Blinking Revealed by Spectroelectrochemistry of Single Quantum Dots. Nature 2011, 479, 203—207.

(25) Yuan, G.; Gomez, D. E.; Kirkwood, N.; Boldt, K.; Mulvaney, P. Two Mechanisms Determine Quantum Dot Blinking. *ACS Nano* **2018**, *12*, 3397–3405.

- (26) Frantsuzov, P. A.; Volkan-Kacso, S.; Janko, B. Model of Fluorescence Intermittency of Single Colloidal Semiconductor Quantum Dots Using Multiple Recombination Centers. *Phys. Rev. Lett.* **2009**, 103, 207402.
- (27) Kuno, M.; Fromm, D. P.; Hamann, H. F.; Gallagher, A.; Nesbitt, D. J. "On"/"Off" Fluorescence Intermittency of Single Semiconductor Quantum Dots. J. Chem. Phys. 2001, 115, 1028–1040.
- (28) Busov, V. K.; Frantsuzov, P. A. Models of Semiconductor Quantum Dots Blinking based on Spectral Diffusion. *Opt. Spectrosc.* **2019**, *126*, 70–82.
- (29) Frantsuzov, P.; Kuno, M.; Jánko, B.; Marcus, R. A. Universal Emission Intermittency in Quantum Dots, Nanorods and Nanowires. *Nat. Phys.* **2008**, *4*, 519–522.
- (30) Frantsuzov, P. A.; Marcus, R. A. Explanation of Quantum Dot Blinking without the Long-Lived Trap Hypothesis. *Phys. Rev. B: Condens. Matter Mater. Phys.* **2005**, 72, 155321.
- (31) Park, Y.-S.; Lim, J.; Makarov, N. S.; Klimov, V. I. Effect of Interfacial Alloying versus "Volume Scaling" on Auger Recombination in Compositionally Graded Semiconductor Quantum Dots. Nano Lett. 2017, 17, 5607–5613.
- (32) Rosen, S.; Schwartz, O.; Oron, D. Transient Fluorescence of the Off State in Blinking CdSe/CdS/ZnS Semiconductor Nanocrystals Is Not Governed by Auger Recombination. *Phys. Rev. Lett.* **2010**, 104, 157404.
- (33) Tenne, R.; Teitelboim, A.; Rukenstein, P.; Dyshel, M.; Mokari, T.; Oron, D. Studying Quantum Dot Blinking through the Addition of an Engineered Inorganic Hole Trap. ACS Nano 2013, 7, 5084–5090.
- (34) Zhao, J.; Nair, G.; Fisher, B. R.; Bawendi, M. G. Challenge to the Charging Model of Semiconductor-Nanocrystal Fluorescence Intermittency from Off-State Quantum Yields and Multiexciton Blinking. *Phys. Rev. Lett.* **2010**, *104*, 157403.
- (35) Seth, S.; Ahmed, T.; Samanta, A. Photoluminescence Flickering and Blinking of Single CsPbBr₃ Perovskite Nanocrystals: Revealing Explicit Carrier Recombination Dynamics. J. Phys. Chem. Lett. 2018, 9, 7007–7014.
- (36) Nirmal, M.; Dabbousi, B.; Bawendi, M. G.; Macklint, J. J.; Trautmant, J. K.; Harrist, T. D.; Brus, L. E. Fluorescence Intermittency in Single Cadmium Selenide Nanocrystals. *Nature* 1996, 383, 802–804.
- (37) Park, Y. S.; Bae, W. K.; Pietryga, J. M.; Klimov, V. I. Auger Recombination of Biexcitons and Negative and Positive Trions in Individual Quantum Dots. ACS Nano 2014, 8, 7288–7296.
- (38) Spinicelli, P.; Buil, S.; X, X. Q.; Mahler, B.; Dubertret, B.; Hermier, J. P. Bright and Grey States in CdSe-CdS Nanocrystals Exhibiting Strongly Reduced Blinking. *Phys. Rev. Lett.* **2009**, *102*, 12501
- (39) Yarita, N.; Tahara, H.; Saruyama, M.; Kawawaki, T.; Sato, R.; Teranishi, T.; Kanemitsu, Y. Impact of Postsynthetic Surface Modification on Photoluminescence Intermittency in Formamidinium Lead Bromide Perovskite Nanocrystals. J. Phys. Chem. Lett. 2017, 8, 6041–6047.
- (40) Reid, K. R.; McBride, J. R.; Croix, A. D. L.; Freymeyer, N. J.; Click, S. M.; Macdonald, J. E.; Rosenthal, S. J. Role of Surface Morphology on Exciton Recombination in Single Quantum Dot-in-Rods Revealed by Optical and Atomic Structure Correlation. ACS Nano 2018, 12, 11434–11445.
- (41) Kim, T.; Jung, S. I.; Ham, S.; Chung, H.; Kim, D. Elucidation of Photoluminescence Blinking Mechanism and Multiexciton Dynamics in Hybrid Organic–Inorganic Perovskite Quantum Dots. Small 2019, 15. 1900355.
- (42) Gibson, N. A.; Koscher, B. A.; Alivisatos, A. P.; Leone, S. R. Excitation Intensity Dependence of Photoluminescence Blinking in CsPbBr₃ Perovskite Nanocrystals. *J. Phys. Chem. C* **2018**, *122*, 12106–12113

- (43) Li, B.; Huang, H.; Zhang, G.; Yang, C.; Guo, W.; Chen, R.; Qin, C.; Gao, Y.; Biju, V.; Rogach, A. L.; Xiao, L.; Jia, S. Excitons and Biexciton Dynamics in Single CsPbBr₃ Perovskite Quantum Dots. *J. Phys. Chem. Lett.* **2018**, *9*, 6934–6940.
- (44) Yuan, G.; Ritchie, C.; Ritter, M.; Murphy, S.; Gómez, D. E.; Mulvaney, P. The Degradation and Blinking of Single CsPbI₃ Perovskite Quantum Dots. *J. Phys. Chem. C* **2018**, 122, 13407–13415.
- (45) Hu, F.; Zhang, H.; Sun, C.; Yin, C.; Lv, B.; Zhang, C.; Yu, W. W.; Wang, X.; Zhang, Y.; Xiao, M. Superior Optical Properties of Perovskite Nanocrystals as Single Photon Emitters. ACS Nano 2015, 9, 12410–12416.
- (46) Tachikawa, T.; Karimata, I.; Kobori, Y. Surface Charge Trapping in Organolead Halide Perovskites Explored by Single-Particle Photoluminescence Imaging. J. Phys. Chem. Lett. 2015, 6, 3195–3201.
- (47) Halder, A.; Pathoor, N.; Chowdhury, A.; Sarkar, S. K. Photoluminescence Flickering of Micron-Sized Crystals of Methylammonium Lead Bromide: Effect of Ambience and Light Exposure. J. Phys. Chem. C 2018, 122, 15133–15139.
- (48) Merdasa, A.; Tian, Y.; Camacho, R.; Dobrovolsky, A.; Debroye, E.; Unger, E. L.; Hofkens, J.; Sundstrom, V.; Scheblykin, I. G. Supertrap" at Work: Extremely Efficient Nonradiative Recombination Channels in MAPbl₃ Perovskites Revealed by Luminescence Super-Resolution Imaging and Spectroscopy. ACS Nano 2017, 11, 5391—5404.
- (49) Pathoor, N.; Halder, A.; Mukherjee, A.; Mahato, J.; Sarkar, S. K.; Chowdhury, A. Fluorescence Blinking Beyond Nanoconfinement: Spatially Synchronous Intermittency of Entire Perovskite Microcrystals. *Angew. Chem.* **2018**, 130, 11777–11781.
- (50) Zhang, A.; Dong, C.; Ren, J. Tuning Blinking Behavior of Highly Luminescent Cesium Lead Halide Nanocrystals through Varying Halide Composition. J. Phys. Chem. C 2017, 121, 13314– 13323.
- (51) Raino, G.; Nedelcu, G.; Protesescu, L.; Bodnarchuk, M. I.; Kovalenko, M. V.; Mahrt, R. F.; Stöferle, T. Single Cesium Lead Halide Perovskite Nanocrystals at Low Temperature: Fast Single-Photon Emission, Reduced Blinking, and Exciton Fine Structure. ACS Nano 2016, 10, 2485–2490.
- (52) Zhang, A.; Bian, Y.; Wang, J.; Chen, K.; Dong, C.; Ren, J. Suppressed Blinking Behavior of CdSe/CdS QDs by Polymer Coating. *Nanoscale* **2016**, *8*, 5006–5014.
- (53) Li, B.; Zhang, G.; ZaoWang; Li, Z.; RuiyunChen; ChengbingQin; YanGao; LiantuanXiao; Jia, S. Suppressing the Fluorescence Blinking of Single Quantum Dots Encased in N-type Semiconductor Nanoparticles. Sci. Rep. 2016, 6, 32662.
- (54) Mahler, B.; Spinicelli, P.; Buil, S.; Quelin, X.; Hermier, J.-P.; Dubertret, B. Towards Non-Blinking Quantum Dots: The Effect of Thick Shell. *Proc. SPIE* **2009**, 7189, 718903.
- (\$5) Tang, X.; Yang, J.; Li, S.; Liu, Z.; Hu, Z.; Hao, J.; Du, J.; Leng, Y.; Qin, H.; Lin, X.; Lin, Y.; Tian, Y.; Zhou, M.; Xiong, Q. Single Halide Perovskite/Semiconductor Core/Shell Quantum Dots with Ultrastability and Nonblinking Properties. Adv. Sci. 2019, 6, 1900412.
- (56) Mondal, N.; De, A.; Samanta, A. Biexciton Generation and Dissociation Dynamics in Formamidinium and Chloride-Doped Cesium Lead Iodide Perovskite Nanocrystals. J. Phys. Chem. Lett. 2018, 9, 3673–3679.
- (57) Chen, J.; Messing, M. E.; Zheng, K.; Pullerits, T. Cation-Dependent Hot Carrier Cooling in Halide Perovskite Nanocrystals. *J. Am. Chem. Soc.* **2019**, *141*, 3532–3540.
- (58) Dong, C.; Qian, H.; Fang, N.; Ren, J. Study of Fluorescence Quenching and Dialysis Process of CdTe Quantum Dots, Using Ensemble Techniques and Fluorescence Correlation Spectroscopy. J. Phys. Chem. B 2006, 110, 11069–11075.
- (59) Patra, S.; Samanta, A. A Fluorescence Correlation Spectroscopy, Steady-State, and Time-Resolved Fluorescence Study of the Modulation of Photophysical Properties of Mercaptopropionic Acid Capped CdTe Quantum Dots upon Exposure to Light. J. Phys. Chem. C 2013, 117, 23313–23321.

(60) Yettapu, G. R.; Talukdar, D.; Sarkar, S.; Swarnkar, A.; Nag, A.; Ghosh, P.; Mandal, P. Terahertz Conductivity within Colloidal CsPbBr₃ Perovskite Nanocrystals: Remarkably High Carrier Mobilities and Large Diffusion Lengths. *Nano Lett.* **2016**, *16*, 4838–4848. (61) Mosconi, E.; Angelis, F. D. Mobile Ions in Organohalide Perovskites: Interplay of Electronic Structure and Dynamics. *ACS Energy Lett.* **2016**, *1*, 182–188. (62) Chen, S.; Wen, X.; Sheng, R.; Huang, S.; Deng, X.; Green, M. A.; Ho-Baillie, A. Mobile Ion Induced Slow Carrier Dynamics in Organic—Inorganic Perovskite CH₃NH₃PbBr₃. *ACS Appl. Mater. Interfaces* **2016**, *8*, 5351–5357.



pubs.acs.org/JPCC Article

Individual Particle-Level Picture of Charge Carrier Recombination in Bi-Doped CsPbBr₃ Nanocrystals

Tasnim Ahmed, Apurba De, Sumanta Paul, and Anunay Samanta*



Cite This: J. Phys. Chem. C 2021, 125, 2156-2162



Read Online

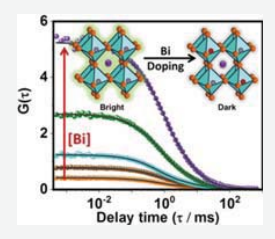
ACCESS

Metrics & More



Supporting Information

ABSTRACT: Doping is an important strategy for both introducing new properties and modifying the intrinsic properties of a semiconductor. In this work, we investigate Bi-doped CsPbBr₃ nanocrystals (NCs), which are less toxic and weakly luminescent compared to the parent system, employing ultrafast pump-probe and fluorescence upconversion techniques and single-particle-based fluorescence correlation spectroscopy technique to obtain individual particle-level understanding of the charge carrier recombination pathways and dynamics in these systems. The results reveal the heterogeneity of the system in terms of photoluminescence (PL) brightness/efficiency of the individual NCs. Three different types of NCs (bright, dim, and dark) have been identified in doped samples that arise from the difference in the extent of doping and consequent variation in the density of Bi-induced states; the latter act as traps for the electrons and assist in nonradiative recombination of charge carriers. An ultrafast trapping process (~2 to 6 ps), which



renders a majority of the Bi-doped NCs into dark ones, is found to be the primary cause of weak PL of the doped systems. The individual particle-level information obtained in this work using a combination of techniques provides new insight into the low PL of Bi-doped CsPbBr₃ perovskite NCs.

1. INTRODUCTION

Lead halide-based perovskites have attracted great attention as next-generation semiconducting materials for photovoltaic and optoelectronic applications because of their broad absorption with high cross section, long carrier diffusion length, intrinsic defect tolerance, and high photoluminescence quantum yield (PLQY). $^{1-9}$ Moreover, the properties of these materials can be tuned by adjusting the composition, size, and dimensionality of the systems. $^{6.10}$ As doping is another strategic route through which these materials can be endowed with new properties, $^{11-13}$ a large number of studies have also been performed on perovskites doped with various dopants, which include both isovalent $^{14-21}$ and heterovalent ions 21,22 with respect to Pb^{2+} for different purposes such as controlling the optoelectronic performance, structural stability, crystal growth, light conversion, and partial replacement of toxic lead. 10,21,23

While the effect of doping an isovalent metal ion on the optical properties of the perovskites has been studied quite extensively $^{14-19,21}$ not much studies have been performed on heterovalent metal-ion dopants. 21,22,24 Among different heterovalent dopants, less toxic Bi^{3+} has received utmost attention as its ionic radius and electronic structure are very similar to those of $\mathrm{Pb}^{2+,25}$ Bi^{3+} -doped perovskite films, nanocrystals (NCs), and large single crystals (SCs) have been studied. $^{24-33}$ As far as the optical properties are concerned, Bi doping results in a significant drop of PLQY of the perovskites. 24,25,28,30,32 For example, Bi doping (5%) of the MAPbBr₃ SCs leads to \sim 99% reduction in PL intensity and carrier lifetime. 28,30 A very recent ultrafast time-resolved THz spectroscopy study shows a notable decrease in charge carrier mobility in MAPbBr₃ film

on Bi doping, attributed to enhanced electron-trapping defects, leading to a decrease in PL efficiency and carrier lifetime. 32 A decrease of PLQY from 78 to 8% (for 2.1% doping) and a substantial decrease of carrier lifetime are also reported for CsPbBr₃ NCs by Mohammed and co-workers.^{24,25} All of these measurements provide an average PL behavior of the NCs, without revealing any information on the PL characteristics of individual NCs. For example, an overall decrease in PLQY of the system on Bi doping can result from (shown in Scheme 1) (i) a decrease in the PL brightness (photon counts per unit time) of each particle, (ii) a decrease in the number of bright particles due to the conversion of some of these particles to dark ones, and (iii) both (i) and (ii). We attempt to obtain individual particle-level information of these doped NCs employing fluorescence correlation spectroscopy (FCS), ultrafast transient absorption (TA), and PL upconversion (UC) techniques, which were not used previously for the study of these systems.

2. METHODS

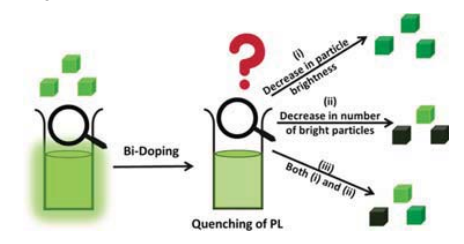
2.1. Materials. Cesium carbonate (99.9%), lead bromide (98%), bismuth bromide (98%) oleic acid (OA, 90%),

Received: November 6, 2020 Revised: December 25, 2020 Published: January 12, 2021





Scheme 1. Possible Reasons for PL Quenching on Bi Doping



oleylamine (OAm, 70%), 1-octadecene (ODE, 90%), and methyl acetate (anhydrous, 99.5%) were purchased from Sigma-Aldrich. Hexane (HPLC grade) was purchased from Finar. These chemicals were used without any purification.

2.2. Synthesis of Undoped and Doped NCs. Cs₂CO₃ (0.102 g), OA (0.312 mL), and ODE (5 mL) were mixed in a 50 mL double-neck round-bottom (RB) flask and heated at 120 °C in vacuum for 1 h. This led to the formation of a clear solution of cesium oleate (Cs-oleate), which was kept at 100 $^{\circ}\text{C}$ (to avoid solidification) under N_2 atmosphere. In another 50 mL double-neck RB flask, ODE (5 mL), PbBr₂ (0.188 mmol), OA (0.5 mL), and OAm (0.5 mL) were loaded and the mixture was heated at 120 °C under vacuum for at least 1 h. After complete solubilization of PbBr2, the mixture was transferred into a N2 atmosphere. Temperature was then increased to 170 °C, and 0.4 mL of a preprepared Cs-oleate solution was injected into it. The reaction mixture was immediately cooled (5-10 s) in an ice-water bath. Then, methyl acetate was added to the reaction mixture in a ratio of 1:2 (v/v) (reaction mixture:methyl acetate) and centrifuged at 6000 rpm for 10 min. The precipitate was dispersed in hexane or ODE according to the need. These NCs were subsequently treated with a mixture of OA (0.1 mL) and OAm (0.1 mL). For the synthesis of Bi-doped CsPbBr₃ NCs, BiBr₃ (2%, 5%, 10%, or 20 mol % PbBr₂) was also used along with PbBr₂, OA, and OAm during synthesis following the method discussed above

2.3. FCS Study. These measurements were performed using a commercial setup, which consisted of a confocal fluorescence microscope (MicroTime 200, PicoQuant) equipped with an inverted microscope (Olympus IX71) with a water-immersion objective (UPlansApo NA 1.2, 60×). The excitation (405 nm) was made using a pulsed diode laser (PDL 828 S Sepia II, PicoQuant) with a repetition rate of 10 MHz, a pulse width of 176 ps, and an excitation power of 0.3 μ W. A drop of solution (nM) of the NCs in ODE was placed on a coverslip for FCS measurement. Under this condition, the average number of excitons generated per pulse was estimated to be \sim 0.2. Fluorescence from the samples was collected by the same objective and passed through a dichroic mirror and filtered using a 430 nm long-pass filter to cut off the exciting light. A pinhole (50 µm diameter) was used for cutting of the out-of-focus signal before being directed to the single-photon avalanche photodiodes (SPADs). The fluorescence correlation traces were generated by cross-correlating signals from two SPAD detectors, for which the signal was directed to two SPADs using a (50/50) beam splitter. Data acquisition was performed using SymPhoTime software-controlled PicoHarp 300 time-correlated single-photon counting (TCSPC) module in a time-tagged time-resolved method.

The correlation function for fluorescence intensity fluctuation is given by 34

$$G(\tau) = \langle \delta F(t) \delta F(t+\tau) \rangle / \langle F(t) \rangle^{2} \tag{1}$$

where F(t) is the average fluorescence intensity, and $\delta F(t)$ and $\delta F(t+\tau)$ are the fluctuations from the average fluorescence intensity in the observation volume (due to diffusion and any other process(es)) at times t and $(t+\tau)$, respectively, which are given by

$$\delta F(t) = F(t) - \langle F(t) \rangle \text{ and } \delta F(t+\tau)$$

= $F(t+\tau) - \langle F(t) \rangle$ (2)

2.4. Transient Absorption Measurement. These measurements were performed using a femtosecond transient absorption setup, the details of which have been described in one of our earlier studies.³⁵ Briefly, the setup consisted of a mode-locked Ti:sapphire oscillator (Mai-Tai, Spectra-Physics), which produced ~100 fs pulses (~30 nJ) with a center wavelength at 800 nm (80 MHz). A part of its output was directed to a regenerative amplifier (Spitfire Ace, Spectra-Physics), which was pumped by the frequency-doubled output (527 nm) of a Nd:YLF laser (Empower, Spectra-Physics). The amplified 800 nm laser beam (~4.2 mJ, 1 kHz) was divided into two parts. The major portion was directed to an optical parametric amplifier (TOPAS-Prime, Spectra-Physics) to generate a 400 nm excitation pulse (~100 fs). The other portion was passed through a variable optical delay line and then directed to a rotating CaF2 crystal to produce the white probe pulse. The probe beam was divided into two parts and used as signal and reference beams. The pump and signal beams were focused onto a rotating sample cell maintaining a collinear geometry for better spatial overlap of the two. The transmitted signal and reference beams were received by a multichannel photodiode array through a polychromator and further processed to record the difference in absorbances (ΔA) as a function of wavelength and pump-probe delay. All measurements were carried out by maintaining a low pump fluence (2 μ J cm⁻²) to avoid any undesired nonlinear processes

2.5. Fluorescence Upconversion Measurement. In these measurements, the 800 nm, 100 fs, 80 MHz output of the mode-locked Ti:sapphire laser (Mai Tai) was directed to a second-harmonic generating BBO crystal to generate 400 nm pulses, which were used for excitation of the samples in a spectrometer (FOG 100, CDP systems, Russia). The laser beam was passed through a dichroic mirror, which reflected the 400 nm pulses and transmitted the 800 nm pulses. The 800 nm laser beam, which served as the gate beam, was passed through an optical delay line. The PLs from the sample and gate beams were mixed in a sum-frequency generating crystal (BBO) to produce the upconverted PL. The upconverted beam was finally directed to the photomultiplier tube through a monochromator. All measurements were carried out maintaining low excitation fluence (0.05 μ J cm⁻²), keeping the absorbance same for all of the systems. The instrumental resolution was found to be ~200 fs.

3. RESULTS AND DISCUSSION

The undoped and Bi-doped CsPbBr₃ NCs with different Bi contents were prepared following reported procedures, ^{6,24} the

details of which are provided in the Methods section. To eliminate any possible contribution of surface-adsorbed Bi on the optical properties of the NCs, the doped samples were thoroughly washed with methyl acetate and dispersed in hexane/ODE, treated using optimum amounts of OA and OAm, and used for studies (see the SI for details). The last treatment, which was not recommended in the reported procedure, ²⁴ was to make up for possible removal of some of protective ligands from the surface during washing.

The Bi content in doped NCs, estimated by the inductively coupled plasma optical emission spectrometry (ICP-OES) measurements, was found to be 0.3, 0.5, 2.7, and 8.2%, respectively, for the 2, 5, 10, and 20% of Bi-feed solutions. The TEM images (Figure S1) of the undoped and doped (8.2% Bi) CsPbBr₃ NCs show no notable change in morphology (a cubic shape with an average edge length of ~9 nm). The HR-TEM images indicate (Figure S1) a lattice spacing of ~0.59 nm for the (100) planes in both doped and undoped systems and confirm the negligible influence of doping on the crystal structure of the NCs. Similar PXRD peak positions (Figure S2) for the undoped and doped NCs further support this statement. No change in the crystal structure of the NCs upon doping is understandable as both Pb²⁺ and Bi³⁺ have an identical ionic radius (~119 pm).²⁵

Doping, however, leads to a change in color of the colloidal dispersion, as observed by the naked eye, from green (0% Bi) to brown (8.2% Bi) (Figure 1).²⁴ The electronic absorption

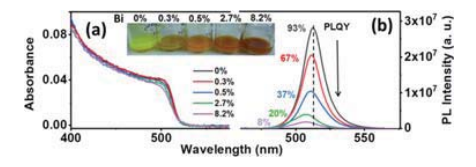


Figure 1. (a) Absorption and (b) emission spectra (λ_{ex} = 400 nm) of Bi-doped (0, 0.3, 0.5, 2.7, and 8.2%) CsPbBr₃ NCs dispersed in hexane.

spectra of the NCs show (Figures 1a and S3) a reduction of the excitonic peak intensity and slight blue shift of the peak position with an increase in Bi content. The PL spectra (Figures 1b and S4) of the samples also show a progressive blue shift with increasing Bi content in the NCs. A shift in PL peak position from 513 to 506 nm is observed between undoped and 8.2% doped NCs. A similar shift, observed earlier for Bi-doped CsPbBr₃ NCs and PbS quantum dots, was attributed to the Burstein–Moss effect. ^{24,36,37} The increase in Bi content also leads to progressive quenching of PL. The PLQY drops from ~93% (undoped) to ~8% (8.2% Bi-doped) with no significant change in the width of the PL spectra (FWHM, 17-20 nm). Although this drastic decrease in PLQY is consistent with the literature, 24,25 the PL quenching can be due to surface defects arising from surface-adsorbed Bi or/and detachment of the surface ligands. These possibilities are however ruled out by washing the doped NCs with methyl acetate and treating them with the ligands, OA and OAm. Additional control experiments (vide SI) were performed to establish that the PL quenching of CsPbBr3 NCs in our study was solely due to Bi doping.

We have studied the spectral and temporal characteristics of the transients produced on photoexcitation of the undoped and doped NCs using femtosecond pulses under similar experimental conditions to understand the influence of doping on the charge carrier dynamics. The TA spectra (Figure 2a)

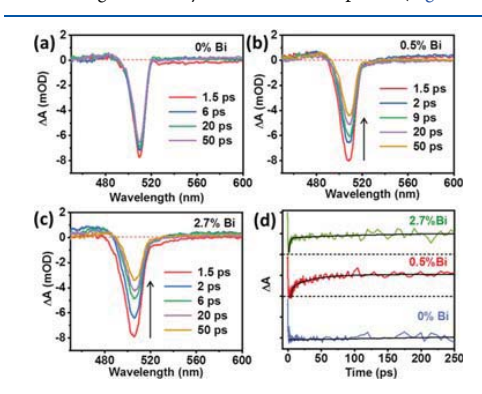


Figure 2. TA spectra of (a) 0%, (b) 0.5%, and (c) 2.7% Bi-doped CsPbBr₃ NCs dispersed in hexane ($\lambda_{\rm ex}$ = 400 nm). (d) Comparison of the bleach recovery kinetics monitored at their respective bleach maximum (505–509 nm) of the samples with different Bi contents.

are found to be characterized by a sharp bleach signal at \sim 509 nm, which arises due to filling of the band edge states by the charge carriers. ^{38,39} Even though the spectral features are quite similar for the undoped and doped NCs, with an increase in Bi content in the samples, a blue shift (509–505 nm) of the bleach peak is observed (Figure 2), which is consistent with the shift of the excitonic peak in the steady-state absorption spectra.

The bleach recovery kinetics of the undoped CsPbBr3 NCs is found to be single exponential (Figure 2d) with a time constant of >500 ps⁴⁰ (Table S2), which represents the excitonic recombination of the charge carriers. 17,39 For the doped samples, the bleach recovery is, however, biexponential. In addition to the slow component (>500 ps), another ultrafast component, whose value decreases with an increase in Bi content, is observed. For example, the lifetime decreases from 3.2 to 1.9 ps with an increase in dopant content in the NCs from 0.5 to 2.7% (Table S2). This time constant corresponds to the trapping process. It is thus evident that Bi doping promotes rapid nonradiative recombination of the charge carriers through the dopant-introduced trap states and quenches the PL of the NCs. Careful inspection of the data reveals that even though the maximum bleach amplitudes (measured under identical conditions) are similar for undoped and 0.5 and 2.7% doped NCs, it is substantially (75%) lower for the 8.2% Bi-doped sample (Figure S5), indicating that for this sample, all photogenerated charge carriers do not return to the band edge states; some are leaked through another channel in competition with the hot carrier cooling process. 41,42 Hence, it is evident that while carrier trapping becomes faster with an increase in Bi content, for the sample with a higher Bi content, trapping of the hot carriers is also an important process. The hot carrier trapping process is further confirmed by acceleration of the formation of the bleach kinetics for 8.2% Bidoped NCs compared to the other samples (Figure S5).

Additional insight into the low PLQY of the Bi-doped CsPbBr₃ NCs is obtained from FCS measurements. In this technique, we measure the fluctuations of PL of a highly dilute solution (nM) of the NCs in a small volume of the sample

(typically \sim 1 fL) using a confocal fluorescence microscope. For this purpose, we have studied solutions of the NCs (in ODE) with identical absorbance at the excitation wavelength of 405 nm (see the SI for details). The measured time dependence of the fluorescence correlation data of the undoped and doped NCs is shown in Figure 3. The data are

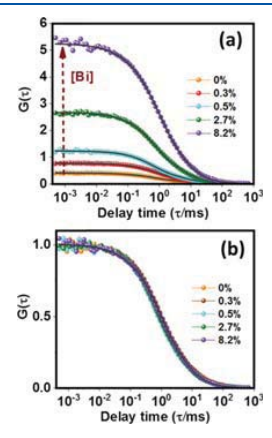


Figure 3. Fluorescence correlation curves of Bi-doped (0, 0.3, 0.5, 2.7, and 8.2%) $CsPbBr_3\ NC\ solutions\ in\ ODE\ in\ (a)\ absolute\ and\ (b)\ normalized\ scales.$

found to be best represented by a model (eq 3), according to which the PL fluctuations arise from (i) diffusion of the NCs in and out of the observation volume and (ii) involvement of the trap states, which are represented by a stretched exponential decay component. This model has been used previously for metal-chalcogenide quantum dots as well as for perovskite NCs. $^{43-46}$ The amplitude of correlation at time $\tau,\ G(\tau),$ is expressed as

$$G(\tau) = \left[1 + \frac{T}{1 - T} \exp\left(-\frac{\tau}{\tau_{\rm T}}\right)^{\beta} \right] 1 / \langle N \rangle \left(1 + \tau/\tau_{\rm D} \right)^{-1}$$

$$\left(1 + \tau/\kappa^2 \tau_{\rm D} \right)^{-1/2}$$
(3)

where $\tau_{\rm D}$ is the diffusion time of the NCs, $\langle N \rangle$ is the average number of particles undergoing reversible PL intensity fluctuation in the observation volume, T is the fraction of particles in their "off" state, $\tau_{\rm T}$ is the dark-state relaxation time or blinking time, β is a stretching exponent having a value between 0 and 1, indicating the distribution of $\tau_{\rm T}$, κ (= ω_z/ω_{xy}) is the structure parameter of the observation volume, and ω_z and ω_{xy} are the longitudinal and transverse radii, respectively. The per-particle brightness (PPB) of the NCs is given by I/

 $\langle N \rangle$, where I is the average count rate of the PL intensity trace. 47

The time dependence of the fluorescence correlation data of the samples and the fits to eq 3 are shown in Figure 3. With an increase in Bi content, the G(0) value, which is the amplitude of correlation at time zero, increases (Table 1), but the shape of the correlation curves remains the same despite the significant difference in PL efficiency of different samples. A close look at different parameters associated with blinking (Table 1), as obtained from the analysis of the data, shows that the β value is not very far from unity (~0.8) for undoped NCs, indicating that only a few trap states contribute to PL blinking of these systems. This is in agreement with the high PLQY (~93%) of the undoped NCs. 43 Interestingly, even though the doped systems exhibit much lower PLQY, the blinking parameters such as T, τ_T , and PPB including the β values are very similar for doped and undoped samples. No notable effect of doping on the blinking dynamics (in the microsecond to millisecond time scale) of the NCs, as observed here, is possible only when undoped NCs are present in an ensemble of doped NCs. Considering that G(0) is defined as $1/[\langle N \rangle(1$ - T)], its value can increase (Figure 3a) with a decrease of $\langle N \rangle$ or/and increase in T. However, as the T value remains unchanged on doping (Table 1), it is thus evident that the increase in the G(0) value for a higher dopant content is due to a decrease in $\langle N \rangle$ (Table 1). This decrease in the $\langle N \rangle$ value for a higher dopant content could be due to the conversion of bright NCs to permanently dark ones and also due to particles, which exhibit slow blinking dynamics ($au_{\mathrm{T}} > au_{\mathrm{D}}$) and is not captured here.

The excited-state dynamics of the systems were further studied by monitoring the PL decay profiles with a time resolution of ~200 fs using the PL UC technique.³⁵ Figure 4a depicts the normalized PL decay profiles of undoped and 0.5 and 2.7% Bi-doped NCs. While the undoped NCs exhibit a single-exponential PL decay with a time constant >500 ps, the doped NCs show a biexponential decay behavior with an additional fast component due to the carrier trapping process. With an increase in the doping content from 0.5 to 2.7%, this decay component becomes faster (from 6.2 to 3.4 ps) and the PL intensity at time zero decreases progressively (Figure 4b). For the 8.2% Bi-doped NCs, the initial PL counts drop to such a low level that the PL decay dynamics cannot be measured under similar experimental conditions. This decrease in timezero PL intensity can be due to (i) hot carrier trapping or/and (ii) increase in the number of dark particles.⁵⁰ However, as the TA data indicated the same bleach amplitude for 0.5 and 2.7%doped NCs, it is evident that with an increase in Bi content from 0.5 and 2.7%, the number of photoluminescent NCs decreases. This finding is consistent with that obtained from the FCS study that confirms the conversion of fraction of bright NCs to permanently dark ones. A quantitative analysis

Table 1. Estimated Blinking Parameters, G(0), $\tau_{\rm D}$, $\langle N \rangle$, β , $\tau_{\rm T}$, T, and PPB Values of the Bi-Doped (0, 0.3, 0.5, 2.7, and 8.2%) CsPbBr₃ NCs, As Obtained from FCS Measurements

Bi content (%)	G(0)	$\tau_{\mathrm{D}} \; (\mathrm{ms})$	$\langle N \rangle$	β	$\tau_{\mathrm{T}} \; (\mathrm{ms})$	T	PPB (K cps)
0	0.44 ± 0.02	4.1 ± 0.27	5.6 ± 0.41	0.78 ± 0.01	0.63 ± 0.03	0.52 ± 0.05	3.27 ± 0.21
0.3	0.71 ± 0.03	4.2 ± 0.25	3.01 ± 0.37	0.79 ± 0.02	0.77 ± 0.05	0.49 ± 0.02	3.72 ± 0.28
0.5	1.2 ± 0.15	3.8 ± 0.28	1.73 ± 0.20	0.83 ± 0.06	0.60 ± 0.06	0.47 ± 0.03	3.93 ± 0.20
2.7	2.7 ± 0.21	3.9 ± 0.27	0.91 ± 0.15	0.80 ± 0.03	0.65 ± 0.03	0.46 ± 0.04	3.59 ± 0.25
8.2	5.3 ± 0.25	4.1 ± 0.26	0.43 ± 0.02	0.75 ± 0.05	0.75 ± 0.05	0.48 ± 0.02	3.27 ± 0.28

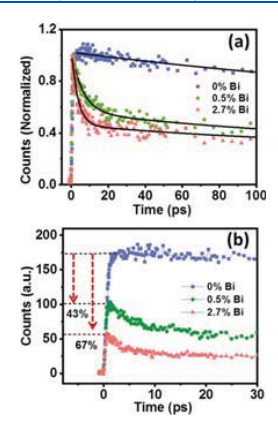
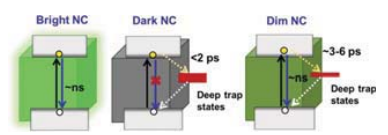


Figure 4. PL decays of different Bi-doped (0, 0.5, and 2.7%) CsPbBr₃ NCs (dispersed in hexane) obtained in PL UC measurement (λ_{ex} = 400 nm) in (a) normalized and (b) absolute scales.

of the time-zero PL intensity reveals ${\sim}43$ and ${\sim}67\%$ conversions of the NCs into the dark ones for 0.5 and 2.7% Bi-doped NCs, respectively.

Replacement of Pb²⁺ by Bi³⁺ in CsPbBr₃ NCs creates deep electron trap states, which serve as nonradiative recombination channels for the carriers and quenches the PL^{24,25,28,51} Our measurements (TA, PL UC and FCS) not only confirm that an efficient nonradiative ultrafast carrier recombination pathway introduced by the dopant is responsible for the low PL efficiency of the system, but they provide the first particle-level insight into the lower PL efficiency of the Bi-doped CsPbBr₃ NCs. Let us combine the findings of three different measurements and attempt to construct the picture that we obtain from this study (Scheme 2).

Scheme 2. Recombination Processes in $Bi\text{-}Doped\ CsPbBr_3$ NCs, Which Comprise a Mixture of Three Different Kinds of NCs



The FCS study reveals two important pieces of information. First, there remain some NCs that exhibit blinking characteristics remarkably similar to those of the undoped NCs that remain undoped in the doped samples. Second, the decrease of number of observable photoluminescent particles upon doping, *i.e.*, conversion of the photoluminescent particles into dark ones could be one of the possible reasons for lowering the PL efficiency upon Bi doping.

The decrease of PL intensity at t = 0 in PL UC study further confirms the conversion of some bright NCs into permanently dark ones. However, if there were only bright and dark NCs, the PL decay kinetics would not have been affected. The short-lifetime component arises from the NCs with intermediate brightness, which is termed as dim NCs. These particles are characterized by short PL lifetimes, in which nonradiative

recombination of the carriers competes with the radiative recombination processes, but does not prevent it completely (like in dark NCs). The fraction of bright NCs converting into dark ones upon doping is estimated to be ~69% (0.5% Bi) and ~84% (2.7% Bi) in FCS measurements (from the drop in the value of $\langle N \rangle$) and ~43 and ~67% for the respective samples in PL UC measurements (from the decrease in PL intensity at t=0). This difference arises because the dim particles appear as dark NCs in FCS measurements as weak PL (comparable to the background signal) of these particles does not allow their detection under identical experimental conditions. \$^{45,52}

A close look at the estimated time constants of the carrier trapping process (Table \$2) shows that the process appears faster in TA measurement than that obtained by the PL UC technique. This is because PL UC measurement probes the dynamics of only the fluorescent particles (bright and dim NCs), whereas the TA studies collect the data for all particles (bright, dim, and dark). With an increase in Bi content as the density of Bi-associated trap states increases, the carrier recombination process becomes faster. The dark and dim NCs differ in terms of the density of the trap states depending on the Bi content in the individual particles.⁵²

4. CONCLUSIONS

In short, investigation of the Bi-doped CsPbBr₃ NCs using a combination of techniques reveals three types of NCs differing in PL brightness and charge carrier recombination dynamics. Nonuniform doping of the NCs is found to be responsible for the heterogeneous nature of the sample. A difference in dopant content leads to a change in the density of the dopant-introduced states and the consequent difference in the rate of trapping of the carriers and PL brightness of the NCs. This study provides first insight into the individual particle-level information on the carrier dynamics and PL efficiency of the Bi-doped CsPbBr₃ NCs.

■ ASSOCIATED CONTENT

Supporting Information

The Supporting Information is available free of charge at https://pubs.acs.org/doi/10.1021/acs.jpcc.0c10037.

Details of PXRD, ICP-OES, and TEM measurement; control experiment, TEM images, and PXRD patterns; normalized absorption, emission spectra, and FCS curves; and tables containing fitting parameters of PL UC and TA measurements of undoped and doped CsPbBr₃ NCs (PDF)

AUTHOR INFORMATION

Corresponding Author

Anunay Samanta — School of Chemistry, University of Hyderabad, Hyderabad 500046, India; orcid.org/0000-0003-1551-0209; Email: anunay@uohyd.ac.in

Authors

Tasnim Ahmed — School of Chemistry, University of Hyderabad, Hyderabad 500046, India; ⊙ orcid.org/0000-0002-5990-3891

Apurba De — School of Chemistry, University of Hyderabad, Hyderabad 500046, India; ⊙ orcid.org/0000-0002-3042-0642

Sumanta Paul – School of Chemistry, University of Hyderabad, Hyderabad 500046, India Complete contact information is available at: https://pubs.acs.org/10.1021/acs.jpcc.0c10037

Notes

The authors declare no competing financial interest.

ACKNOWLEDGMENTS

This work was supported by the J. C. Bose Fellowship (to A.S.) of the Science and Engineering Research Board (SERB) and Institute of Eminence Grants (to University of Hyderabad) of the Ministry of Human Resource and Development (MHRD). The authors thank Dr. M. Durga Prasad for the TEM measurements at the Centre for Nanotechnology, University of Hyderabad. T.A. thanks CSIR, and A.D. and S.P. thank UGC for Fellowships.

REFERENCES

- (1) National Renewable Energy Laboratory NREL. https://www.nrel.gov/pv/assets/pdfs/best-research-cell-efficiencies.20200803.pdf.
- (2) Chen, Q.; Wu, J.; Ou, X.; Huang, B.; Almutlaq, J.; Zhumekenov, A. A.; Guan, X.; Han, S.; Liang, L.; Yi, Z.; et al. All-inorganic Perovskite Nanocrystal Scintillators. *Nature* **2018**, 561, 88–93.
- (3) Gong, M.; Sakidja, R.; Goul, R.; Ewing, D.; Casper, M.; Stramel, A.; Elliot, A.; Wu, J. Z. High-Performance All-Inorganic CsPbCl₃ Perovskite Nanocrystal Photodetectors with Superior Stability. ACS Nano 2019, 13, 1772–1783.
- (4) Kang, J.; Wang, L. W. High Defect Tolerance in Lead Halide Perovskite CsPbBr₃. J. Phys. Chem. Lett. **2017**, 8, 489–493.
- (5) Kovalenko, M. V.; Protesescu, L.; Bodnarchuk, M. I. Properties and Potential Optoelectronic Applications of Lead Halide Perovskite Nanocrystals. *Science* **2017**, 358, 745–750.
- (6) Protesescu, L.; Yakunin, S.; Bodnarchuk, M. I.; Krieg, F.; Caputo, R.; Hendon, C. H.; Yang, R. X.; Walsh, A.; Kovalenko, M. V. Nanocrystals of Cesium Lead Halide Perovskites (CsPbX₃, X = Cl, Br, and I): Novel Optoelectronic Materials Showing Bright Emission with Wide Color Gamut. Nano Lett. 2015, 15, 3692–3696.
- (7) Shi, Z.; Li, Y.; Zhang, Y.; Chen, Y.; Li, X.; Wu, D.; Xu, T.; Shan, C.; Du, G. High-Efficiency and Air-Stable Perovskite Quantum Dots Light-Emitting Diodes with an All-Inorganic Heterostructure. *Nano Lett.* **2017**, *17*, 313–321.
- (8) Swarnkar, A.; Chulliyil, R.; Ravi, V. K.; Irfanullah, M.; Chowdhury, A.; Nag, A. Colloidal CsPbBr₃ Perovskite Nanocrystals: Luminescence beyond Traditional Quantum Dots. Angew. Chem., Int. Ed. 2015, 54, 15424–15428.
- (9) Zhou, Q.; Bai, Z.; Lu, W.-g.; Wang, Y.; Zou, B.; Zhong, H. In Situ Fabrication of Halide Perovskite Nanocrystal-Embedded Polymer Composite Films with Enhanced Photoluminescence for Display Backlights. *Adv. Mater.* **2016**, *28*, 9163–9168.
- (10) Zhou, Y.; Chen, J.; Bakr, O. M.; Sun, H.-T. Metal-Doped Lead Halide Perovskites: Synthesis, Properties, and Optoelectronic Applications. *Chem. Mater.* **2018**, *30*, 6589–6613.
- (11) Abram, R. A.; Rees, G. J.; Wilson, B. L. H. Heavily Doped Semiconductors and Devices. Adv. Phys. 1978, 27, 799–892.
- (12) Khan, A.; Das, A. Diffusivity–Mobility Relationship for Heavily Doped Semiconductors Exhibiting Band Tail. *Phys. B* **2010**, 405, 817–821.
- (13) Palankovski, V.; Kaiblinger-Grujin, G.; Selberherr, S. Dopant-Dependent Band Gap Narrowing in Compound Semiconductor Devices. *Mater. Sci. Eng. B* **1999**, *66*, 46–49.
- (14) De, A.; Das, S.; Mondal, N.; Samanta, A. Highly Luminescent Violet- and Blue-Emitting Stable Perovskite Nanocrystals. *ACS Mater. Lett.* **2019**, *1*, 116–122.
- (15) Chen, J.-K.; Ma, J.-P.; Guo, S.-Q.; Chen, Y.-M.; Zhao, Q.; Zhang, B.-B.; Li, Z.-Y.; Zhou, Y.; Hou, J.; Kuroiwa, Y.; et al. High-Efficiency Violet-Emitting All-Inorganic Perovskite Nanocrystals Enabled by Alkaline-Earth Metal Passivation. *Chem. Mater.* 2019, 31, 3974–3983.

- (16) Yong, Z.-J.; Guo, S.-Q.; Ma, J.-P.; Zhang, J.-Y.; Li, Z.-Y.; Chen, Y.-M.; Zhang, B.-B.; Zhou, Y.; Shu, J.; Gu, J.-L.; et al. Doping-Enhanced Short-Range Order of Perovskite Nanocrystals for Near-Unity Violet Luminescence Quantum Yield. J. Am. Chem. Soc. 2018, 140, 9942—9951.
- (17) Das, S.; De, A.; Samanta, A. Ambient Condition Mg²⁺ Doping Producing Highly Luminescent Green- and Violet-Emitting Perovskite Nanocrystals with Reduced Toxicity and Enhanced Stability. *J. Phys. Chem. Lett.* **2020**, *11*, 1178–1188.
- (18) De, A.; Mondal, N.; Samanta, A. Luminescence Tuning and Exciton Dynamics of Mn-doped CsPbCl₃ Nanocrystals. *Nanoscale* **2017**, *9*, 16722–16727.
- (19) Mondal, N.; De, A.; Samanta, A. Achieving Near-Unity Photoluminescence Efficiency for Blue-Violet-Emitting Perovskite Nanocrystals. ACS Energy Lett. 2019, 4, 32–39.
- (20) Wang, H.-C.; Wang, W.; Tang, A.-C.; Tsai, H.-Y.; Bao, Z.; Ihara, T.; Yarita, N.; Tahara, H.; Kanemitsu, Y.; Chen, S.; et al. High-Performance $CsPb_{1-x}Sn_xBr_3$ Perovskite Quantum Dots for Light-Emitting Diodes. *Angew. Chem., Int. Ed.* **2017**, *56*, 13650–13654.
- (21) Luo, B.; Li, F.; Xu, K.; Guo, Y.; Liu, Y.; Xia, Z.; Zhang, J. Z. B-Site Doped Lead Halide Perovskites: Synthesis, Band Engineering, Photophysics, and Light Emission Applications. *J. Mater. Chem. C* **2019**, *7*, 2781–2808.
- (22) Swarnkar, A.; Mir, W. J.; Nag, A. Can B-Site Doping or Alloying Improve Thermal- and Phase-Stability of All-Inorganic CsPb X_3 (X = Cl, Br, I) Perovskites? ACS Energy Lett. 2018, 3, 286–289.
- (23) Seth, S.; Ahmed, T.; De, A.; Samanta, A. Tackling the Defects, Stability, and Photoluminescence of CsPbX₃ Perovskite Nanocrystals. *ACS Energy Lett.* **2019**, *4*, 1610–1618.
- (24) Begum, R.; Parida, M. R.; Abdelhady, A. L.; Murali, B.; Alyami, N. M.; Ahmed, G. H.; Hedhili, M. N.; Bakr, O. M.; Mohammed, O. F. Engineering Interfacial Charge Transfer in CsPbB₇ Perovskite Nanocrystals by Heterovalent Doping. J. Am. Chem. Soc. 2017, 139, 731–737.
- (25) Yin, J.; Ahmed, G. H.; Bakr, O. M.; Bre'das, J.-L.; Mohammed, O. F. Unlocking the Effect of Trivalent Metal Doping in All-Inorganic CsPbBr₃ Perovskite. ACS Energy Lett. **2019**, *4*, 789–795.
- (26) Abdelhady, A. L.; Saidaminov, M. I.; Murali, B.; Adinolfi, V.; Voznyy, O.; Katsiev, K.; Alarousu, E.; Comin, R.; Dursun, I.; Sinatra, L.; Sargent, E. H.; Mohammed, O. F.; Bakr, O. M. Heterovalent Dopant Incorporation for Bandgap and Type Engineering of Perovskite Crystals. J. Phys. Chem. Lett. 2016, 7, 295–301.
- (27) Hu, Y.; Bai, F.; Liu, X.; Ji, Q.; Miao, X.; Qiu, T.; Zhang, S. Bismuth Incorporation Stabilized \(\alpha\)-CsPbI_3 for Fully Inorganic Perovskite Solar Cells. \(\alpha\)CS Energy Lett. \(\frac{2017}{2017}\), 2, 2219—2227.
- (28) Nayak, P. K.; Sendner, M.; Wenger, B.; Wang, Z.; Sharma, K.; Ramadan, A. J.; Lovrincic, R.; Pucci, A.; Madhu, P. K.; Snaith, H. J. Impact of Bi³⁺ Heterovalent Doping in Organic–Inorganic Metal Halide Perovskite Crystals. *J. Am. Chem. Soc.* **2018**, *140*, 574–577.
- (29) Lozhkina, O. A.; Murashkina, A. A.; Shilovskikh, V. V.; Kapitonov, Y. V.; Ryabchuk, V. K.; Emeline, A. V.; Miyasaka, T. Invalidity of Band-Gap Engineering Concept for Bi³⁺ Heterovalent Doping in CsPbBr₃ Halide Perovskite. J. Phys. Chem. Lett. 2018, 9, 5408-5411.
- (30) Yamada, Y.; Hoyano, M.; Akashi, R.; Oto, K.; Kanemitsu, Y. Impact of Chemical Doping on Optical Responses in Bismuth-Doped CH₃NH₃PbBr₃ Single Crystals: Carrier Lifetime and Photon Recycling. *J. Phys. Chem. Lett.* **2017**, *8*, 5798–5803.
- (31) Zhou, Y.; Yong, Z.-J.; Zhang, K. C.; Liu, B. M.; Wang, Z.-W.; Hou, J.-S.; Fang, Y.-Z.; Sun, H. T.; Song, B.; et al. Ultrabroad Photoluminescence and Electroluminescence at New Wavelengths from Doped Organometal Halide Perovskites. J. Phys. Chem. Lett. 2016, 7, 2735–2741.
- (32) Ulatowski, A. M.; Wright, A. D.; Wenger, B.; Buizza, L. R. V.; Motti, S. G.; Eggimann, H. J.; Savill, K. J.; Borchert, J.; Snaith, H. J.; Johnston, M. B.; Herz, L. M. Charge-Carrier Trapping Dynamics in Bismuth-Doped Thin Films of MAPbBr₃ Perovskite. J. Phys. Chem. Lett. 2020, 11, 3681–3688.

- (33) Meng, R.; GuangbaoWu; Zhou, J.; Zhou, H.; HonghuaFang; Loi, M. A.; Zhang, Y. Understanding the Impact of Bismuth Heterovalent Doping on the Structural and Photophysical Properties of CH₃NH₃PbBr₃ Halide Perovskite Crystals with Near-IR Photoluminescence. Chem. Eur. J. 2019, 25, 5480–5488.
- (34) Heuff, R. F.; Swift, J. L.; Cramb, D. T. Fluorescence Correlation Spectroscopy Using Quantum Dots: Advances, Challenges and Opportunities. *Phys. Chem. Chem. Phys.* **2007**, *9*, 1870–1880.
- (35) Mondal, N.; Samanta, A. Complete Ultrafast Charge Carrier Dynamics in Photo-Excited All-Inorganic Perovskite Nanocrystals (CsPbX₃). Nanoscale **2017**, *9*, 1878–1885.
- (36) Stavrinadis, A.; Rath, A. K.; Arquer, F. P. G. ad.; Diedenhofen, S. L.; Mage'n, Cs.; Martinez, L.; So, D.; Konstantatos, G. Heterovalent Cation Substitutional Doping for Quantum Dot Homojunction Solar Cells. *Nat. Commun.* 2013, 4, No. 2981.
- (37) Kamat, P. V.; Dimitrijevic, N. M.; Nozik, A. J. Dynamic Burstein-Moss Shift in Semiconductor Colloids. *J. Phys. Chem. Lett.* **1989**, 93, 2873–2875.
- (38) Mondal, N.; De, A.; Das, S.; Paul, S.; Samanta, A. Ultrafast Carrier Dynamics of Metal Halide Perovskite Nanocrystals and Perovskite Composites. *Nanoscale* **2019**, *11*, 9796–9818.
- (39) Wu, K.; Liang, G.; Shang, Q.; Ren, Y.; Kong, D.; Lian, T. Ultrafast Interfacial Electron and Hole Transfer from CsPbBr₃ Perovskite Quantum Dots. *J. Am. Chem. Soc.* **2015**, 137, 12792–12795.
- (40) Exact estimation of this long time-constant is not possible in this setup, which is suited for measurements in the fs-ps time window. (41) Mondal, N.; Paul, S.; Samanta, A. Photoinduced 2-way Electron Transfer in Composites of Metal Nanoclusters and Semiconductor Quantum Dots. Nanoscale 2016, 8, 14250–14256.
- (42) Yu, P.; Wen, X.; Lee, Y.-C.; Lee, W.-C.; Kang, C.-C.; Tang, J. Photoinduced Ultrafast Charge Separation in Plexcitonic CdSe/Au and CdSe/Pt Nanorods. J. Phys. Chem. Lett. 2013, 4, 3596–3601.
- (43) Ahmed, T.; Seth, S.; Samanta, A. Mechanistic Investigation of the Defect Activity Contributing to the Photoluminescence Blinking of CsPbBr₃ Perovskite Nanocrystals. ACS Nano 2019, 13, 13537– 13544.
- (44) Seth, S.; Mondal, N.; Patra, S.; Samanta, A. Fluorescence Blinking and Photoactivation of All-Inorganic Perovskite Nanocrystals CsPbBr₃ and CsPbBr₂I. *J. Phys. Chem. Lett.* **2016**, *7*, 266–271.
- (45) Ito, S.; Toitani, N.; Pan, L.; Tamai, N.; Miyasaka, H. Fluorescence Correlation Spectroscopic Study on Water-Soluble Cadmium Telluride Nanocrystals: Fast Blinking Dynamics in the μs-ms Region. J. Phys.: Condens. Matter 2007, 19, No. 486208.
- (46) Patra, S.; Samanta, A. A Fluorescence Correlation Spectroscopy, Steady-State, and Time-Resolved Fluorescence Study of the Modulation of Photophysical Properties of Mercaptopropionic Acid Capped CdTe Quantum Dots upon Exposure to Light. J. Phys. Chem. C 2013, 117, 23313–23321.
- (47) Dong, C.; Qian, H.; Fang, N.; Ren, J. Study of Fluorescence Quenching and Dialysis Process of CdTe Quantum Dots, Using Ensemble Techniques and Fluorescence Correlation Spectroscopy. J. Phys. Chem. B 2006, 110, 11069—11075.
- (48) Dong, C.; Liu, H.; Ren, J. Assessing the Blinking State of Fluorescent Quantum Dots in Free Solution by Combining Fluorescence Correlation Spectroscopy with Ensemble Spectroscopic Methods. *Langmuir* **2014**, *30*, 12969–12976.
- (49) Yao, J.; Larson, D. R.; Vishwasrao, H. D.; Zipfel, W. R.; Webb, W. W. Blinking and Nonradiant Dark Fraction of Water-Soluble Quantum Dots in Aqueous Solution. Proc. Natl. Acad. Sci. U.S.A. 2005, 102, 14284–14289.
- (50) Lai, R.; Wu, K. Picosecond Electron Trapping Limits the Emissivity of CsPbCl₃ Perovskite Nanocrystals. *J. Chem. Phys.* **2019**, 151, 194701–194706.
- (51) Mosconi, E.; Merabet, B.; Meggiolaro, D.; Zaoui, A.; Angelis, F. D. First-Principles Modeling of Bismuth Doping in the MAPbI₃ Perovskite. J. Phys. Chem. C 2018, 122, 14107–14112.
- (52) Durisic, N.; Godin, A. G.; Walters, D.; tter, P. G.; Wiseman, P. W.; Heyes, C. D. Probing the "Dark" Fraction of Core Shell Quantum

Dots by Ensemble and Single Particle pH-Dependent Spectroscopy. ACS Nano 2011, 5, 9062–9073.

Controlling Photoluminescence and Understanding Charge Carrier Recombination and Transfer Dynamics of Perovskite Nanocrystals

by Tasnim Ahmed

Submission date: 07-Apr-2021 12:47PM (UTC+0530)

Submission ID: 1552606690

File name: Thesis_Tasnim_Ahmed_7-4-21.pdf (8.87M)

Word count: 24875 Character count: 128992

Controlling Photoluminescence and Understanding Charge Carrier Recombination and Transfer Dynamics of Perovskite Nanocrystals

Ivali	ocrystals		S) // // // / / / / / / / / / / / / / /		
ORIGINA	ALITY REPORT				
3 SIMILA	9% ARITY INDEX	5% INTERNET SOURC	36% ES PUBLICATIONS	5% STUDENT PAPERS	
PRIMAR	RY SOURCES				
1		The second secon	a De, Sumanta F lividual Particle-L	Paul, 15%) con blication
	Doped C		ier Recombination ystals ", The Jou 2021	on in Bi- urnal of	man
2	Samanta Defect A Photolun	a. " Mechanistic ctivity Contribu ninescence Bli	a Seth, Anunay c Investigation of uting to the nking of CsPbBr s ", ACS Nano, 2		
3	Samanta Defect A Photolun	n. "Mechanistic ctivity Contribu ninescence Bli	a Seth, Anunay Investigation of Iting to the nking of CsPbBr s", ACS Nano, 2	3	

Submitted to University of Hyderabad,

	4	Hyderabad Student Paper	3%
	5	Nianhui Song, Haiming Zhu, Shengye Jin, Tianquan Lian. "Hole Transfer from Single Quantum Dots", ACS Nano, 2011 Publication	1%
Dwn publication	. 6	Tasnim Ahmed, Sudipta Seth, Anunay Samanta. "Boosting the Photoluminescence of CsPbX (X = Cl, Br, I) Perovskite Nanocrystals Covering a Wide Wavelength Range by Postsynthetic Treatment with Tetrafluoroborate Salts ", Chemistry of Materials, 2018 Publication	1%
	7	www.ncbi.nlm.nih.gov Internet Source	<1%
	8	researchonline.jcu.edu.au Internet Source	<1%
	9	pubs.acs.org Internet Source	<1%
	10	Sudipta Seth, Navendu Mondal, Satyajit Patra, Anunay Samanta. "Fluorescence Blinking and Photoactivation of All-Inorganic Perovskite Nanocrystals CsPbBr and CsPbBr I ", The Journal of Physical Chemistry Letters, 2016 Publication	<1%
		Rudolf Rigler, Michel Orrit, Thomas Basché.	

Petter Persson, Villy Sundström. "Ultrafast Electron Dynamics in Solar Energy Conversion", Chemical Reviews, 2017

<1%

Publication

50

Submitted to University of Birmingham Student Paper

<1%

Exclude quotes

On

Exclude matches

< 14 words

Exclude bibliography On